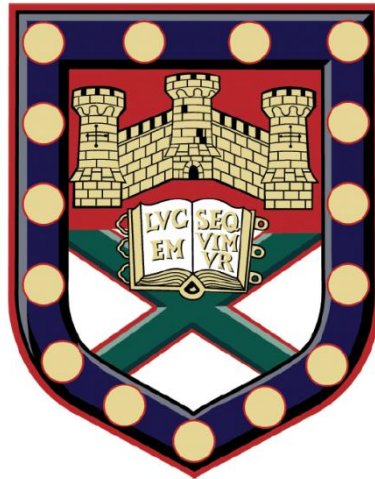


Investigations into the Potential of Constructing Aligned Carbon Nanotube Composite Materials through Additive Layer Manufacture



Robert J. A. Allen

College of Engineering, Mathematics and Physical Sciences

University of Exeter

A thesis submitted for the degree of

Doctor of Philosophy

June 2013

**Investigations into the Potential of Constructing Aligned Carbon Nanotube
Composite Materials through Additive Layer Manufacture**

Submitted by Robert James Anthony Allen to the University of Exeter

as a thesis for the degree of

Doctor of Philosophy in Engineering

In June 2013

This thesis is available for Library use on the understanding that it is copyright material and that no quotation from the thesis may be published without proper acknowledgement.

I certify that all material in this thesis which is not my own work has been identified and that no material has previously been submitted and approved for the award of a degree by this or any other University.

Signature:

Acknowledgements:

The undertaking of the works contained in this thesis has been a privilege and a pleasure and I am extremely grateful to all who have made this possible. It is only through the help of many people that this thesis has come to completion and although clearly not extensive the following provides a list of those who have extended significant and invaluable aid over the past three years:

- Firstly I would like to thank the late Prof. Alexander Savchenko, his excellent tuition was invaluable during the final years of my undergraduate studies and without his guidance and belief it is unlikely that I would have chosen to pursue the course of this PhD.
- I extend many thanks to my supervisors, Prof. Kenneth Evans, Dr Oana Ghita, Dr Benjamin Farmer, and Dr Mark Beard who have all provided extensive assistance and support throughout.
- Much gratitude is given to the Engineering and Physical Sciences Research Council (EPSRC) and EADS Innovation Works for providing the financial support necessary to undertake these investigations.
- Much credit is owed to the Engineering Workshop and its Staff, in particular Pete Gerry, Martin Simpson, Roger Perret, and Dave Baker. Their help in producing custom equipment has been crucial.
- Thanks to the Engineering Instrument Pool (EIP) for the loan of a high speed camera to conduct the experiments detailed in **Chapter 6**.
- Thanks as well to the many staff and students at the university who have made the last few years so enjoyable, Thanks to: Lesley Wears, Tom Hughes, Will Newby, Nunzio Palumbo, Chris Taylor, David Barnes, Wayne Miller, Stephen Mellor, Mathew Johns, Marc-Antoine Boucher, Giovanni Stranno, Asmi Rizvi, Pierre Aumjaud, Paul BrookBank, Monica Craciun, Yat-Tarng Shyng, Linda Urlu and Pete Jerrard.
- Thanks to my friends for being so adventurous, and providing relief from my studies by exploring everywhere from Lands' End to the French Alps, Thanks to: Freddie Withers, Tom Bointon, Edward Halliday, Lucy Sainsbury, Ellis Woods, Lucy Halliday, Tom Bonning-Snook, Greg Simpson, Jim Hirst, Tom Bailey, Ben Goddard, Chris White, Nathan Shumoogum, and Jack Dyer to name but a few.
- Extended thanks to all of my family who have always been invaluablely supportive in many different ways throughout my studies to date.
- Finally, Many many thanks to my partner Laura Taylor for all her support throughout these past few years.

Publications:

- [1] **R. J. Allen**, O. Ghita, B. Farmer, M. Beard, and K. E. Evans, 'Mechanical testing and modelling of a vertically aligned carbon nanotube composite structure', *Compos. Sci. Technol.*, vol. 77, pp. 1–7, Mar. 2013.
- [2] **R. J. Allen**, O. R. Ghita, B. L. Farmer, M. A. Beard, and K. E. Evans, 'Wetting Mechanisms of Vertically Aligned Carbon Nanotube (VACNT) Composite Structures in readiness for Additive Layer Manufacture', *15th Eur. Conf. Compos. Mater. ECCM15*, June 2012
- [3] B. L. Farmer, **R. J. Allen**, O. R. Ghita, M. A. Beard, and K. E. Evans, 'Strategies to combine nanocomposite and additive layer manufacturing techniques to build materials and structures simultaneously', *15th Eur. Conf. Compos. Mater. ECCM15*, June 2012
- [4] B. L. Farmer, M. A. Beard, O. Ghita, **R. J. Allen**, and K. E. Evans, 'Assembly Strategies for Fully Aligned and Dispersed Morphology Controlled Carbon Nanotube Reinforced Composites Grown in Net-Shape', *MRS Online Proc. Libr.*, vol. 1304, 2011.

Investigations into the Potential of Constructing Aligned Carbon Nanotube Composite Materials through Additive Layer Manufacture

Abstract

Since their discovery Carbon Nanotubes (CNTs) have attracted much interest from many fields of the scientific community owing to their range of unique and impressive properties. Measurements of the mechanical properties of these nanoscale molecules have shown strengths up to five times greater than that of steel at only a quarter of the density. Consequently many have attempted to unlock these remarkable properties by creating nano-composite structures where CNTs effectively reinforce materials with little increase in density. Unfortunately the tendency of CNTs to form agglomerations when allowed to disperse in fluid suspensions has made this process non trivial, and led to difficulties in achieving effective reinforcement when simply mixing CNTs into a matrix material. As a result it has become clear that new approaches to composite construction will be required if effective composite reinforcement using CNTs is to be achieved.

Recent advances in CNT synthesis using Chemical Vapour Deposition (CVD) where tall forests of these nanoparticles are grown from the vapour phase have begun to solve the agglomeration problem. These forests are produced in aligned and dispersed arrays, and wetting of these structures with polymer matrices has demonstrated improvements in modulus of several hundred percent. These improvements arise as the CNTs retain both the dispersion and alignment of the forest when incorporated into the matrix thus overcoming the difficulties observed using traditional manufacture methods. New complications arise when attempting to extend these promising results to larger scale composite components owing to the typically millimetre size of CVD grown vertically aligned CNT (VACNT) forests. From these results it follows that to create large composite parts it will be required to incorporate many individually CVD grown VACNT forests into a single composite structure.

Strategies to achieve such a composite are being developed, with a range of ideas extending from knowledge gained from the emerging technology of additive manufacture (AM) described as ‘...the process of joining materials to make objects from 3D model data, usually layer upon layer....’. Indeed it is desirable to reinforce materials used in AM processes and the nano scale diameter of CNTs makes them the perfect choice owing to their high aspect ratios at the micron scale. In this thesis

investigations are conducted into the feasibility of manufacturing CNT composite structures using CVD grown forests and AM techniques. These investigations include measurement of the anisotropic mechanical properties of composite samples, and studies of the wetting interactions that occur between CNT forests and polymer materials. Composite samples are constructed and tested mechanically in the transverse orientation and results compared to traditional fibre composite reinforcement models in order to understand the material properties that can be expected if such an AM process is achieved. Results show greater mechanical improvements in transverse modulus than expected, and these results are attributed to the wavy nature of individual CNTs within forest structures providing multi directional reinforcement to the matrix material. Further studies are conducted to investigate the flow of molten thermoplastic materials into CNT forest structures under capillary driven flow. Thermoplastics were allowed to flow into VACNT forests before being cooled and inspected using micro x-ray computed topography (μ -CT) to gain an understanding of the wetting mechanism. Results from μ -CT scans show that the polymer flows into the structure in peaks of similar radius. Finally dynamic investigations were conducted into the fast capillary driven flow of a low viscosity thermoset resin into VACNT forests using a high speed camera. Results are fitted to traditional models for dynamic capillary driven flow in porous media and an effective radius and porosity is calculated for VACNT forests. Experimental values illustrate that these nanoscale structures still fit to traditional flow models of fluids where the height of capillary rise is proportional to the square of the elapsed time. These results provide a further step in understanding methods of incorporating many VACNT structures into polymeric matrices to achieve large scale effective polymer VACNT composite materials.

Contents

| | |
|---|-----------|
| Acknowledgements | 5 |
| Publications | 7 |
| Abstract | 9 |
| Contents | 11 |
| List of Figures | 15 |
| List of Tables | 22 |
| 1 Introduction, Motivation, and Outline | 23 |
| 1.1 Introduction | 23 |
| 1.2 Key Historical Events and Motivation | 25 |
| 1.3 Thesis Outline | 27 |
| 2 Introduction to Carbon Nanotube Science, Carbon Nanotube Composites and Polymer Composite Additive Manufacture Processes | 31 |
| 2.1 Introduction | 31 |
| 2.2 Carbon Nanotube Science | 31 |
| 2.2.1 Introduction | 31 |
| 2.2.2 Carbon Nanotube Science | 32 |
| 2.2.3 Mechanical Properties | 34 |
| 2.2.4 Thermal Properties | 36 |
| 2.2.5 Electrical Properties | 36 |
| 2.2.6 Characterisation of CNT | 38 |
| 2.2.7 Functionalisation of CNT | 39 |
| 2.3 Synthesis of CNTs | 40 |
| 2.3.1 Background | 40 |
| 2.3.2 Arc Discharge CNT Synthesis | 40 |
| 2.3.3 Laser Ablation CNT Synthesis | 42 |
| 2.3.4 Chemical Vapour Deposition CNT Synthesis | 43 |
| 2.3.5 Solar Energy CNT Synthesis | 47 |
| 2.3.6 Electrolysis CNT Synthesis | 48 |
| 2.3.7 Flame CNT Synthesis | 48 |
| 2.3.8 Bulk Polymer CNT Synthesis | 48 |
| 2.4 CNT Composites | 49 |
| 2.4.1 Background | 49 |
| 2.4.2 Dispersion of CNTs in a Matrix | 49 |
| 2.4.3 Polymer-CNT Composites | 51 |
| 2.4.4 Polymer Matrix-CNT Interactions | 56 |
| 2.4.5 Mechanical Testing of CNT-Polymer Composites | 57 |
| 2.5 Additive Manufacturing of Polymer Composite Materials | 58 |
| 2.5.1 Introduction to Additive Manufacturing | 58 |
| 2.5.2 Selective Laser Sintering | 59 |
| 2.5.3 Laser Engineered Net Shaping | 60 |
| 2.5.4 Three Dimensional Printing | 60 |

| | |
|---|------------|
| 2.5.5 Stereo Lithography | 61 |
| 2.5.6 Laminated Object Manufacture | 62 |
| 2.5.7 Fused Deposition Modelling | 62 |
| 2.5.8 Nanocomposites | 63 |
| 2.5.9 Conclusions | 64 |
| 2.6 Strategies to Assemble Carbon Nanotube Composite Structures with Controlled Morphology through Additive Manufacture Methodologies | 65 |
| 2.6.1 Introduction | 65 |
| 2.6.2 CNT composite Additive Manufacture Approaches | 68 |
| 2.6.2.1 Filled Polymer Sintering Approach. | 69 |
| 2.6.2.2 In-Situ CNT Introduction Approach | 71 |
| 2.6.2.2.1 In-Situ CNT Growth | 71 |
| 2.6.2.2.2 Detached Ex-Situ CNT Growth | 73 |
| 2.6.3 VACNT Forest Patterning and Net Shape | 82 |
| 2.6.4 Summary | 83 |
| 3 Synthesis of Vertically Aligned Carbon Nanotubes using the Sabretube Chemical Vapour Deposition System | 85 |
| 3.1 Introduction | 85 |
| 3.2 Production of Catalysts for use in ‘Sabretube’ CVD Processes | 86 |
| 3.3 CVD Growth of VACNT Structures using the Sabretube System | 89 |
| 3.3.1 The Sabretube Chemical Vapour Deposition System | 90 |
| 3.3.1.1 The Pre-Heater System | 90 |
| 3.3.1.2 CVD Chamber and Suspended Silicon Heating Platform. | 91 |
| 3.3.1.3 Mass Flow Controllers and LabView Software | 93 |
| 3.3.2 Typical VACNT Synthesis Process using the Sabretube | 94 |
| 3.3.3 Growth Mechanics of VACNT produced using CVD | 97 |
| 3.3.4 Examples of VACNT Forests Produced using the Sabretube System | 101 |
| 4 Fabrication, Modelling and Mechanical Analysis of a Vertically Aligned Carbon Nanotube Composite Structure | 113 |
| 4.1 Introduction | 113 |
| 4.2 Fabrication of Large Millimetre Scale VACNT Composite Structures for Mechanical Analysis. | 114 |
| 4.2.1 Fabrication Materials | 114 |
| 4.2.2 Resin Infiltration of VACNT Forests | 116 |
| 4.2.3 Curing of VACNT Composite Samples | 118 |
| 4.2.4 Machining of VACNT Composite Samples | 119 |
| 4.3 Mechanical Analysis of Large Millimetre Scale VACNT Composite Structures | 122 |
| 4.3.1 Dynamic Mechanical Thermal Analysis: Experimental Techniques | 122 |
| 4.3.2 Dynamic Mechanical Thermal Analysis: Results. | 123 |
| 4.3.3 Micro Tensile Testing: Experimental Techniques | 125 |
| 4.3.4 Micro Tensile Testing: Results | 126 |
| 4.3.5 Thermo Gravimetric Analysis: Experimental Techniques | 127 |
| 4.3.6 Thermo Gravimetric Analysis: Results | 128 |
| 4.4 Modelling of a VACNT Composite Material | 131 |
| 4.4.1 Modelling a VACNT Composite Material using Uniaxially Aligned Fibre Models | 131 |
| 4.4.2 Modelling a VACNT Composite Material with Wavy Fibre Models | 134 |
| 4.5 Discussions and Conclusions | 139 |

| | |
|--|------------|
| 5 Investigations into the wetting mechanisms of vertically aligned CNT structures | 143 |
| 5.1 Introduction | 143 |
| 5.2 Static Capillary Rise in VACNT Forest Structures | 144 |
| 5.3 Simple Dynamic Capillary Rise in Capillary Tubes | 154 |
| 5.4 Application of Simple Dynamic Capillary Rise to VACNT Structures | 156 |
| 5.5 Experimental Investigations into VACNT Forest Wetting Mechanisms | 158 |
| 5.6 Experimental investigations into VACNT forest wetting mechanisms with EVA 40wt% | 163 |
| 5.7 Experimental confirmation of early stage capillary rise in VACNT structures during capillary driven wetting using μ -CT analysis. | 171 |
| 5.8 Conclusions. | 174 |
| | |
| 6 Experimental Investigations and Modelling of Dynamic Capillary Driven Wetting in VACNT Forest Structures | 175 |
| 6.1 Introduction | 175 |
| 6.2 Experimental Investigations into Dynamic Capillary flows in VACNT Forest Structures | 176 |
| 6.2.1 Materials | 176 |
| 6.2.2 Measurement of the Fluid Surface Tension of the LY3505/XB3403 Resin system | 177 |
| 6.2.3 Details of the PHOTRON Fastcam XLR Hi-speed Camera System | 179 |
| 6.2.4 Monitoring of Dynamic Capillary Rise using the PHOTRON Fastcam XLR Hi-speed Camera System. | 180 |
| 6.3 Modelling of Dynamic Capillary Rise in VACNT Forest Structures | 184 |
| 6.3.1 Simple Capillary Rise Phenomenon in VACNT Forest Structures | 185 |
| 6.3.2 Modelling of Dynamic Capillary Rise in Porous Media and Structures. | 185 |
| 6.4 Analysis of Experimental Video Data | 187 |
| 6.5 Fitting Experimental Data to the Porous Lucas-Washburn Model | 190 |
| 6.6 Conclusions | 193 |
| | |
| 7 Conclusions | 197 |
| 7.1 Conclusions | 197 |
| 7.2 Key Questions and Further Work | 201 |
| 7.3 Feasibility of an industrial approach to multi layer VACNT composites through ALM | 202 |
| | |
| References | 205 |

List of Figures

| | | |
|------|--|----|
| 1.1 | Example of AM manufacturing technology, AM processes build parts from 3D model data in an additive fashion. A- 3D model Data, B- FDM printing of part, C- Finished component. | 23 |
| 2.1 | A comparison of C ₆₀ , Buckminsterfullerene, and a single-walled CNT | 32 |
| 2.2 | a) A diagram showing how the chiral vector of a zigzag and an armchair CNT lie on a single graphene layer. b) & c) Side profiles of a zigzag and armchair CNT respectively .. | 34 |
| 2.3 | a) An example of sp ³ hybridisation in a methane molecule, note the 3-D structure, and b) an example of 2-D sp ² bonding in an ethylene molecule | 35 |
| 2.4 | Examples of aligned CVD CNTs grown at The University of Exeter both images are of the same sample at different magnifications | 43 |
| 2.5 | Detail of the CVD ‘SabreTube’ equipment in use at The University of Exeter | 45 |
| 2.6 | CNT forests partially embedded in silicone layers, a) an SEM image where the layer marked ‘A’ is embedded and ‘B’ is free, and b) an optical image of the sample. Images taken from [156] | 55 |
| 2.7 | An example of AM in industrial use, note how the final part is constructed of several components as a result of a limit on build size in this process. (Images courtesy of EADS IW) | 59 |
| 2.8 | Examples of fibre orientations in fibre reinforced composites, A - Continuous Aligned, B - Discontinuous Aligned, C – Discontinuous Random, D – Woven | 67 |
| 2.9 | A simplified step by step schematic of the SLS strategy for CNT composite production, 1-Example CNT composite fibre and chopped CNT composite powder particles, 2- Examples of CNT-composite powder particles, 3-Aligned CNT composite powder particle distributed on an SLS build platform, 4-Bulk alignment of fluidised powder particles with an electromagnetic field, 5-Sintering of powder particle through heat, 6- Example of controlled fibre alignment in a bulk composite. Adapted from [195] | 70 |
| 2.10 | A simplified step by step schematic of the SLS strategy for in-situ CNT composite production, 1-General Schematic of the system, 2-A feed stock layer is deposited by the hopper and then laser sintered, 3-The printing head deposits a layer of catalytic particles, 4-Suitable Gases are introduced and PECVD VACNT growth occurs, 5- Another feedstock layer is deposited on top of the VACNTs, 6-The next layer is sintered leaving the VACNT partially embedded, 7-Another layer of catalytic particles is deposited, 8-PECVD VACNT growth, 9- Another feedstock layer is deposited, 10- Sintering of the next feedstock layer. Adapted from [199] | 72 |
| 2.11 | A simplified step by step schematic of the SL strategy for detached ex-situ CNT composite production, Adapted from [200] | 74 |
| 3.1 | Schematic of the suggested catalyst structure used in much of MIT’s work with the Sabretube system, not to scale | 87 |
| 3.2 | Images of the components of the Edwards electron beam evaporation system. A- Overview of the system, B-Detailed view of the evaporation table, C-Details of the electron gun and target crucibles, D-The retrofitted quartz crystal oscillator for the FTM-2400 system | 88 |

| | | |
|------|--|-----|
| 3.3 | Key components of the pre-heater system in disassembled form. Dirty pre-heater tubes can be cleaned by heating in a traditional furnace to 1050 °C and then rinsing with acetone once cooled. The heater coil is usually fixed in place using fire cement but this has been removed to expose the coil in this image | 90 |
| 3.4 | Simplified schematic of the suspended heater system and overall Sabretube system . . | 91 |
| 3.5 | Images of the suspended heater system and overall Sabretube system. The entire CVD furnace is located inside of a fume cupboard for health and safety reasons | 92 |
| 3.6 | A-Image of the MFCs the LCD display can be used to confirm the correct gas flows, this is particularly useful in the case that the gas bottles are running low, B-Screenshot of the LabView software with a typical VACNT ‘recipe’ programmed | 93 |
| 3.7 | Details of the suspended heater system showing the catalyst with mounted silicon cap ready for CVD VACNT synthesis | 95 |
| 3.8 | AFM scans of annealed catalyst samples. The scans were conducted in tapping mode and were conducted on the same catalyst sample. The data reveals the small catalytic islands that lead to VACNT growth | 98 |
| 3.9 | Schematic of tip growth CNT synthesis. 1-As produced catalyst, 2-Catalyst after annealing to form catalyst nanoparticles, 3-CNT growth is initiated, Carbon diffuses through the catalyst and the catalysts lifts off from the substrate, 4-Fully developed CNT growth. [98] | 99 |
| 3.10 | Schematic of base growth CNT synthesis. 1-As produced catalyst, 2-Catalyst after annealing to form catalyst nanoparticles, 3-CNT growth is initiated, Carbon diffuses through the catalyst but the catalyst remains substrate bound, 4-Fully developed CNT growth. [98] | 100 |
| 3.11 | SEM images of two forests structures grown from the catalyst that was supplied with the Sabretube system. Although the exact catalyst structure is unknown it is supposed to consist of 1.0 nm of Fe deposited on 10 nm Al ₂ O ₃ , the forests are short and do not reach the edge of the substrate likely due to an insufficient thickness of Fe. This occurs as with an insufficient thickness of Fe catalyst the formation of islands that initiate individual VACNT growth is hindered, resulting in an imperfect special density of such islands. Consequently early termination of CNT growth occurs | 102 |
| 3.12 | Examples of disordered CNT forest structures. Although the CNTs in these structures are over a 1 mm in height the areal density of the catalytic islands is too low resulting in a loss of self organisation of the VACNTs and consequent collapse of the aligned forest structure. It appears that small areas of the catalytic islands have formed resulting in pillars of different heights being produced across the catalyst substrates area. The structure of tall VACNT forests is self supporting hence these isolated pillars are prone to collapsing at such high aspect ratios | 103 |
| 3.13 | Top view of the right hand image in Figure 3.11 , and a zoomed in view of a split in a VACNT forest where the forest falls apart due to low catalyst density, losing its uniform structure. These images provide details of the collapsing VACNT structure, and show small bundles of VACNT bridging between the falling towers. It appears that the sections of VACNT are considerably more prone to collapse when the CSA of the pillars is smaller, resulting in many small pillars that appear fully collapsed at short heights compared to those with larger CSAs | 104 |
| 3.14 | SEM images of a well aligned and uniform VACNT forest of 1 mm in height. This forest was produced using the catalyst developed specifically for this work and consisting of 1.5 nm of Fe deposited onto 30 nm of Al ₂ O ₃ as discussed previously. These forests illustrate the desired choice of forest structure for producing composite materials using CNT and are representative of the forests used throughout this Thesis. | 105 |

| | | |
|------|--|-----|
| 3.15 | Higher magnification SEM images of a well aligned VACNT forest structure, at high magnification individual bundles of VACNT are apparent and appear to be wavy and less well organised; this effect is discussed further in Chapter 4 . Although it appears that individual fibres are clear under SEM analysis these fibres actually represent small bundles of many VACNT in the left hand image. On the right hand side individual wavy VACNT are just resolvable. | 106 |
| 3.16 | Further High magnification images of VACNT structures, the right hand image reveals the entangled individual CNTs that exist within an individual CNT bundle that appears highly organised at lower magnifications. These images show how the CNTs are self supporting and require a significant areal density to achieve uniform high aspect ratio growth | 107 |
| 3.17 | Images of the same large VACNT forest, the CNTs located at the edges of the forest have peeled away on this sample, these excess CNTs can be removed through careful use of a razor blade if required. It is believed that this effect occur when forests begin to reach heights that are greater than 1mm as the edges of the forest are no longer sufficiently self supported by the overall structure. Small strings of VACNT are visible that bridge the gap between the main forest and peeled edge and indicate an approximate height of growth at which the peeling initiated. | 108 |
| 3.18 | Defects in the top surface of a VACNT forest marked with white squares, left hand side is a small hole likely caused by a dust particle, and right a small CNT pillar protrudes from the surface, the cause of which is unknown, the right hand image shows the detail of this pillar at higher magnification. It appears that the VACNT in this region have experienced an extended growth lifetime compared to the surrounding forest. This could result from a small contamination of the catalyst, for instance the presence of water has recently been shown to enhance CVD growth lifetimes [108]. . . | 109 |
| 3.19 | The left image is a high magnification image of the defect caused by a dust particle present during CNT growth, and right hand shows the detail of the CNT that can fall away at the edges of particularly large forest structures. It provides a detailed image of the bridging CNTs that provide evidence that initially the forest grew as a fully aligned structure, however at a certain height the edges fall away. Edge defects can be removed using a razor blade and are not observed in shorter CVD grown forests . . . | 110 |
| 3.20 | Optical microscope images of large VACNT forests, VACNT are known to be highly effective at absorbing optical radiation and consequently observing their structure using optical microscopy is particularly difficult although it is possible to gain an idea of the overall forest size [212] | 111 |
| 4.1 | Examples of Long Sabretube Grown VACNT forests used for composite coupon production. A-Optical Image of a large VACNT forest, this particularly forest reaches several millimetres in height. B-A composite SEM image, constructed of two separate SEM images, which details the side of a large area VACNT forest. It is possible to see how the edges of the forest appear to have separated which is often the case when forests reach heights of greater than 2mm | 115 |
| 4.2 | An image of the aluminium cast and silicone mould used for VACNT composite fabrication. In the fore ground of the image are two examples of neat resin samples before being machined for testing. The square shaped cut outs were included for testing purposes and are not used to produce the samples tested later in this chapter . | 117 |
| 4.3 | A schematic of the resin mould illustrating how the VACNT forest was infiltrated using the mixed resin | 118 |

| | | |
|------|--|-----|
| 4.4 | A schematic of the cured composite when removed from the silicone mould. The blue dashed line is indicative of where approximately where Neat Resin samples are machined from and the red dashed line indicates where VACNT samples are machined from | 119 |
| 4.5 | An Optical image of VACNT composite and Neat Resin samples that have been freshly machined for DMTA testing. Note how the VACNT composite (left hand side) appears almost completely black despite only containing a relatively low volume fraction (~2 vol%) of VACNT reinforcements | 120 |
| 4.6 | A photos of the low speed saw. The saw is fitted with a micrometer to position the blade in the desired location. To ensure clean and uniform cuts the saw is also fitted with a counterbalance system which allows the user to control the force applied to the saw blade during cutting | 121 |
| 4.7 | A photo of micro tensile test coupons that have been machined ready for testing. A penny is included to illustrate the size of these samples; again the VACNT composite sample appears black and is on the right hand side | 121 |
| 4.8 | Photos of the Mettler Toledo DMA861e the left hand image is the full machine with the furnace open revealing the clamps, and the right hand image details the clamping system. The thermocouple used to measure sample temperatures during experiment is visible in the right hand image | 122 |
| 4.9 | A schematic illustrating a close up view of how a sample is clamped during single cantilever DMTA testing. The schematic indicates the CNT alignment axis, the direction of the applied load, and the transverse direction in which the samples storage modulus is being measured | 123 |
| 4.10 | Plot of Storage Modulus against Sample Temperature for the first batch of VACNT composite samples | 124 |
| 4.11 | Plot of Storage Modulus against Sample Temperature for the second batch of VACNT composite samples | 124 |
| 4.12 | Plot of Storage Modulus against Sample Temperature for the third batch of VACNT composite samples | 125 |
| 4.13 | The Deben micro tensile test stage used in micro tensile testing experiments, for clarity it has been removed from the microscope assembly | 126 |
| 4.14 | An example of stress strain plots for a VACNT composite coupon and a Neat resin coupon. The plots illustrate how tensile modulus and breaking strain were calculated from the data | 127 |
| 4.15 | The Netzch TGA used to conduct TGA experiments under Nitrogen flow | 128 |
| 4.16 | Examples of TGA plots that were used in the calculation of VACNT volume fractions in VACNT composite samples. The first graph illustrates that VACNTs are unaffected by the TGA process and the second details the difference between VACNT composite and neat resin samples observed at elevated temperatures | 130 |
| 4.17 | Example Schematic of a continuous uniaxially aligned fibre composite material. Although this is a 2D schematic the transverse direction is isotropic throughout the plane and the schematic can be thought of as a cross section of the material | 131 |
| 4.18 | SEM images of the same VACNT forest at different magnifications, at low resolution the CNTs appear very straight but at higher magnifications the wavy structure becomes significant | 133 |
| 4.19 | Schematic of the wavy composite structure illustrating how waviness is calculated from an assumed sinusoidal form of the CNT reinforcements. | 135 |
| 4.20 | SEM images of the VACNT composite sample fracture surfaces at different magnifications. The axial direction is marked and fibre alignment appears visible | 136 |
| 4.21 | High magnification SEM image of an as grown VACNT forest structure indicating how the average VACNT waviness was calculated | 137 |

| | | |
|------|---|-----|
| 4.22 | Plot of the curved Rule of mixtures model for both Transverse and Axial directions as a function of fibre waviness. The line along the y axis indicates uniaxial straight fibre reinforcement. The plot indicates that extremely wavy fibres will provide greater reinforcement in the Transverse orientation than the axial | 138 |
| 4.23 | Detailed plot of the wavy model with experimental data included from this work for Transverse Modulus and literature values for Axial modulus from Beard et al.'s [215] work | 138 |
| 4.24 | A detailed plot of the transverse moduli for VACNT composite samples against VACNT waviness including calculated theoretical values and both experimentally measured values. The measured value of VACNT waviness is also plotted with upper and lower bounds based on the standard deviation of measured VACNTs. This plot is a zoomed region of Figure 4.23 | 140 |
| | | |
| 5.1 | A simple schematic detailing the calculation of contact angle at a three phase interface | 145 |
| 5.2 | Examples of capillary rise, A, where the contact angle is between 0° and 90°, and B, where the value of the contact angle is between 90° and 180° resulting in a negative capillary rise | 146 |
| 5.3 | A -An example of a rectangular array of solid cylinders in a matrix with unit cell marked in red, and B a unit cell close up with parameters 'r' and 'd' defined | 147 |
| 5.4 | Plot detailing how VACNT Radius affects Equilibrium Capillary Rise for parameters from Table 5.1 | 149 |
| 5.5 | Plot detailing how VACNT spacing affects Equilibrium Capillary Rise for parameters from Table 5.1 | 150 |
| 5.6 | Plot detailing how Surface Tension affects Equilibrium Capillary Rise for parameters from Table 5.1 | 151 |
| 5.7 | Plot detailing how Contact Angle affects Equilibrium Capillary Rise for parameters from Table 5.1 | 151 |
| 5.8 | Plot detailing how Fluid Density affects Equilibrium Capillary Rise for parameters from Table 5.1 | 152 |
| 5.9 | A comparison detailing how the various parameters affect equilibrium capillary rise, the point where the lines cross illustrates the value achieved from using the parameters detailed in Table 5.1 , ~15 m. | 153 |
| 5.10 | A plot of the dynamic capillary rise models for water in a glass capillary of radius 100µm illustrating the implicit model as well as the two asymptotic solutions and also illustrating where each approximation is most accurate. | 156 |
| 5.11 | Example plots of the Lucas-Washburn/Washburn implicit models using parameters of mixed LY3505 resin and different values of the capillary radius. | 157 |
| 5.12 | Dipping rig for the partial embedment of VACNT forest structures. The heated stage is accurately controlled using an electronic PID controller and is heated using two cartridge heaters embedded in the stage. | 159 |
| 5.13 | Simplified schematic of the partially embedded VACNT production mechanism using the custom rig imaged in Figure 5.12 | 160 |
| 5.14 | SEM images of the interaction between the LDPE and VACNT forest at the interface region. | 161 |
| 5.15 | DSC traces for the three polymers tested. | 162 |
| 5.16 | Complex viscosity plotted against temperature for the three polymers. | 163 |

| | | |
|------|---|-----|
| 5.17 | A comparison between SEM and μ -CT images for the same area of Sample 1. In B distinguishing features have been marked, the polymer appears to flow in a peaked fashion over the majority of the forest but also appears to fill minor forest defects that likely form during CVD production. | 164 |
| 5.18 | A comparison between SEM and μ -CT images for a different area of Sample 1. A large circular defect is present that appears to have channelled polymer flow in the forests interior although this is not clear at the surface of the forest as seen under SEM. Again the majority of the forest appears to channel polymer flow in peaks | 165 |
| 5.19 | A Comparison of images from the corner of Sample 2, from this perspective it is observed that as well as flowing inside the interior the polymer also rides up the exterior of the forest slightly. | 166 |
| 5.20 | A Zoomed image of Sample 2 detailing the peaked structure apparent in the forests interior, the marked yellow line indicates the polymer CNT interface visible under SEM. It appears that the CNT extend to a greater height than the peaks of polymer visible in the CT scan. It is also of interest to note that the surface of the VACNT forest structure remains relatively smooth under SEM imaging. | 167 |
| 5.21 | A-C , Comparisons of SEM and μ -CT images of sample 3. This sample had a circular portion of the forest missing in the centre owing to the presence of a dust particle during CVD growth of the forest. The presence of which allows an estimation of the height of the rise of the polymer in the forests interior. The final image D illustrates that the peaks appear fairly uniform in the uniform defect free regions of the wetted VACNT structure. | 167 |
| 5.22 | Illustration of average peak diameter approximation using the VGstudio software environment the left hand images are indicative of individual xray scans used in the construction of the 3D model. Estimations of peak diameter were calculated at approximately half the total height of the peak. | 170 |
| 5.23 | Plot of the Lucas Washburn prediction of the evolution of capillary rise in a VACNT structure with an approximate capillary radius of 120 μ m, from μ -CT measurements, using the same parameters as in Figure 5.11. | 171 |
| 5.24 | Simplified schematic of the modified partially embedded VACNT production mechanism using the custom rig imaged in Figure 5.12. | 172 |
| 5.25 | SEM and μ -CT analysis results of using the modified sample production technique detailed in Figure 6.24 to wet VACNT forest structures. | 173 |
| | | |
| 6.1 | Computer analysis of a pendant drop taken from a still from video data collected using the Photron XLR camera for the measurement of fluid surface tension. The measurement of the values of d_e and d_s are shown. | 177 |
| 6.2 | The PHOTRON Fastcam XLR installed at Exeter. | 180 |
| 6.3 | A simplified schematic of the hydraulic syringe system used to control z-axis displacement of the VACNT forest (not to scale), note how large displacements on the smaller volume syringe correspond too much smaller displacements of the larger volume syringe. | 181 |
| 6.4 | Example of a VACNT forest mounted and ready to be <i>dipped</i> into the resin bath, the camera has been focused onto the silicon growth substrate. | 182 |
| 6.5 | Overall schematic of the Camera and VACNT <i>dipping</i> experimental arrangement, B -Zoomed detail of the resin bath and VACNT forest mounting arrangement, Note that neither schematic is to scale. | 184 |
| 6.6 | A Simple schematic of a typical camera still frame, the dashed red boxes indicate cropped sections of the images that were zoomed and used for repeat readings of the total wetting time for each sample. | 188 |

| | | |
|------|--|-----|
| 6.7 | Example frame images detailing the various stages of dynamic capillary rise for a single VACNT forest sample undergoing the dipping procedure. Example time scales are provided below each individual frame to provide an indication of the length of the process. | 189 |
| 6.8 | Plot of experimental data for total wetting times fitted to a porous model for dynamic capillary rise of neat LY3505 resin in a VACNT forest structure. | 191 |
| 6.9 | Plot of experimental data for total wetting times fitted to a porous model for dynamic capillary rise of mixed LY3505 resin in a VACNT forest structure. | 192 |
| 6.10 | Plot of experimental data for total wetting times fitted to a porous model for dynamic capillary rise of both neat LY3505 and mixed LY3505 resin in a VACNT forest structure. | 193 |
| | | |
| 7.1 | Simplified schematic of the current theoretical reinforcing mechanism in a multilayer composite an increase in modulus of approximately 20 % in the transverse orientation and 120 % in the axial direction can be expected with only a 2 vol% loading of VACNTs, not to scale. | 199 |
| 7.2 | Implications of the peaked flow regime on a multilayer composite constructed through the capillary driven wetting of multiple VACNT forests. It is likely that such peaks will improve interlayer bonding through the increased contact area between layers. | 200 |

List of Tables

| | | |
|-----|--|-----|
| 2.1 | A Table summarising the advantages and disadvantages of the three most common methods of CNT synthesis. | 47 |
| 3.1 | Schematic of a typical VACNT growth procedure conducted at The University of Exeter using the Sabretube system. In the images the VACNT forest reaches several millimetres in height. | 95 |
| 4.1 | Values of variables used in calculating Reuss and Voigt predicted moduli for a VACNT composite. | 132 |
| 4.2 | A comparison of Rule of Mixtures predictions for straight and curved fibre reinforcement and experimental Data for improvement for Axial and Transverse Moduli. Transverse experimental data has been measured during this work and Axial by Beard et al [215] | 139 |
| 5.1 | Parameters used in the calculation of equilibrium capillary rise for materials in use in Chapter 4. | 148 |
| 6.1 | Experimental values of surface tension measured using the pendant drop method. | 179 |
| 6.2 | Experimental values for total wetting time and VACNT forest height for both Neat LY3505 and LY3505/XB3403 mixture experiments, Viscosity values from the manufacturer's datasheet are also included | 189 |

Chapter 1

Introduction, Motivation and Outline

1.1 Introduction

The development of innovative manufacturing techniques packaged as Additive Manufacturing (AM) methods has provided engineers and scientists with the means to construct novel architectures using a bottom up approach in contrast to traditional subtractive top down methods. These processes are broadly defined through an ASTM standard as a ‘process of joining materials to make objects from 3D model data, usually layer upon layer, as opposed to subtractive manufacturing methodologies, such as traditional machining’. Currently AM technologies are frequently used as a tool for the rapid manufacture of components from a vast range of materials, including but not limited to, photopolymer resins, metals, ceramics, and thermoplastics [1]. **Figure 1.1** demonstrates an example of a simple AM process known as fused deposition modelling (FDM) [2]. This process is one of the simplest AM methods in use and builds components from extruded tracks of material, in this case a thermoplastic.

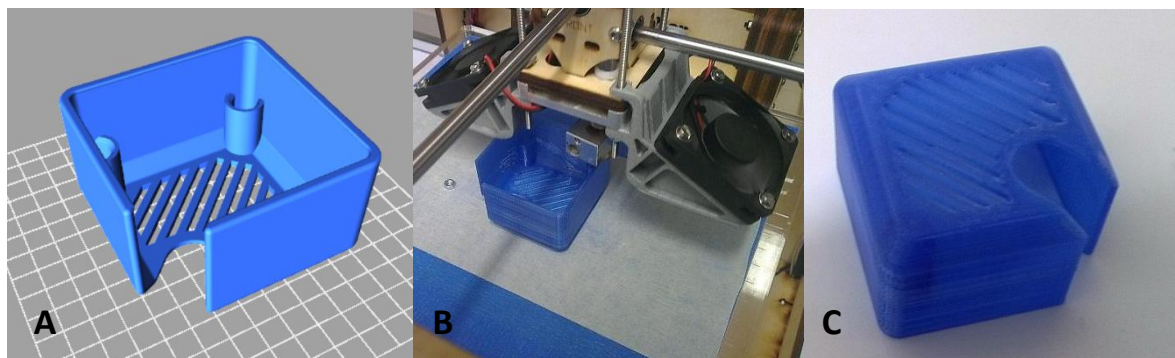


Figure 1.1: Example of AM manufacturing technology, AM processes build parts from 3D model data in an additive fashion. **A-** 3D model Data, **B-** FDM printing of part, **C-** Finished component

Despite great improvements in the performance of components produced using AM techniques over the past twenty years there is still significant desire within the field to match or better material properties when compared to those produced using traditional methods of manufacture [3]. More recently comparable mechanical properties have been observed particularly in metallic AM methods, for example in the Electron Beam Melting of Titanium powders to form solid components. Indeed the EBM melting of Titanium components provides an excellent example of the potential of

AM manufacturing for use as a tool in high value manufacturing such as the aerospace industry where such technologies are blossoming. Although success has been achieved in the AM of metals, polymer processes are lagging behind and the mechanical properties of components produced in such a fashion often fall considerably short of those produced traditionally using methods such as injection moulding. In a bid to improve polymer AM methods much research is underway to incorporate polymer composite materials into AM feed stocks using various approaches which are usually specific to the precise AM technique employed. The development of traditional polymer composites has illustrated the potential of these light weight high performance materials to find a wide range of applications from consumer products to aerospace components. It is hoped that the use of polymer composites in AM will enhance the properties of current polymer feed stocks, mechanically or otherwise, and current research is already beginning to illustrate the potential of multi material AM for a vast range of applications [4].

In composite science literature both experimental and theoretical works combined have illustrated that precise microstructure of a composite is critical in achieving the desired performance from components constructed from composite materials [5]. For example in fibre based composites the precise orientation and dispersion of reinforcing fibres in a polymer matrix are critical in achieving high performance. Consequently the marriage of AM methodologies and composite materials has great potential to allow precise control of a components microstructure by using 3D model data to define the location and even orientation of filler components throughout the interior of a complex structure. In doing so it will be possible to build both components and materials simultaneously thus providing the potential to construct highly specific parts for unique applications. Furthermore, producing components in such a fashion also holds potential for realising graded multi-functional materials where a filler component can be added to a feedstock material in varying volume fractions thus modifying the material properties of a structure throughout its volume providing additional functionality. For example the addition of conductive components could create built in circuits or sensors where the flow of electrical current can be controlled by a conductive network which exists throughout the interior of a 3D structure [6]. When considering the mechanical reinforcement of a polymer matrix the optimum choice of filler material is often considered to be a form of high modulus fibre. Fibres are high aspect ratio structures which allow a strong interaction between their surface and the polymer matrix whilst retaining the ability to transfer load across the material through their elongated form. Indeed the uniform distribution of such fibres in polymeric matrices has already shown highly effective reinforcement and such materials are frequently in use in a wide range of current applications.

In tandem to the properties of its components the final properties of composite materials are also highly dependent on the distribution and orientation of the composite structure as mentioned previously. This is particularly true when considering fibrous materials that can often be considered as a 1 dimensional reinforcement where significant enhancement of the composite structures mechanical properties are only observed in the axial direction of an individual fibre. As a consequence various techniques are currently utilised to precisely control the orientation and distribution of fibres in composite materials. For example, in Carbon Fibre panels long pre-woven (or even unidirectional) fibres are often employed which can be impregnated with thermoset resins to form components with excellent in-plane properties but poor out of plane properties. Another example is the use of advanced mixing techniques such as ultrasonication to create uniform distributions of solid components within a fluid matrix prior to curing. Although numerous techniques for controlling microstructure exist so far no technique truly offers precise microstructure control of fibre orientation throughout a component as maybe possible through the use of AM methods.

This work seeks to investigate the potential of using the recently discovered nanoscale fibres termed Carbon Nanotubes (CNTs) to reinforce a polymer matrix in a controlled fashion using an AM process.

CNTs are now well known for boasting superior mechanical properties when compared to most, if not all, current fibre reinforcements [7]. Consequently significant research has been conducted in a bid to realise the remarkable properties of these materials observed at the nanoscale into macroscale components through their incorporation in composite materials. Despite almost twenty years of intensive research the effective reinforcement of polymers on a macroscale using CNTs has remained for the most part an elusive target. The problems in realising effective reinforcement using CNTs can in large be attributed to the unavoidable difficulties involved in achieving a high volume fraction and uniform dispersion of these nanoscale particles in a matrix material [8]. As a consequence it is hoped that the development of a CNT reinforced AM process will assist in furthering both the fields of composite materials for AM, and also the general development of CNT composite materials simultaneously by allowing precise orientation and distribution of these nanoscale particles throughout the microscale layers that exist in many AM manufacturing techniques.

1.2 Key Historical Events and Motivation

This work has been for the most part motivated by two high profile research fields that have emerged in the last thirty years. The first of these fields was born from the first recognised discovery

of CNTs in 1991 by Sumio Iijima whilst working at the NEC Research Facility in Japan. Iijima's original paper entitled 'Helical microtubules of graphitic carbon' has now received over 29000 individual cites, and many more papers in the field exist that do not cite his work. Despite the response that Iijima's paper generated some evidence exists for the discovery of CNTs prior to the publication of Iijima's work. Indeed CNTs may have inadvertently been synthesised previously by several groups, for example by Davis et al. who identified 10nm diameter carbon filaments with catalytic Iron particles embedded in the structures tip that were most likely Multi Walled CNTs (MWCNTs) [9]. However the defining feature of Iijima's work is the precise identification of the graphitic structure of CNTs through the use of electron microscopy thus confirming CNTs as new allotropes of Carbon and consequently sparking a significant research effort.

The second source of motivation for this work stems from the recently developed set of engineering tools now commonly referred to as 3D printing or Additive Manufacturing. Investigations into AM methods were first envisaged shortly after the development of commercially available 2D printers. Initial developments took two significant routes lead by Charles Hull and Scott Crump who are now the founders of 3D systems and Stratysys respectively. Although manufacturing in an additive fashion has been conducted extensively, for example welding maybe considered an additive method, it is the development of advanced computer control systems leading to the automation of the process that defines AM as a unique technology. The development of the hardware and software required for 2D printers is not extensively different from that in use by modern 3D printers and is sufficient to provide precise resolution on the micron scale. The following chronological list illustrates key historical events that have provided motivation for the undertaking of this work:

- **1953** - W. R. Davis et al. publish their paper entitled 'An unusual form of Carbon'. They report the growth of carbon filaments from iron oxide contained in brick samples when exposed to a Carbon Monoxide atmosphere at temperatures of the order of 450 °C. [9]
- **1985** – H. Kroto et al. publish their work describing the synthesis of a new carbon allotrope. The molecules consist of a cage of 60 Carbon atoms and are called 'buckminsterfullerene' after Buckminster Fuller who designed geometrically intricate domes with near identical structure. [10]
- **1986** - Charles Hull patents a new manufacturing process which will become the Stereo Lithography AM process, he goes on to develop his techniques and found 3D systems. [11]
- **1988** – Scott Crump develops a Fused Deposition Modelling process as a new method of Additive Manufacture. He founds Stratysys and begins development of a commercial system. [2]

- **1991** – S. Iijima synthesises Multi Walled Carbon Nanotubes (MWCNT) in arc discharge deposited in a similar experimental method to that used in the production of C₆₀ by Kroto et al. This publication creates a boom in CNT based research. [12]
- **1996** – First release of commercial 3D printer products by zcorp, Stratysys, and 3D systems.
- **2000** – M-F. Yu et al. measure the Young's Modulus of an individual MWCNT by fixing it between two Atomic Force Microscope tips. They report values as high as 63 GPa providing significant experimental evidence of the high strength of CNTs. [7]
- **2000s** – Development of Windform XT, the first commercially available short carbon fibre reinforced AM feedstock material. [13]
- **2004** – Li et al. Report the first spinning of CNT yarns directly from a Chemical Vapour Deposition furnace. These yarns offer great potential for use in composite materials. [14]
- **2005** – Open source RepRap project founded by Adrian Bowyer. The project aims to produce a printer that can replicate itself and sparks the development of many low cost FDM projects. [15]
- **2008** – Wardle et al. report the first highly effective reinforcement of a high performance resin using CNTs. They incorporate a high volume fraction vertically aligned CNT forest into a low viscosity thermoset material. [16]
- **2012** – S. J. Leigh et al. develop a conductive feedstock for FDM. The material, entitled 'Carbomorph', consists of a thermoplastic matrix containing Carbon Black particles. It can be used to print structures with in-built sensors. [6]
- **2013** – Many commercially available products exist which contain CNTs. These range from high performance composites such as those used in boat hulls or sports equipment, to transparent conductor for use in electronics. [17]

The above list is not an extensive list of historical events concerning AM and CNT composite research, but is intended to highlight key factors that are explicitly relevant in the scope of this thesis. This work aims to expand on knowledge gained from prior research outlined above to ascertain the feasibility of introducing CNT reinforcements to an AM process in a controlled fashion.

1.3 Thesis Outline

This project began from a desire to improve current AM processes with polymeric materials by introducing a controlled reinforcement to the structure. CNTs provide an ideal candidate for this reinforcing filler as they can exhibit high aspect ratios without exceeding the AM processes z-axis resolution. Furthermore CNTs have excellent mechanical properties thus indicating the potential for significant mechanical reinforcement even at low volume fractions. In investigating the potential of

this novel method for constructing nanocomposite materials through AM, significant investigations into the interactions of vertically aligned arrays, or forests, of CNTs and fluid polymers have been undertaken. Additionally mechanical investigations of large single layer VACNT composite samples have been undertaken and comparisons between experiment results and theoretical models been sought. These results have revealed how the alignment of the reinforcing CNT at the composites microstructure combined with the nanostructure of the individual CNTs can greatly influence the degree of reinforcement achieved in the material. The following chapters detail the findings of investigations conducted to assess the feasibility of building net shape Nanocomposite components using additive manufacture:

Chapter 2 provides a brief review of the relevant literature in the fields of Carbon Nanotube Science, the current state of the art research in CNT based composite materials, and also that of the use of polymer composite materials in additive manufacture to date. It also details an in-depth discussion of the various strategies that have been identified in order to incorporate CNTs to a current AM process. Although many other possibilities exist these ideas were identified as possibilities based on the current state of research across the fields. Three ideas are presented including the inclusion of CNTs in both a selective laser sintering (SLS) process and a stereolithography (SLA) process as interlayer reinforcements.

Chapter 3 presents the experimental methods used throughout the studies detailed in this work. In particular it provides details of the methods used for producing the large scale CVD grown vertically aligned CNT forests that are used in the later chapters of this thesis. It includes methods used for catalyst production as well as the CVD recipes used to grow the VACNT forests. Example scanning electron micrographs of some CVD grown forests are also presented.

Chapter 4 presents experimental works to examine the influence of the precise micro structure of the individual CNTs contained within a VACNT array on its potential to reinforce a thermoset resin. Single layer VACNT resin composite samples are produced which are large enough to be tested using Dynamic Mechanical Thermal Analysis (DMTA) and micro tensile testing. Experimental results are compared to a wavy VACNT reinforcement model and good agreement between the two is observed.

Chapter 5 details investigations conducted into the interactions that occur between VACNT forests and molten thermoplastic polymers. VACNTs are brought into contact with molten polymers in an attempt to achieve partially wetted forests by solidifying the thermoplastic through cooling after contact with the forest. Successfully embedded samples are analysed using scanning electron

microscopy and x ray micro computed tomography. Results indicate complex flow patterns occurring in the interior of the forest structure.

Chapter 6 describes experimental investigations into the dynamic capillary driven wetting of VACNT forests with a low viscosity thermoset resin. Forests are precisely dipped using a custom rig and the wetting process is carefully monitored using a high speed camera fitted with a monozoom lens. Video data is then analysed frame by frame to provide an estimation of the total time to required to fully wet a VACNT forest of a given height under capillary driven flow. Experiments are conducted for VACNT forests of various heights and then fitted to a modified Lucas-Washburn model demonstrating that the capillary flow is in the early stages of the dynamic process and providing a means to predict the evolution of the capillary driven flow.

Chapter 7 summarises the significance of the results found in the course of this work and places them within the context of their implications in the feasibility of producing a CNT reinforced AM process. Furthermore suggestions are made as to how further work could be conducted in order to continue investigating the challenges that must be overcome in order to achieve such a process.

Chapter 2

Introduction to Carbon Nanotube Science, Carbon Nanotube Composites and Polymer Composite Additive Manufacture Processes

2.1 Introduction

This section details a review of the state of the art research in the relevant fields. It contains details of the remarkable properties of CNTs, methods of CNT synthesis, current CNT composite progress, as well as the current progress in composite materials for AM.

2.2 Carbon Nanotube Science

2.2.1 Introduction

The first recognized discovery of Carbon Nanotubes (CNTs), graphitic tubes of a single carbon layer, is often credited to the work of Iijima [12], who in 1991 published the first details of this new allotrope of carbon. This discovery was made soon after the published work of Kroto et al. [10] showed the existence of buckminsterfullerene in 1985, see **Figure 2.1**, as another distinct allotrope of carbon besides graphite, diamond and amorphous structures. Buckminsterfullerene is often described as a closed cage of 60 carbon atoms with a similar structure to a football, where six hexagons surround a pentagon causing the curvature of the molecule's surface. It is these pentagons that cause the structure to differ from that of graphene, a single layer of graphite, and form a closed structure. The name of the allotrope buckminsterfullerene is a tribute to the late 'Richard Buckminster Fuller' who was known for his geodesic dome designs that resembled fullerene-like structures. Indeed it was whilst experimenting with the production method for fullerenes that Iijima's discovery came about, and fullerenes were also produced in the very same experiment. Although the paper showed accurate imaging of CNT structure, some authors [18] believe that evidence for the existence of CNTs was shown and also published [9], [19] prior to Iijima's work, even as early as 1953.

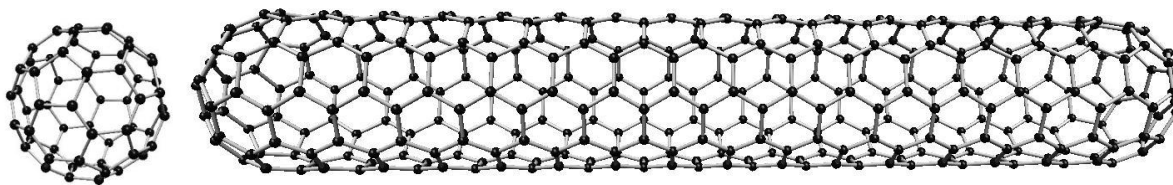


Figure 2.1: A comparison of C₆₀, Buckminsterfullerene, and a single-walled CNT.

Despite this it is important to remember that these carbonaceous structures only showed similar physical properties to CNTs and their structure was not well understood or characterised in sufficient detail when compared to the specific characterisation contained in Iijima's work. There is also evidence of theoretical predictions of the existence of CNTs before their discovery as shown by Fowler [20] who saw possibilities of these graphitic structures. As well as these early examples of possible CNT existence it is more than likely that Iijima himself came remarkably close to finding these remarkable nanostructures but failed to notice their importance at the time [21].

Since the publication of CNT existence in 1991, a flurry of research was initiated to better characterize and understand the properties and structure of CNTs. In fact CNT discovery has led to an entirely new field of research based almost solely around the remarkable features of these nanoparticles and their endless possible applications. These properties include impressive mechanical, electrical and thermal properties which will be discussed in due course. This review aims to provide an assessment of the current state of published research in taking the exciting nanoscale properties of CNTs and incorporating them into a polymer, or other matrix, in order to exploit these advantages on a millimetre scale and above. This will involve assessing the known properties of individual CNTs as well as looking into synthesis techniques along with characterization methods. It is only by gaining a clear understanding of these areas that one can hope to fully understand the possible benefits of producing CNT composites and any applications that these materials may fulfil.

2.2.2 Carbon Nanotube Structure

In general CNTs fall into two main structural groups, Multi Walled CNTs (MWCNTs), and Single Walled CNTs (SWCNTs). The first tubes synthesised by Iijima [12] were reported to be MWCNTs which were identified using high resolution transmission electron microscopy and typically had between two and fifty walls creating a concentric tube structure. Iijima also reported an inter wall distance in these tubes of ≈ 0.34 nm which is similar to the inter-layer separation in bulk graphite.

MWCNTs with two walls are sometimes referred to as Double Walled CNTs (DWCNTs), and some [22] believe them to be of particular interest as they are the bridge between SWCNTs and MWCNTs and consequently possess properties of both types of CNT. In 2003 Flahaut et al. reported a specific method for the production of samples containing 77% DWCNTs which may be of importance in future CNT research [22]. Flahaut suggested that the structure of DWCNTs would allow functionalisation of the outer tube whilst maintaining the graphitic properties of the inner tube. The first synthesis of SWCNTs was reported in 1993, soon after the first discovery of MWCNTs, by two groups independently [23], [24]. It is said that SWCNTs can be referred to as ‘ideal’ CNTs as they are reported to have few defects in their graphitic structure and are of small diameter, typically of the order of a few nanometres, leading to suggestions that they may behave as ‘Quantum wires’ [25]. Overall it is clear that both types of CNTs may be able to lend themselves to some highly unique applications and as a result it is well recognised that the purification of different types of tubes will be an important achievement. Although purification remains challenging, modern techniques of production have shown potential for the production of nanotubes of specific dimensions in larger quantities and improved purities [22], [26], [27], and will be discussed later.

Another important structural feature of CNTs is the chirality which arises from their hexagonal lattice structure. Considering nanotubes as a rolled up sheet of graphite, it is clear that the helical structure of the tube can vary considerably as noticed by Iijima [12]. The helical nature of nanotubes was confirmed in 1993 by Ge and Sattler who probed individual nanotubes using a scanning tunnelling microscope [28]. The helical nature of an individual CNT is described using the unit vectors of the two-dimensional lattice in a standard geometric format originally defined by Hamada et al. [29] as shown in **Figure 2.2**. The helicity of a CNT is then defined using these unit vectors to describe a chiral vector defined below [30],

$$\mathbf{C}_h = n\mathbf{a} + m\mathbf{b}$$

where \mathbf{C}_h is the chiral vector, \mathbf{a} and \mathbf{b} are the unit vectors, and n and m are integer values ($0 \leq |m| \leq n$) defining the specific CNT. The chiral vector is always orthogonal to the axis of the tube and effectively corresponds to the circumference of the tube, meaning that in rolled form the ends of the vector will meet, see **Figure 2.2**. This means the diameter of a CNT, d_{CNT} , can be calculated as follows [30],

$$d_{CNT} = \mathbf{C}_h / \pi = \frac{a_{C-C}\sqrt{3}}{\pi} \sqrt{n^2 + m^2 + nm}$$

where the value of a_{C-C} is about 0.142 nm and is the nearest neighbour distance in graphite.

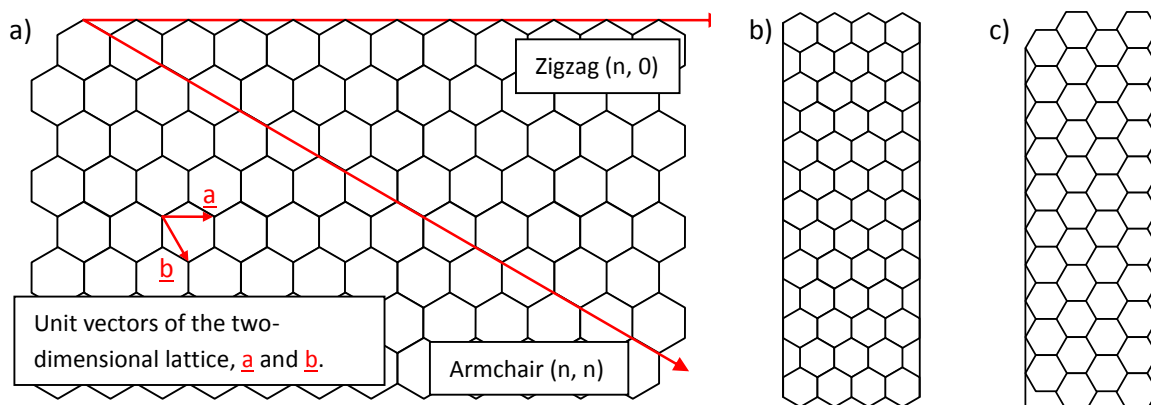


Figure 2.2: a) A diagram showing how the chiral vector of a zigzag and an armchair CNT lie on a single graphene layer. b) & c) Side profiles of a zigzag and armchair CNT respectively [30]

A final point concerning CNT structure with application to composites is the existence of certain defects in synthesised tubes and some unusual structural irregularities as follows. It has been shown that CNTs can be produced with a bamboo like structure consisting of small hollow compartments separated by graphitic layers [31] although mechanical properties were not investigated. CNTs have also been reported to grow in spiral or helix shapes [32], and it has been suggested that this coiled structure arises from pentagon-heptagon pair formation in the graphitic walls of the tubes causing the curvature of the CNT structure [33]. Another paper [34] has also reported the synthesis of SWCNTs with encapsulated buckminsterfullerene molecules described by the author as ‘nanoscopic peapods’. Although these intricate structural morphologies are of great interest, and may provide key details in understanding the growth mechanisms of these complex carbon structures this work focuses on simpler CNT structures as they are in general better understood.

2.2.3 Mechanical properties

It is well reported that CNTs exhibit some remarkable mechanical properties leading many people to believe that they are the strongest material currently known to man with high tensile strengths of up to 63 GPa reported [7] for MWCNTs. There is much speculation about the use of CNTs in ultra strong fibre reinforced composites due to this strength as well as their large length to diameter ratio, reported up to 28,000,000:1 for a SWCNT [35] and more recently 132,000,000:1 [36], although often lower for typical MWCNTs depending on the method of synthesis. This makes CNTs highly desirable for use in mechanical applications but the implementation of these properties in macro scale structures had proved non-trivial. A paper published in 2006 [37] included an interesting discovery of

CNT inside a sabre that was forged in the 17th century from a lost recipe for Damascus steel. Historically these blades were known for being sharper and stronger than other weapons of the time and it is highly possible that this could be a result of the CNTs contained within them. The remarkable strength of CNT can be accredited to the ability of Carbon atoms to form different types of covalent bond depending on the hybridisation of the atoms [38]. In diamond carbon atoms are bonded in the sp^3 hybridised state, where the four valence electrons are shared equally between nearest neighbours. It is this that provides diamond with its strong isotropic state that it is known so well for. Graphite on the other hand forms the sp^2 hybridisation state that leads to stronger in plane bonding of three of the valance electrons leaving the fourth to be delocalized among the remaining atoms similar to metallic bonding. In graphite this leads to a layered structure of graphene layers held together by weak Van der Waals bonding between the sheets of 2-D carbon giving it its conductive and lubricating properties. This type of sp^2 bonding is the same as that in CNTs, except due to the tubular structure of CNTs there are no weak interlayer bonds resulting in their strong characteristics. **Figure 2.3** shows examples of the hexagonal structure of sp^2 bonding and the tetrahedral structure of sp^3 bonding in different hydrocarbon molecules.

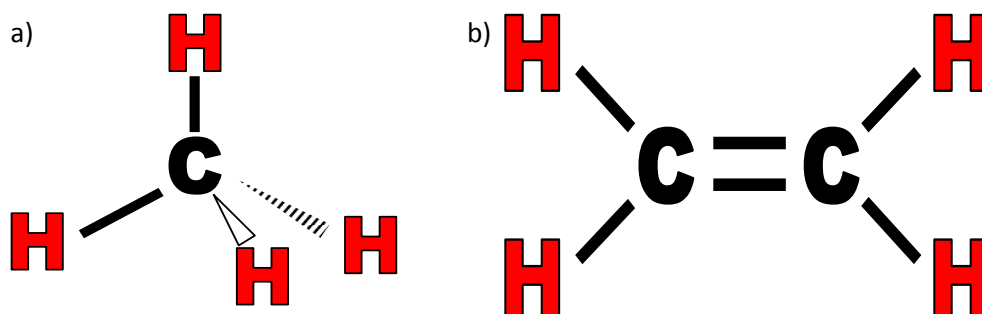


Figure 2.3: a) An example of sp^3 hybridisation in a methane molecule, note the 3-D structure, and b) an example of 2-D sp^2 bonding in an ethylene molecule

The measurement of the strength of a single CNT is certainly no easy task due to its nanodimensions. In 2000 this was achieved via the use of a technique which allowed the attachment of a single CNT to the tip of an atomic force microscope (AFM) [26]. Using this technique an individual CNT was joined between two AFM tips allowing measurement of its tensile strength [7]. These strengths are measured to be up to 100 times the strength of steel even though CNTs are only a fraction of the density [40] owing to the atomic weight of carbon atoms when compared to Iron and other metals.

It is these properties that make CNTs highly attractive for use as a filler material in advanced composites, as the inclusion of CNTs in a polymer, or other, matrix could provide a method of employing these exciting properties on a macro scale. As with all fibre composites an accurate understanding of CNT-matrix interactions, and of the CNT breaking mechanism, are crucial in advancing towards the large scale production of such composites.

2.2.4 Thermal Properties

CNT have also been reported to have valuable thermal properties, with thermal conductivities that are greater than 3000 W/m.K for a MWCNT at room temperature [41] and as high as 6600 W/m.K for a SWCNT [42], which is higher than that of diamond and the basal plane of graphite [43]. This is believed by some [42] to be down to the large phonon mean free paths present in these structures. More recently the accuracy of these values has been questioned with other groups reporting considerably lower values of thermal conductivity of CNT [44] suggesting precise thermal properties are still not well understood. CNT are also known to possess excellent thermal stability and experiments have shown them to be thermally stable in a vacuum up to temperatures of 2800 °C [40]. It has also been shown that CNT can absorb microwave radiation resulting in various effects such as light emission, intense heat, out gassing and structural reconstruction [45]. These effects have been utilised to cure CNT/matrix composites with as little as 1 wt% CNT and results show a similar cure quality as conventional thermal curing of the samples [46]. The high thermal conductivity of CNT has also been used to help introduce CNT to a thermoplastic through the absorption of microwave radiation. Sunden et al. [47] placed an array of vertically aligned CNTs (VACNTs) attached to a silicon substrate tip down on a Polycarbonate layer. The substrate and the VACNTs were then heated using microwaves and the excellent thermal conductivity of the VACNTs resulted in high temperatures at the polymer interface. This locally raised the polymer above its glass transition temperature and resulted in the VACNTs being anchored in the polymer whilst remaining vertically aligned. When considering composite materials the conductive properties of CNTs lend themselves to creating thermally conductive composites that could be used in many applications, particularly in the automotive and aerospace industries where the dissipation of heat is critical [48]. In fact composites with 1 wt% CNT filler have already been shown to increase the thermal conduction of a polymer matrix by 125 % [49] and higher for larger CNT concentrations.

2.2.5 Electrical properties

CNTs have also been shown to exhibit extraordinary electrical conductivity, which has been reported to be 1000 times higher than that of traditional copper wires [40], [50]. This has led to some large

scale interest into CNT-polymer composites with the ability to conduct electricity through a percolating network of CNT [48]. It is the graphitic nature of the structure of CNTs that leaves a delocalized electron from the sp^2 hybridization of the carbon atoms which in turn allows electrical conduction. An interesting effect occurs from the chiral nature of SWCNTs and it is documented that the conductivity of a SWCNT is controlled by its defining chiral vector. Saito et al. whilst working as visiting scientists at Massachusetts Institute of Technology (MIT) reported that SWCNTs could conduct as a metal if they were of the armchair structure and would act as a semiconductor if they were zigzag SWCNTs [51]. From structural simulations the same group realised that the chiral vector was a critical factor in CNT conductivity and formulated which vectors would allow metallic conduction and which would act as semiconductors based on the density of states available and the location of the Fermi level for each structure. Overall it was hypothesized that only 1/3 of all SWCNTs would be metallic and the rest semiconducting. The electrical properties of MWCNTs are known to resemble those of graphite, as the smaller inner tubes structures are superimposed by the structure of the larger outer tubes [38] and the band gap of a semiconducting CNT tends to zero as the diameter increases. This has been shown by experimentally obtaining the band structure of a single MWCNT and comparing this with that of graphite [52].

Other experiments [53], [54] have shown potential for use of CNTs as excellent field emission devices particularly when the ends of the CNTs are opened by laser heating in a vacuum [53]. Using CNTs as field emitters could create electron sources [54] that could be useful in many applications, from simple lab equipment to electron microscope beams. It has also been shown experimentally that the emission properties of CNTs could allow the production of flat panel displays that are 'nanotube-based' [55]. Another group [56] proposed the use of CNT as 'Supercapacitors' and carried out experiments separating two SWCNT by a layer of polymer in order to create a capacitor. The use of CNT as capacitors has also shown application to Li-ion battery technology where the use of CNT coated paper can be used to make highly effective current collectors [57]. CNTs have also been used to operate as nanoscale transistors that function at room temperature [58]. These devices rely on a semiconducting SWCNT mounted between two electrodes. The SWCNT can be switched between an insulator and a conductor by applying different gate voltages to the electrodes, hence performing as a transistor.

2.2.6 Characterisation of CNTs

The characterisation of CNTs has been an important technique since their first discovery [12] as in nearly all CNT applications it is of interest to know the structure of any CNTs that are produced. Currently there are several methods of spectroscopy and microscopy available to assess the types of CNT present in a given sample. The first techniques used to identify the structure of CNTs were carried out by Iijima et al. [12] and published in the same paper as the discovery of CNTs. They used high resolution transmission electron microscopy (TEM) to identify the number of walls present in various MWCNTs. Scanning electron microscopy (SEM) is useful when dealing with CNTs but even the best SEM available will struggle to resolve a single CNT. The greatest use of SEM is in imaging bundles of as produced tubes to gauge an estimate at the length of the tubes present in the sample. As previously discussed the chiral structure of CNTs has important implications to their electrical properties and thus identifying chirality is useful, particularly for electrical applications. Recent advances in scanning tunnelling microscopy (STM) have allowed imaging of structures on the atomic scale and applying this to CNTs has been shown to reveal their chirality [59]. The same images can also be used to confirm the hexagonal lattice structure and quality of the graphitic structure of each individual CNT. Another useful application of STM is that the tip of an atomic force microscope can be used to manipulate CNTs both testing them mechanically [7] and orientating them into a desired position [60].

One of the most important techniques for identifying CNTs is the use of Raman spectroscopy in order to detect the unique atomic structure of CNTs [61]. An important known use of Raman spectroscopy in identifying CNTs is the dependence of the radial breathing mode (RBM) on the diameter of the CNT [62]. This allows the RBM for a batch of tubes to be measured and an approximate diameter for the CNT to be deduced. SWCNT can be more accurately identified by Raman spectroscopy as their structure is nearly always more perfect than that of MWCNT as they contain fewer defects or impurities [23]. As Raman spectroscopy relies on the use of optical light it can only be focused to about one micron, despite this, effective measurement can be performed on individual SWCNT as long as they are well isolated [61], [63]. More importantly micro Raman of SWCNTs has revealed a method for non-destructively identifying the chiral vector of individual SWCNTs and consequently allowing precise knowledge of their electronic structure and properties [63]. Finally a further useful result of this non destructive testing in composite manufacture is the use of Raman spectroscopy to assess any damage to CNTs during composite processing, for example as used by Kwon et al. [64].

2.2.7 Functionalisation of CNTs

Functionalisation of CNTs refers to the modification of the surface of CNTs, usually by the covalent bonding of a molecule to the carbon structure. Such a process is desirable as certain chemical groups could provide CNTs improved surface properties, such as better fibre-matrix interaction in composites [65]. Often when functionalising CNTs it is important that the CNTs are purified and often activated to allow the covalent attachment of chemical groups [66]. One of the first used methods of purification of MWCNT is oxidization at high temperature, (>700°C) in a suitable environment, leading to the removal of most amorphous carbon and other nanoparticles [67]. Activation of CNT is another important procedure in functionalisation and is usually performed as a 'cutting' procedure in which CNT are treated with sulphuric or nitric acid and sonicated creating oxidizing conditions. This causes the CNT to be cut down into many pieces which are approximately 100-300nm in length [68]. Often this process leaves the CNT open ended which allows the covalent attachment of a variety of oxygenated groups including carboxylic and hydroxyl groups [65], although the reduction in aspect ratio of individual CNTs may affect their efficiency as fibre reinforcements in composite structures. Following from this a similar technique was used by Shaffer et al. to obtain an electrostatic stabilised dispersion of cut CNTs in water [69], [70]. Once activated, a great deal of chemical groups can be attached to the CNT, for example Gojny et al. [71] attached amine groups to CNTs creating amino-functionalised CNTs. They showed that this not only has potential improvements for CNT-Matrix interactions but also helped prevent agglomeration and to disperse the CNTs better, as a result of the modified CNT surface properties.

Riggs et al. [72] also reported better dispersion of MWCNTs when functionalised with the soluble poly (vinyl acetate-co-vinyl alcohol) group via ester linkages. This resulted in 'polymer-bound' CNTs that were soluble in both organic solvents and water, forming homogenous solutions that are surprisingly highly coloured. CNTs have also been functionalised with many other polymers such as poly-vinylbutryal (PVB) [73] and poly (styrene-co-*p*-(4-(4'-vinylphenyl)-3-oxabutanol)) (PSV) [74]. These functionalisations have also achieved soluble functionalised CNTs in specific polymers. As well as the addition of complex chain molecules, simpler functionalisation of CNTs has also been studied in detail. A good example is that of the fluorination of CNTs where fluorine atoms are attached to the sidewalls of the tubes and the results confirmed by infra-red spectroscopy to show the presence of covalent C-F bonds [75]. Interestingly the fluorination of SWCNTs appears to be reversible in a similar technique used with graphene involving the use of a defluorinating agent. Importantly this process has been shown to leave the graphitic structure of the CNTs intact [75]. More recently it has been shown that SWCNT can also be bonded covalently to Fullerene molecules to form what has

been termed as 'nano-buds' [76] and have shown 'promising field emission properties' when compared to as produced SWCNTs.

2.3 Synthesis of CNTs

2.3.1 Background

Since the first synthesis of CNTs there have been many attempts to find methods of producing CNTs using various novel techniques. Much of this interest has been due to the lack of methods for large scale cost effective production of high quality CNTs with potential to be scaled up to a commercial level. As with all production, if an economically viable technique for CNT synthesis cannot be found then there is to be little benefit from the years of research put into the area. This section aims to assess the main advantages and disadvantages of the various techniques and provide an insight into these processes.

2.3.2 Arc Discharge CNT Synthesis

The arc discharge method of CNT synthesis is regarded by many to be one of the simpler processes, and is also the first process where CNTs were observed to be synthesised [12]. The process involves the use of two graphite electrodes placed in an inert atmosphere, usually of Helium. Both electrodes are water cooled, and the anode, which is usually of slightly smaller diameter, is mobile allowing it to be brought closer to the cathode as required. The anode is then moved to within less than 1 mm of the cathode allowing a 100 A current to pass between the two causing the creation of a plasma that is of temperatures of around 4000 K [77]. This causes the graphite anode to be vaporized and in turn deposited on the cathode resulting in the synthesis of CNTs, amongst other carbonaceous structures, during the process the anode is moved continually closer to the cathode to maintain a constant distance as it is consumed. It is also possible to include a metal catalyst in the electrodes allowing synthesis of MWCNTs and SWCNTs depending on the presence and type of catalyst [77].

In the case of purely graphitic electrodes the resulting CNTs are usually MWCNTs [12] that are formed on the cathode, although impurities such as amorphous carbon and fullerenes are always present. During the process carbon structures have also been observed to be formed in a deposit that builds up on the reactor walls, although Iijima noticed no MWCNTs contained within this soot. By varying the pressure of He in the reactor, Ebbesen et al., showed that the rate of formation and the total yield of CNTs can be drastically improved, with a maximum efficiency seen at pressures of 500 torr [78]. The deposit formed on the cathode usually consists of a hard grey outer shell and a softer fibrous core, the core consists of about two thirds MWCNT and the remaining third consisting of other carbon nanoparticles [79]. The MWCNTs produced in this technique usually consist of

approximately between 2 and 50 layers and are not normally of lengths greater than 1 μm , in a typical arc-discharge experiment [12]. This process of synthesis is generally considered to be highly energetic and as a result despite good yields it still remains high cost. Variations on this technique have shown the possibility of cost reduction by carrying out the process in liquid nitrogen thus removing the need for a vacuum and cooling system. This technique was demonstrated by Jung et al. [80] in 2002 and shows promising yields and no contamination of the MWCNT with nitrogen atoms as a result of the process being carried out in a dewar of the liquid. Due to the relatively simple steps involved in this method and the high yield produced, there is clearly some potential for scaled up mass production.

The production of SWCNT through an arc-discharge process requires the integration of a metal catalyst into one of the graphite electrodes. This process was first published by Iijima in 1993 [23], and involved the incorporation of iron filings into a dimple in a vertical cathode used in the apparatus. Interestingly the formation of SWCNTs does not occur on the electrodes as seen with MWCNT, but rather they are formed in the soot that is left on the walls of the reaction chamber. Another distinct difference in this synthesis is that SWCNTs were only found to form when methane was present in the chamber as well as inert argon unlike in the case of MWCNTs. In the same issue of Nature, Bethune et al. [24] also reported synthesis of SWCNTs through a very similar method although they used cobalt as their catalyst and reported much more consistency in the diameters of the SWCNTs that were produced. Since these first experiments many reports have shown that a wide range of metal catalysts can be used to synthesise SWCNTs through the arc discharge method including mixtures of metals and mixtures of metals and graphite powders as well. Larger scale synthesis of SWCNTs has also been reported using this method allowing the production of gram scale quantities of approximately 80 % purity [81].

In summary the arc discharge method has been shown to produce various forms of CNT in a well repeatable process. The main downfalls of the technique are the formation of many impurities in the produced CNTs and the problems involved with removing these in order to obtain pure samples of CNT as well as the high energetic cost involved. Also it is often the case that the purification process can be damaging to the fine structure of the individual CNTs [78]. The other problem with arc discharge is the limitation of the length, about 1 μm [12], of the CNTs produced as it is clear that some applications would favour longer CNTs. Finally CNTs produced via this technique are formed in a so called 'spider web' style where they are highly entangled with each other unlike other techniques such as Chemical Vapour Deposition (CVD) which allows the production of aligned CNT

[82]. As a result practical processing of arc-discharge CNTs can be challenging furthering the need for improved CNT production methods.

2.3.3 Laser Ablation CNT Synthesis

The laser ablation technique of CNT synthesis uses laser radiation to vaporise a graphite target inside of a furnace leading to the formation of CNTs. The set up typically consists of a high power laser, of at least 500 W [83], that is focused onto a graphite target and can be continuous or pulsed. The target is typically positioned in a quartz tube that is evacuated, filled with a flowing inert atmosphere and placed inside of a furnace that is typically heated to 1200 °C. The laser radiation then causes the vaporisation of the graphite target and the particles in the gas phase travel down the tube in the inert flow where they are collected on a water-cooled conical copper collector. It is here that CNT are collected although CNTs have also been found to be present on the walls of the quartz tube and also in other areas that are down flow of the target [84–86].

Similarly to arc-discharge, MWCNTs and SWCNTs can both be synthesised depending on the composition of the target. Purely graphitic targets yield MWCNTs as originally found by Guo et al. [84] in the first production of CNT through the laser ablation technique. After this report many groups experimented with similar procedures in order to understand the effectiveness of this new method and it was soon shown by the same group that SWCNTs could be produced by including metal catalysts in the targets [85]. Other than the target composition, the power and type of the laser is known to affect the quality and quantity of CNTs produced. Zhang et al. [83] showed in 2001 that the yield of SWCNT was greatly improved with higher laser power, with the best results at laser powers greater than 800 W. They also showed that at low powers, less than 500 W, the laser was not powerful enough to produce high enough temperatures for the ablation process to occur. Most laser ablation synthesis involves the use of an Nd:YAG laser with either the primary beam of wavelength 1064 nm [84] or secondary beam of wavelength 532 nm [86].

Later experiments attempted to use a larger wavelength, 10.6µm, CO₂ laser causing some notable effects on the synthesised SWCNTs as follows. The most interesting point of using a continuous CO₂ laser to synthesise SWCNTs is that Raman spectroscopy of produced samples has revealed that the average diameter of SWCNTs produced increases by approximately 0.3nm [83] illustrating a degree of control over SWCNT dimensions. Another important effect was that using a CO₂ laser the synthesis of SWCNTs was possible at room temperature where as other experiments had shown that the yield of SWCNTs always increased with temperature [84] and was minimal at room temperature. Other groups have also used different techniques to attempt to increase the yield from laser

ablation. After noticing that catalyst containing targets became metal rich over time Yudasaka et al. [87] synthesized SWCNT using separate metallic and graphitic targets positioned face to face. Their experiments revealed a method of expanding the effective life span of targets used for laser ablation CNT production, which is important in producing CNTs in larger quantities. A further area of research, as with most CNT production methods, is the effect of the catalyst on the process. It has been found that by using a mixture of catalysts, usually Ni or Co based, can increase the yield of SWCNTs many times [88] with yields greater than 70 %. The yield of laser ablation is also dependant highly on the atmosphere inside the reactor, with successful synthesis being reported in both Argon [85] and Nitrogen [89] atmospheres. Strangely in the presence of a helium atmosphere almost no SWCNT synthesis is observed despite keeping all other parameters constant [89] and also at pressures below 200 Torr the soot deposits are dominated by amorphous carbon. Munoz et al. report the greatest yields of CNTs at pressures between 200 and 400 Torr [89].

In conclusion, similarly to arc discharge CNTs, laser ablation produces tangled CNT that are difficult to separate from the amorphous carbon and other impurities formed during the process. This said yields are fairly good, approximately 70% [88], when the process is fully optimised. The main downfall of laser ablation is that it is only feasible on a lab scale due to the fact that the power of the laser will always be limited allowing the ablation of only small amounts of the target at any time. As well as this it is a highly energy intensive process which drives up the cost of manufacture despite the possibility of production at room temperature.

2.3.4 Chemical Vapour Deposition CNT Synthesis

CVD of carbon containing gases has been studied for many years prior to the discovery of CNTs, some of the earliest reports of carbon deposition over iron catalysts date back to the 1960s [90]. This specific report concerns the formation of various carbon structures via the decomposition of carbon monoxide over iron surfaces in a furnace at 550°C. Despite the well known process of CVD it was not until 1993 that the technique was used to produce samples of CNTs by Jose-Yacaman et al. [91]. These CNTs were grown via the decomposition of a flowing acetylene/nitrogen mixture over iron particles at 700°C for several hours. The process produced MWCNTs of up to 50µm in length which formed due to the catalytic nature of the iron particles.

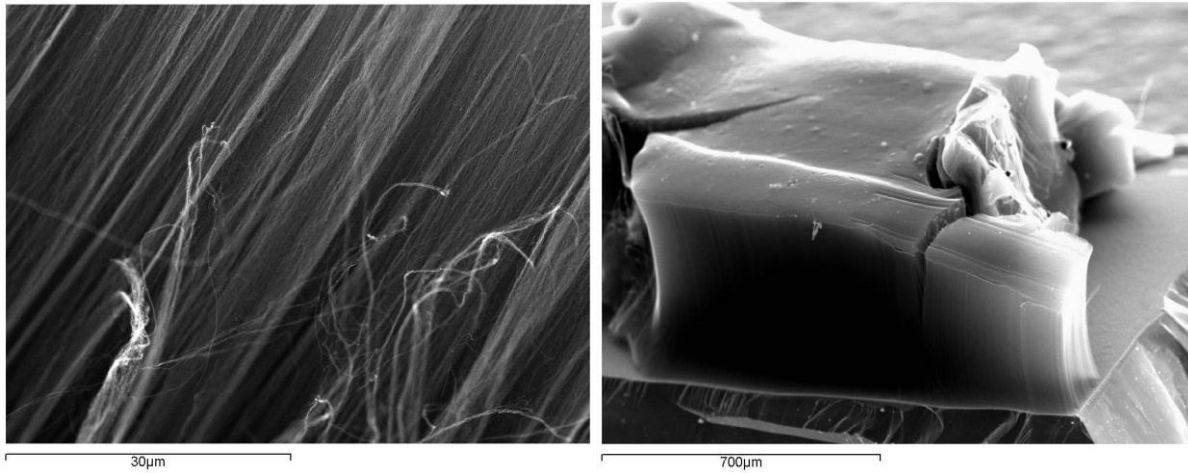


Figure 2.4: Examples of aligned CVD CNTs grown at The University of Exeter both images are of the same sample at different magnifications

The basic design of a CVD set up is actually rather simple, and does not involve any particularly expensive apparatus when compared to arc discharge and laser ablation processes. It consists of a quartz tube placed inside a furnace with a gas flow from one end of the tube to the other through the furnace. A crucible is positioned in the centre of the furnace and filled with a catalyst, typically a metal such as iron or cobalt, that is known to aid the decomposition of the flow gases and also to favour the formation of CNTs. Due to the low cost involved it was quickly realized that CVD had a lot of potential for large-scale production of CNTs and as a result many different variations of the standard CVD set up were quickly developed and tested [82], [91–93]. Early methods of CVD CNT production often produced a thin film of randomly orientated MWCNTs that contained many amorphous carbon impurities and often the as grown CNTs were coated in a layer of amorphous carbon [94]. In 1996 Li et al. used a mesoporous silica substrate embedded with iron nanoparticles to catalyse CNT grown through CVD [93]. This report had important implications for the future of CVD as the CNTs produced grew in an aligned ‘forest’ that grew approximately perpendicular to the substrate. An example of an aligned CVD CNT forest grown using ‘sabretube’ apparatus is shown in **Figure 2.4** under different SEM magnifications and the ‘sabretube’ CVD system in use is shown in **Figure 2.5**. All mentioned CVD experiments thus far have resulted in MWCNT growth however by fine adjustment of the settings; Kong et al. reported growth of individual SWCNTs on to patterned wafers in 1998 via the decomposition of methane gas [95]. Expanding on this, millimetre length SWCNTs have also been formed on flat substrates that appear to be orientated in the direction of the flow gas [96], and even more recently SWCNTs of length of 4cm that grew at rates of $11\mu\text{m/s}$ although these were more randomly orientated [35].

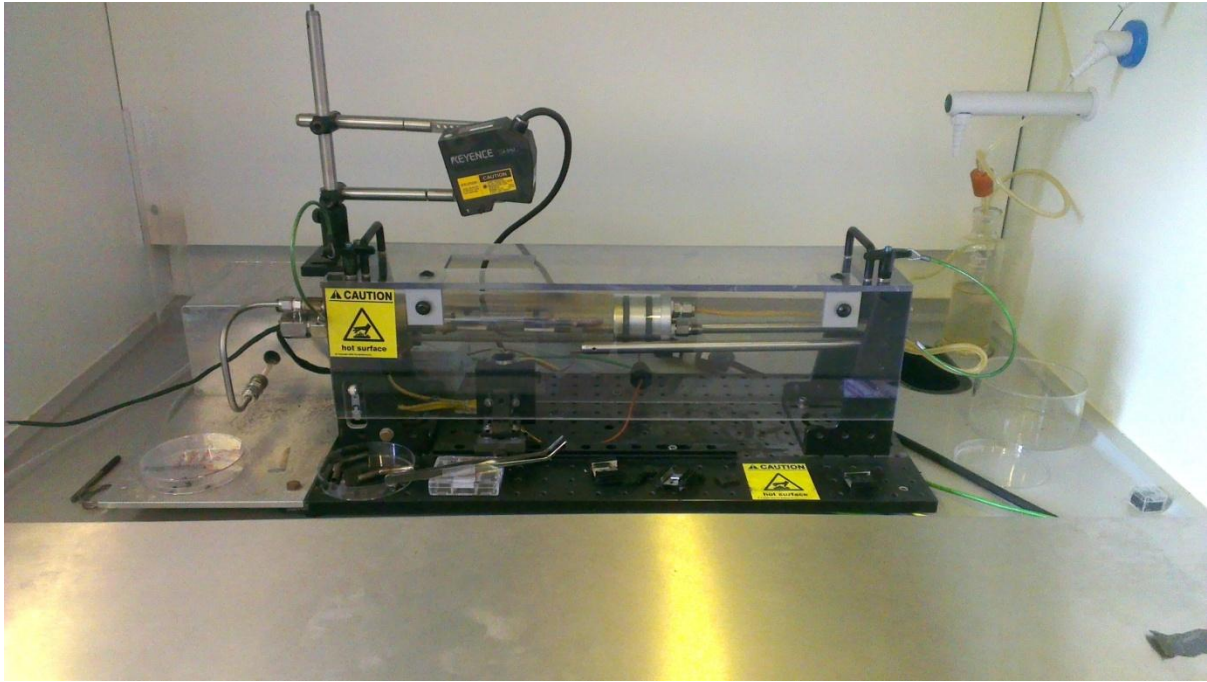


Figure 2.5: Detail of the CVD 'SabreTube' equipment in use at The University of Exeter.

CVD is clearly highly dependent on the presence of a catalyst to form CNTs as even MWCNTs will not grow without its presence unlike in previously mentioned techniques. This has sparked many groups to investigate the effect of various catalysts on the CVD process in order to optimise the procedure. A growth mechanism for CNTs based on vapour phase growth using metal catalysts has been proposed via both tip and root growth of the CNTs [97], evidence of this has also been seen in the presence of catalyst particles embedded in the roots and tips of CNT. As well as this mechanism there is other evidence [98] in the literature to suggest that the annealing of a thin film of catalyst in specific atmospheres leads to the formation of nanoparticles of catalyst on the substrate and each particle gives rise to a single CNT. This has been shown by the production of CNTs of different diameters via the use of different transition metal catalysts and different thin film thicknesses [99], [100]. As a result of this annealing process, it has been observed that the presence and composition of a buffer layer under the catalyst can have a significant impact on CNT growth [101]. Although originally SiO_2 [93] buffer layers were used recent experimentation has shown longer and more prolonged growth via the use of Al_2O_3 [101] buffer layers. The annealing process is also dependant on the thickness of the metal catalyst layer and the ability of the process to form nanoparticles suitable for the initiation of CNT growth. Bronikowski et al. [102] showed a peak in CNT length occurred with relation to the thickness of the catalyst layer with a maximum occurring between 1 and 2 nm. This is believed to be a result of thicker layers resulting in too much catalyst being present

meaning that small nanoparticles of the catalyst will not form under heating in an inert and then reducing atmosphere [103]. Further details of the chemistry involved in the CVD process is detailed later in **Chapter 3** of this work.

Another useful technique with CVD synthesis is the ability to create substrates with a patterned catalyst layer through photolithography resulting in the production of patterned CNT forests [82], [104]. Despite the focus of producing carefully constructed thin film catalyst layers deposited on substrates for CNT growth another group has also recently reported the growth of CNTs onto bulk alloy. Talapatra et al. found that CNTs could grow on bulk samples of inconel, an alloy consisting mainly of nickel, chromium and iron, in various geometries [105]. These CNTs were also observed to grow in a vertically aligned fashion perpendicular to the surface of the metal similarly to those that were substrate grown, although smaller final lengths, of approximately 300 μm , were observed. In order to improve the CVD process some groups have experimented with growing CNTs using a plasma enhanced CVD (PECVD) set up. This process has been shown to not only improve the alignment of the CNTs but also to lower the production temperature [92]. This is particularly desirable when producing CNTs on glass substrates for use in electronic devices such as in field emission applications [53] as temperatures greater than 666 °C can damage even the most advanced glass substrates [92]. Furthermore plasma enhanced CVD growth has been shown to improve CNT alignment when compare to self aligned VACNT structures by Bower et al. who proposed that CNT could be switched from a wavy to an aligned state by switching the plasma on and off respectively [106], [107] A final development in CVD growth of CNTs is the use of water vapour in CVD systems to promote so called 'super growth' of CNT forests. Using this process CNT forests have now been grown to taller heights with CNT growing to greater than 2 mm in height in larger areas as originally shown by Hata et al. [108].

In summary CVD production of CNTs shows great potential for low cost large scale production which is greatly desired. Recently the ability to grow CNTs on a moving substrate has been demonstrated hinting towards the possibility of a constant CNT production process [109]. Also a technique for the removal of CNT from a moving substrate has been suggested by a member of the same group at Massachusetts Institute of Technology [110]. As well as this by carefully selecting catalysts and buffer layers deposited on the substrate, the dimensions and quality of the CNTs produced can be controlled. CVD also allows the production of the longest CNTs to date, which is highly desirable for many applications particularly in electronics and advanced CNT composites. Finally the total CVD production time for CNT can be well under an hour for a large batch of CNT produced to lengths of several millimetres, where the area of growth is only limited by the size of the reactor available [26].

Arc-Discharge, Laser ablation and CVD are by far the most common techniques of CNT synthesis and show the most promise for commercial application and are comparatively summarised in **Table 2.1**. Although other CNT production techniques exist these have been studied considerably less and as a result are only reviewed in brief as follows.

| Method | Advantages | Disadvantages |
|----------------|---|--|
| Arc Discharge | High yields | CNT often entangled, Highly Energetic, Post processing of CNT required, Short CNT aspect ratios |
| Laser Ablation | High Yields of Pure CNT | CNT often entangled, Highly Energetic, Post processing of CNT required, Short CNT aspect ratios |
| CVD | Very High yield, Suited to automation, Low energetic cost, Pure CNT produced, Can produce highly ordered CNT structures such as forests, CNT can have large aspect ratios | Large scale production often lowers product quality (aspect ratio), precise CNT structure is catalyst driven so precise control is required for reliable production. |

Table 2.1: A Table summarising the advantages and disadvantages of the three most common methods of CNT synthesis

2.3.5 Solar Energy CNT Synthesis

The method of CNT production through the use of solar energy can be compared to that of laser ablation in that sunlight is focused using a solar furnace resulting in the vaporization of a graphitic target. This technique was first used to produce fullerene samples in 1993 by Chibante et al. [111] who believed that solar production could lead to cleaner fullerenes with less damage to their overall structure usually caused by photochemical destruction during synthesis. The synthesis of CNTs produced by solar energy was first reported in 1996 at a conference and later in a paper by Laplace et al. [112]. They produced a mixture of both SWCNTs and MWCNTs in an argon atmosphere using the same technique as Chibante et al. [111], but incorporating a catalyst into the graphite target. Through the adjustment of precise experimental conditions they found that the structure of the CNTs produced could be varied including the length and the number of walls present. Similarly to laser ablation these CNTs are formed in tangled networks containing nanoparticle impurities and overall the technique appears to hold little promise for mass production of useful CNTs.

2.3.6 Electrolysis CNT Synthesis

The synthesis of CNTs has also been reported through an electrolysis process [113], [114]. This process involved a graphite crucible filled with lithium chloride with a graphite rod dipped inside. The salt was heated to above its melting point before a current was passed through the system causing the cathode rod to be consumed through electrolysis. Carbon nanostructures formed in the liquid salt which was then cooled and removed by dissolving in water. The carbon nanostructures contained in the resulting solution can then be removed and viewed under TEM allowing the observation of MWCNTs. The CNTs formed in this process are quite varied and it is clear that the precise conditions of the set up affect the quality of the yield greatly. Although interesting, low quality CNTs and low yields limit this techniques usefulness in practical CNT production.

2.3.7 Flame CNT Synthesis

The production of various Carbon structures such as fullerenes [115] in hydrocarbon flames was originally observed in 1991. Although carbon soot deposits have been observed from flames for centuries it was not until 2000 that CNTs were first observed within these deposits [116]. These CNTs were observed to be formed when an acetylene/nitrogen flame had a metallocene vapour injected to it acting as a catalyst for CNTs formation. This experiment produced a range of SWCNTs although a lot of amorphous carbon embedded with metal particles was also found to be present in the collected soot. Another group [117] found that MWCNTs could be grown on a Ni-Cr wire placed in a methane flame. They proposed a catalytic root growth mechanism similar to that of CVD growth but different as they believed the catalyst particles to be metal oxides that were formed during the process thus hinting at the possibilities of low cost large scale manufacture.

2.3.8 Bulk Polymer CNT Synthesis

The production of CNTs via heat treatment, a form of pyrolysis, of a polymer was first reported in 1996 by Cho et al. [118]. They found that by heating a specific polymer on an alumina boat, at temperatures up to 400 °C, produced CNT samples from the polymer. The samples were then left to cool and dispersed in ethanol in order to allow the observation of the CNTs. These CNTs were identified as MWCNT with lengths of less than 1 µm. More recently another report [119] used a similar process where polypropylene was used as a carbon source for CNT synthesis. They used a specific combustion process at temperatures of 630-830 °C combined with Ni compound catalysts to form MWCNTs. They showed that at higher temperatures it appeared that the yield of MWCNT was increased, by up to 10 %, and also that the form of the Ni catalyst played a significant role in the process.

2.4 CNT Composites

2.4.1 Background

The inclusion of CNTs in composite materials is of interest for several reasons that arise from the properties of individual CNTs. The most desirable of these are the remarkable mechanical properties of individual CNTs [7] and also their excellent conductive properties both thermal [41], [42] and electrical [40], [50]. Consequently by using CNTs as a filler in a matrix these properties have the potential to be scaled up resulting in very unique composite characteristics. Although this process sounds simple the nanoscale nature of CNTs has made composite production remarkably difficult in practice, mainly due to the strong interaction of van der Waals forces between individual tubes [40], [65]. As a result of this interaction, as formed MWCNTs and SWCNTs tend to aggregate into bundles or 'ropes', particularly when allowed to disperse in a suspension. In order to form effective composite materials it is necessary that any filler used should be well dispersed in order to maximize the surface area contact between filler and matrix [121] as well as ensuring uniform reinforcement. Although the main focus in this review will be the inclusion of CNTs in polymer matrices, it should also be noted that CNT fillers have already been tested in ceramics [121], [122] and metals [123] as well.

2.4.2 Dispersion of CNTs in a Matrix

There are several techniques currently available for aiding the dispersal of CNTs in a matrix via physical mixing and blending techniques. The main issue with the agglomeration of CNTs in a composite is that they tend to form rope-like bundles [124] resulting in slipping between CNTs and causing a great weakness in any composite structure. The most effective method of physical dispersion thus far has been to sonicate mixtures of matrix and CNT for prolonged periods in order to obtain dispersion. Many groups [125], [126], report uniformly dispersed CNT in polymer composite samples using sonication processes, and also often find modest improvements to composite properties. In most cases reinforcement is often less than expected, when considering the mechanical properties of individual CNTs [7]. For example Qian et al. report improvements in elastic modulus of ~ 36-42 % and tensile strength of ~ 25 % [126] in CNT-polystyrene composites. The main downfall of the sonication dispersion method is that during the highly energetic process the CNTs can be damaged [127] and are commonly shortened considerably [128], [129]. Mukhopadhyay et al. report the conversion of well graphitized CNTs into amorphous nanofibres after 24hrs of 2W ultrasonication in ethanol solution [127]. This discovery hinders the use of sonication to disperse CNTs as these effects will decrease the strength of the CNT resulting in weaker composites.

When using sonication to disperse CNTs there are three common strategies, the first is to use a surfactant to facilitate the dispersion of the CNTs before mixing with a polymer. This method was employed by Gong et al. [130] who used a non-ionic surfactant to disperse CNTs before mixing with epoxy to create composite samples. The second method is, instead of a surfactant, using a solvent to aid dispersion of CNTs through sonification, then mixing with a matrix similar to methods using a surfactant. Ausman et al. report the effective dispersion of SWCNTs in the organic solvent *N*-methylpyrrolidone (NMP) [131] although some agglomeration was still observable and the process was carried out with short (<300nm) SWCNTs. The final sonication method is to mix CNT with an uncured or molten polymer, then sonicate the mixture to disperse the CNT before curing or cooling to form a composite. Although this process seems simpler than using a surfactant or solvent, molten polymers and uncured resins are often viscous and CNTs are known to further increase viscosity thus inhibiting dispersion of the CNTs [132]. An example of this process is the work of Kim et al. [133] who sonicated a mixture of CNTs and epoxy resin to disperse the CNTs, before using the resin to make carbon fibre multi scale composite samples.

Another mechanical method of dispersing CNT is to use high speed stirring to overcome the attraction between individual CNT. Similar to sonication this technique is often carried out in solvents, or surfactants, but can be used in simple uncured polymer-CNT mixtures [134]. This method was used by Sandler et al. in 1999, they used high speed mixing of a resin, ethanol and CNT mixture to create well dispersed composites with enhanced electrical conductivities [135]. High shear forces have also been used to physically overcome the Van der Waals attraction between CNT in order to aid dispersion. For example Ajayan et al. demonstrated that cutting thin, 50-200nm, slices from a bulk CNT-polymer resin sample resulted in the alignment of the CNT within the polymer resin [136] as revealed by TEM although mechanical tests have not been conducted. Another group [137] used the mechanical stretching of a CNT-thermoplastic composite to aid the alignment and distribution of the CNT. They found that by heating the samples to a temperature of 100 °C and stretching the sample by up to 330 % the previously tangled CNT became elongated and aligned.

Many previously mentioned reports [135–137], utilise a combination of physical dispersion techniques to create well structured CNT-polymer composites. Another process for aiding CNT dispersion is to functionalise the CNT prior to mixing with a matrix. The use of functionalisation to aid dispersion has also been investigated by Mickelson et al., who dissolved fluorinated SWCNTs in propanol up to 1 mg/ml [138]. They found that the mixtures formed metastable states and that light sonication in alcohol solvents did not remove the fluorine from the SWCNTs, but that the tubes could be precipitated from the mixtures using hydrazine to yield unfluorinated SWCNTs. Geng et al.

[139] then used this technique to form fluorinated SWCNT poly-(ethylene oxide) composites and reported considerably better dispersion of the functionalised SWCNTs compared to as produced SWCNTs, when imaged using SEM. Many groups aiming for well dispersed tubes use CNTs produced by either the arc-discharge [137] or laser ablation [139] synthesis methods. More recently the ability to use CVD to produce aligned arrays of CNTs has resulted in investigations into using these arrays as fillers without any high energy mixing. Sunden et al. [47] used localized microwave heating of aligned CNT arrays to anchor the CNTs into a polycarbonate layer, with the aim of fixing the CNT for use in Microelectromechanical Systems (MEMS). They achieve the embossing of VACNT forests, of up to 200 μm in height, into the polymer layer using a hot press technique, and report the successful retention of the forests original dispersion and alignment. Similarly another group [140] experimented with the wetting of aligned arrays of CNT pillars with a thermoset polymer and found that the aligned nature of the forests resulted in capillary driven wetting along the axis of alignment. This technique can then be used to create polymer composites. Importantly both of these techniques do not require the use of any solvent/surfactant to disperse CNT but rather rely on the dispersion of the forests defined by the growth conditions and the penetration of the matrix molecules into the aligned forests. The alignment of CNTs in polymer matrices has shown several advantages over randomly orientated mixtures of CNTs and polymers and is desirable for many composite applications. Cebeci et al. [141] report that aligned CNT nanocomposites show better mechanical and electrical properties than randomly orientated CNT composites, they also report that the aligned composites show increasing modulus with volume fraction % and discuss models to explain measured reinforcement values.

2.4.3 Polymer-CNT Composites

The many techniques for dispersing CNTs are often tailored to the nature of the polymer matrix to be used in the composite. One of the most commonly tested types of polymers in CNT composites are various thermosetting resins, mainly due to their low viscosity and known effectiveness in other composites such as carbon fibre. Gojny et al. [142] used a 'three roll mill' to mechanically disperse various CNT morphologies into a low viscosity epoxy resin that was cured via use of a chemical hardener. They observed that low, 0.1 - 1.0 % volume, amounts of CNTs in the resin did lead to mechanical reinforcement of the resin but only by a small fraction compared with the neat samples. They also noted, through the use of electron microscopy, that high loading of the matrix with CNTs resulted in more agglomeration after dispersion than in samples with lower, 0.1 % volume, CNT loading highlighting the ever present dispersion problem. The same group [143] measured the conductive properties of similar samples, reporting that this method of producing randomly

orientated CNT-epoxy composites was effective at creating conductive composites. They also showed that only a low weighting of 0.1 % was required to reach the percolation threshold for CNTs, and attributed this to the high aspect ratio of the CNTs allowing the formation of conducting networks. Similar results were achieved by Moisala et al. [48] using the sonification method of CNT dispersion using a similar epoxy and hardener.

Li et al. [144] performed mechanical tests on coiled CNT epoxy composites, which were produced using a sonication method and then cured inside of a mould again through the use of a hardener. They also showed a modest increase, from 5 GPa to 7 GPa, for 5 % CNT weighted composite compared with neat resin. The experiments also showed an increasing trend between CNT volume fraction and elastic modulus although levels of reinforcement are still considerably lower than those expected theoretically. Another group [14] developed a unique method for spinning CNT fibres whilst working at the University of Cambridge; they managed to continuously draw a fibre, of approximately 50µm diameter, from a CVD furnace onto a rotating spindle. These fibres were then used in later experiments, published by Mora et al. [145], to form composites. Samples were produced using an epoxy-hardener mixture inside of a mould to create samples for both compression and tensile testing. This technique allows high volume % loading of the resin with CNTs and the results of these recent experiments showed an increase in tensile strength of greater than 5 times, at 27 % CNT fibre volume fraction. Wardle et al. [16] also showed the possibility of loading epoxy with high volume fractions of CNTs. They found that by bi-axially mechanically compressing an as grown aligned forest of CVD produced CNTs they could increase the density of the forests. They then submersed the samples in resin creating CNT composite samples with up to 22 % volume fraction VACNTs. They believe like many others that in order for successful mechanical reinforcement of a matrix with CNTs it is critical to move towards high volume fraction aligned composites.

Another use of epoxy in CNT-composites has been its inclusion in so called multi-scale composites that often incorporate CNTs combined with one or more other fillers. Siddiqui et al. [146] looked at glass fibres that had been coated with a CNT-epoxy layer in an attempt to enhance the tensile strength of the fibres with a goal of enhancing the strength of fibreglass composites. They used sonication methods to disperse the CNTs and found an increase between 200 and 500 MPa for the fibres depending on the gauge length at a 0.3 wt% CNT loading. Interestingly at higher volume fractions, 0.5 wt%, the effect was reversed and this is believed to be due to agglomeration of the CNT in the matrix further illustrating the inherent difficulties in dispersing CNTs. Garcia et al [147], [148] used CNT-epoxy composite to reinforce a commercially available alumina cloth. They employ

an interesting method where CNTs are grown directly on to the fibres using CVD. This involves the coating of the fibres with catalytic particles before the decomposition of ethylene gas in a CVD furnace resulting in the growth of CNTs radially around the fibre axis. This CNT-alumina cloth is then saturated in thermoset polymer resin to create a multi-scale laminate composite. In mechanical testing they found that composites created with CNTs showed a 69 % increase in interlaminar shear strength when compared to the regular composite. The group managed to produce 3 layer samples of up to 8cm² in area, which was limited by the furnace size, showing high potential for scaled up applications. Another group [149] attempted to use epoxy-CNT combinations, mixed using 'high-shear calendaring equipment', as a reinforcement for a carbon fibre composite. This proved to be less effective though as the random orientation of the CNT allowed for agglomeration and did not effectively increase inter-fibre bonding as Garcia's method did, so no notable increase in modulus or strength was observed. The group did however show that the inclusion of CNTs reduced the coefficient of thermal expansion by up to 32% which could be useful in applications where thermal expansion of composites is problematic. This is thought to be a result of the highly conductive nature of CNTs dispersing heat faster than the standard matrix and at least shows some prospect of individual CNT properties being effective on a macroscopic scale.

The attractiveness of resins for use as a polymer matrix in composites can be attributed to a few key points. These are that resins can be produced with a low viscosity facilitating mixing processes, and that there are various methods of curing resins available such as chemically, thermally, or even through exposure to UV radiation [150]. As a result resins are often manufactured in the composite industry to meet specific criteria in order to effectively fulfil specific applications based on many factors such as cure times and viscosity. Although experimentation with resins is common, in reality it may well be desirable to use CNTs as a reinforcing or conductive filler in a wide range of materials for multiple applications. Other groups have experimented with the use of many different polymers to create CNT composites. Kim et al. [151] used a similar technique to many others involving ultrasonification to disperse CNTs in a Poly (vinylidene fluoride), (PVDF). This meant that the samples contained CNTs in a randomly positioned orientation and it is likely that agglomeration occurred with increasing CNT content. The formed samples were tested mechanically using Dynamic Mechanical Analysis (DMA) in an attempt to record any change in the elastic modulus as a result of CNT loading. They found an increase in the modulus of just less than 40 % when the matrix was loaded with 1.0 wt% CNTs. Another report [152] focuses on the spinning of SWCNT-nylon composite fibres. They again use sonification to disperse the CNTs before mixing with molten nylon by mechanical stirring and further sonification. Once cured, the CNT-composite was 'chopped' before being loaded in to a custom spinneret and a nylon fibre, of 400 µm diameter, drawn through via

nitrogen driven extrusion. This process may lead to a degree of alignment of the CNTs in the direction of the extrusion although this is not confirmed. Importantly they report effective reinforcement through the use of CNTs as a filler, with Young modulus increasing by almost 200 % for a 1.5 wt% loading. They also observed that the tensile strength of the fibres was almost doubled although break strain decreased indicating that the fibres had been made 'stronger but less flexible' as a result of CNT reinforcement. Jia et al. [153] used poly (methyl methacrylate) as the matrix for their CNT composite samples. They dispersed the CNT in the monomer and used *in situ* polymerisation in order to create their composite samples. An important point is that the CNTs used were grown using a CVD technique, although little alignment occurred in this process, but before mixing they were ground resulting in the reduction in the length of the CNTs. It is likely that this shortening process causes the CNTs to be less likely to agglomerate but may alter their effectiveness as reinforcing fibres. When forming the polymer the group added a free radical initiator to the mixture in order to polymerise the composite samples. Interestingly they observed that the addition of the initiator to the mixture had little effect on the viscosity which dramatically increased when added to neat monomer. They also found that three times as much initiator was required to get the mixture to a mouldable viscosity and initiate curing when CNTs were present indicating that CNTs have a strong effect on the process. The samples they produced showed some increase, about 25 %, in the tensile strength of the samples with 7.0 wt% CNT and that higher loading of the composite, ~10 wt% resulted in very brittle samples.

Poly (ether ether ketone) (PEEK) CNT composites have also been produced, using a melt processing technique [154], that contained various morphologies of SWCNTs. These composites have been produced with SWCNTs weightings up to 1.0 wt% using SWCNTs which were produced by both the arc-discharge and laser ablation methods. The group also looked at the difference between samples loaded with as produced CNTs and CNTs that had been purified and processed. Their results show mild reinforcement of PEEK with the largest increase, approximately 27 %, in storage modulus being observed with 1.0 wt% Laser Ablation CNTs that had been processed prior to mixing. It was also observed that little reinforcement occurred when CNTs were not processed prior to mixing; this is likely due to inadequate dispersion of the longer tubes in the matrix resulting in agglomeration of the CNTs and weaknesses in the structure. It is likely that due to the processing of the CNTs involving high energy sonication that CNTs are shortened considerably thus aiding their dispersion in the matrix. Apart from these composites, many similar experiments have been carried out with other polymers although these were mostly done in processes that result in the random orientation of the CNTs within the matrix at relatively low, usually well below 10 wt%, CNT content. As a consequence of this the results are similar to those discussed and the composites show little or no mechanical

reinforcement as a result of the CNTs, although improvements in conductivity are often observed. Polymers that have also been used for CNT composites include poly (vinyl chloride) (PVC) [44], poly (vinyl alcohol) [70], poly (ethylene oxide) (PEO) [139], Polystyrene (PS) [126], and low density polyethylene (LDPE) [155] amongst many others.

In 2007 Sansom et al. [156] reported the ‘controlled partial embedding’ of CVD CNT forests into a thin silicone film. They used a spin coating technique to distribute a uniform thin film of 30 μm in thickness, after this the CNT forest, or ‘nanocarpet’, is partially dipped into the film using glass slides as supports and gravity to embed the CNTs. Once embedded the silicone composite was thermally cured before the careful removal of the silicon substrate used for the CNT growth. SEM analysis of the resulting sample clearly reveals the aligned CNTs anchored into the silicone layer with the rest, approximately 66 %, of the CNT exposed, as shown in **Figure 2.6**. This type of anchoring provides useful prospects for the possibility of layered composites as well as anchoring of CNT for exploiting their field emission properties in electrical applications. However despite the apparent control over the wetting process observed in these tests important observations are the short lengths of the CNTs used and the volume limited approach to the wetting process, thus meaning that scaling this method up may not be practical. In the same report the group also managed to anchor CNT forests at both ends leaving a matrix free section of CNT in between two layers of silicone composite. They also attempted some mechanical tensile testing of these samples, however they used an adhesive to attach the samples and during the testing this adhesive failed before the sample thus meaning they could only quote a greater than value for the tensile strength. This ‘anchoring strength’ is described in the report as being greater than or equal to 64.5kPa.

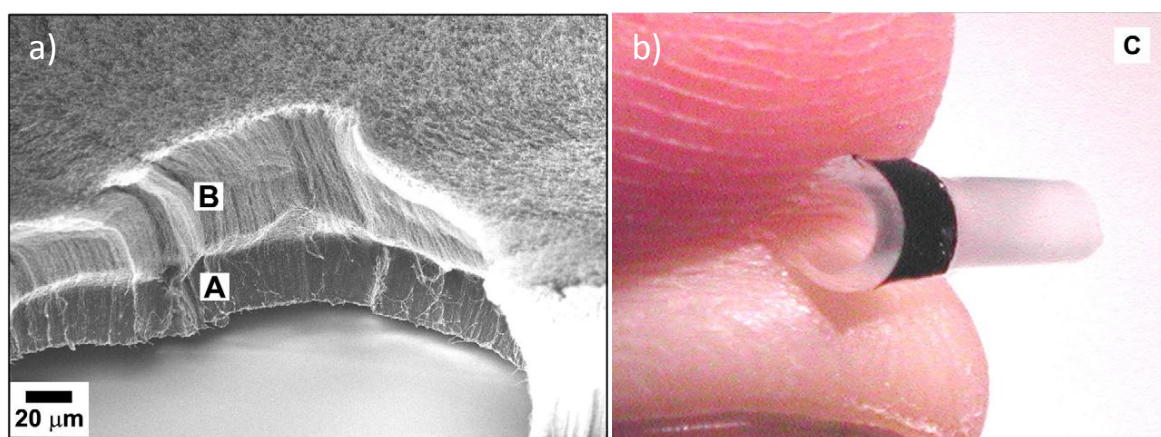


Figure 2.6: CNT forests partially embedded in silicone layers, a) an SEM image where the layer marked ‘A’ is embedded and ‘B’ is free, and b) an optical image of the sample. Images taken from [156]

2.4.4 Polymer Matrix-CNT interactions

Apart from the proper dispersion and alignment of CNT within a matrix in order to form effective composites, it is also important to consider the interactions between a single CNT and the surrounding polymer. These interactions are crucial in providing reinforcement to a polymer through the use of CNT as a filler material. Barber et al. [157] used Nishijima's technique for the attachment of a single CNT to an AFM tip [39] in order to test the 'nanotube-polymer interfacial strength'. They found that by heating a thin film, 300 nm, of a thermoplastic, polyethylene-butene, whilst performing AFM, that the CNT could be embedded into the polymer. A 'jump-in' of the tip was observed and the CNT is immersed about 10 nm into the polymer, this is thought to be caused by a wetting effect. The tip can be further pushed into the polymer by applying a load using the AFM to create an average immersion of 40 nm. From this work, by testing a multitude of depths and diameters, a fit to the relationship between pullout area and pullout force was calculated allowing the interfacial separation stress to be measured. This stress was established to be 47 MPa for these samples, whereas previous, non-CNT, fibre pull out tests, where weak interaction with the matrix exists usually result in stresses below 10 MPa, thus indicating that bonding between CNT and matrix is highly effective. They suggested this was likely because covalent bonding was occurring between the CNT and the matrix, most likely due to 'defects in the outer shell of the nanotube itself'.

Another example of experimenting with matrix-CNT interaction is shown by Garcia et al. [110] who looked at joining layers of a prepreg composite with an aligned CNT-epoxy layer. They showed a significant increase, up to three times, in the Mode II fracture toughness of the samples indicating that the CNTs had indeed penetrated the plies and effectively provided interlaminar reinforcement. SEM images of the fractured samples confirm that the CNTs penetrate at least 10 μm into each ply forming a so called 'nanostich' between the layers. This indicates a strong interaction between the matrix and CNTs, and helps to prevent delamination significantly which is crucial in laminated composites. In order to increase the strength of matrix-CNT interactions, it has been proposed that CNTs maybe functionalised, as discussed, by the covalent attachment of specific molecules in order to modify interactions with the polymer matrix. Gojny et al. [142] report the comparison of composites consisting of as grown CNT and amino functionalized CNT combined with epoxy. Their results show that the amino functionalized CNT composite shows approximately a 6 % improvement in Young modulus and a 3 % improvement in tensile strength when compared to an as grown CNT reinforced epoxy. They credit these improved properties to enhanced matrix-CNT interaction between the amino functionalised CNT and the epoxy matrix. Functionalisation has also been shown to improve mechanical properties by Geng et al [139], who report up to a 300 % increase in tensile

strength through the incorporation of fluorinated CNT in a PEO matrix. Others [152] have also used carboxylated CNT to improve matrix interactions with effective reinforcement of the matrix being observed, notably an increase in Young's modulus of 153 %. Dyke and Tour [158] synthesised functionalized SWCNT specifically tailored to interact strongly with the PDMS matrix they used in their samples. The covalently attached molecule contained a benzene ring, an acyl group and finished in a hydroxyl group. They believe this molecule will allow strong covalent bonding between the functionalised SWCNTs and the PDMS, with results showing a 300 % increase in yield strength but little change in the yield strain. This means that the CNT reinforcement did not make the samples brittle as seen in many other CNT composites [153].

2.4.5 Mechanical testing of CNT-Polymer composites

Other than the difficulties in the production of CNT-polymer composites there are also complications in accurately testing the mechanical properties of samples. Experiments that use various mixing methods to disperse CNTs randomly in a matrix lend themselves to traditional mechanical testing. This is due to the possibility of producing bulk samples in standard moulds used for testing polymers both in compression, and tensile testing. As discussed previously these composites with randomly orientated, and usually low wt%, CNTs appear to provide little reinforcement to the matrix overall, although useful improvement in the conductive nature of many polymers has been observed. These shortfalls are particularly apparent when considering the mechanical properties of the individual CNT and standard rule of mixtures models for fibre reinforced composite materials. The production of aligned CNT composites usually results in microscale samples being produced due to the lab scale of most CVD furnaces, despite their ability to be scaled up. Some of the largest lab grown aligned CVD-CNT forests are around 10x10 mm [26] in area and 2.5 mm [82] in length, where the dimension of most interest is the length which is often considerably less than 2.5 mm, although CVD processes are constantly being improved as previously discussed. Testing the strength and modulus of such a thin sample is practically difficult, particularly when a high level of accuracy is desired. A helpful tool in assessing these properties is dynamic mechanical analysis (DMA) as used by Wang et al. to measure mechanical properties of their thin film CNT-epoxy composite samples, [159] which can be used to assess changes in the mechanical properties of millimetre scale samples.

Another technique used by Garcia et al. [160] is nanoindentation, which they used to assess the hardness of small samples of aligned CNT composites. They report a 219 % increase in Young's modulus at 2 % CNT volume fraction whilst similar randomly orientated experiments [161] report only a change of 100 % maximum. Another technique to allow the mechanical testing of thin films of CNT-polymer composite is to use a layer by layer manufacturing method in order to build up a

composite that is thick enough to be tested using standard apparatus. Mamedov et al. [162] constructed SWCNT-Polyelectrolyte composites based on the layer by layer method. They constructed modified bilayer films, to increase interlayer interaction, with typically between 30 and 40 layers per sample and CNT weightings of up to 50%. Their results demonstrate remarkable increases in tensile strength with their samples showing ultimate tensile strengths of 220 ± 40 MPa, which is of the order of 'ultrahard ceramics and cements' such as silicon monocarbide, $T=300$ MPa. The tensile strength of their samples was also considerably higher than that of Carbon fibre composites for example polypropylene filled with 50 % carbon fibres has an ultimate tensile strength of 53 MPa. This result is particularly remarkable when considering they did not use aligned CNT forests, but created samples up to 1 μ m thick by the repeated dipping of a substrate into a SWCNT-polyelectrolyte solution. However SEM images do reveal that this may have aided alignment of the SWCNT in the 2-D plane due to the thickness of the films being less than the length of the CNT. Consequently the out of plane composite properties maybe lower and highly ordered CNT alignment in a single direction was not seen as shown with CVD CNT.

2.5 Additive Manufacturing of Polymer Composite Materials

2.5.1 Introduction to Additive Manufacturing

The emerging technology of additive manufacture (AM) has allowed the rapid prototyping of parts for use in many industries from biomedical to aerospace. AM has recently been defined by ASTM as the 'process of joining materials to make objects from 3D model data, usually layer by layer, as opposed to subtractive manufacturing methodologies, such as traditional machining'. **Figure 2.7** provides an example of current technology that has been used to create prototype polymer parts that have been used in industry. More recently improvements in these technologies has allowed the use of such parts in final products [163] extending the use of these technologies beyond the prototyping stage. Thus far the best mechanical performance of such parts is achieved through various systems focused around metal powder consolidation techniques such as Selective Laser Sintering/Melting (SLS/SLM) [164] and Three Dimensional Printing (3DP) [165]. Although AM of polymer parts has shown excellent morphology control with previously unachievable net shape, the mechanical properties of such parts are a long way from those observed in advanced composite materials such as Glass Reinforced Polymers (GRP), and Carbon Fibre Reinforced Polymers (CFRP), that are being increasingly used in advanced engineering application such as the aerospace industry. This said the latest range of polymer SLS technologies have now been employed using engineering

polymers such as polyetherketone (PEK) and polyetheretherketone (PEEK) [166], which have begun to solve some of the problems associated with polymer AM such as low glass transition temperatures that were previously troublesome.

In a bid to improve mechanical properties of AM polymer materials an influx of research has been conducted into the incorporation of various composite materials into polymer AM processes. The use of such composites spans a range of purposes, but can largely be divided into two categories; these are the use of an additional material to aid the manufacture process, such as the use of binders in 3DP [167], and the addition of a material to alter the physical properties of the final product. This review will focus on the later, looking at attempts which have been made to implement composite materials in the market leading AM methods, and the problems that arise usually as a result of the manufacture process.

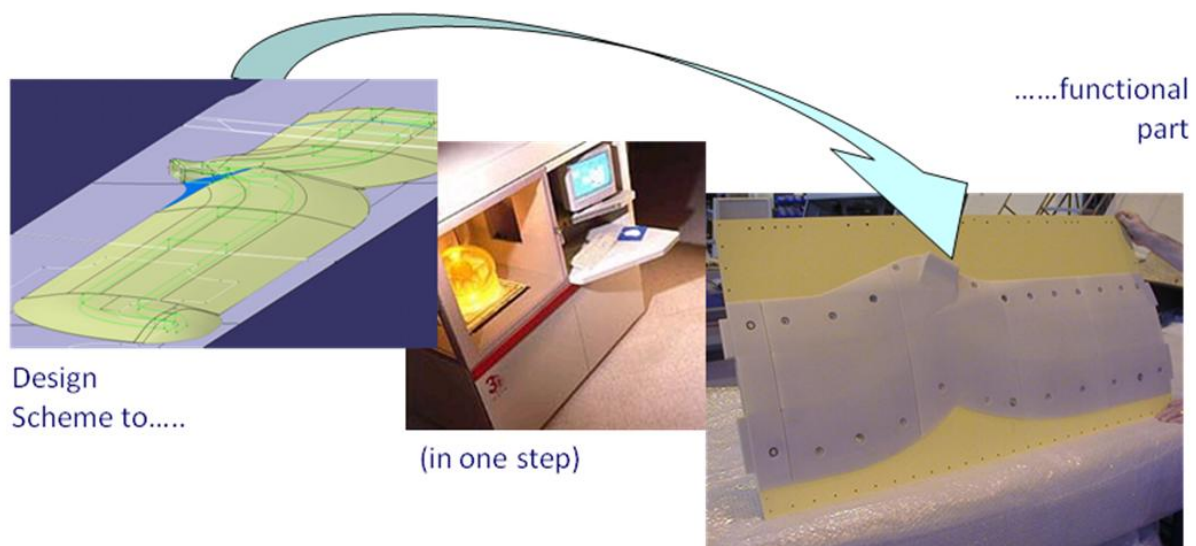


Figure 2.7: An example of AM in industrial use, note how the final part is constructed of several components as a result of a limit on build size in this process. (Images courtesy of EADS IW)

2.5.2 Selective Laser Sintering

Selective Laser Sintering (SLS) is one of the most widely used AM processes due to its commercial availability and ability to manufacture ready to use items which require little or no finishing processes [168]. The process relies on the sintering of a powder bed usually using laser radiation where the feed material is deposited layer by layer. Once a layer has been sintered, the bed then retracts in the z-axis before a further powder layer is deposited. The inclusion of composites in such a process thus lends itself to two potential mechanisms, the first being that both matrix and filler are

mixed in the required quantities prior to being used as the powder feed [169] and the second is that the feed powder is pre manufactured in a composite nature [13].

Several current focuses in composite materials for SLS have looked at using powder mixtures of various polymers and hydroxyapatite (HA), with a focus on biocompatibility, although improved mechanical properties have also been reported [170]. In other processes fillers have been coated with the matrix material prior to mixing in order to solve problems of agglomerations of the filler occurring within the matrix [171]. Effective results have been achieved by using nano scale alumina particles coated in polystyrene as reinforcements in a polystyrene matrix with increases in impact strength of 50 %. In conventional composites it is often desirable to use high aspect ratio fillers in order to provide the maximum possible reinforcement to the polymer matrix such as in CFRP panels. This often means that reinforcing fillers are of a fibrous nature. However in an SLS process this represents a practical challenge as the even distribution of the powder over the bed will be affected if the length of a fibre exceeds the thickness of an individual layer. This also leads to a problem where even when fibre fillers are included the reinforcement they provide is only intralayer, and no interlayer reinforcement exists. This said the use of fibre reinforcements has shown to be moderately effective and a selection of fibre/polymer powders are commercially available for use in SLS processes. These include polymer/glass fibre as well as polymer/‘short’ carbon fibre mixtures [13]. The current market leading commercially available SLS composite material is windformXT, a short CF reinforced polymer material that has shown much improved mechanical properties as well as thermal stability and is already in use in the advanced automotive industry [13].

2.5.3 Laser Engineered Net Shaping

Laser Engineered Net Shaping (LENS) is similar in principle to SLS, however rather than the feed material being supplied in the powder bed it is fed directly into the beam through the deposition head [172]. Although these similarities exist, much of the current research into LENS manufacturing is based around Metals and Metal Matrix Composites, which usually contain metal or ceramic filler such as Ti-TiC, which has been used to improve surface wear properties of Titanium components [173]. As there is little use of polymer materials in LENS processes this is all that will be mentioned in this review.

2.5.4 Three Dimensional Printing

Three Dimensional Printing (3DP) involves the deposition of a powder layer followed by the ‘printing’ of a binder to bond the powder in the desired structure [167]. In principle this means that almost all 3DP processes produce composite parts but the nature of these is to aid the production process

rather than improve the properties of the final material. In fact in some cases the binder is often removed and the final structure impregnated with a suitable material in order to overcome the problems of low density parts associated with the process [165]. 3DP is also well recognised as being one of the major AM technologies that allow for Functionally Graded Materials (FGM) where the properties of the material vary throughout the bulk, such as suggested by Jackson et al. [174].

However due to the nature of the 3DP process production of high performance polymer composite parts is challenging, largely owing to the porous structure and low accuracy of the systems compare to SLS techniques. In general the technology is recognised and credited for its rapid speed, low cost and versatility, and as a result has already found use in the pharmaceutical industry in tablet production where composition rather than mechanical performance is the highest priority [165].

2.5.5 Stereo Lithography

The process of Stereo-Lithography (SL) differs from those discussed thus far mainly through the use of a liquid feedstock as opposed to the powder based systems mentioned previously. Clearly this is of fundamental importance when considering methods of integrating composite materials into such a system. The basis of SL technology is to deposit a layer of 'liquid' photo curable polymer which can in turn be selectively cured using laser radiation of the required frequency. The use of composite materials in such a process thus involves the mixing of the filler into the feed polymer, and as a result challenges arise with regard to achieving uniform dispersion of the filler throughout the liquid layer [176]. Despite these problems SL remains the main process in which research has been carried out to investigate the effectiveness of fibre-reinforced composites in AM.

When using an SL process the dimensions of such fillers cannot exceed the thickness of the layer as deposited by the process; else an even bed between layers would not be achieved similarly to SLS. However fibre mats have been used in an SL process leading to improved mechanical properties but in doing so the complexity of the system is increased, which in turn increases the production time of components. Further problems arise with regard to the photo curing of the polymer as it is possible for fillers to absorb or reflect incoming radiation thus causing an uneven cure throughout each individual layer. This has led to the majority of successful SL composite experiments being based around glass based fillers which allow the transmission of UV radiation and resultantly an even cure of the polymer layer [177]. More recently the developments of systems using a paste rather than a liquid as the feedstock have begun to overcome some of these problems, particularly the achievement of uniform filler distribution [178]. Currently SL technology provides another leading

composite material within the industry, which is commercially known as 'bluestone' and has shown improvement in mechanical properties as well as significantly improved thermal stability [179].

2.5.6 Laminated Object Manufacture

Laminated Object Manufacture (LOM) uses a more simplistic approach than most other methods of AM manufacture where models are constructed using sheets of material that are pre-cut or cut in-situ and then bonded together to create a 3-D structure [1]. As a result of this manufacturing process most examples of this technique produce composite materials consisting of the sheet material and binder used to join the sheets. Progression of the use of composites in such technology generally relies on improvement of composite sheets that are suitable for use in such a process. As expected parts produced using such a process exhibit many of the problems associated with the base materials used such as delamination of layers, as the process is essentially an extension of the methods used for production of composite panels.

LOM processes have also been shown to be effective for production of FGMs as it is possible to change the sheet material between subsequent layers [180]. In theory it would be possible to use a vast range of materials allowing control of a wide range of physical properties throughout a sample, however including such a range into an automated process is likely to prove difficult. LOM structures can also be pyrolysed post construction in order to remove binders, or combust them, leaving behind a porous structure which can then be infiltrated to create a high density final composite structure [181].

2.5.7 Fused Deposition Modelling

Fused deposition modelling (FDM) is an AM process where solid feed material is fed directly into a heated deposition head and extruded into place. It often relies upon the use of viscous materials with low temperature melt allowing natural solidification of the material after deposition. As with several fore mentioned technologies the use of composites in such a process relies around development of suitable feedstock materials. It is important that such a material is still well suited to the production process as well as providing the desired properties required from the composite material in question. This means that many materials for FDM will require the addition of surfactants and plasticisers in order to ensure that the viscous properties of the material meet the requirements of the machine and particularly that the feed stock is capable of acting as a piston within the nozzle and forcing molten material to be extruded under load.

Masood and Song investigated the use of a Nylon/Iron feed stock material for FDM where 'fine' and 'coarse' Iron particles were included in the feedstock at varying concentrations [182]. They report

effective reinforcement of the Nylon with results suggesting that the larger Iron filler particles resulted in a greater improvement in tensile stress, and with finer fillers providing significant improvement in tensile strain at breaking. Other experiments involving composites and FDM have aimed to use ceramic based composites where a polymer binder is used in the feedstock to aid the FDM process. This polymer binder can then be 'burned out' and the subsequent porous parts are then sintered to increase material density and finally infiltrated with a material such as liquid Aluminium [183].

The use of fibre reinforced composites is troublesome as any reinforcements will have to pass through the extrusion head limiting the maximum aspect ratio of such reinforcements. Another problem is that often the inclusion of fibres in polymer composites often decreases the ductility of the material. This is a significant problem for FDM as the feed material is usually supplied as a spool and the process relies on the ability of the material to be wound, although such properties can often be improved by the addition of plasticisers as mentioned previously. Despite such problems effective reinforcement has been achieved in such a process using a polymer/short glass fibre composite material [184]. Results report improved tensile strengths of up to 100 % but also show that in order to provide such reinforcement careful selection of material composition is critical and that strengths in the stacking direction can be significantly reduced, particularly with certain compositions.

2.5.8 Nanocomposites

The use of nano materials in AM of polymer composite has already begun to be investigated by various groups. The use of nano fillers is desirable in AM processes as the nano dimensions of the filler can provide high aspect ratio reinforcement within a single layer, unlike traditional microscopic fillers. Initial findings from such studies show that reinforcement and property improvement are possible, but also highlight various problems that are often process related. Kim and Creasy investigated the feasibility of nylon 6/nano clay composites for SLS processing [185]. They find that the presence of nano particles inhibits the flow of the long chain polymer molecules increasing the viscosity of the melted material and as a result also inhibits the sintering process.

Other investigations into nanocomposites have focused around the area of Functionally Graded Materials (FGMs), with some work being carried out into gradient refractive index lenses (GRIN). This research looks at using a 3DP technology combined with ceramic nano fillers to allow production of flat lenses as opposed to traditional lens shapes and profiles by changing the refractive index throughout the material [186]. Other investigations have used Nylon/Nanosilica composites to

demonstrate FGM [187]. These experiments showed that SLS can indeed be used for FGM but did not show any significant increases in mechanical properties of the composite components.

Chu et al. developed a new process called the Nano Composite Deposition System (NCDS) [188], this system deposits a photo-curable polymer resin before machining to ensure a high level of accuracy on the millimetre scale. The process can use both neat resin and composite materials made by dispersing nano fillers within the matrix. In their study they use MWCNTs as well as hydroxyapatite particles. Results show that the composite materials show improved tensile strengths, with a 40 wt% HA composite showing almost a 1000 % improvement, the CNT composite however only showed a smaller improvement of around 10 % likely due to MWCNT agglomerating in the resin as seen in many other MWCNT composite experiments [142]. Mild improvements resulting from the inclusion of small amounts of MWCNT in resin have also been observed using a SL process. This process also reported problems arising from agglomeration of the MWCNT even with loading being as low as 0.025 % in the resin [176].

A final example of the use of nano materials in AM is shown using 3DP [189]. Although this process relies on the use of nano materials in post processing and is based around standard plaster 3DP. The results have shown that by taking a porous structure as produced by 3DP and impregnating it with an epoxy/Carbon Nano Fibre (CNF) mixture, a conductive component can be produced. During this process it became apparent that traditional nanocomposites problems still exist in AM processing, and without intense mechanical mixing of the resin agglomerations of CNF were abundant throughout the structures. Overcoming such issues may prove troublesome, particularly when considering Carbon based fillers as it is well known that such particles are likely to agglomerate quickly whilst in solution.

Despite such problems success has been achieved in using nanocomposites in AM, with the best example again being the commercially available 'bluestone' resin mixture for SL processing. Although the exact composition of the material is unknown due to its commercial nature, it is known that the material is mostly likely a resin containing nano ceramic fillers based on its insulating characteristics [179].

2.5.9 Conclusions

A brief review of the current progress of using polymer matrix composites in the various AM processes has been discussed. Thus far such composites have failed to achieve the properties of their traditionally manufactured counterparts although mild success has been shown and it is clear that much research is underway. It is apparent that the key factors in using such materials in AM

processes is often governed by the specific process itself, and as such it is difficult to provide specific solutions to problems that will cover the wide range of available AM technology. As a result many areas of such research focus primarily on specific processes and on development of composites that are suitable for use as unique feedstock materials.

Considering the above, it may be the case that in order to effectively introduce polymer composites to AM a different approach might be the best solution, and rather than tailoring materials to suit current technology, the tailoring of a machine to suit the materials might prove more effective. The use of nano materials as fillers may allow effective reinforcement without such involvement, as shown by 'bluestone', but it is clear that particularly in the field of carbon, and fibre based composites much work will be required before the desired level of reinforcement is observed.

Despite desired mechanical properties not being achieved it should be noted that FGMs have shown success in AM using composites. This includes both mechanical grading of material properties as well as other physical properties such as electrical conductivity. The addition of fillers has also helped to improve the thermal stability of AM polymers, and has led to the use of parts straight from the process in the advanced automotive industry, even in 'under bonnet' applications where temperatures exceed 100 °C [13]. Current literature shows that the development of polymer composite materials for AM is well underway and that these materials will help to take polymer AM away from prototyping and towards actual engineering application as is currently being observed in AM of metal components.

2.6 Strategies to Assemble Carbon Nanotube Composite Structures with Controlled Morphology through Additive Manufacture Methodologies

2.6.1 Introduction

Fibre reinforced composite materials are of vital importance in a wide range of engineering applications and have existed in various forms for thousands of years. Despite the use of such materials in large scale applications such as steel reinforced concrete in industrial structures the use of fibre composites in smaller scale advanced engineering application was hindered until the development of Glass Reinforced Plastics (GRPs) in the 1940s. GRPs illustrated that fibre reinforcement of polymer matrix materials could be used to make strong light weight composites that could rival metals for use in modern engineering applications and the desire to understand, improve, and development these materials created an entire field of research. Early mathematical models of fibre composites were developed in the form of the well known Rule of Mixtures equations that are still used today [190], [191]. These equations are based on theoretical and

experimental understanding of composite structures and classical mechanics of materials and can be used to calculate theoretical properties of fibre composites. Accurate estimation of composite behaviour using rule of mixture relies on knowing the mechanical properties of the fibres and their dimensions, the mechanical properties of the matrix, the volume fraction of each component, and the distribution and geometry of the fibres within the matrix, and is discussed further in **Chapter 4**. For now whilst considering composite assembly strategies only a qualitative understanding of the various techniques to improve fibre composite performance is of importance.

A composite material's mechanical properties are a function of those of its components, and as a result they are directly related, so unsurprisingly increases in fibre and matrix mechanical properties will result in improved composite performance. Consequently a great deal of research has been conducted into the development of advanced polymer matrices and fibre reinforcements. Other than the mechanical properties of these materials, further improvements in composite properties can be expected by improving the aspect ratio of the fibres allowing higher fibre volume fractions and improved fibre matrix interactions. Considering these factors it is clear why so many researchers have investigated CNT polymer composites, as CNTs fulfil both criteria of high aspect ratio and high strength fibres. Consequently CNTs seem like a logical progression of fibre composites however two crucial parameters in fibre composites, the dispersion and alignment of the fibres within the matrix, become difficult to control at the nanoscale. When considering fibre alignment in composites such as GRPs fibres are often randomly orientated or specifically aligned depending on application. 3-D randomly orientated fibre composites, where the fibres are evenly dispersed throughout the matrix in random orientations, are isotropic structures where the fibres provide equal reinforcement to the matrix in all directions. Such composites are often created by mechanical mixing of matrix and fibres before curing and are often similar to many of the methods attempted thus far when using CNTs in composite structures. As discussed in earlier, CNTs are difficult to effectively disperse in a polymer matrix when using traditional dispersion techniques such as ultrasonification and high shear mixing [65]. Consequently achieving an even distribution of CNTs throughout a matrix material is challenging even at low volume fractions and often composite samples contain fibre agglomerations and matrix rich regions causing weaknesses in the structure. In many applications it can also be desirable to align fibres within a matrix in order to provide greater levels of reinforcement in specific axes or planes. For example the use of woven Carbon Fibre (CF) sheets in Carbon Fibre Reinforced Polymer (CFRP) panels creates composites that are considerably stronger in the plane of the weave than perpendicular to it depending on the specific weave. Further more in some applications fibre composites are used to create rods where the fibres align in a single direction thus creating uniaxially aligned fibre composite structures. **Figure 2.8** illustrates a selection of possible fibre

composite microstructure morphologies although clearly many others are possible depending on specific fibres and processing methods. In summary, to create effective fibre composite structures accurate control of microstructure morphology is critical.

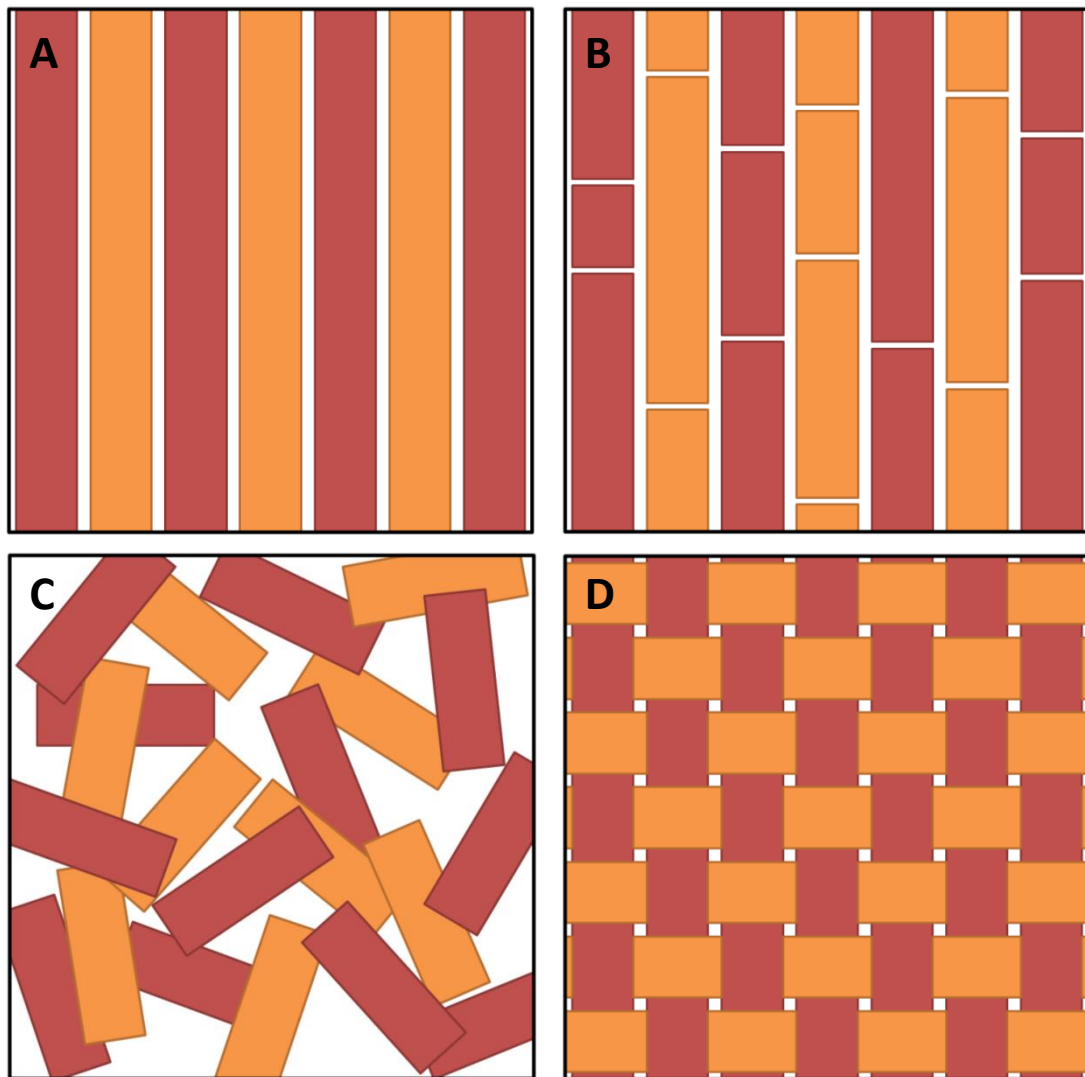


Figure 2.8: Examples of fibre orientations in fibre reinforced composites, A - Continuous Aligned, B - Discontinuous Aligned, C – Discontinuous Random, D – Woven [5]

Regarding the uniaxial alignment of CNTs in a matrix some recent results have published mechanical properties for CNT composite samples produced using VACNT forests where the CNTs remain dispersed and aligned after the manufacture process even at fibre volume fractions as high as 20 vol% [16]. These experiments illustrated that effective reinforcement could be achieved using CNTs as long as the CNTs remained evenly dispersed and aligned in the matrix. An important consideration is the size limitations that are inherent with these aligned and dispersed CNT

composite samples that exist as a result of the CNTs being produced as aligned forests in a CVD reactor. Consequently it is of interest to develop manufacture techniques that incorporate many different VACNT forest structures into a bulk composite. The realisation of the need for novel manufacture methods in order to introduce controlled morphology to create useful CNT composite materials can be well summarised by a quote from Professor Alan Windle. He states “..we need to make materials containing a high volume fraction of nanotubes which are both straight and very well aligned. It will mean an approach radically different to simply stirring (or sonicating) CNTs into a polymer melt or resin, as if they were the ultimate magic filler” [192]. Farmer et al. considered the problems associated with manufacturing composites using Additive Manufacturing (AM) and the problems associated with manufacturing CNT composites and proposed that both problems might be solved simultaneously [193]. These ideas evolve from attempting to extract the best parts from both the emerging technologies of Nanocomposites and AM as follows. Firstly any filler material for use in an AM process should not interfere with the manufacture process, and in the case of fibre reinforcements this often occurs when the length of the fibre reinforcements exceed, or are comparable to, the thickness of an individual layer. Usually this means that fibre reinforcements must be short, less than 100 µm in length, and as a result often the aspect ratio of such fibres is low leading to poor reinforcement when compared to traditional composites. However CNTs are of considerably smaller diameter, typically 2-25 nm, and as a result CNTs have the potential to reinforce AM materials whilst retaining a high aspect ratio [38]. AM processes are famous for allowing excellent topology control when creating structures and thus the introduction of CNTs at a microscale during such a process could create CNT composite samples with precisely controlled microstructures as well. Perhaps even more interesting is the idea that a process could be developed in which CNTs effectively ‘stitch’ individual layers together helping to combat any delamination effects that may occur as a result of the manufacturing process.

This chapter will describe and discuss “*Strategies to combine Nanocomposite and additive layer manufacturing techniques to build materials and structures simultaneously*”, as it is the manufacturing techniques proposed within these works that has provided much of the motivation for this project [194].

2.6.2 CNT Composite Additive Manufacture Approaches

In Additive Manufacture of composite materials there are two common approaches to introducing fibre reinforcements to the process depending on the specific technique in use. One method is to simply mix the filler and material before the process thus providing a composite feedstock, and the other is to introduce the filler and the matrix to the process separately. As AM covers a wide range

of techniques invariably there are a multitude of possibilities for introducing fibres to the process, but these two main ideas have been considered for introducing VACNTs to AM and will be discussed accordingly.

2.6.2.1 Filled Polymer Sintering Approach

The idea of filled polymer sintering pivots on the production of a suitable feedstock and in essence is based around current methods for additive manufacturing of thermoplastics. As typical powders for SLS processes have diameters of the order of 50 μm it could be possible to produce such powder particles which contain many aligned CNT reinforcements [195]. As discussed, the production of large scale aligned CNT composite samples is difficult, but success has been achieved with smaller samples that are produced from individual VACNT forest structures. Although small these samples are still considerably larger than a powder particle for SLS hence the production of such particles remains feasible despite being challenging on a large scale. Furthermore aligned CNT fibres have also been spun such as those synthesised by Li et al. directly from a CVD furnace [14], but perhaps more relevantly the electrospinning of polymer CNT composites for example in the works of Ko et al. [196]. They use an electrospinning process which uses electric charge to draw a thin jet from a CNT-polymer solution before curing and spooling. The fibres produced are continuous and contain up to 4 wt% SWCNTs and are between 50 and 100 nm in diameter and exhibit superior mechanical properties to those produced using neat polymer. Such fibres then have the potential to be finely chopped in order to produce a suitable feedstock for a CNT composite SLS process as described. Obviously if such a material was developed and used in a traditional SLS thermoplastic powder processes the result would be a well dispersed random fibre composite. Interestingly the multifunctional properties of CNTs may allow further manipulation of composite microstructure through their interactions with strong electromagnetic fields that could allow alignment of the CNTs and the composite powder respectively with the field or otherwise. Park et al. showed that alignment of SWCNTs in a polymer matrix was possible using an AC field for electrical applications suggesting that CNT might exhibit some polarity in specific electromagnetic fields [197]. In order to aid the alignment process, the application of an ultrasonic horn in order to agitate the powder particles will allow them to rotate freely within the field and only a small force will be required for alignment to occur. If alignment is controllable it would be possible to create uniaxially reinforced CNT polymer structures or even to vary the field throughout a build in order to create functionally graded composite structures. **Figure 2.9** illustrates a simplified schematic of the filled polymer approach.

This filled polymer particle approach provides an interesting strategy for the assembly of Nanocomposite materials in net shape. However as stated the development of the process hinges on the development of feedstock materials in particulate form and as a result is not directly addressed in detail as a part of this thesis.

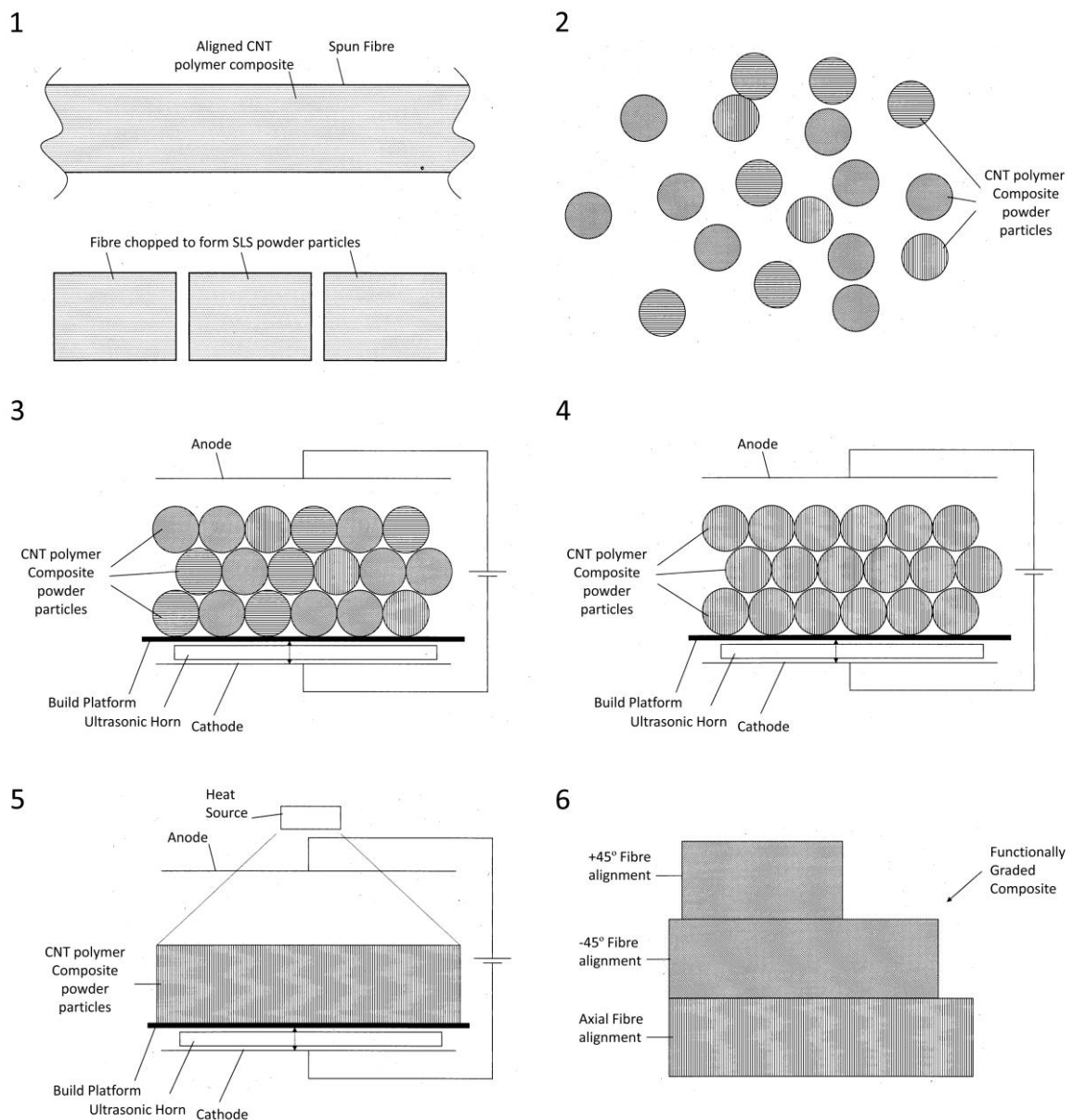


Figure 2.9: A simplified step by step schematic of the SLS strategy for CNT composite production, 1-Example CNT composite fibre and chopped CNT composite powder particles, 2-Examples of CNT-composite powder particles, 3-Aligned CNT composite powder particle distributed on an SLS build platform, 4-Bulk alignment of fluidised powder particles with an electromagnetic field, 5-Sintering of powder particle through heat, 6- Example of controlled fibre alignment in a bulk composite. Adapted from [195].

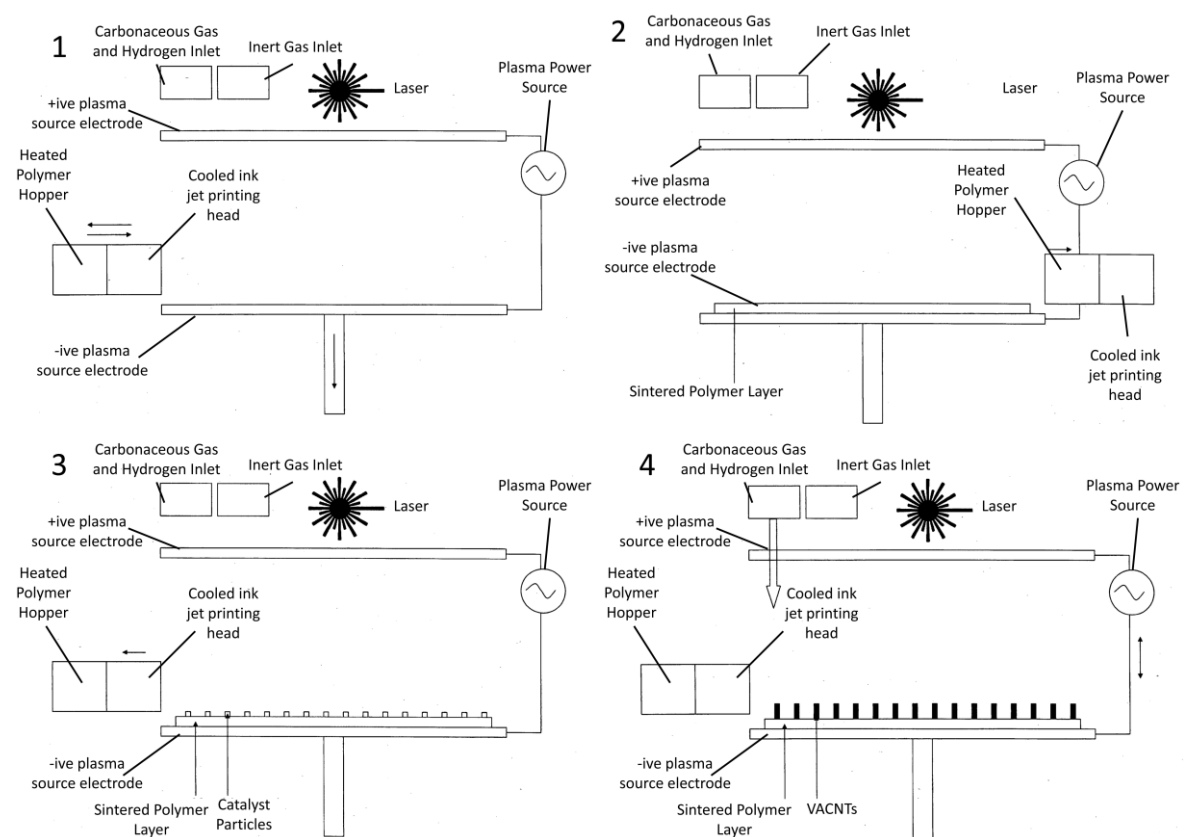
2.6.2.2 In-situ CNT introduction approach

In situ approaches to producing CNT composite structures through additive manufacture are based on introducing CNTs to a polymer during the AM process. Farmer et al. have suggested two main approaches to the process [193]. Both processes involve the introduction of CVD produced VACNT forests to a polymer matrix and are primarily based on SLS and SL methods of AM respectively.

2.6.2.2.1 In-situ CNT Growth

The in-situ CNT growth approach is to grow the CNT in-situ on each layer thus removing the need to manipulate the CNTs into the correct orientation and dispersion to provide effective reinforcement. Considering the many available methods of CNT synthesis a vast range of approaches to this strategy exist however perhaps the simplest and most appropriate is the use of a CVD process. As the CNTs would need to be produced inside of an ALM environment it is useful to produce CNTs at as lower temperature as possible, ideally less than 500 °C which is achievable using a plasma enhanced CVD (PECVD) process [107]. Producing CNTs at a lower temperature is critical as this method relies on depositing the catalyst directly onto the sintered layers and then growing CNT from the vapour phase in-situ via the introduction of a suitable flowing gas environment. Catalytic particles can be selectively deposited in a number of ways and the process will be dependent on the feedstock material in use, but could be simply printed in suspension similarly to the method employed by Ago et al [198]. They utilise a system where iron and cobalt nanoparticles are printed using a typical ink jet print head (IJP) to accurately deposit catalyst particles in any 2D shape or pattern, the particle can then be used to grown CNTs using a CVD technique. For this approach to be effective the catalytic PECVD growth of VACNTs onto a sintered feedstock layer is critical but far from the only key development required for the process. In order to provide intra layer reinforcement it will also be required that fibre reinforcements extend between layers, an accomplishment currently not achieved in AM polymer composite materials. This will involve the partial embedding of CNTs in to the layer through capillary driven wicking of the polymer into the VACNT forest structures. The Interactions between VACNT forest structures and fluids are highly complex and difficult to control and is discussed in depth later in **Chapters 4-6** of this work. A final point to consider is that ideally fibres would be interlocked with each other, and initially it was suggested individual CNTs might slide past each other, however further studies have revealed that although VACNTs forests appear very straight and aligned when viewed using low resolution SEM, they are in fact much more wavy and entangled when viewed individually thus making this approach unfeasible [193]. To counteract this problem it has been suggested that small microscale VACNT forests consisting of many VACNTs can be used instead and still provide effective reinforcement to the structure. By producing a CNT

composite in this fashion it may be possible to provide intra and inter layer aligned fibre reinforcement at a micro scale to an AM composite material. **Figure 2.10** illustrates a simplified schematic of an SLS process in which the VACNT reinforcements are grown in-situ from catalytic particles using CVD, note that the VACNTs in the schematic might represent individual CNTs or in fact small forests or pillars of VACNTs. A final point is that the PECVD may also be used to adjust the angle of alignment of the VACNTs as they are being produced by changing the angle of the build platform of direction of the plasma field, allowing further control of composite microstructure. For simplicity these details are not included in the schematic.



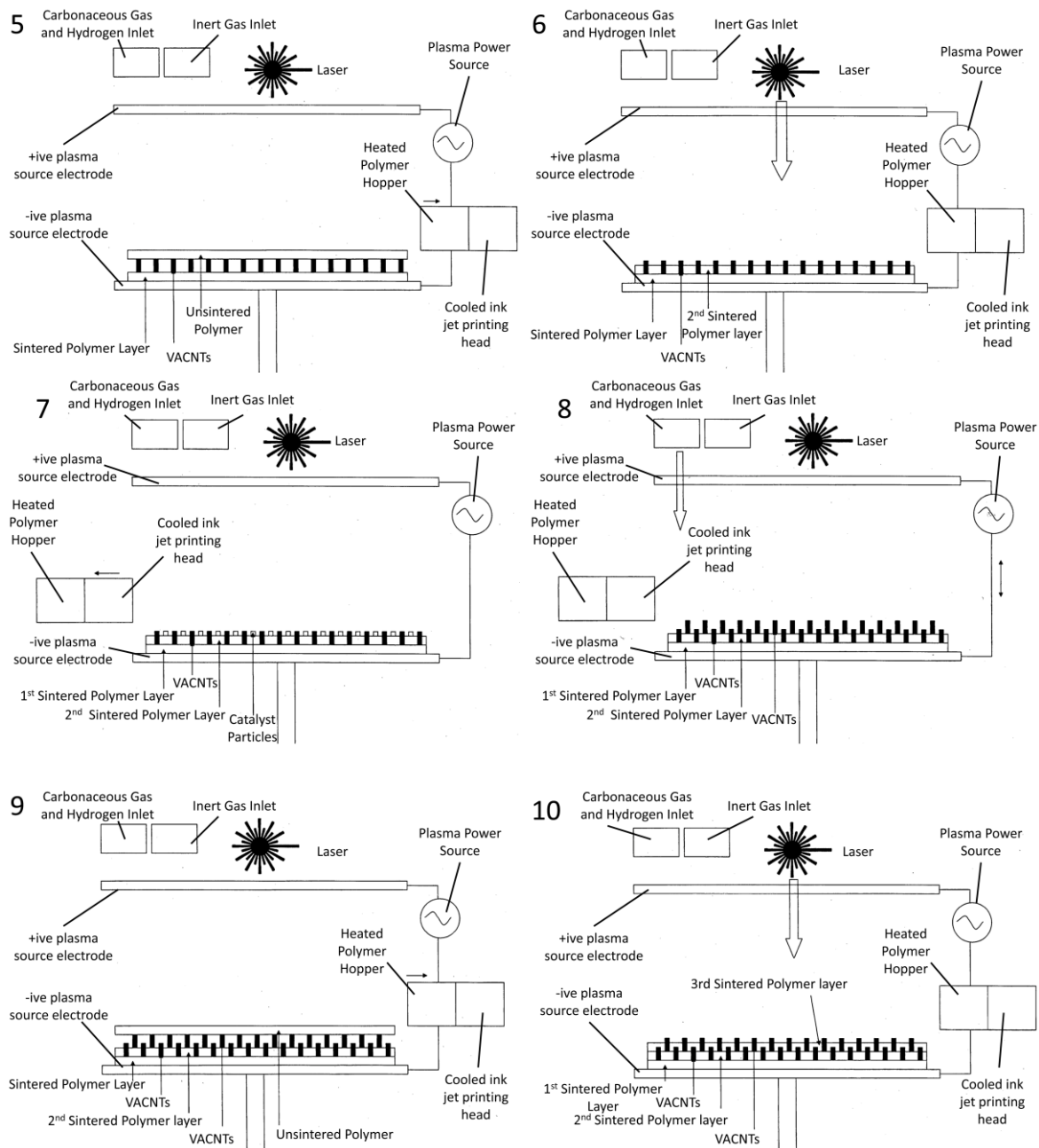
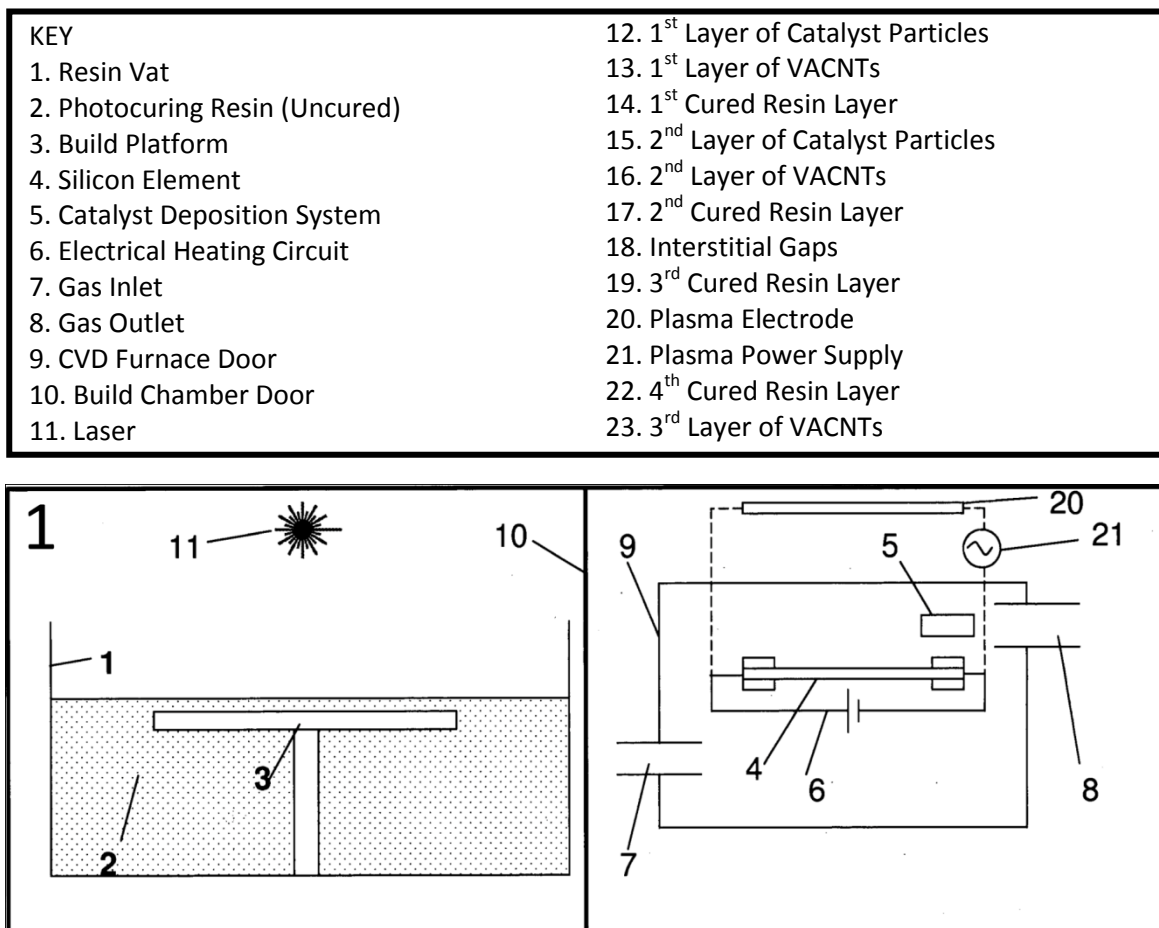


Figure 2.10: A simplified step by step schematic of the SLS strategy for in-situ CNT composite production, 1- General Schematic of the system, 2-A feed stock layer is deposited by the hopper and then laser sintered, 3- The printing head deposits a layer of catalytic particles, 4-Suitable Gases are introduced and PECVD VACNT growth occurs, 5-Another feedstock layer is deposited on top of the VACNTs, 6-The next layer is sintered leaving the VACNT partially embedded, 7-Another layer of catalytic particles is deposited, 8-PECVD VACNT growth, 9- Another feedstock layer is deposited, 10-Sintering of the next feedstock layer. Adapted from [199].

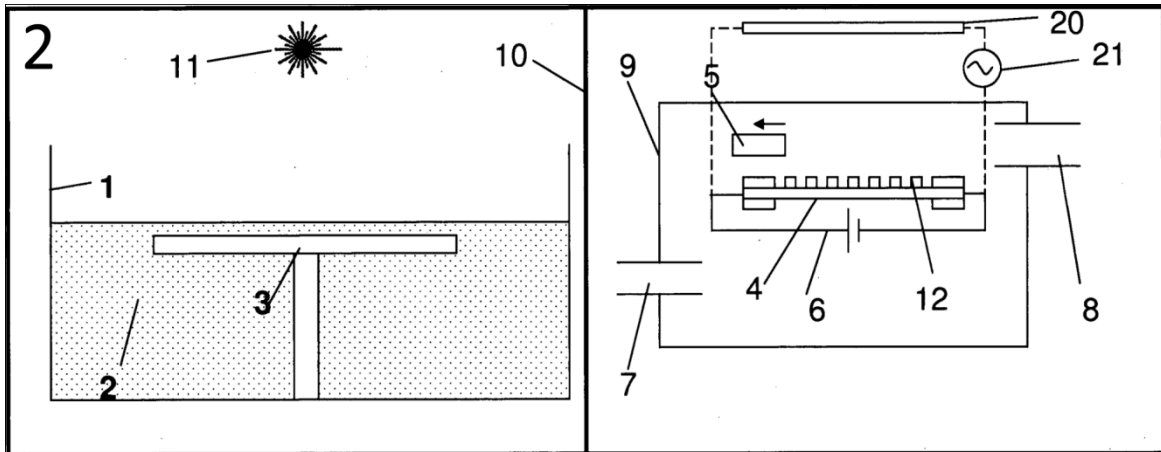
2.6.2.2.2 Detached Ex-situ CNT Growth

The detached ex-situ approach still relies on introducing CNTs in-situ within the process but the CNTs are produced in a separate CVD chamber attached to the AM build chamber. As a result the AM

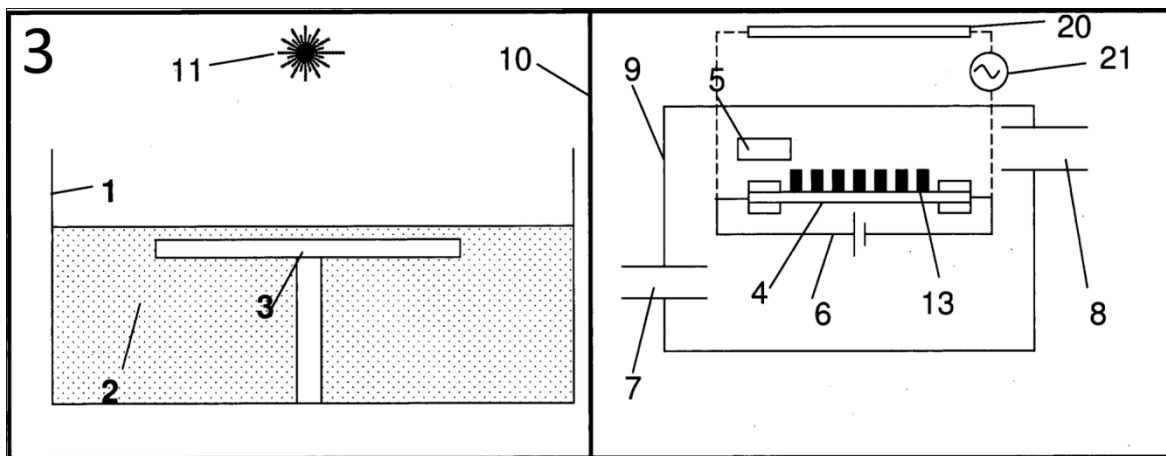
build environment and CNT growth environment remain separate allowing more control over each individual process. Consequently the need for expensive PECVD is removed and a standard low cost CVD process can be used at higher temperatures, although plasma enhancement can still be included if desired to improve VACNT growth. Using plasma could also allow control of the orientation or alignment angle of the VACNTs as discussed for the in situ approach if desired. Separation of the ALM and CVD chambers also eliminates the need to grow VACNTs onto polymer layers and a more effective traditional Silicon substrate with appropriate buffer layer can be used repeatedly. For such a process to be viable an SL process incorporating a carefully selected thermoset resin would be used. In this case the VACNTs will again have to be partially wetted through capillary effects in order to effectively reinforce the structure which is the greatest challenge in realising this process and is discussed in detail later in this thesis. The process is best described using a step by step schematic and this is detailed in **Figure 2.11**, once again the VACNT's may represent individual CNT or in fact small pillars of VACNTs.



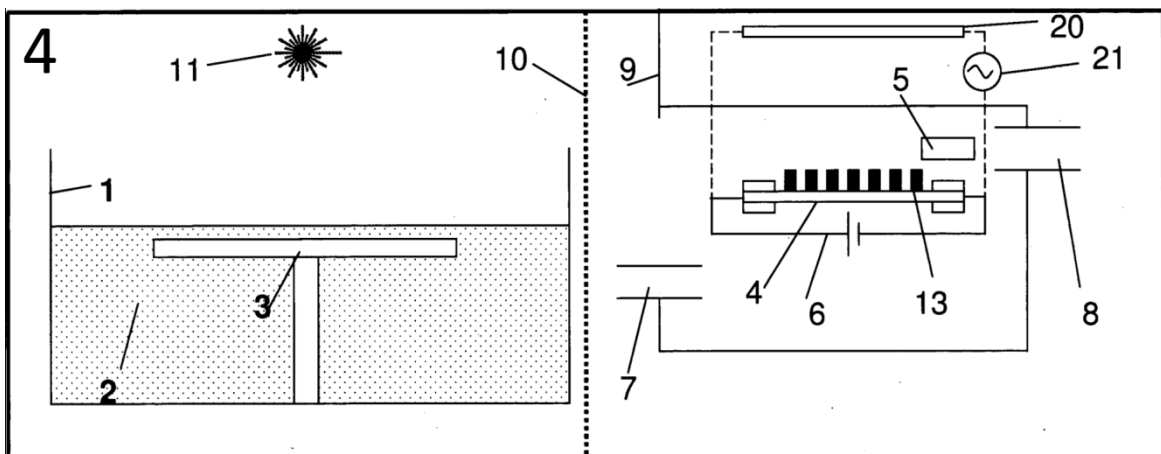
1-General Schematic of the system



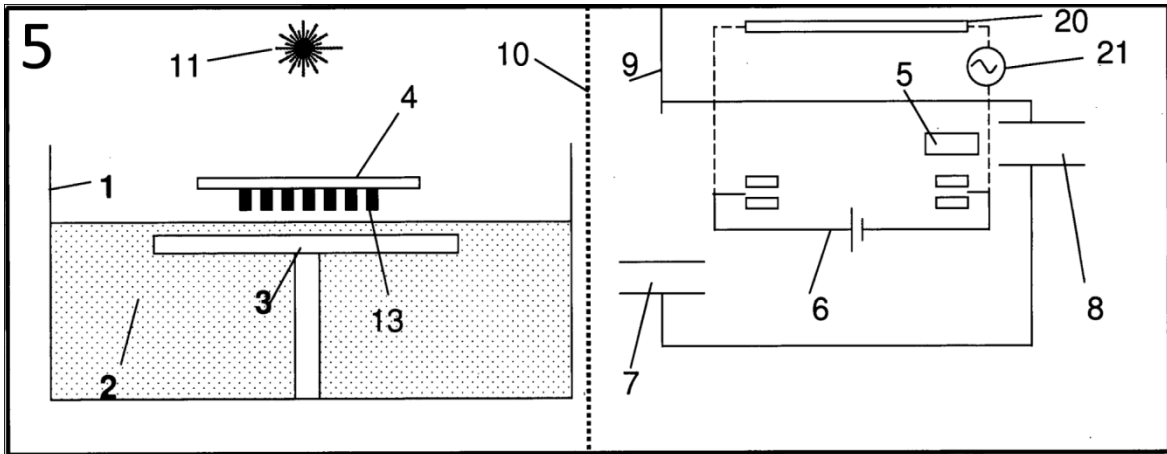
2-A catalyst layer is deposited in the CVD chamber (right hand side)



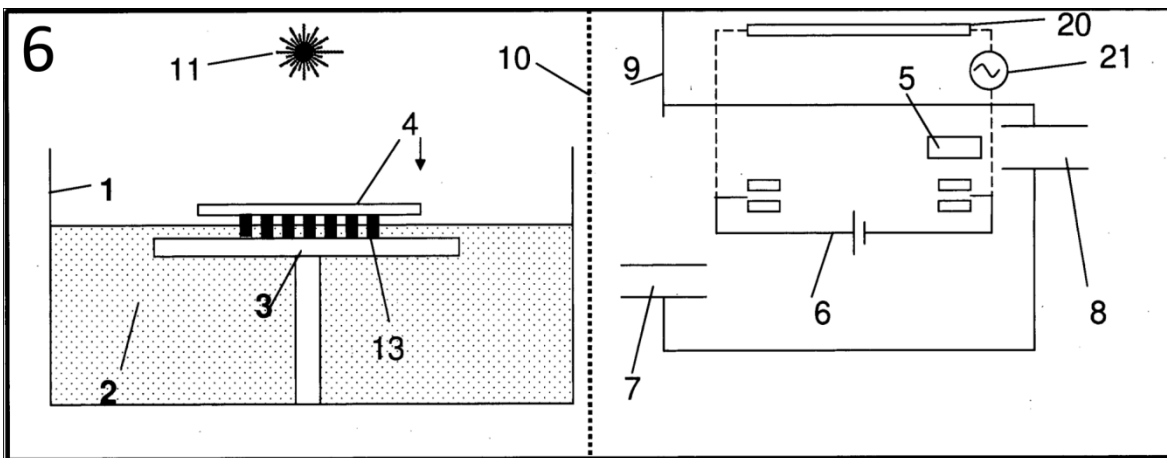
3-VACNTs are grown in the CVD chamber



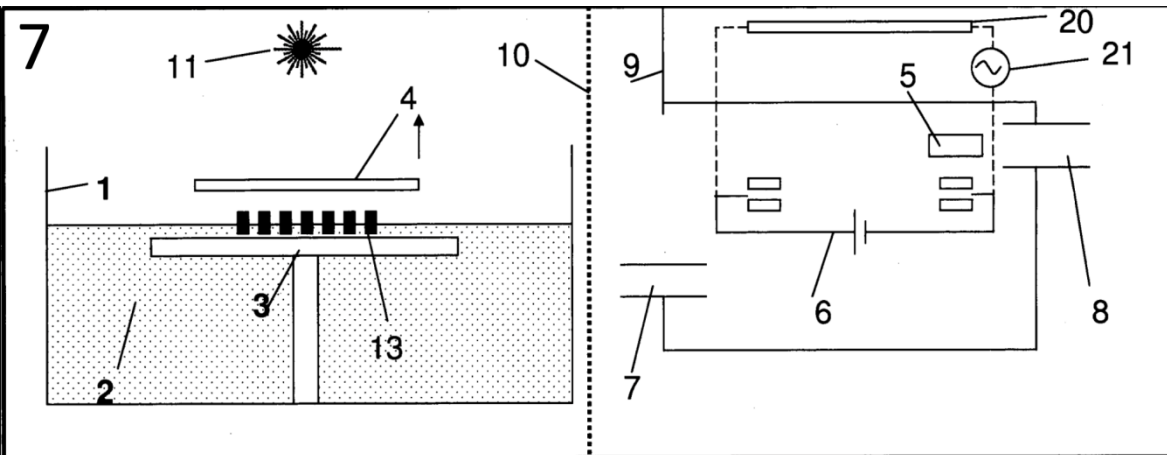
4-The CVD chamber and ALM chamber doors are opened



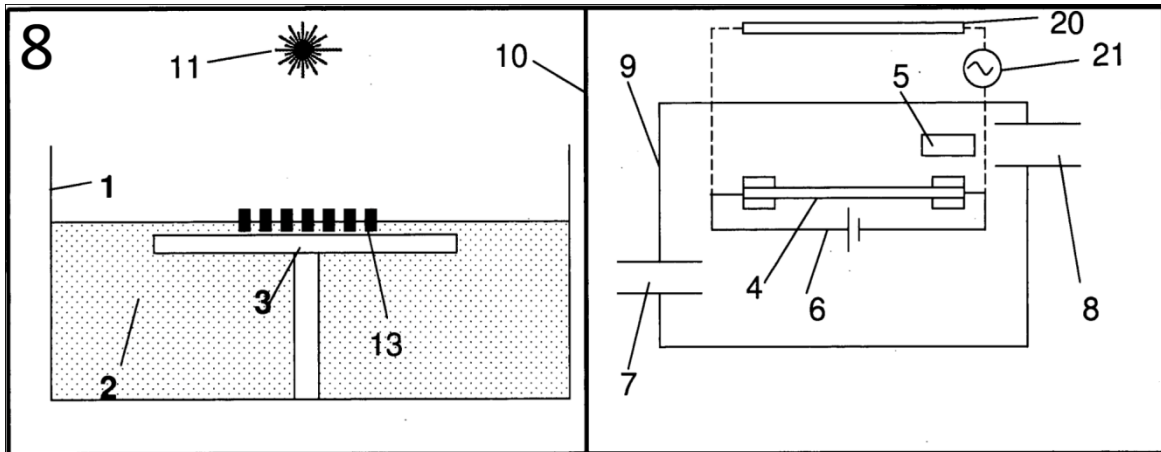
5-The VACNTs are transferred to the ALM chamber



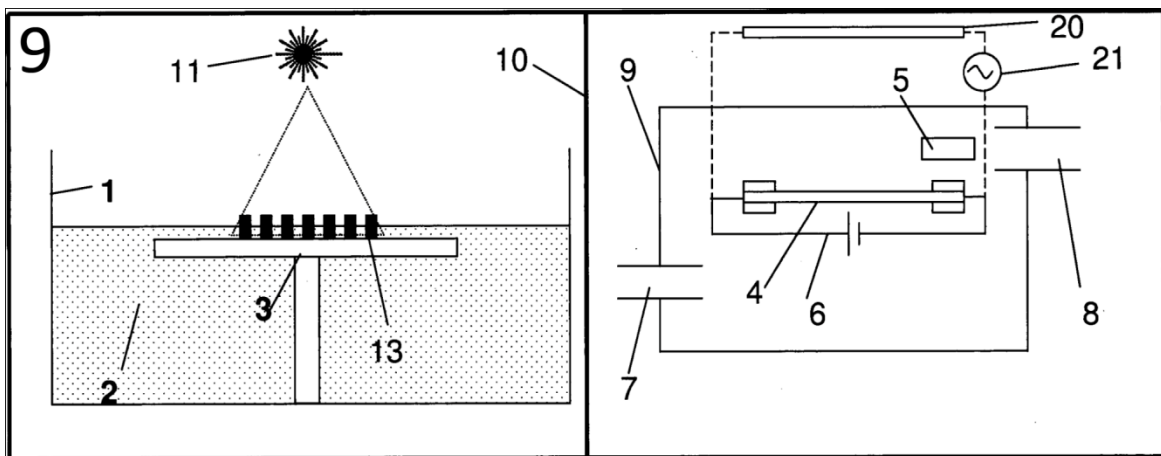
6-The VACNTs, still attached to the growth substrate, are dipped in the resin leaving them partially embedded



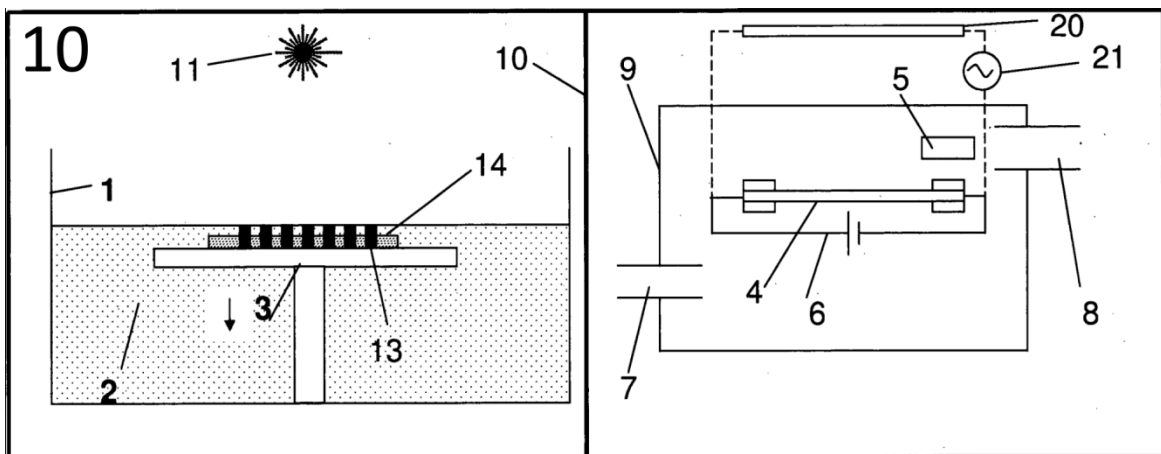
7-The growth substrate is removed from the VACNT forest



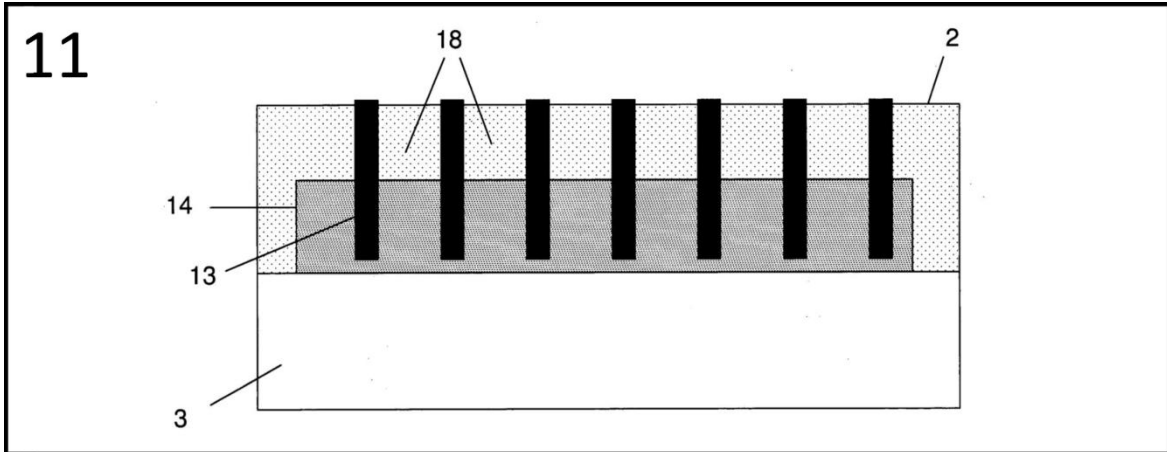
8- The growth substrate is returned to the CVD chamber



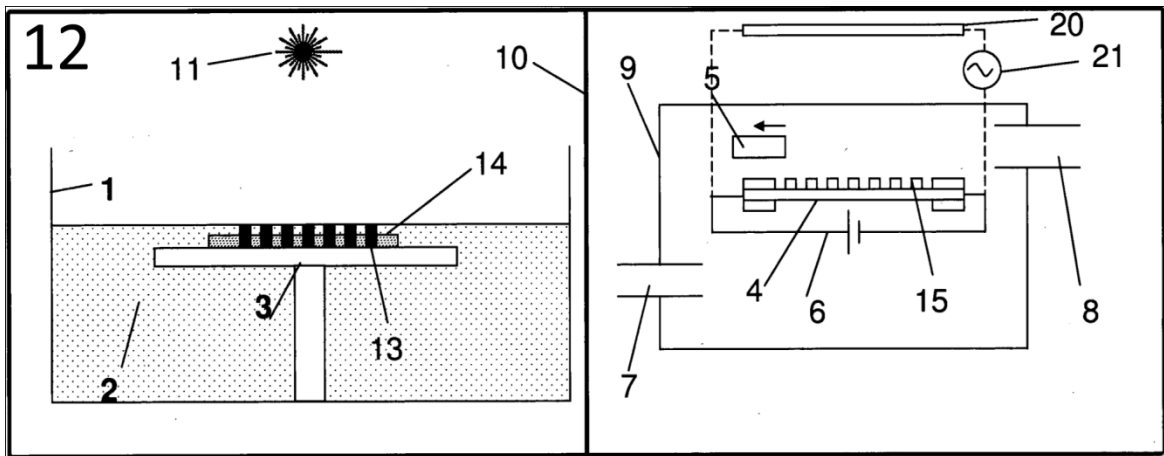
9-The 1st layer of resin is selectively cured using laser radiation



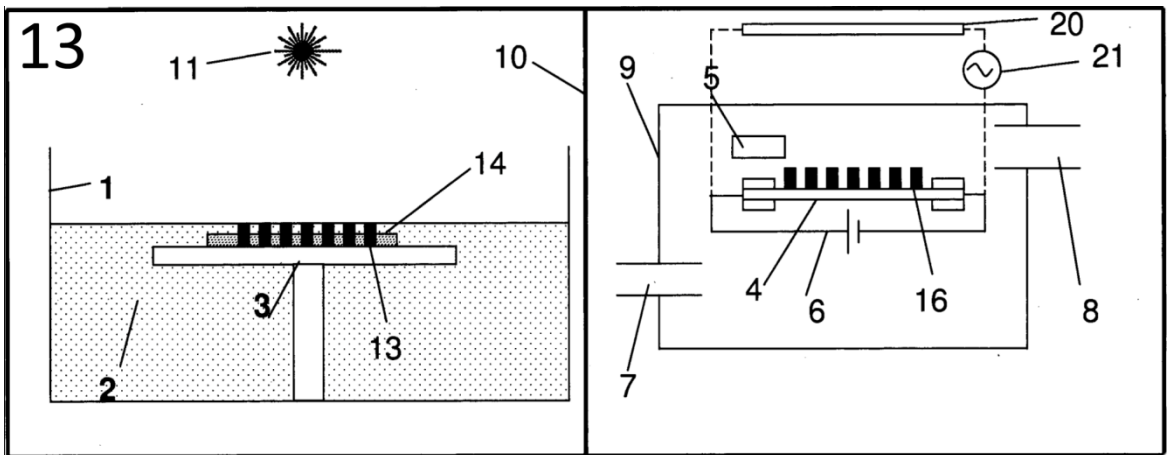
10-The build platform is lowered by the layer thickness



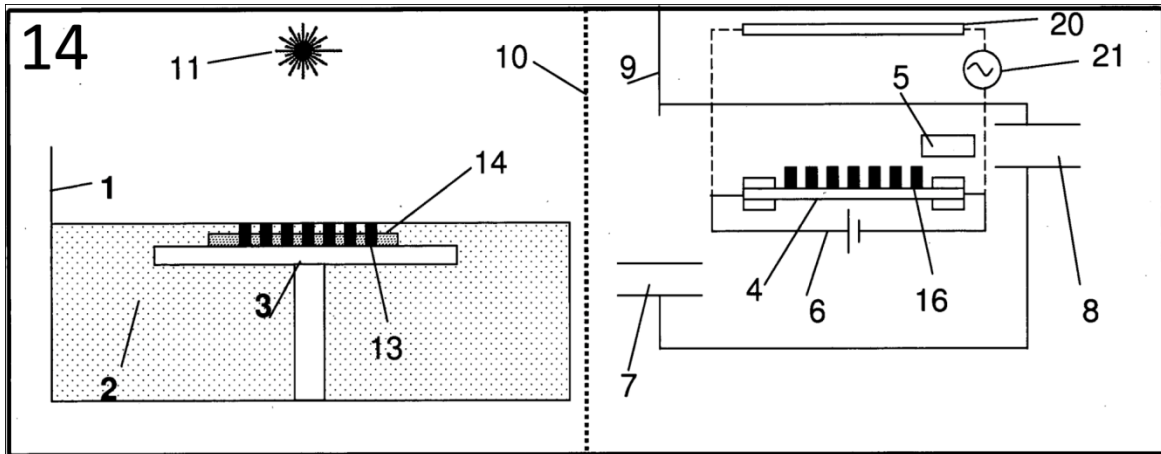
11-Zoomed in view of the present stage of composite production



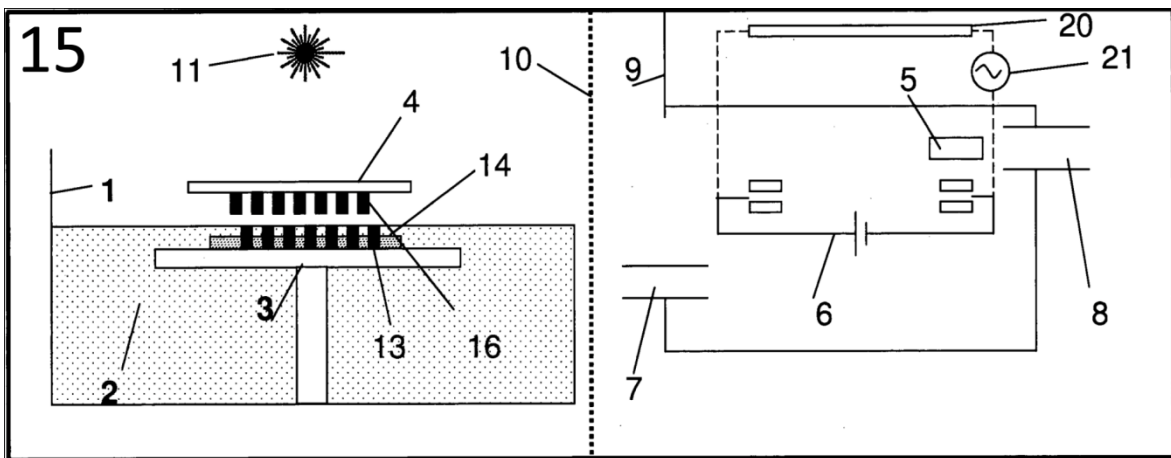
12-A second catalyst layer is deposited



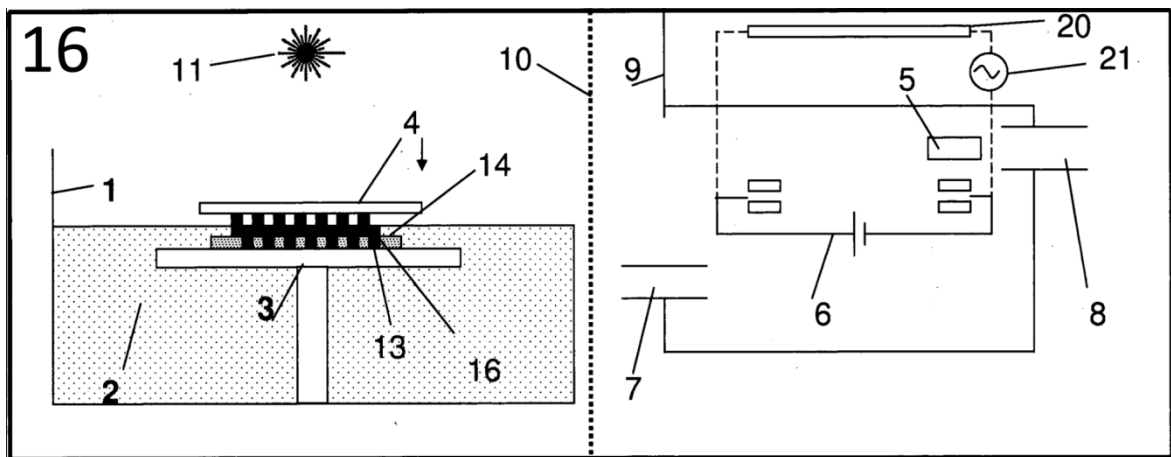
13-VACNTs are grown in the CVD chamber



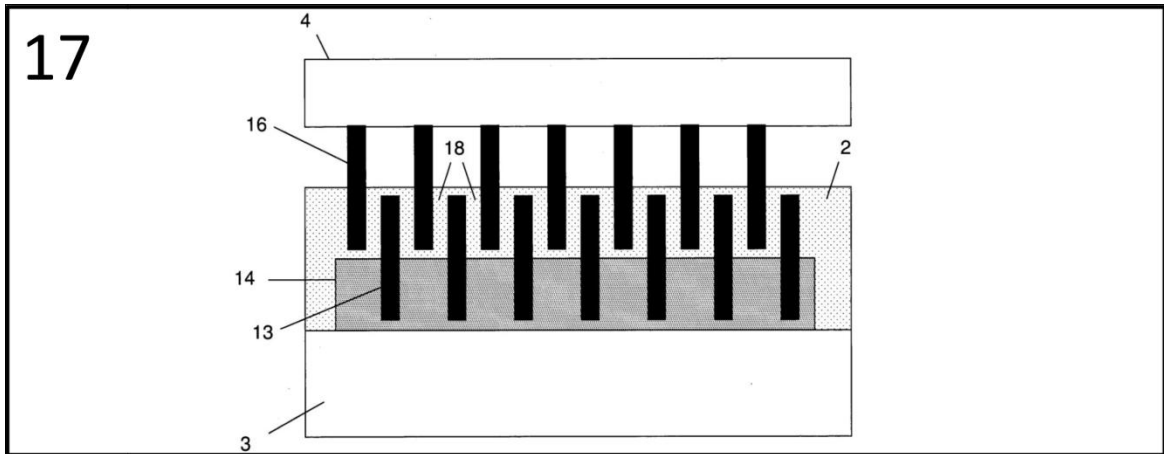
14- The CVD chamber and ALM chamber doors are opened



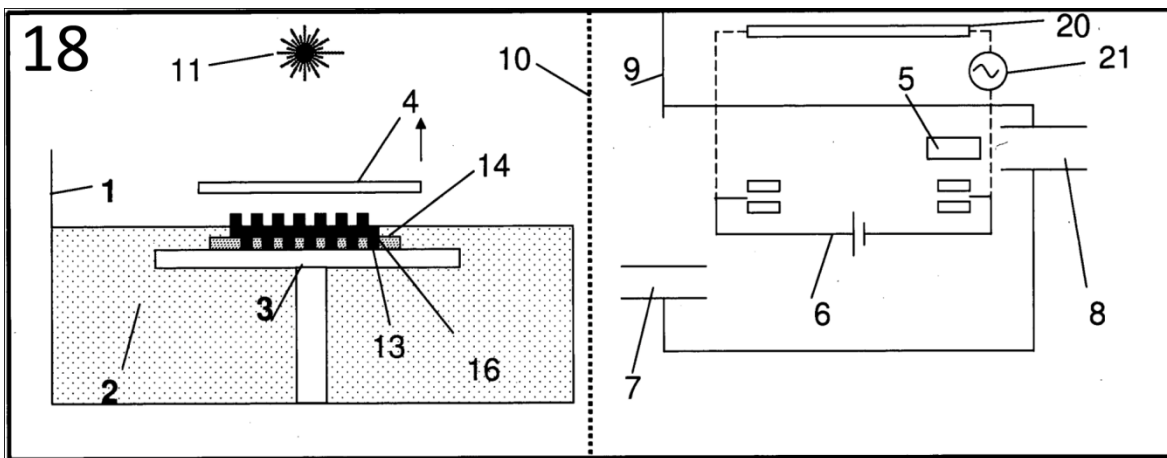
15-The 2nd VACNT layer is accurately positioned



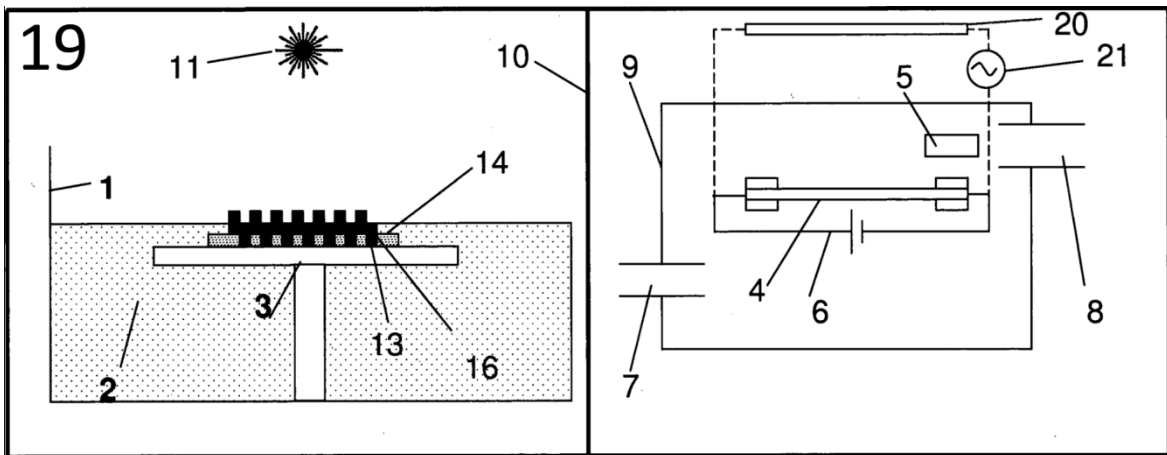
16-The second VACNT layer is dipped



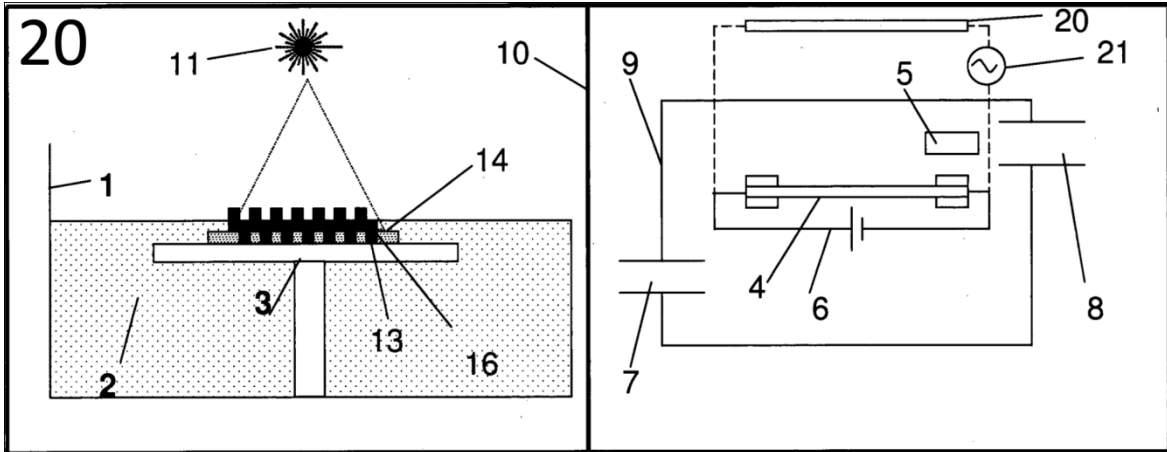
17- Zoomed in view of the present stage of composite production



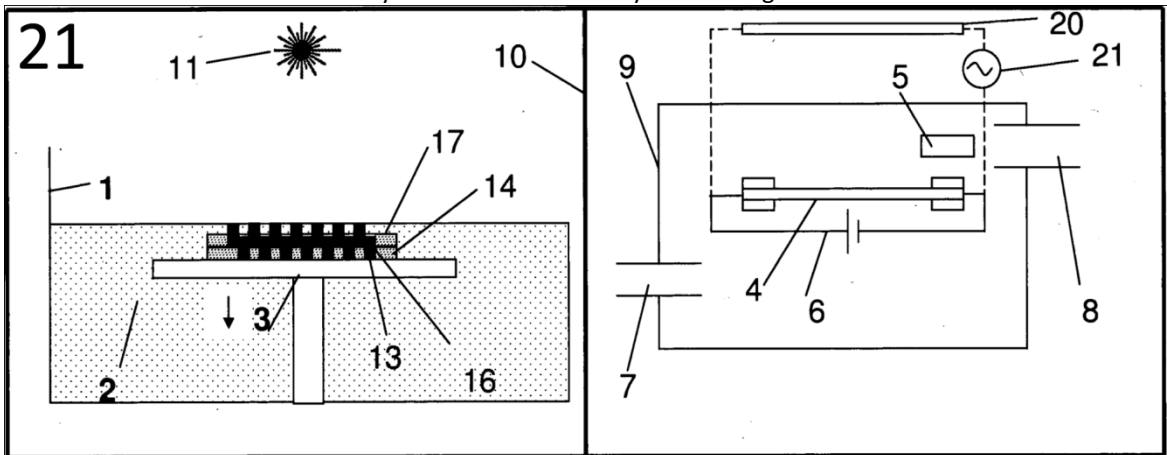
18- The growth substrate is removed from the VACNT



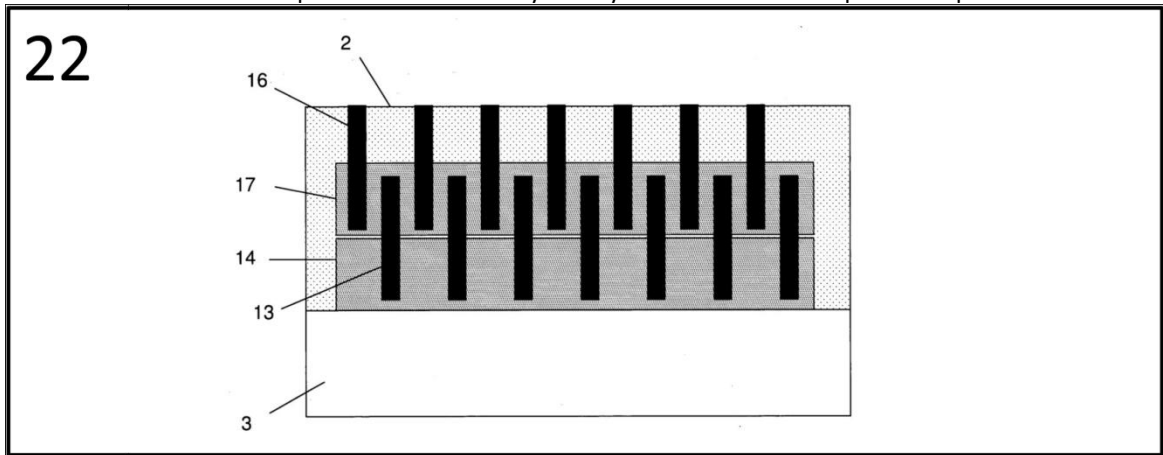
19- The growth substrate is returned to the CVD chamber



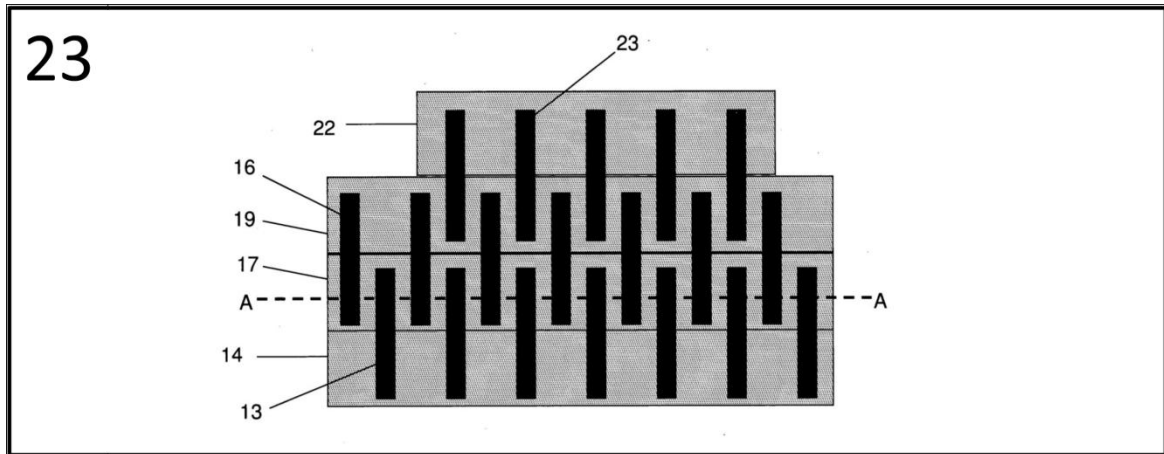
20- The 2nd layer of resin is selectively cured using laser radiation



21- The build platform is lowered by the layer thickness and the process repeats



22- Zoomed in view of the present stage of composite production microstructure with 3 layers.



23-Example of VACNT composite microstructure with 3 layers

Figure 2.11: A simplified step by step schematic of the SL strategy for detached ex-situ CNT composite production, Adapted from [200].

2.6.3 VACNT Forest Patterning and Net Shape

The methods detailed previously aim to use AM techniques to build CNT-composite materials at a micrometer scale allowing accurate control over composite microstructure. In doing so it is hoped that effective reinforcement using VACNTs will be achieved and many current difficulties in CNT composite manufacture overcome. However as well as solving CNT composite manufacture problems, it is also important that if achievable these processes will incorporate the benefits of AM processing as well, allowing the accurate control of the net shape of CNT composite parts. This point is not made especially clear in the previous schematics in order to increase their clarity but can be included in such systems in similar methods to current technologies.

In the case of the filled polymer approach no further complexity is required as the sintering process is laser controlled and the CNTs are already present within the feedstock. This means the path of the laser can be calculated from 3D model data for each individual layer thus producing a composite part in net shape in the same approach as current technologies. When the CNTs are manufactured during the process further complication arise as CNTs are only required in areas where the feedstock material will be solidified through sintering or photo curing. The ability to pattern catalysts for CVD growth of VACNTs has been mention previously and can also be employed in this instance to build reinforced structures in net shape. In the in-situ CNT growth method the catalyst can simply be patterned by printing the catalyst suspension at the required resolution directly onto the previous consolidated feedstock layer. The printer head can be programmed according to the 3D model data in an identical fashion to the laser for each individual layer and then VACNTs will only grow from

these catalytic sites when CVD is initiated. The same process can be applied when producing CNTs in a separate chamber as in the later case described, however different methods of catalyst production are also viable options such as patterned electron beam deposition. Using electron beam deposition is known to produce more accurate catalytic films that can be used to grow taller VACNT structures with higher aspect ratios that could be beneficial [82]. In contrast, electron beam evaporation is an energy intensive process, and VACNT structures can grow from catalysts deposited from suspension thus ultimately this may be the fastest and most cost effective solution.

2.6.4 Summary

The strategies discussed in this chapter present a selection of methods for incorporating CNT composites into AM processes in order to produce structures that are effectively reinforced at a macroscale using these nanoscale fibres. It is clear that although these strategies present some interesting ideas, further understanding of the interactions between VACNT forests and fluid polymers is required. The capillary driven wetting of VACNTs with fluid polymers is currently not well understood and precise control of this process is required to build composite structures in this fashion. It is the feasibility of these approaches that provides inspiration for many of the investigations carried out within this work although an understanding of CNT and fluid polymer interactions may have many more applications across many scientific fields.

Chapter 3

Synthesis of Vertically Aligned Carbon Nanotubes using the Sabretube Chemical Vapour Deposition System

3.1 Introduction

Synthesis of CNTs has been the subject of intensive research since the first discovery of these intriguing new carbon allotropes. As discussed a vast range of synthesis techniques have been investigated with varying levels of success when considering key manufacturing parameters such as CNT quality, and process efficiency. When considering aligned composites the use of CVD to produce ordered self organised forests of aligned CNTs is particularly appealing. Indeed CVD production of CNTs is the subject of much ongoing research to develop effective and efficient CNT synthesis as well as being responsible for the production of some of the most extreme CNT to date [36]. For example individual CNTs that stretch to over 15 cm in length have been synthesised by Wang et al. using a modified CVD production process [36]. CVD has also shown potential to allow accurate control over various properties of synthesised CNTs include their height, diameter, and number of walls amongst others [201]. During these studies a novel CVD furnace system known as the ‘Sabretube’ is utilised. This desktop system was originally designed by Anastasios John Hart whilst working at the Massachusetts Institute of Technology (MIT) [202]. This novel approach to the CVD process provides an ideal lab scale production facility which allows the accurate adjustment of various parameters independently of each other as well as in-situ monitoring of the process. A detailed discussion and explanation of the controllable variables will be discussed later in this chapter.

Despite much success in CVD production of CNTs across the field of research using many different furnace systems the specifics of the process remain complex and a great diversity in results have been observed. In general there are two main areas of consideration when explaining these observations, the first is the precise CVD process in use including, the equipment, the condition of the equipment, and the precise parameters used in the system, and the second is the catalyst employed. In many works the catalyst is fine tuned to fit the individual process, and often precise catalyst production is critical in achieving high yields of useful CNTs. Although a vast range of catalysts have been used to produce CNTs in CVD processes the most common and successful methods have involved using transition metal catalysts such as iron or cobalt [103]. As well as

different materials choices being available the form of the catalyst is known to be critical in reliable CVD production. Catalyst structures range from bulk catalysts to thin films deposited on various substrates, with the later providing a vast scope of possibilities considering the range of film deposition techniques that are currently available. Such techniques include the evaporation of deposited suspensions containing catalysts particles as well as precise deposition techniques such as sputter coating [203]. In this work a method of electron beam evaporation, similar to that used by many groups and inspired by works conducted at MIT is employed and precise details of catalyst manufacture are detailed in due course.

This chapter details the precise CVD methods of VACNT synthesis that have been utilised throughout these works including the optimisation process that was conducted in order to produce the largest VACNT forests possible using the available facilities.

3.2 Production of Catalysts for use in ‘Sabretube’ CVD Processes

The Sabretube CVD furnace has been designed specifically for use with catalysts that have been deposited onto silicon substrates, primarily for growth of VACNT forests at a lab scale. Silicon substrates make an ideal choice for catalyst substrates for many reasons but perhaps the most important of these are their thermal stability and relatively high thermal conductivity of $149 \text{ Wm}^{-1}\text{K}^{-1}$. As well as excellent thermal properties silicon wafers also provide extremely smooth surfaces when polished and can be cut to required sizes simply using diamond scribes or other diamond cutting tools. These properties that make silicon substrates ideal for use in CVD environments also make them ideal substrates for thin film deposition processes, and they are often the choice of material for thin film deposition substrates. Although abundant in compound forms, refinement of silicon to levels that are pure enough for research and industrial applications is an energy intensive process which drives up the cost of silicon wafers that are cut from large monocrystalline silicon ingots often produced using the Czochralski process [204]. Although expensive the catalytic nature of the CVD process provides a means for reuse of silicon substrates and although substrate recycling is not often practiced at a lab scale it is a commercially viable option when considering mass CVD production of VACNTs or indeed an AM process as discussed in **Chapter 2**.

In their works based on the Sabretube system Meshot and Hart discusses effective catalyst structures at depth and recommend a layered thin film structure produced using electron beam evaporation [26]. Similar structures have been used throughout the literature to produce well aligned CNT forests of up to several millimetres in height, although variations in catalyst film thickness and production methods are often reported. As this work employs the use of a Sabretube

system experiments were conducted to replicate the catalyst used in MIT's procedure, where a layered catalyst consisting of an oxidised silicon wafer coated with a buffer layer of Al_2O_3 followed by a catalyst layer of Fe are deposited using electron beam evaporation. A schematic of the catalyst structure is illustrated in **Figure 3.1**, where the silicon wafers are purchased pre-oxidised and the SiO_2 layer has been grown thermally via dry oxidation in a commercial process.

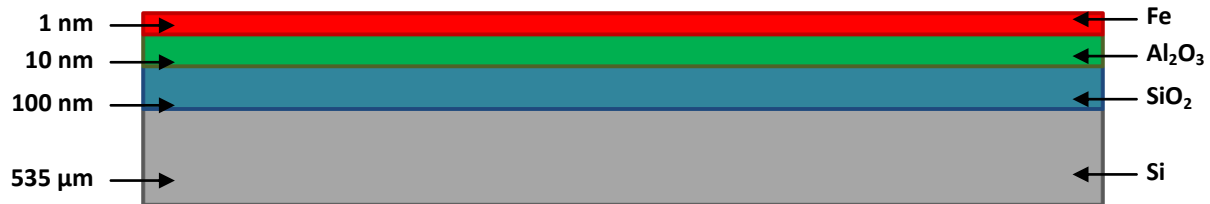


Figure 3.1: Schematic of the suggested catalyst structure used in much of MIT's work with the Sabretube system, not to scale.

Various publications from MIT suggest that the ideal thicknesses of the buffer and catalyst layer are 10 nm and 1 nm respectively, as shown above, for the Sabretube system although fine tuning of the catalyst is often required for specific furnaces and processes [98]. Consequently a series of experiments were undertaken to investigate the most effective catalyst for use in the system installed at the University of Exeter. Thin film deposition substrates were cut from type N doped silicon wafers of 525 μm thickness that were thermally oxidised with a 100 nm film of SiO_2 and supplied by IDB Technologies [205]. Electron beam evaporation depositions were conducted using an Edwards's electron beam evaporation system that was recently retrofitted with a FTM-2400 quartz crystal film thickness monitor (FTM) supplied by Kurt J. Lesker and pictured in **Figure 3.2** with the evaporator itself. The FTM allows precise control and stabilisation of the film deposition rate at rates as low as $\sim 0.1 \text{ \AA/s}$ and at accuracies approaching $\sim 0.01 \text{ \AA/s}$. Such high degrees of accuracy are crucial when constructing catalysts as film thicknesses need to be accurate at the nanoscale in order to achieve reliable and repeatable VACNT growth. Evaporations of both buffer and catalyst layers were conducted during a single pump down cycle at pressures below 5×10^{-6} torr. A High Tension voltage of 4.2 kV was used to accelerate the incident electron beam sourced from a molybdenum ring element carrying a filament current of 20-27 A during the evaporation. Although the catalyst layer is responsible for initiating CNT growth the importance of the buffer layer has also been discussed and investigated by many and has been shown to vastly improve the quality of VACNT structures grown using this technique when compared to substrates without a buffer layer for reasons discussed later [206]. Although a buffer layer is frequently used questions have been raised concerning the significance of the thickness and constitution of such a layer with some reporting

considerable effects on the CVD process when varying the thickness of the buffer layer by only relatively small amounts [101]. Throughout this work a buffer layer thickness of 30 nm of Al_2O_3 was used in order to ensure consistency as this work is concerned with reliable and consistent CNT production. Furthermore no significant effects on CNT synthesis were observed for changes in buffer layer thicknesses between 10 nm and 50 nm, when using the process described hereafter, and it is the deposition of the catalyst film that appears of utmost importance.

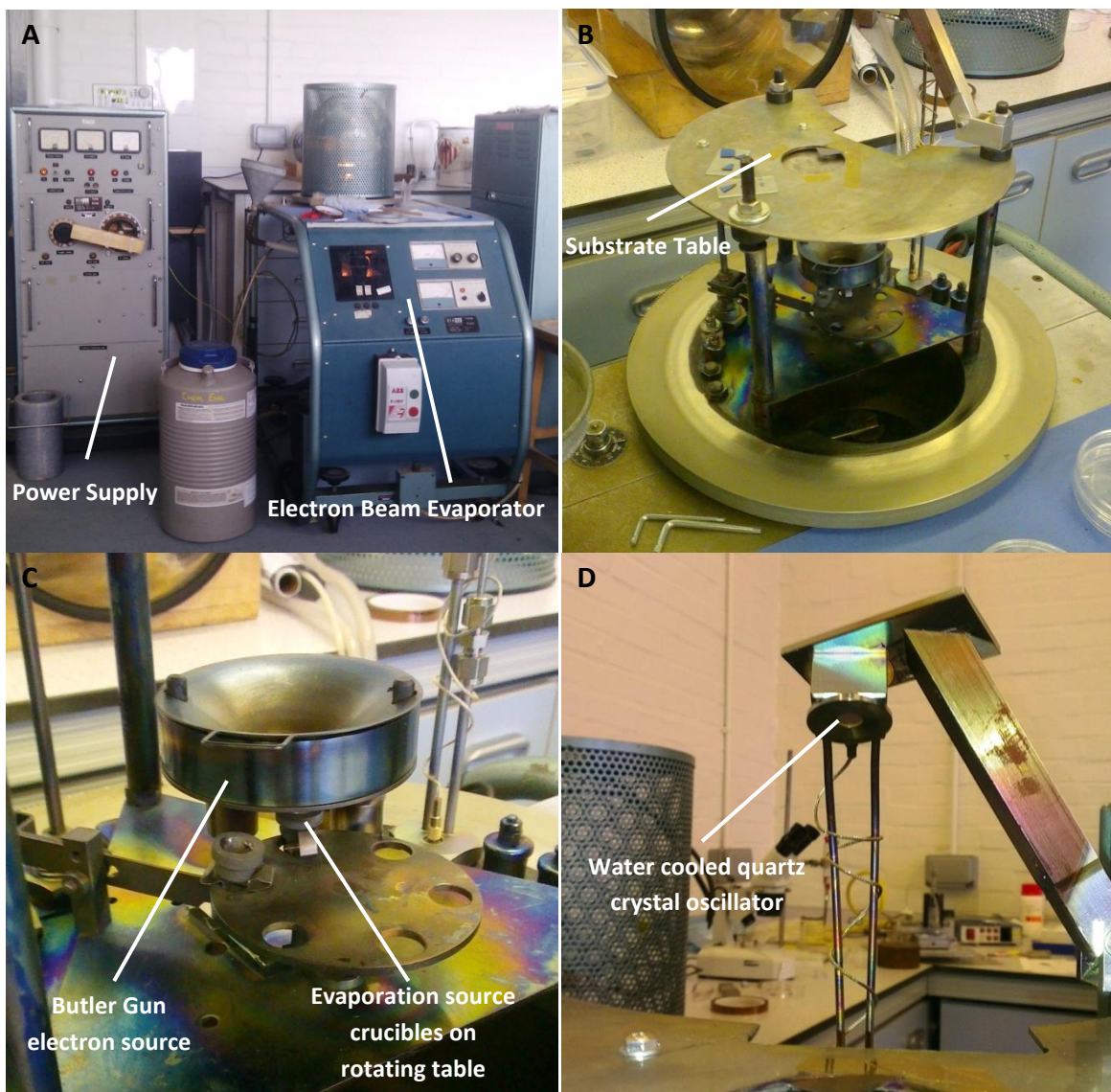


Figure 3.2: Images of the components of the Edwards electron beam evaporation system. A-Overview of the system, B-Detailed view of the evaporation table, C-Details of the electron gun and target crucibles, D-The retrofitted quartz crystal oscillator for the FTM-2400 system

Deposition of the buffer layers was conducted at a rate of $\sim 1.0 \text{ \AA/s}$ and typically lasts for around 300 s of substrate exposure in order to deposit the required 30 nm thickness, although it is often the case that deposition rates decay thus often longer exposure times may be required to reach full

thickness. It should be noted that the accurate evaporation of Iron to form thin films can be performed using simpler thermal evaporators, but such processes are not suitable for the evaporation of Al_2O_3 . It is for this reason that an electron beam evaporator is employed as literature has shown improved CVD growth of VACNTs for catalysts that have had both buffer and catalytic layers deposited in a single pump down cycle [98]. The evaporator deposits material onto a circular area of diameter of ~ 5 cm that is shielded by a mechanically operated shutter, allowing production of ~ 20 cm² of catalyst per cycle. Once evaporation of the buffer layer is completed the system is allowed to cool for at least 30 minutes before rotating the crucible platform ready for deposition of the catalyst layer. As well as cooling the system the waiting period also allows time for the vacuum inside the system to stabilise at the desired level and for any contaminate particles from the previous evaporation to be removed. As it is the Iron film that forms catalytic particles which initiate CNT formation, as discussed later in this chapter, it is critical that this film is deposited accurately and evenly onto the substrate. In order to achieve highly uniform and accurate catalytic films at such low thicknesses it is necessary to evaporate the Iron at the lowest possible rate. In order to achieve such low evaporation rates a simple procedure is followed in which the filament current is increased until steady evaporation of the Iron begins as measured by the FTM. The current is then slowly lowered until the lowest rate possible of evaporation is reached which is around 0.08-0.20 Å/s depending on the various variables involved, in particular the volume of material remaining in the evaporation crucible. Experiments were conducted using thin iron catalyst films ranging from 0.5-5.0 nm in thickness with the best results for VACNT growth achieved using films of 1.5 nm in thickness. Although keeping a constant deposition rate is desirable, in practice using this technique typically results in a decaying rate of evaporation as the volume of material in the crucible decreases during the process. Consequently in practice it typically takes around 30-60 s to deposit the required thickness of Iron which equates to an average rate of deposition of around 0.35 Å/s although fluctuations are inevitable. Once the evaporations are completed the system can be cooled and the catalyst substrate removed and stored ready for use in the CVD growth of VACNT structures using the Sabretube system.

3.3 CVD Growth of VACNT Structures using the Sabretube System

The next section of this chapter will provide an in depth description of the CVD process that is used to produce all VACNT materials tested throughout this work. It will cover an explanation of the equipment, the typical growth process and parameters employed, mechanisms of CVD VACNT growth discussed in the literature, and finally some examples of VACNT forest structures grown at the University of Exeter.

3.3.1 The Sabretube Chemical Vapour Deposition System

The Sabretube system is a novel take on standard chemical vapour deposition procedures for a number of reasons as follows and is particularly suited to the lab scale production of VACNTs.

3.3.1.1 The Pre-Heater System

The first unique feature of the system is the incorporation of a coil pre-heater that heats the flowing gas en route to the CVD chamber. The pre-heater unit is controlled using a proportional–integral–derivative (PID) controller coupled with a thermocouple that is manually operated by the user and can be set to temperatures of up to ~ 1100 °C. The thermocouple is contained in a quartz tube of ~ 18 mm internal diameter that has the ni-chrome heater coil tightly coiled around it. This larger outer quartz tube also houses the flow environment tube which passes through the pre-heater carrying the desired gas flow. The entire heater is then housed in an insulating box for protection and to improve its efficiency. The system has also been specifically designed to allow fast replacement of the so called ‘pre-heater tubes’ that often become dirty after extensive use due to a build up of carbon deposits on the tubes interior and require replacement, **Figure 3.3** pictures the key components of the pre-heater system.

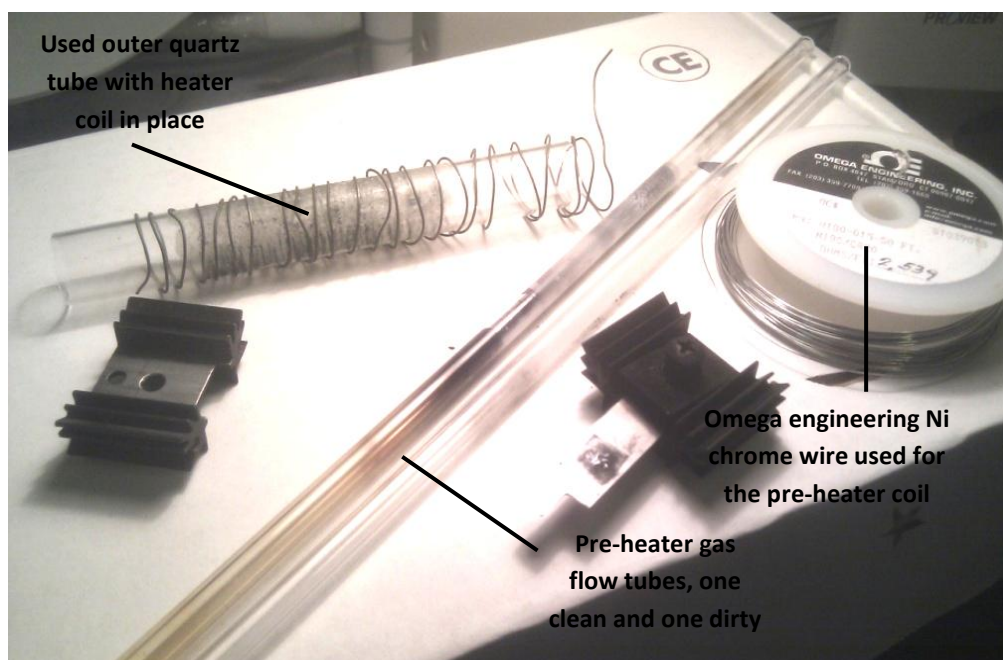


Figure 3.3: Key components of the pre-heater system in disassembled form. Dirty pre-heater tubes can be cleaned by heating in a traditional furnace to 1050 °C and then rinsing with acetone once cooled. The heater coil is usually fixed in place using fire cement but this has been removed to expose the coil in this image.

3.3.1.2 CVD Chamber and Suspended Silicon Heating Platform

The majority of traditional CVD furnaces consist of a simple ceramic tube system that is heated externally usually through the use of resistive heater coils. The Sabretube system uses a novel technique where samples are heated using a resistive heater element that is cut from a suitably doped silicon wafer. This provides the system with several benefits over traditional furnaces particularly for use in a laboratory environment. The temperature of the element is again controlled using a PID controller but this time it is coupled with an infra red (IR) sensor that monitors the temperature of the heater element. Using an IR sensor is only possible as a result of incorporating the suspended heater, as unlike traditional furnaces the process can be monitored optically as there are no heater coils surrounding the quartz furnace tube. As silicon is an excellent conductor of heat and conducts electricity well when suitably doped, as in this case, the system provides very fast and accurate temperature control, and can be heated at rates of up to 1500 °C/min. Such accurate control of the system temperature is invaluable when fine tuning CVD growth of VACNT structures to achieve tall uniform forests. The silicon element is typically around 50 mm in length and 12-15 mm in width, and consequently the largest VACNT forest samples that can be produced using this system are around 10 mm x 25 mm in area. Optical access to the CVD process also provides a means of monitoring the development of the VACNT growth process visually and furthermore the system is installed with a laser interferometer that measures the real time height that the VACNT forest has reached. Coupled with the excellent heater control this allows the user to terminate forests growth at any point very quickly which is not possible using traditional CVD furnaces, and allows the manufacture of different height CNT forests as required. **Figures 3.4 and 3.5** provide details of the suspended heater system and also an overview of the quartz tube furnace in a schematic and photos respectively.

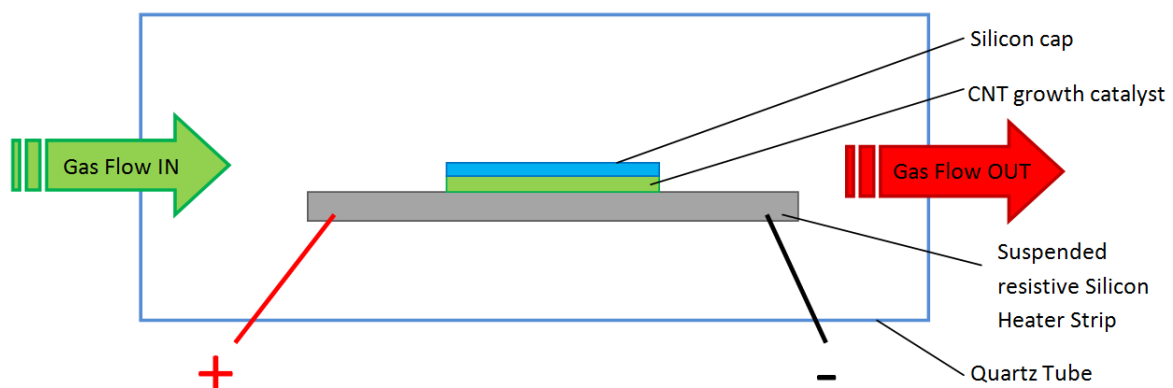


Figure 3.4: Simplified schematic of the suspended heater system and overall Sabretube system.

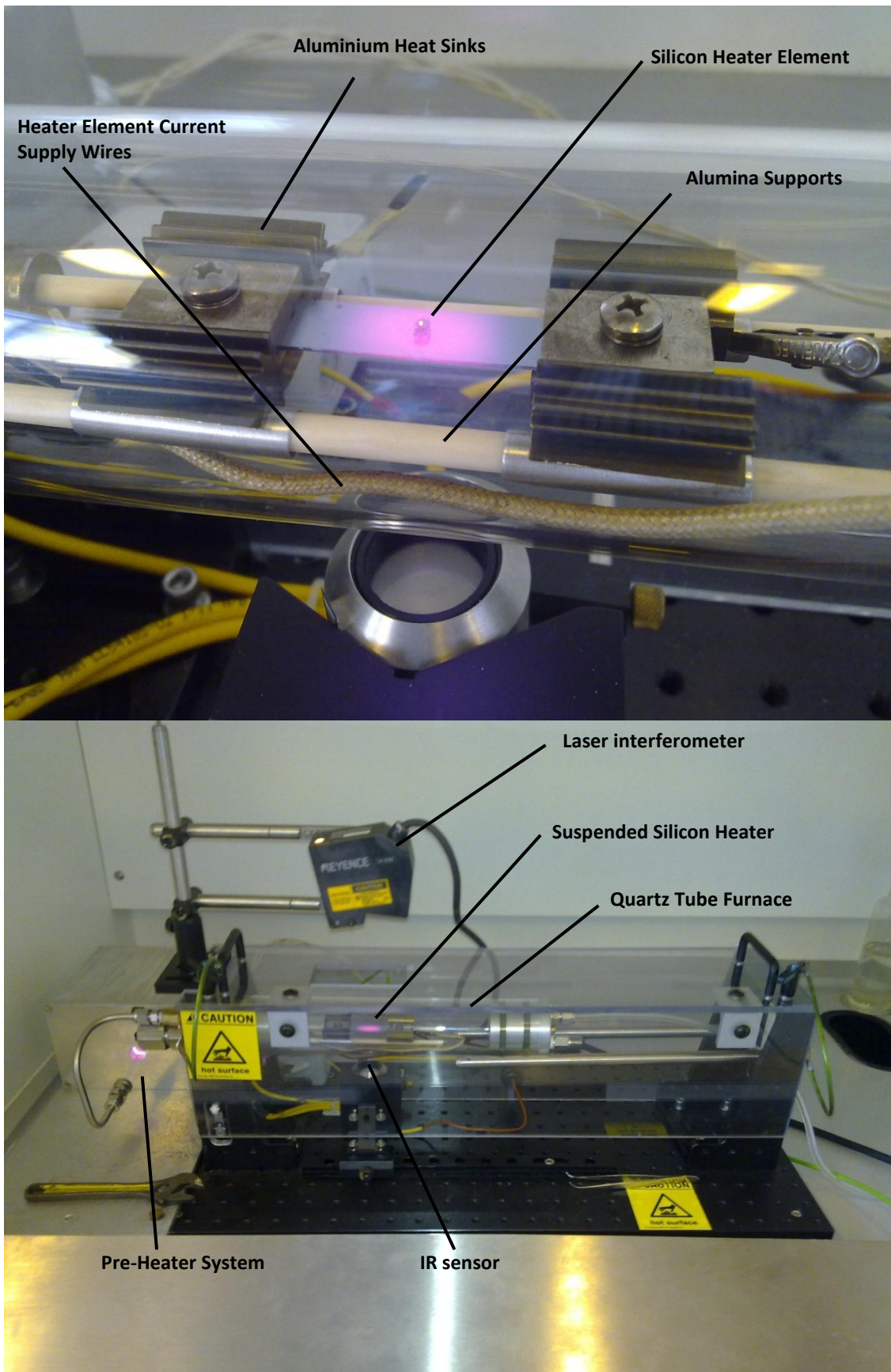


Figure 3.5: Images of the suspended heater system and overall Sabretube system. The entire CVD furnace is located inside of a fume cupboard for health and safety reasons.

3.3.1.3 Mass Flow Controllers and LabView Software

All CVD systems rely on precise control of the flowing gas environment inside the furnace at all times during the process to ensure controlled deposition and reliable repeatability. The Sabretube system uses three individual Mass Flow Controllers (MFCs), manufactured and calibrated by Aalborg, to control the flow of the three source gases required for the process. These MFCs can then be controlled using LabView software allowing automated control of the gas flow to fit the users individual 'recipe' for VACNT growth. The specific system in use employs a custom LabView program to control the MFCs as well as the PID controller for the suspended heater element. The software allows the user to define individual steps in the process, which can accurately control flow parameters, as well as controlling the heating rate of the element and its final temperature. Another important point concerning the Sabretube system is that it is not designed for use with a vacuum pump, as is the case for many CVD systems. Instead the system relies on the use of an inert gas flow environment to ensure no oxidation or combustion occurs within the furnace. Removing the need for a vacuum is useful as it not only lowers the cost of CNT production but also reduces the total time required to produce VACNT samples. **Figure 3.6** details an example of the LabView software user interface as well as an image of the MFC units.

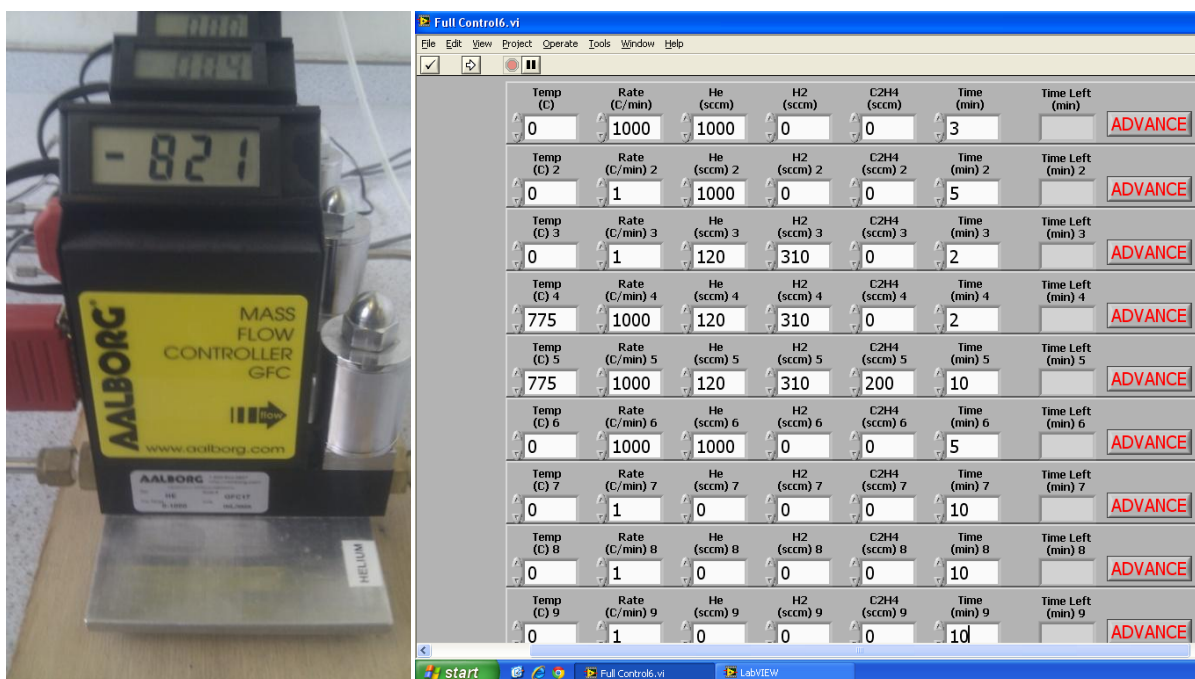


Figure 3.6: A-Image of the MFCs the LCD display can be used to confirm the correct gas flows, this is particularly useful in the mass case that the gas bottles are running low, B-Screenshot of the LabView software with a typical VACNT 'recipe' programmed.

3.3.2 Typical VACNT Synthesis Process using the Sabretube

It is well known that CVD synthesis of VACNT structures can be a highly temperamental process and fine tuning of various parameters is often vital to achieving high-quality results. Although significant improvements in CVD growth of VACNTs are consistently reported throughout the literature the reliability and repeatability of these processes is often challenging, particularly when tall forest structures are desired. For these reasons the CVD process used in this work was kept as consistent as possible once a useful level of VACNT synthesis had been achieved. In practice many parameters such as flow rates, heater temperatures, and the catalyst itself can be kept consistent but there are some variables that are considerably more challenging to maintain. The majority of these variables relate to the cleanliness of the system which is particularly challenging to address. The reason for this challenge is simple; the most effective synthesis of VACNTs is often achieved when the system is in a state that could be considered 'slightly' dirty. It may seem logical to clean the furnace before each run but unfortunately clean CVD furnaces are often ineffective at producing CNTs likely due to the clean components in the furnace absorbing the reactive carbonaceous species in the flow gases. As a result previous studies using the Sabretube suggest that all furnaces require a 'burn in' time that is not well understood but clearly is critical to effective synthesis of VACNT structures [98]. Unfortunately a simple 'burn in' is not sufficient to then ensure effective synthesis, as with continued use carbonaceous deposits build up within the furnace, and also pre-heater, and the maximum height of synthesised forests begins to decline. Consequently a cyclic approach to VACNT production is necessary where the furnace is used until significant decline in production is observed at which point the system is thoroughly cleaned and any excessively worn or damaged components replaced before entering another 'burn in' cycle.

Before initiating the CVD growth process the catalytic growth substrate must be placed centrally on the silicon heater element. It has been shown that the best results in this process are achieved by placing a cap on top of the substrate which limits the flow of the gases to the substrate and helps to maintain consistency and uniformity in the forest structures. The cap also provides a convenient surface to monitor the height of the forest using the laser interferometer allowing dynamic monitoring of the growth process. To ensure the removal of any particles of dust from the substrate that may have appeared as a result of cutting the catalyst substrate to size, substrates are rinsed in propanol and dried with an air duster before being mounted in place. **Figure 3.7** shows a mounted catalyst substrate ready for CVD VACNT growth.

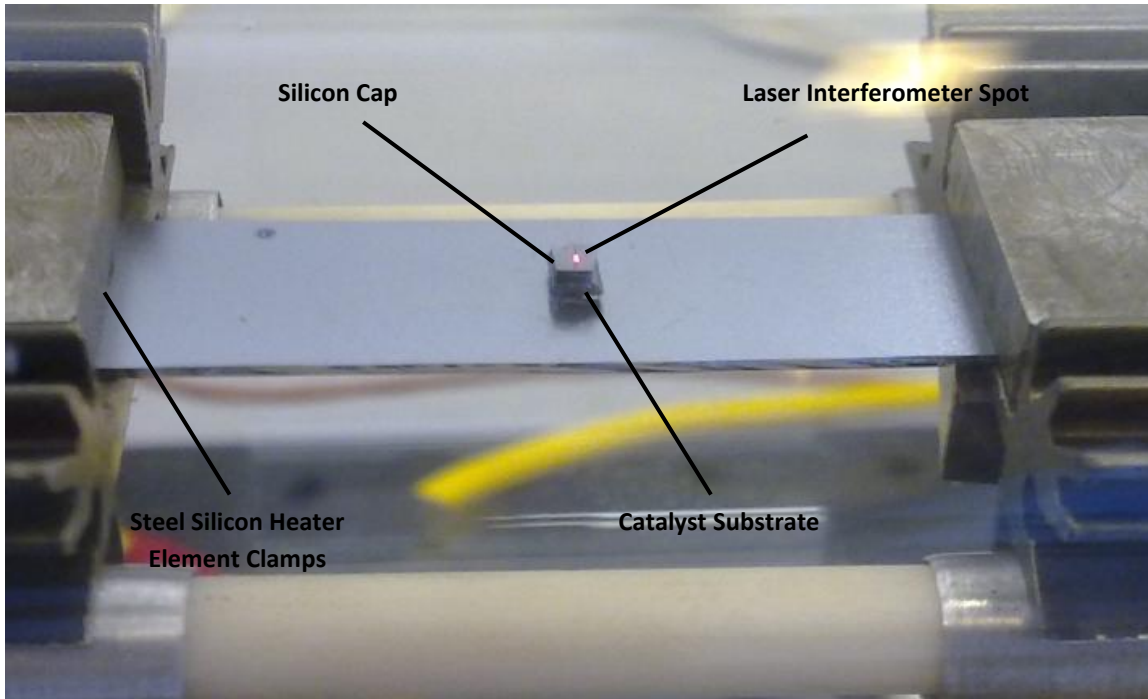





Figure 3.7: Details of the suspended heater system showing the catalyst with mounted silicon cap ready for CVD VACNT synthesis.

The typical CVD process used consists of six distinct stages each with a unique purpose; these stages are pictured and described in **Table 3.1**.

| Stage and Settings | Description | Image |
|---|--|-------|
| STAGE 1 Gas Flow: Helium → 1000 sccm Heater Temperatures: Substrate → 0 °C Pre-Heater → 0 °C Time: 0-180 s | In the first stage of the CVD process the system is flushed with Helium to remove any residual Oxygen and create an inert flowing gas environment. | |

| | | |
|--|---|--|
| <p>STAGE 2</p> <p>Gas Flow: Helium→1000 sccm</p> <p>Heater Temperatures: Substrate→0 °C Pre-Heater→1020 °C</p> <p>Time: 180-480 s</p> | <p>Next the Pre-Heater is ramped to 1020 °C whilst remaining under Helium flow. The pre-Heater activates the carbonaceous species likely by causing minor thermal decomposition of the ethylene in the later stages of the process.</p> |  |
| <p>STAGE 3</p> <p>Gas Flow: Helium→120 sccm Hydrogen→310 sccm</p> <p>Heater Temperatures: Substrate→0 °C Pre-Heater→1020 °C</p> <p>Time: 480-600 s</p> | <p>Once the furnace is purged and the pre-heater is up to temperature the Helium flow is reduced and Hydrogen is added in order to create a reducing environment.</p> |  |
| <p>STAGE 4</p> <p>Gas Flow: Helium→120 sccm Hydrogen→310 sccm</p> <p>Heater Temperatures: Substrate→775 °C Pre-Heater→1020 °C</p> <p>Time: 600-720 s</p> | <p>The heater element is then ramped to 775 °C, this prepares the catalyst for CNT growth, reducing any oxidation of the catalyst, and forming small islands of Iron of around 50 nm which incite the growth of individual CNTs.</p> |  |



| | | |
|---|--|---|
| <p>STAGE 5</p> <p>Gas Flow:</p> <p>Helium→120 sccm</p> <p>Hydrogen→310 sccm</p> <p>Ehtylene→200 sccm</p> <p>Heater Temperatures:</p> <p>Substrate→775 °C</p> <p>Pre-Heater→1020 °C</p> <p>Time:</p> <p>720-1320 s</p> | <p>Finally Ethylene, the carbon source, is introduced and VACNTs begin to grow. In a typical run a forest of 3 mm in height can grow in around 600 s.</p> |  |
| <p>STAGE 6</p> <p>Gas Flow:</p> <p>Helium→1000 sccm</p> <p>Heater Temperatures:</p> <p>Substrate→0 °C</p> <p>Pre-Heater→0 °C</p> <p>Time:</p> <p>1320-1620 s</p> | <p>When growth has terminated or the desired height has been reached the heaters are switched off and the system is purged with Helium. Once cool the VACNT forest can be carefully removed.</p> |  |

Table 3.1: Schematic of a typical VACNT growth procedure conducted at The University of Exeter using the Sabretube system. In the images the VACNT forest reaches several millimetres in height.

The process, or ‘recipe’, detailed above is the process that has been used to produce all VACNT samples used throughout this work in a bid to maintain consistency of these highly varied carbon structures.

3.3.3 Growth Mechanics of VACNT produced using CVD

It is of interest to understand the growth mechanisms of CVD synthesised VACNT forests in order to refine and improve the results of these processes. As mentioned previously by pre-treating the catalyst in stage 4, from **Table 3.1**, of the CVD process the thin film of iron forms small catalytic islands of Iron that float on the Al₂O₃ buffer layer and provide nuclei for individual CNT growth. It is for this reason that the buffer layer is of importance as it provides a smooth non reactive surface for catalyst nucleation to occur. These catalytic islands are identifiable by running the CVD process until stage 4, and then missing out stage 5 thus leaving the catalyst ready for VACNT growth. These

catalytic substrates can then be imaged using Atomic Force Microscopy (AFM) in order to probe these individual catalytic particles and gain an approximation of their diameters. This process was conducted by Meshot et al. who realised that by adjusting the pre treatment stage of the CVD process the diameter of these particles could be varied consequently changing the mean diameter of the CNTs present in the VACNT structures [208]. In order to verify that the catalysts produced using electron beam evaporation were suitable, replica tests were performed using the catalytic films that had been produced in house. AFM analysis was conducted on catalytic substrates that had reached stage 4 of the CVD process using an Explorer AFM and indeed confirmed the formation of these islands, examples images are shown in **Figure 3.8**.

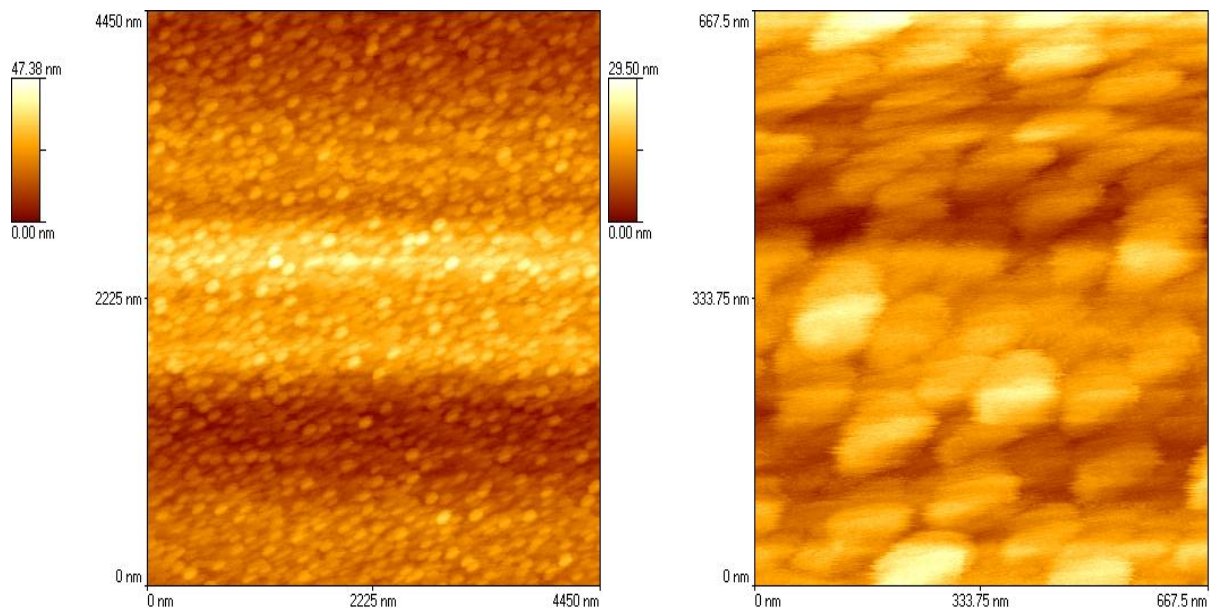


Figure 3.8: AFM scans of annealed catalyst samples. The scans were conducted in tapping mode and were conducted on the same catalyst sample. The data reveals the small catalytic islands that lead to VACNT growth.

The images in **Figure 3.8** are produced from a catalyst sample that was constructed using the experimental methods detailed earlier in this chapter and consisting of 1.5 nm of Iron on a 30 nm Al_2O_3 buffer layer deposited onto an oxidised wafer. The zoomed image is a slower scan of a considerably smaller region of the same catalyst substrate, and reveals the diameter of the catalytic islands to be around the order of ~ 25 nm.

There are two growth mechanisms for VACNTs synthesised using CVD that have been identified in the literature [207], both based on the formations of these small islands from thin film layers. These

are the tip growth and base growth mechanisms of CNT formation. More complex mechanisms have been investigated in the literature but they are not discussed in detail as they do not result in the synthesis of VACNT forests but often entangled mats or other disordered forms of CNTs [36]. In the tip growth mechanism an individual CNT forms under each catalytic island and as the process continues the catalytic particle lifts from the substrate. The particle then remains embedded in the tip of the CNT and the CNT is formed from the tip down, this method had been detailed in the literature by Sinnott et al. amongst others who identified catalytic particles embedded in the tips of CVD grown CNTs [97]. **Figure 3.9** details a simple schematic of the tip growth CNT synthesis mechanism.

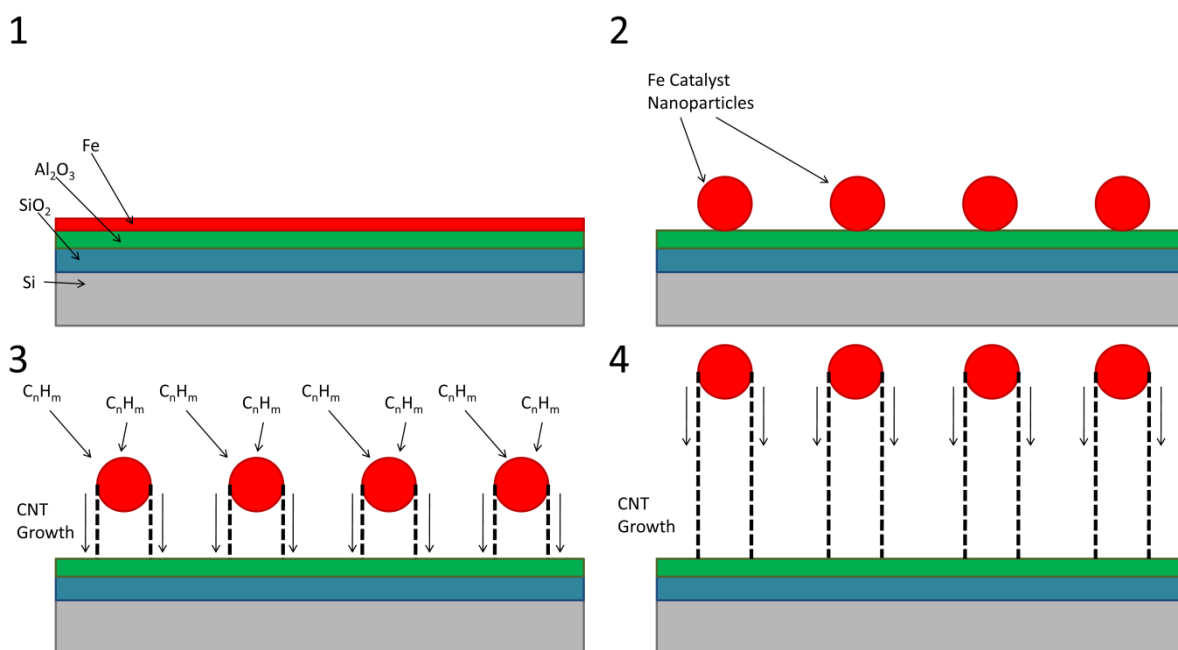


Figure 3.9: Schematic of tip growth CNT synthesis. 1-As produced catalyst, 2-Catalyst after annealing to form catalyst nanoparticles, 3-CNT growth is initiated, Carbon diffuses through the catalyst and the catalysts lifts off from the substrate, 4-Fully developed CNT growth. [98]

The base growth mechanism is a similar process but as the name implies in this scenario the catalytic particles remain substrate bound, and the CNTs lift off from the substrate. Consequently the tips of the CNTs are synthesised first and the base of the CNTs last which is the opposite of the tip growth process. Works using a similar system have established the base growth mechanism as the one which occurs when using the Sabretube system with the catalyst detailed previously, and indeed it has also been shown to be the mechanism that occurs in traditional CVD reactors when using similar catalysts. Bedewy et al. also identify that the initial growth of VACNT using these methods creates a so called ‘crust’ layer of entangled CNT that is believed to occur during the initial synthesis process

as the VACNT self organise themselves into a forest structure [209]. A final point to note is that the growth of VACNT forests is not hindered by lifting the silicon cap used in the Sabretube process. The effect of adding weights to the silicon cap has been investigated experimentally in the literature and it was found that significantly larger weights are required to cause noticeable effect to the VACNT growth process [210]. **Figure 3.10** details a schematic of the base growth CNT synthesis mechanism.

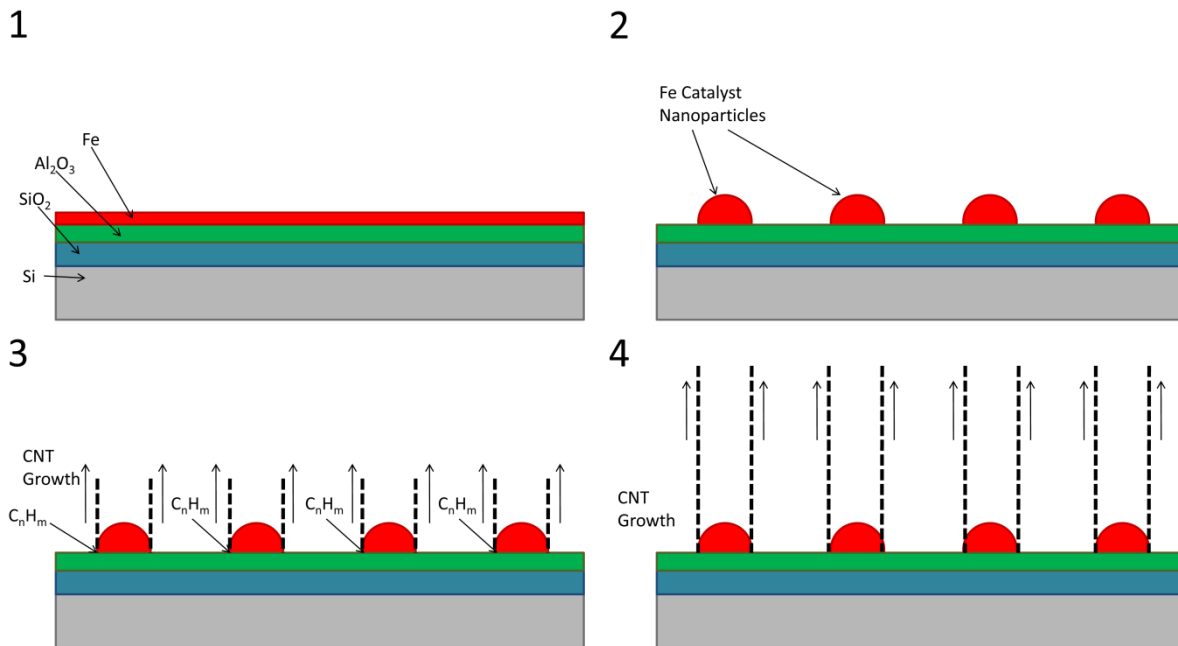


Figure 3.10: Schematic of base growth CNT synthesis. 1-As produced catalyst, 2-Catalyst after annealing to form catalyst nanoparticles, 3-CNT growth is initiated, Carbon diffuses through the catalyst but the catalyst remains substrate bound, 4-Fully developed CNT growth. [98]

In the base growth mechanism that occurs inside of the Sabretube system there are several key points that have been identified. Firstly the carbon source gas in use is ethylene, although many other carbon containing gases may be suitable, which is partially thermally decomposed in the pre-heater prior to entering the CVD reactor. Although the temperature of the pre-heater is higher than the self pyrolysis temperature of ethylene the gas flows through the heater too quickly to allow significant pyrolysis to occur, however the process clearly activates the gas significantly. This activation can be confirmed simply by repeating the process without the use of the pre-heater, in which case little or no growth of VACNTs is observed. Investigations into this activation process have been conducted by Plata et al. who identified a vast range of carbonaceous species by using various gas analysis techniques on samples of gas collected from the different stages in the growth process [211]. It should be noted that their work focused on the environmental impact of the CVD process and found that greater than 1 vol% of the exhaust gases contained methane, a greenhouse gas, as

well as Volatile Organic Compounds (VOCs) and other carcinogenic carbon based materials. Others have conducted similar work on different CVD processes using various other techniques such as in-situ mass spectroscopy; however Plata et al.'s work is more relevant in this case as they use the Sabretube system. These carbonaceous species are then believed to be absorbed into the catalytic Iron particles before being built into VACNT forest structures although precise growth mechanisms are still not well understood. More detailed analysis of the growth process conducted by Bedewy et al. suggests that the termination of synthesis is self activated and occurs as a result of loss of alignment at the base of the forest as measured using synchrotron x-ray scattering. These results suggest that there may also be varying properties in VACNTs along the length of the structures although direct observations of such variations have currently not been measured.

3.3.4 Examples of VACNT Forests produced using the Sabretube System

In this section some example VACNT forest structures will be illustrated as seen under optical microscopy and SEM analysis. The images demonstrate some common problems with VACNT growth that occur when the spatial density of the catalytic islands is incorrect as well as random defects that can occur during synthesis likely due to minor catalyst contamination. Many as grown, VACNT forest samples were examined at various magnifications using a Hitachi S-3200N scanning electron microscope to confirm the overall forest morphology, further SEM of VACNT forests was conducted using an FEI Nova 600 Dual beam system.

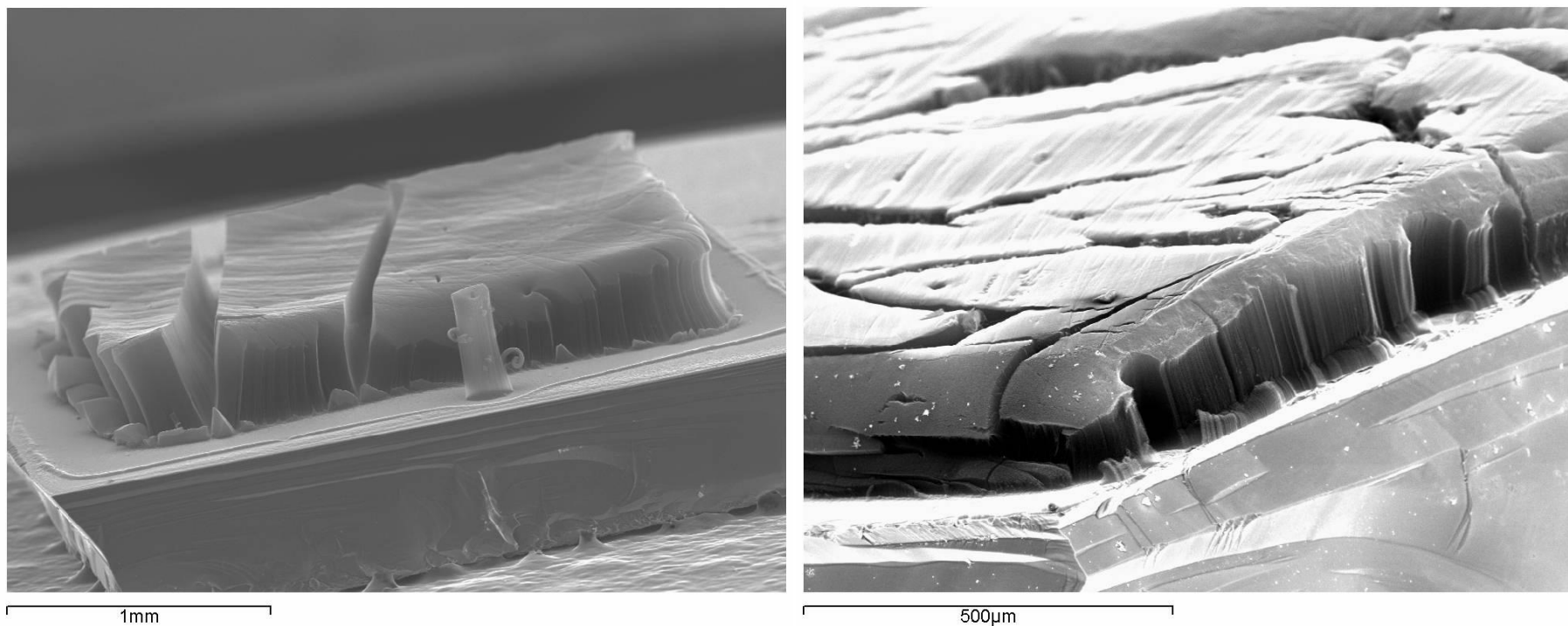


Figure 3.11: SEM images of two forests structures grown from the catalyst that was supplied with the Sabretube system. Although the exact catalyst structure is unknown it is supposed to consist of 1.0 nm of Fe deposited on 10 nm Al_2O_3 , the forests are short and do not reach the edge of the substrate likely due to an insufficient thickness of Fe. This occurs as with an insufficient thickness of Fe catalyst the formation of islands that initiate individual VACNT growth is hindered, resulting in an imperfect special density of such islands. Consequently early termination of CNT growth occurs.

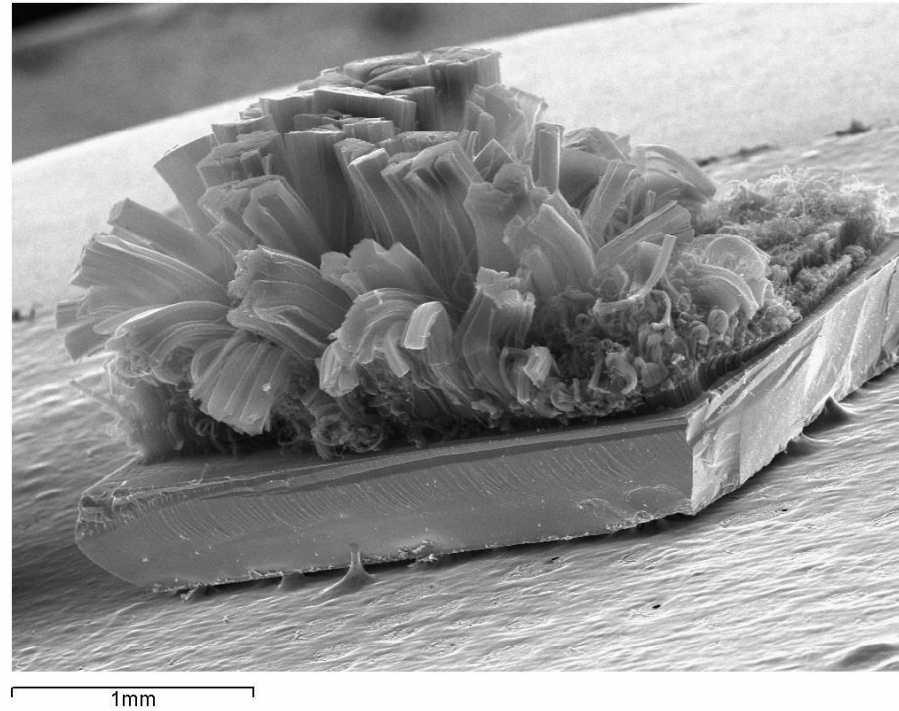
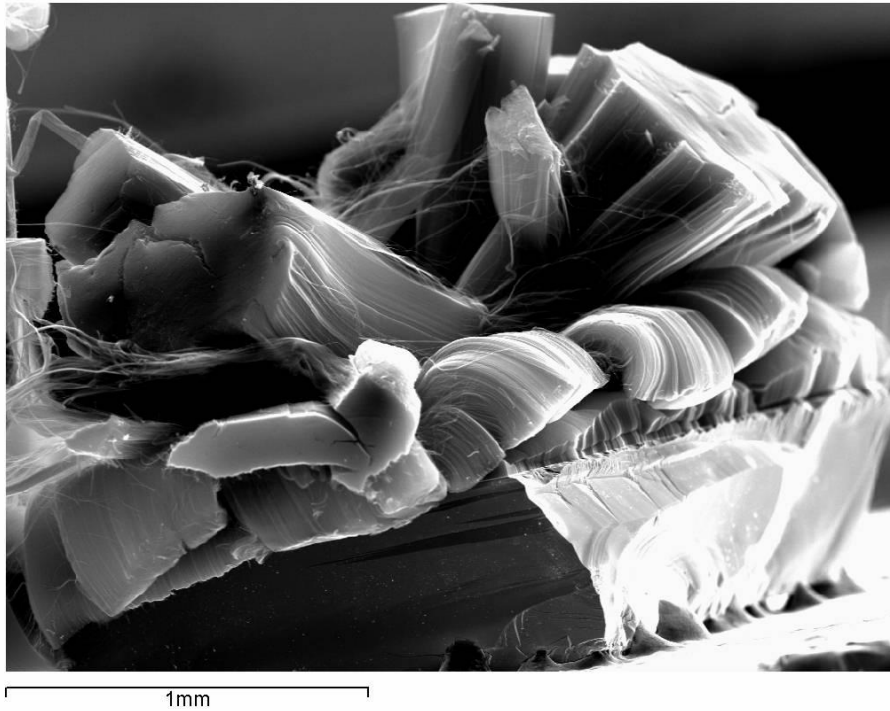


Figure 3.12: Examples of disordered CNT forest structures. Although the CNTs in these structures are over a 1 mm in height the areal density of the catalytic islands is too low resulting in a loss of self organisation of the VACNTs and consequent collapse of the aligned forest structure. It appears that small areas of the catalytic islands have formed resulting in pillars of different heights being produced across the catalyst substrates area. The structure of tall VACNT forests is self supporting hence these isolated pillars are prone to collapsing at such high aspect ratios.

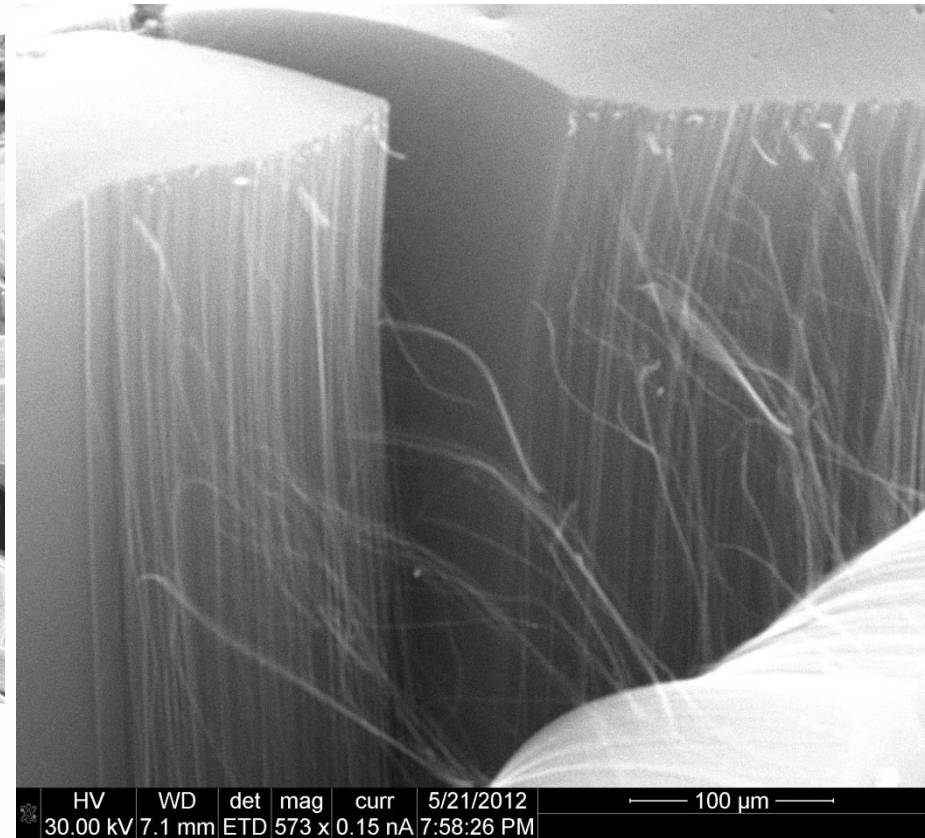
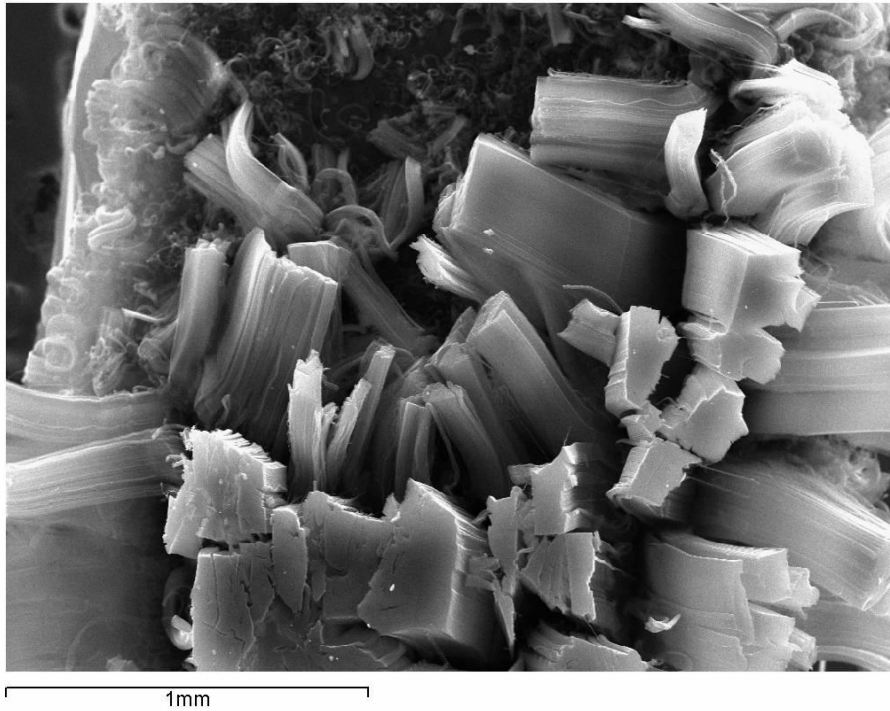


Figure 3.13: Top view of the right hand image in **Figure 3.11**, and a zoomed in view of a split in a VACNT forest where the forest falls apart due to low catalyst density, losing its uniform structure. These images provide details of the collapsing VACNT structure, and show small bundles of VACNT bridging between the falling towers. It appears that the sections of VACNT are considerably more prone to collapse when the CSA of the pillars is smaller, resulting in many small pillars that appear fully collapsed at short heights compared to those with larger CSAs.

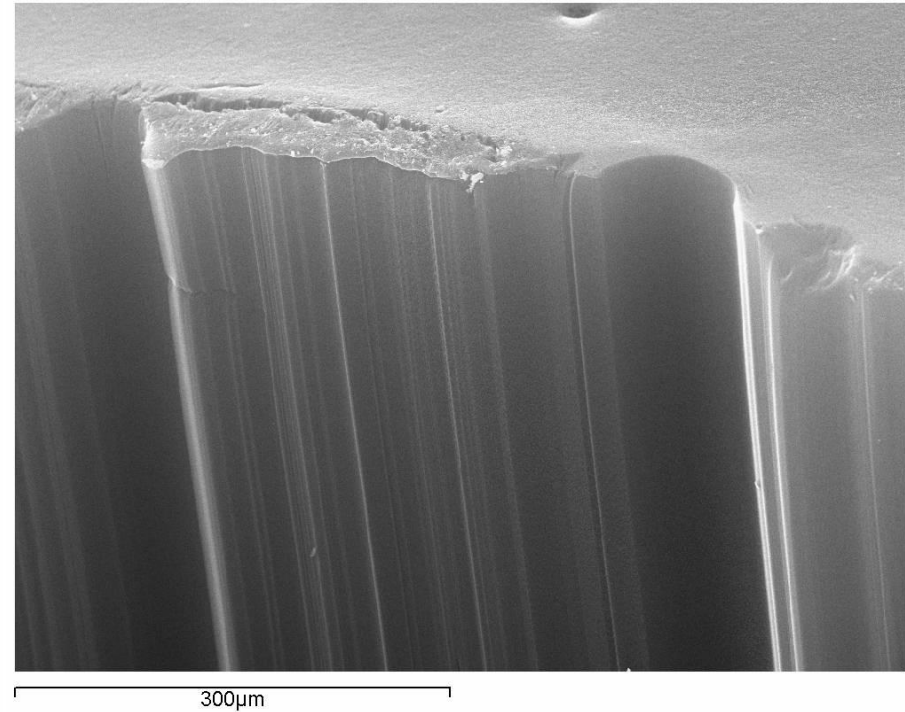
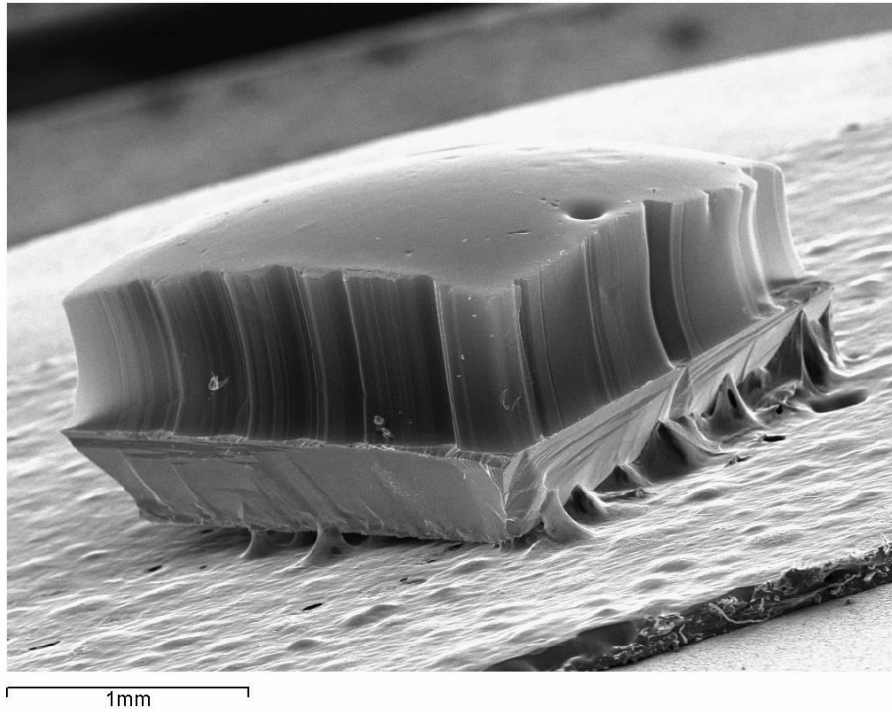


Figure 3.14: SEM images of a well aligned and uniform VACNT forest of 1 mm in height. This forest was produced using the catalyst developed specifically for this work and consisting of 1.5 nm of Fe deposited onto 30 nm of Al_2O_3 as discussed previously. These forests illustrate the desired choice of forest structure for producing composite materials using CNT and are representative of the forests used throughout this Thesis.

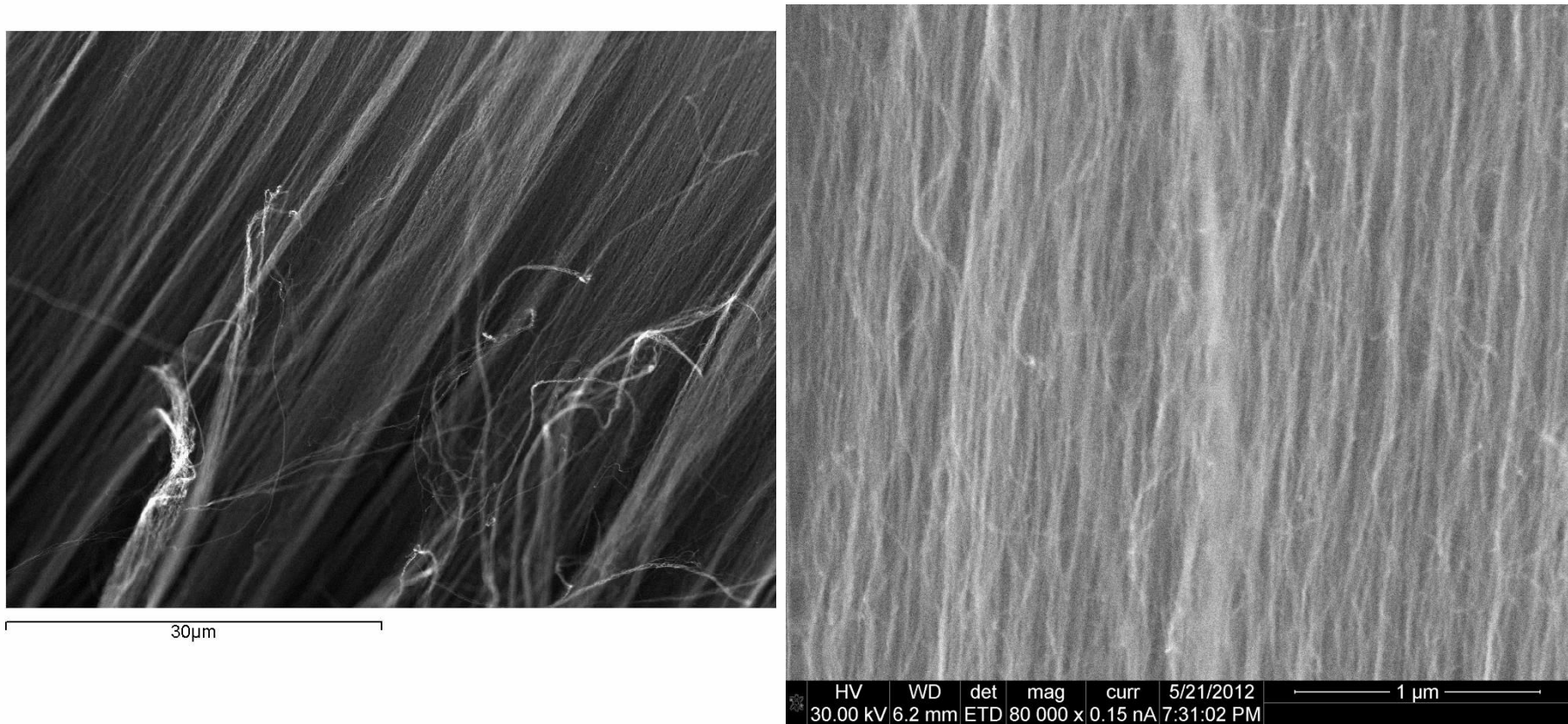


Figure 3.15: Higher magnification SEM images of a well aligned VACNT forest structure, at high magnification individual bundles of VACNT are apparent and appear to be wavy and less well organised; this effect is discussed further in **Chapter 4**. Although it appears that individual fibres are clear under SEM analysis these fibres actually represent small bundles of many VACNT in the left hand image. On the right hand side individual wavy VACNT are just resolvable.

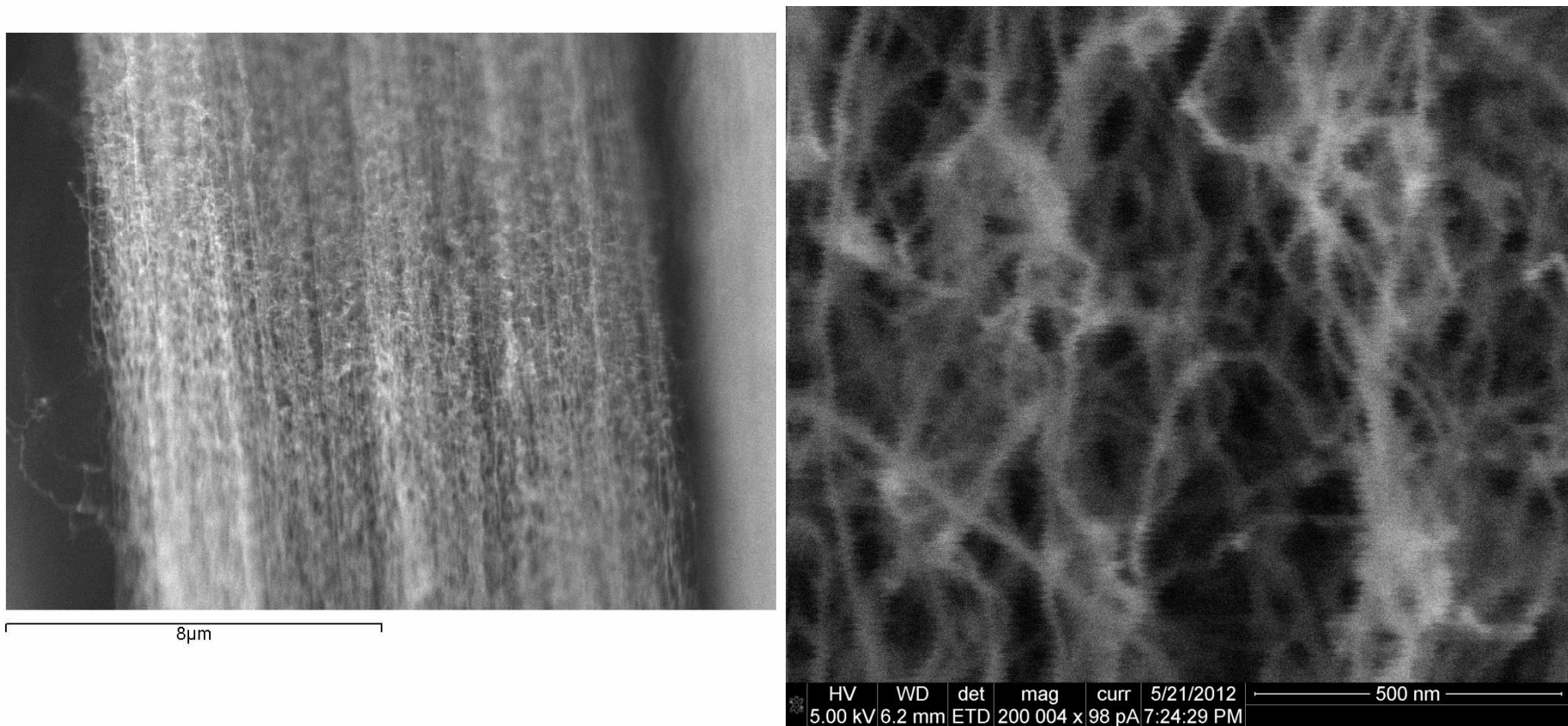


Figure 3.16: Further High magnification images of VACNT structures, the right hand image reveals the entangled individual CNTs that exist within an individual CNT bundle that appears highly organised at lower magnifications. These images show how the CNTs are self supporting and require a significant areal density to achieve uniform high aspect ratio growth.

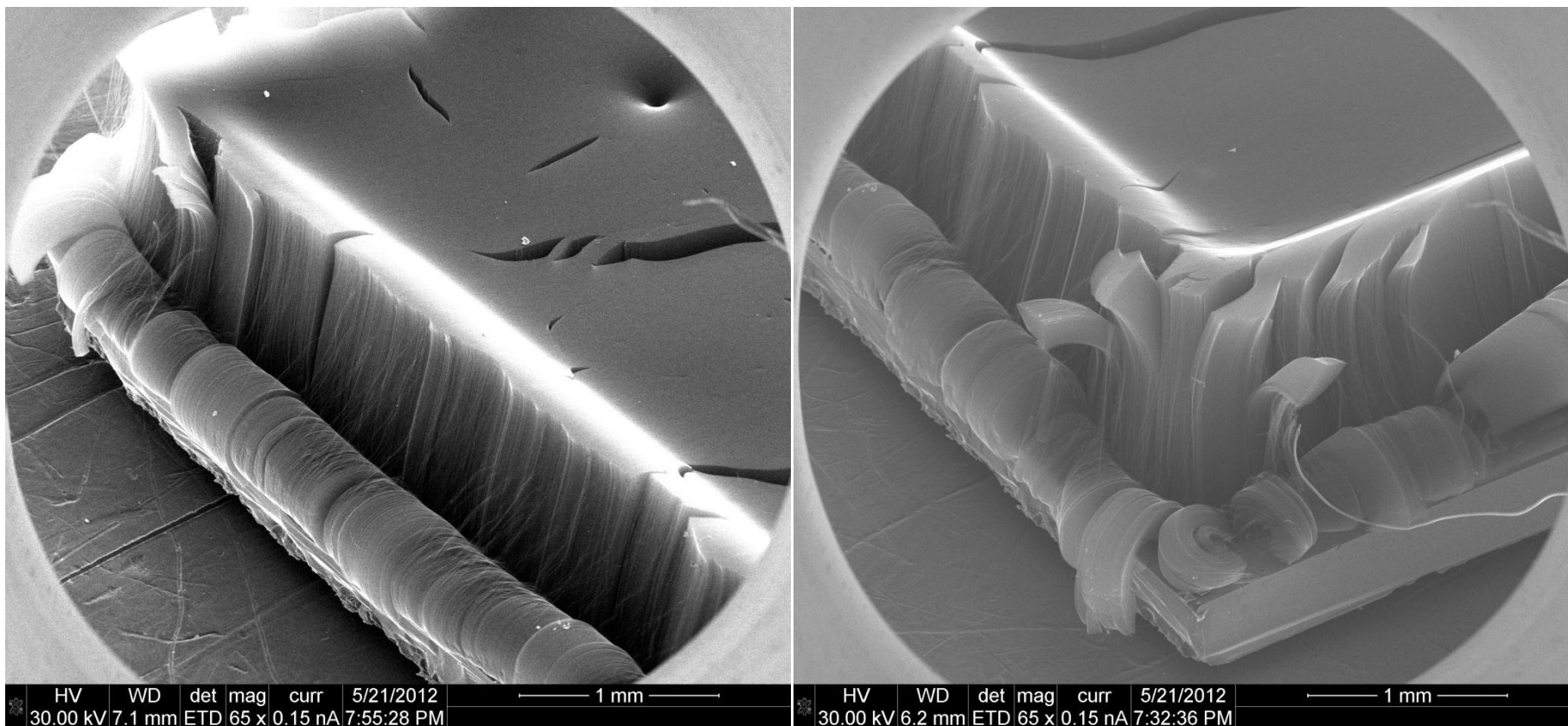


Figure 3.17: Images of the same large VACNT forest, the CNTs located at the edges of the forest have peeled away on this sample, these excess CNTs can be removed through careful use of a razor blade if required. It is believed that this effect occur when forests begin to reach heights that are greater than 1mm as the edges of the forest are no longer sufficiently self supported by the overall structure. Small strings of VACNT are visible that bridge the gap between the main forest and peeled edge and indicate an approximate height of growth at which the peeling initiated.

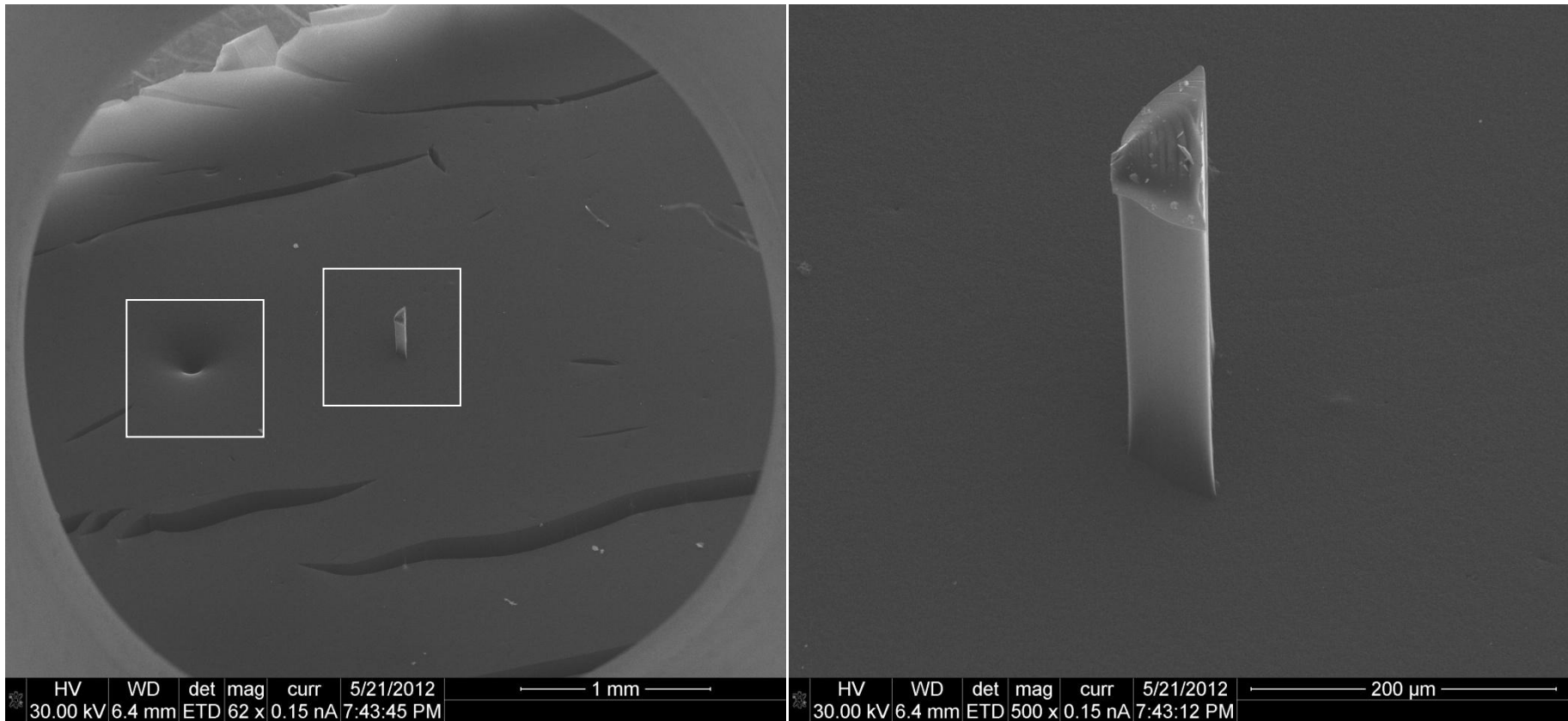


Figure 3.18: Defects in the top surface of a VACNT forest marked with white squares, left hand side is a small hole likely caused by a dust particle, and right a small CNT pillar protrudes from the surface, the cause of which is unknown, the right hand image shows the detail of this pillar at higher magnification. It appears that the VACNT in this region have experienced an extended growth lifetime compared to the surrounding forest. This could result from a small contamination of the catalyst, for instance the presence of water has recently been shown to enhance CVD growth lifetimes [108].

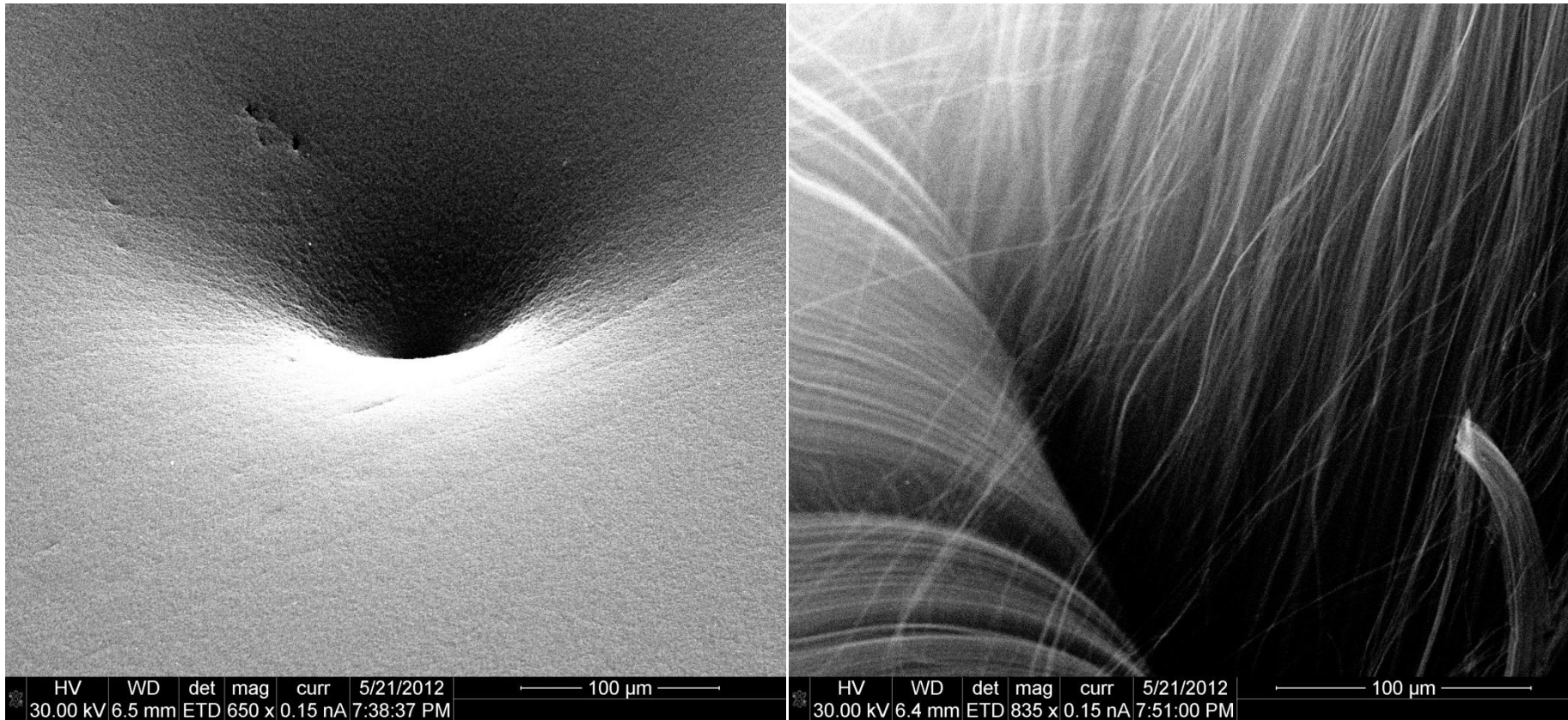


Figure 3.19: The left image is a high magnification image of the defect caused by a dust particle present during CNT growth, and right hand shows the detail of the CNT that can fall away at the edges of particularly large forest structures. It provides a detailed image of the bridging CNTs that provide evidence that initially the forest grew as a fully aligned structure, however at a certain height the edges fall away. Edge defects can be removed using a razor blade and are not observed in shorter CVD grown forests.

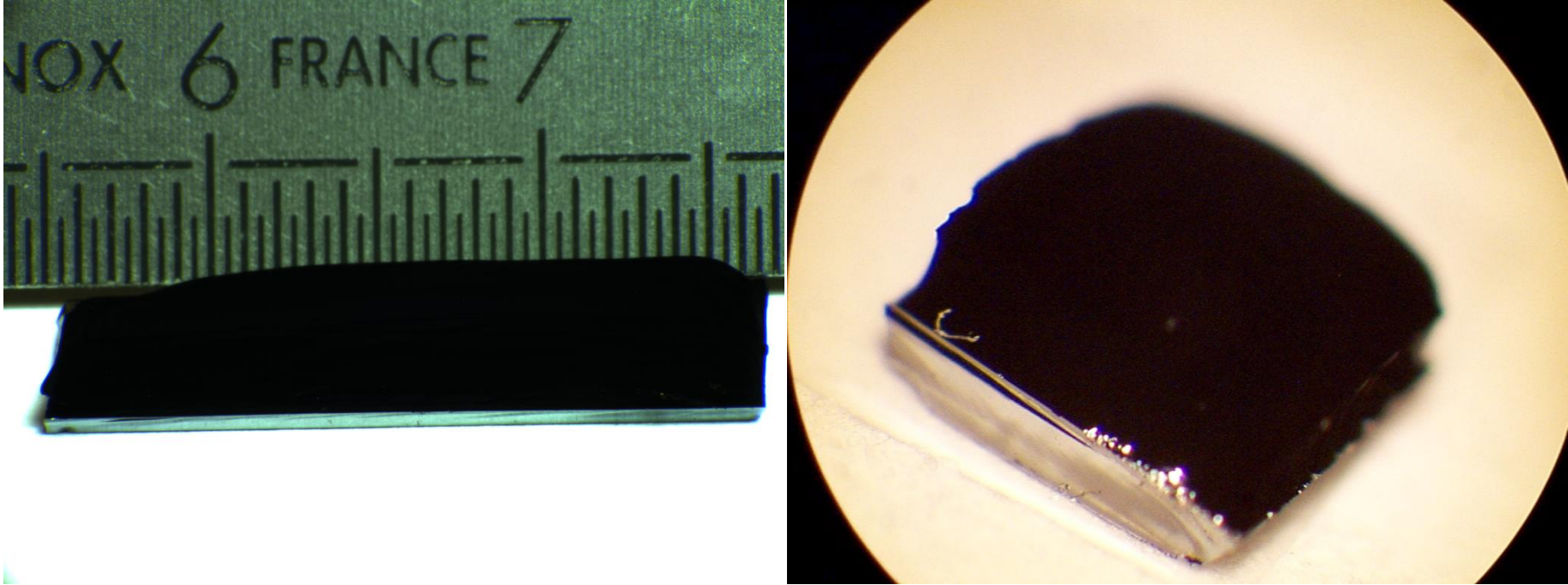


Figure 3.20: Optical microscope images of large VACNT forests, VACNT are known to be highly effective at absorbing optical radiation and consequently observing their structure using optical microscopy is particularly difficult although it is possible to gain an idea of the overall forest size [212].

Chapter 4

Fabrication, Modelling and Mechanical Analysis of a Vertically Aligned Carbon Nanotube Composite Structure

4.1 Introduction

In order to successfully assess the feasibility of a multilayer VACNT composite structure, as discussed in **Chapter 2**, it is of interest to understand the effectiveness of reinforcement that can be introduced to a high performance polymer matrix when using as grown VACNT forests as reinforcements. Measurement of mechanical reinforcement of polymers reinforced using as grown as well as mechanically densified VACNT forest structures has been conducted [213] but this is often performed on micrometer scale samples using nanoindentation techniques to measure the axial reinforcement that occurs in the axis of the nanotube alignment [160]. Currently the effectiveness of reinforcement achieved in VACNT composite structures is known to depend on retaining the dispersion and alignment of the CNT reinforcements during production, as well as the volume fraction of reinforcements contained within samples [16]. However, even the best VACNT composite samples still fall short of predicted values that are calculated using the traditional 'Voigt' and 'Reuss' [190], [191] models for aligned fibre composites as well as the Halpin-Tsai model [142]. More recently it has been suggested that the wavy structure of the individual CNTs contained within a VACNT forest may help to explain this discrepancy in mechanical reinforcement that is currently observed [141]. Results have begun to confirm this by using modified models which incorporate fibre waviness to provide a better prediction of composite properties when compared to data measured in the axial direction for VACNT reinforced composite samples [214]. Consequently some researchers have begun to suggest that after solving problems associated with alignment and dispersion of CNTs in polymer matrices through the use of VACNT forests, or otherwise, that CNT waviness has become the new limiting factor in achieving effective reinforcement.

In this chapter the largest possible VACNT forest structures are grown using the Sabretube and fabricated into composite samples in order to allow millimetre scale testing of samples where the full sample is tested as opposed to nanoindentation techniques where only small volumes of composite samples are tested independently. In producing such large samples it is possible to accurately measure the transverse mechanical properties of composite samples using Dynamic

Mechanical Thermal Analysis (DMTA) as well as Micro Tensile testing techniques. By comparing literature data for the axial reinforcement achieved [215] in similar but smaller composite samples with the data collected for transverse testing it is possible to understand the influence of the angle of axial alignment of these wavy nano scale reinforcements on the mechanical properties of these composite structures. An understanding of this influence is critical when attempting to build multi layer composite components where the alignment of VACNT reinforcements can be controlled at the microstructure level [193]. This is particularly relevant when considering Functionally Graded Materials (FGMs) where mechanical properties vary across the structure or if trying to construct composite materials by controlling VACNT orientation using plasma enhancement, or otherwise, to suit specific applications. These results provide an important step towards realising the potential to use CNTs as fibre reinforcements in polymer composite structures at the macroscale.

4.2 Fabrication of Large Millimetre Scale VACNT Composite Structures for Mechanical Analysis

This section details the fabrication of large VACNT polymer composite samples for mechanical testing.

4.2.1 Fabrication Materials

The VACNTs used to produce the composite samples were manufactured in house using the methods detailed in **Chapter 3**. For these particular experiments forests were produced to form the longest strips possible when considering the size of the resistive silicon heater element. In order to conduct effective mechanical analysis this meant that final sample length were required to be at least 15 mm in length to provide sufficient composite for effective clamping whilst still retaining a 10mm gauge length. Through accurate cutting of pre made catalyst substrate, VACNT forests were grown using catalysts that were approximately 20mm in length and 10 mm in width. These forests were grown to minimum heights of 1.2 mm in order to allow sufficient VACNT forest to produce mechanical test coupons. When producing such large VACNT forests small defects can occur around the edges of the VACNT structures where the external CNTs can appear to fall away from the bulk forest. For this reason the forests were produced to a larger size than required for the test coupons thus allowing any defects in such forests to be removed during the later stages of composite fabrication. **Figure 4.1** details examples of these long VACNT forests viewed both optically and using SEM imaging.

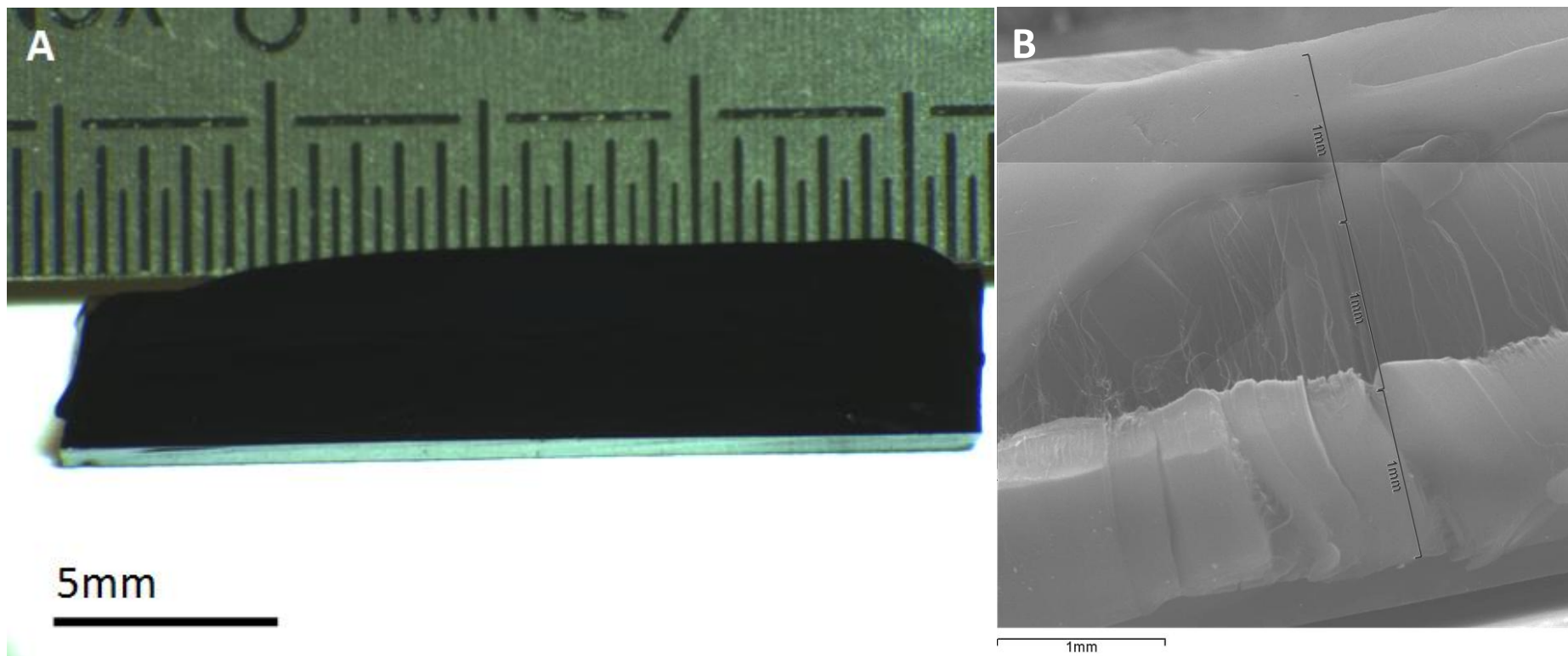


Figure 4.1: Examples of Long Sabretube Grown VACNT forests used for composite coupon production. A-Optical Image of a large VACNT forest, this particular forest reaches several millimetres in height. B-A composite SEM image, constructed of two separate SEM images, which details the side of a large area VACNT forest. It is possible to see how the edges of the forest appear to have separated which is often the case when forests reach heights of greater than 2mm.

The two part epoxy thermosetting resin used as the polymer matrix material in the composites samples was carefully selected based on its cure profile, viscosity, and mechanicals properties once cured. Furthermore a clear resin is desirable as this allows monitoring of the wetting process during the resin infiltration and thus it is possible to confirm that the forest remains aligned and well structured once the process is completed. The resin used is the Araldite LY3505 resin in combination with the Araldur XB3403 hardener supplied by Huntsman [216]. This clear resin has an extended room temperature pot life once mixed which aids sample production, has a low viscosity when mixed, 300-400 mPas at 25 °C, and can be cured at room temperature in 24 hrs or faster at elevated temperatures. This resin is commercially available and is frequently used in many advanced composite applications in the automotive and aerospace industry. Consequently it has excellent mechanical properties when cured and is a suitable choice for creating high performance fibre composite materials.

4.2.2 Resin Infiltration of VACNT Forests

When producing composite samples from as grown VACNT forests there are several key parameters that must be retained during sample production. Most importantly, retaining the dispersion and alignment of the CNTs within the matrix is critical as the purpose of these experiments is to understand the mechanical reinforcement that can be achieved through the use of as grown VACNT forests. The mixed resin in use has been observed to readily wet as-grown VACNT forests through capillary driven effects and consequently it is of importance to avoid any densification of the forest that may occur as the structure collapses due to capillary effects. This densification effect has been observed by various researchers, and is utilised to densify VACNT structures in certain applications [217]. In order to avoid such effects it is important to avoid a three phase interaction between the materials that occurs when the resin-CNT interface interacts with that of the surrounding environment. A simple method of avoiding these interactions is to use a volume of resin that is significantly greater than that of the VACNT forest thus allowing the forest to be fully submersed in the bulk resin. Consequently no densification effects are observed unless the forest is removed from the resin before curing.

In order to produce VACNT composite samples a custom made mould was produced using a carefully machined aluminium cast and a silicone moulding material. The mould consists of several rectangular cut outs that are approximately 10 times the volume of the VACNT forest in use. The silicone mould allows easy removal of the samples once the resin is fully cured and removes the need for any release agents that could potentially contaminate the samples. A picture of the aluminium cast and silicone mould is detailed in **Figure 4.2**.

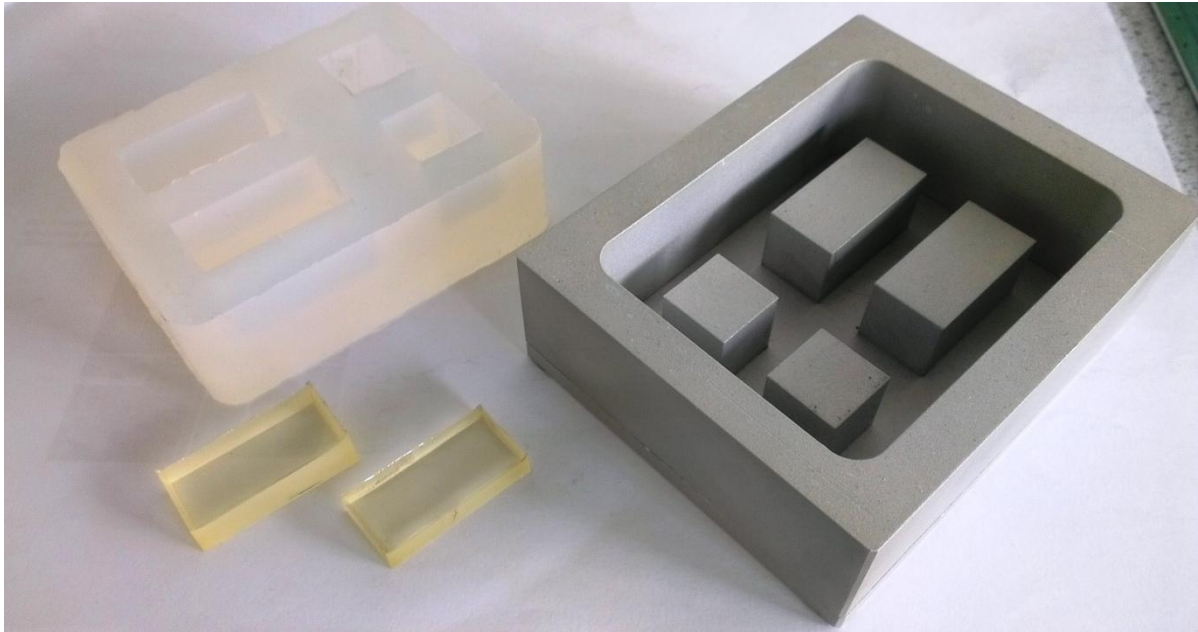


Figure 4.2: An image of the aluminium cast and silicone mould used for VACNT composite fabrication. In the fore ground of the image are two examples of neat resin samples before being machined for testing. The square shaped cut outs were included for testing purposes and are not used to produce the samples tested later in this chapter.

The low viscosity of the resin and hardener used has the added benefit of facilitating the resin hardener mixing process. Resin and hardener were mixed in a ratio of 100 parts to 35 parts by weight using suitably sized syringes to measure out the required amounts into a mixing container that was placed on an accurate digital balance. The mixing container was at least ten times the volume of the total amount of resin being mixed and the mixture was mechanically stirred for 5 minutes until a uniform consistency was achieved. After mixing the resin-hardener mixture contained a large amount of trapped air as a result of mechanical stirring. In any composite it is crucial to remove any trapped air as remaining trapped air can lead to voids and inherent weaknesses in composite structures. In order to remove any trapped air the mixing vessel was placed in a vacuum causing the resin mixture to foam fiercely and dramatically increase in volume hence the use of a large mixing vessel. The vessel was left in a vacuum of approximately 5×10^{-6} torr for at least 30 minutes till no further bubbles were apparent in the mixture and the mixture remained visually still and clear. The mixed resin has a pot life of at least 600 minutes at 23 °C when mixed and consequently the viscosity and other properties of the mixture are not adversely affected during the vacuum processing as the full mixing and deaeration process takes less than 60 minutes. Once the resin mixture was processed VACNT forests were carefully placed substrate down in the bottom of the silicone mould. The resin infiltration process was conducted by filling the mould from the corner with the resin mixture using a suitable syringe that contained the full volume of resin mixture required. The mould was filled quickly without breaking the seal between the resin surface

and tip of the syringe whilst filling the mould thus minimising any further trapped air that may enter the system. Once the mould was filled it was evident that some air remained in the samples that had clearly been trapped in the interior of the VACNT forest, as the resin infiltrates the forest this air is expelled but remains trapped in the bulk resin usually around the VACNT forests surface and edges. Consequently it was necessary to carefully vacuum treat the samples again in order to remove any remaining encapsulated air within the samples. As retaining the as-grown structure of the VACNT was required the vacuum treatment process was conducted using a careful step method in order to avoid any violent foaming of the resin. The mould was placed in the chamber and then the pressure was decreased slowly until entrapped air bubbles began to rise to the resin surface at a steady rate before sealing the chamber at the current pressure. Once the rate of rising bubbles had stopped or significantly decreased the pressure was again lowered until a constant rate of rising air bubbles was achieved once more. In total approximately 10 vacuum steps were required and lasted for about 5 minutes each until the pressure in the chamber reached 5×10^{-6} torr and no more bubbles were observed to form in the resin mixture. **Figure 4.3** shows a simplified schematic of the resin mould and VACNT infiltration process.

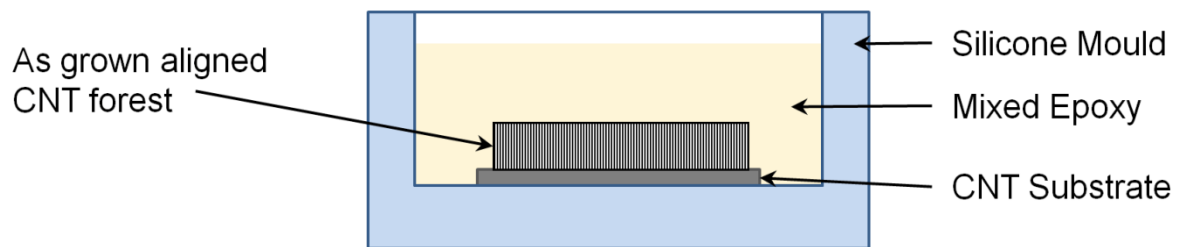


Figure 4.3: A schematic of the resin mould illustrating how the VACNT forest was infiltrated using the mixed resin.

4.2.3 Curing of VACNT Composite Samples

Once the VACNT forest had been fully infiltrated with resin and de-aerated it was placed into a vacuum oven for curing. The manufacturer recommends several cure profiles depending on whether the application requires a fast cure or a low temperature cure. In this work a cure profile was selected that would provide the best mechanical properties according to the manufacturers datasheet [216]. This consisted of heating the mould at 60 °C for 4 hours followed by an increase to 80 °C for a further 6 hours before removing and allowing the samples to cool to room temperature overnight. Once the oven and samples are cooled they can easily be removed from the silicone mould, as it is highly flexible, leaving large fully cured and uncontaminated composite samples that are ready for further processing.

4.2.4 Machining of VACNT Composite Samples

Machining of VACNT composite samples for mechanical testing is a critical stage of the composite production process for a number of reasons. Machining is conducted using a low speed diamond circular saw that can be positioned with micrometre accuracy and is lubricated using a cutting fluid bath during machining. From each cured composite sample both neat resin and VACNT composite samples were machined for mechanical testing. This ensured that the neat resin and VACNT composite samples consisted of precisely the same mix ratio and the exact same cure profile. Ensuring identical mix ratios and cure profiles for sample comparisons is critical as only minor discrepancies can cause significant changes in mechanical properties as shown on the manufacturer's datasheet [216]. It is possible to machine neat resin samples from the composite batches owing to the large volume of matrix used when producing composite samples. As the resin is clear once cured it is possible to optically assess where the substrate bound VACNTs are located and thus machine samples that are purely neat resin and purely VACNT composite material respectively. **Figure 4.4** details a schematic which illustrates the areas of the sample where each sample was machined from.

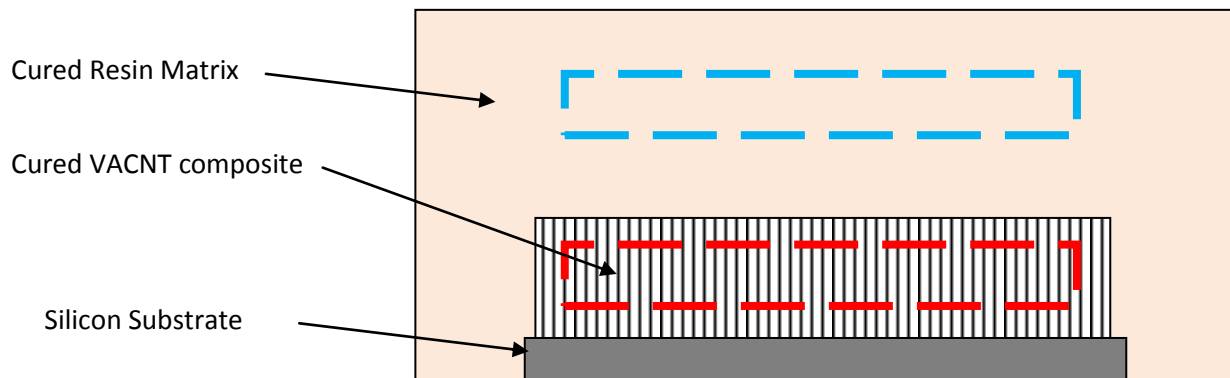


Figure 4.4: A schematic of the cured composite when removed from the silicone mould. The blue dashed line is indicative of where approximately where Neat Resin samples are machined from and the red dashed line indicates where VACNT samples are machined from.

Test coupons were cut from the material in two different sizes in order to suit DMTA and micro tensile testing procedures. DMTA samples were produced having dimensions of approximately 15 x 4 mm area and 1 mm height in the axial direction. Although the height of the VACNT forests often extends beyond 1 mm, there are key benefits to selecting this 1 mm height for DMTA samples. By careful positioning of the sample prior to machining the substrate is removed during the first cut as well as the lower $\sim 100 \mu\text{m}$ of the VACNT forest, the saw can then be moved by a distance of 1 mm plus the width of the blade before conducting a further cut where a slice of the sample of 1 mm

thickness is removed. Using this method to cut samples ensures that the VACNTs remain aligned in the correct direction, removes the catalytic substrate and also removes any catalytic particles remaining from the base growth CVD CNT production process. Furthermore this method removes disordered parts of the VACNT forests structure that may remain at the base, top (crust layer) and edges of the VACNT forest after growth as a result of the growth mechanism [209]. These samples are then simply machined to the required area using the same technique, before being ready for DMTA. Neat resin samples for DMTA testing are cut using the exact same method after the VACNT composite material had been removed. **Figure 4.5** shows an optical image of a neat resin and a VACNT composite sample that have been machined for DMTA and **Figure 4.6** pictures the low speed saw used during sample machining.

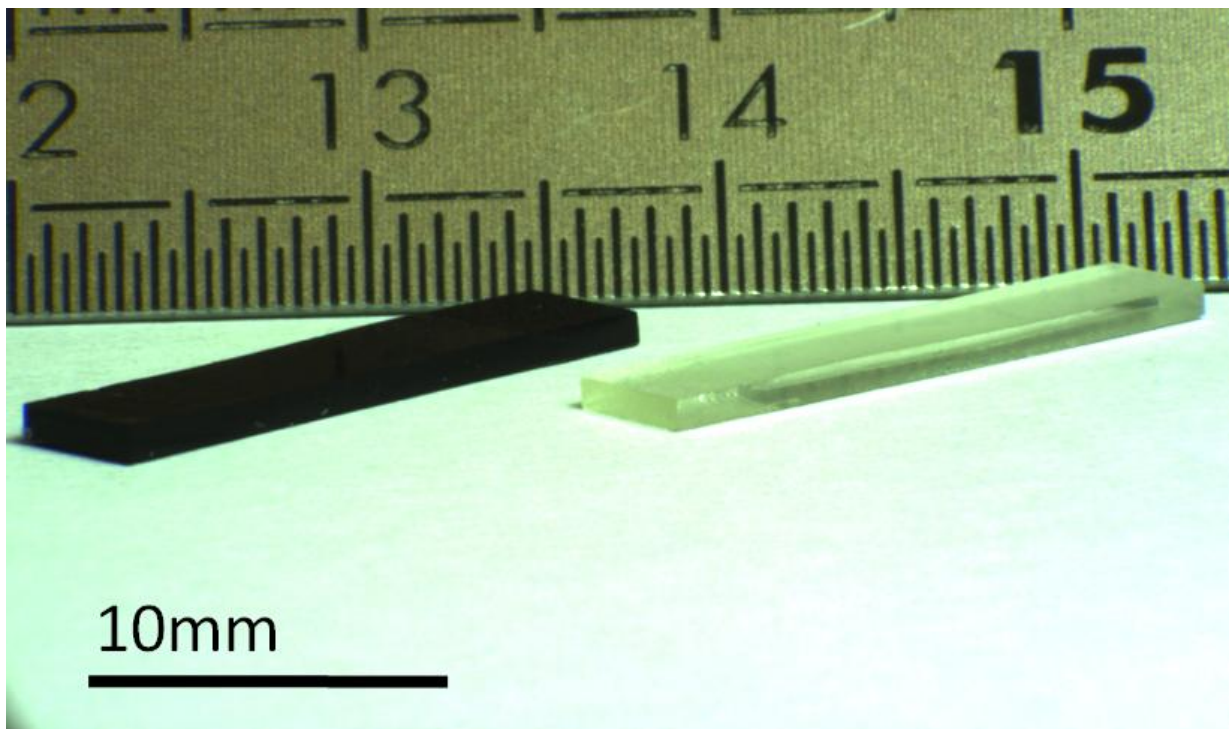


Figure 4.5: An Optical image of VACNT composite and Neat Resin samples that have been freshly machined for DMTA testing. Note how the VACNT composite (left hand side) appears almost completely black despite only containing a relatively low volume fraction (~ 2 vol%) of VACNT reinforcements.

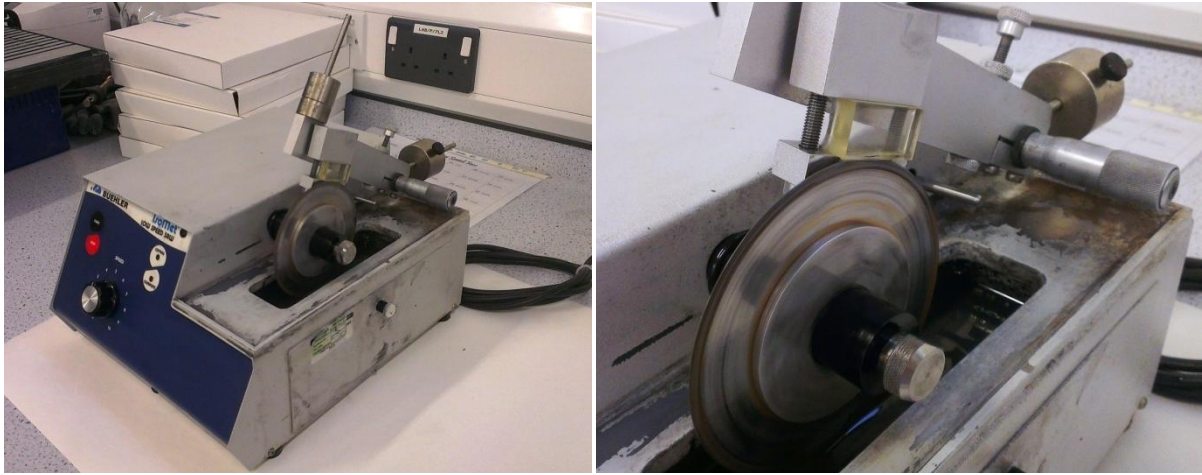


Figure 4.6: A photos of the low speed saw. The saw is fitted with a micrometer to position the blade in the desired location. To ensure clean and uniform cuts the saw is also fitted with a counterbalance system which allows the user to control the force applied to the saw blade during cutting.

Despite the large size of VACNT composite samples produced it is not possible to conduct standard tensile testing on these coupons using a full size tensile test set up. Consequently samples were produced for testing using a micro tensile test rig used for testing smaller scale samples. The Deben micro tensile test rig was fitted with a 20 N load cell thus the maximum applied load was less than 20 N, and in order to ensure the samples break during testing it was necessary to machine their dimensions accordingly. As a result micro tensile test samples were machined in a similar fashion to those for DMTA testing but to dimensions of approximately 15 x 1.5 x 0.2 mm respectively. After machining all samples were accurately measured using a micrometer and all results used to accurately calculate mechanical properties after testing. **Figure 4.7** pictures neat resin and VACNT composite test coupons used for micro tensile testing.

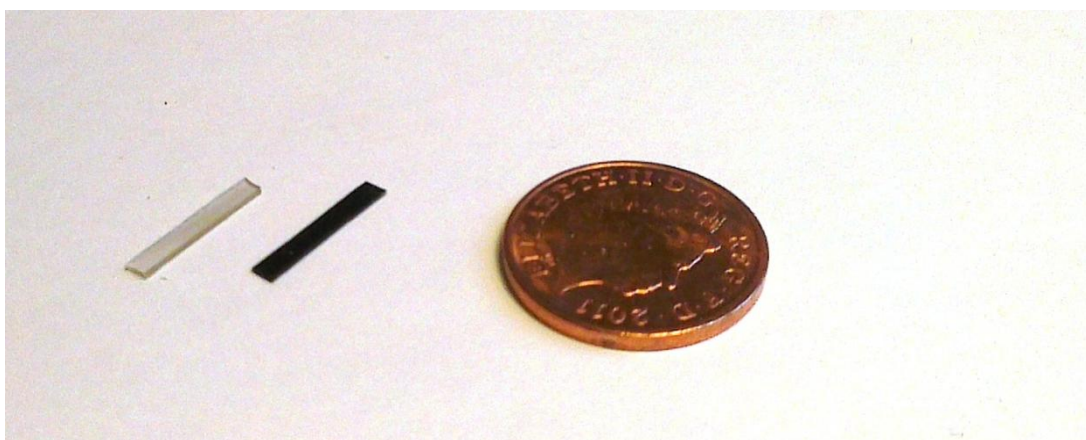


Figure 4.7: A photo of micro tensile test coupons that have been machined ready for testing. A penny is included to illustrate the size of these samples; again the VACNT composite sample appears black and is on the right hand side.

4.3 Mechanical Analysis of Large Millimetre Scale VACNT Composite Structures

The following sections detail mechanical analysis of single VACNT forest composite samples.

4.3.1 Dynamic Mechanical Thermal Analysis: Experimental Techniques

DMTA was conducted on the specially machined samples in the single cantilever mode to measure the level of reinforcement achieved in the transverse direction through reinforcement of the matrix with VACNTs. Experiments were conducted using a Mettler Toledo DMA861e that was fitted with a dual cantilever clamp which allows both dual and single cantilever testing of samples. **Figure 4.8** pictures the DMTA used and also a detailed image of the clamp used in these particular experiments.



Figure 4.8: Photos of the Mettler Toledo DMA861e the left hand image is the full machine with the furnace open revealing the clamps, and the right hand image details the clamping system. The thermocouple used to measure sample temperatures during experiment is visible in the right hand image.

In order to choose effective settings for conducting DMTA analysis several tests were conducted on extra neat resin samples. These tests ensure that sufficient load was applied to samples during the experiments to allow accurate measurement of the storage modulus of the sample whilst remaining in the elastic region of deformation. Consequently measurements were conducted using a sinusoidal load with displacement amplitude of 125.0 μm and a frequency of 1.0 Hz over a dynamic temperature profile between 20.0 $^{\circ}\text{C}$ and 125.0 $^{\circ}\text{C}$ at a heating rate of 3.0 $^{\circ}\text{C}/\text{min}$. Using this temperature range means that the samples will pass through the glass transition point during testing, so any significant effect that the presence of the VACNTs on the composites glass transition temperature can be measured. During the experiments the storage modulus (E'), loss modulus (E'') and tan delta ($\tan \delta$) were measured as functions of the sample temperature. Three sets of neat resin and VACNT composite samples were tested and each test was run twice to ensure that the resin was fully cured and that no post cure effects were occurring during the temperature cycle.

Owing to the clamp structure the gauge length remains fixed as the clamp was untouched between experiments however minor variations in the height and width of samples were accurately measured using a micrometer for each individual sample and then used in further calculations. **Figure 4.9** illustrates a schematic of how the sample is clamped indicating the transverse direction in which the modulus is being measured as well as the direction of the load being applied in the DMTA tests.

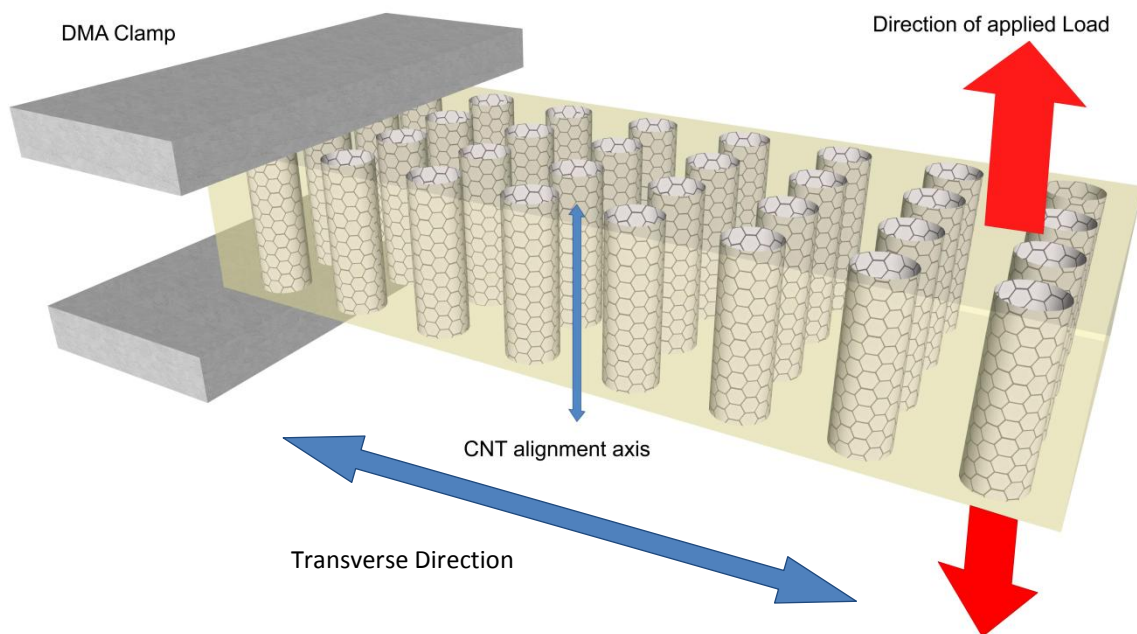


Figure 4.9: A schematic illustrating a close up view of how a sample is clamped during single cantilever DMTA testing. The schematic indicates the CNT alignment axis, the direction of the applied load, and the transverse direction in which the samples storage modulus is being measured.

4.3.2 Dynamic Mechanical Thermal Analysis: Results

Results from DMTA testing were compared for neat resin and VACNT composite that were produced in the same composite production cycle in order to identify mechanical improvements as a result of the VACNT reinforcements. Small variations in the value of the glass transition temperature can be explained through small experimental discrepancies in cure profiles and mix ratios of the resin and hardener as well as the proximity of the thermocouple to the relatively small samples during testing. Furthermore the volume of the steel clamping assembly is large when compared to the composite sample so this may also influence the measurement of sample temperatures recorded during DMTA. **Figures 4.10-4.12** show plots of the Storage Modulus plotted against the sample temperature for the three composite samples that were tested. Each graph shows a repeat of each test for both VACNT composite and the neat resin samples.

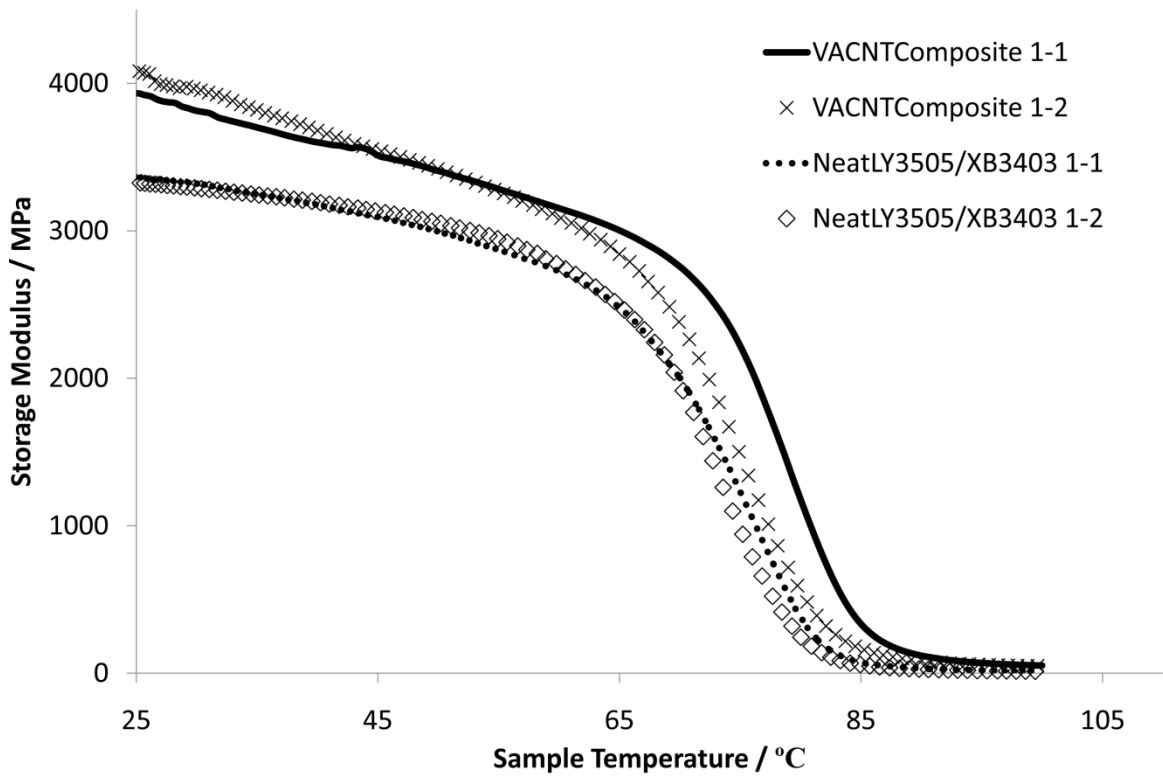


Figure 4.10: Plot of Storage Modulus against Sample Temperature for the first batch of VACNT composite samples.

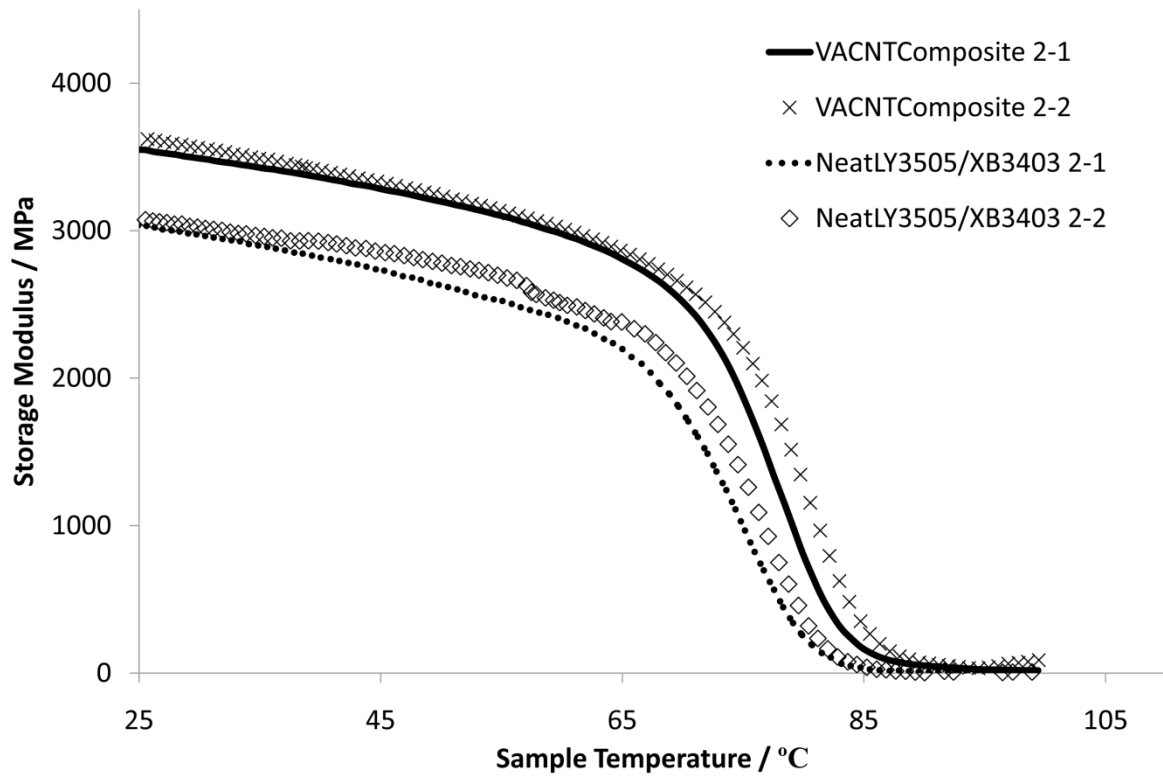


Figure 4.11: Plot of Storage Modulus against Sample Temperature for the second batch of VACNT composite samples.

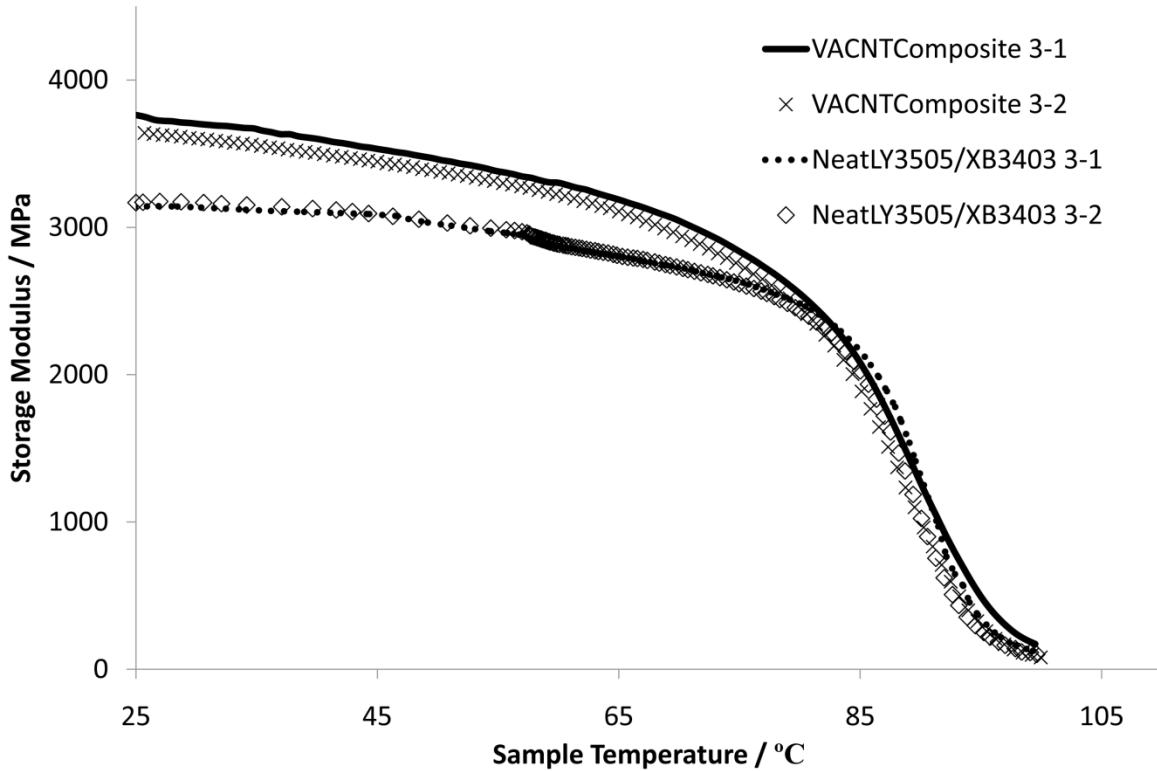


Figure 4.12: Plot of Storage Modulus against Sample Temperature for the third batch of VACNT composite samples.

By repeating DMTA analysis on the same samples two key points are concluded from the repeatability of the experiments when examining measured moduli and T_g values. These are that the resin is fully cured and that no post curing occurs during the temperature sweep and also that no thermal degradation is occurring as a result of the DMTA process. By comparing the values of Storage Modulus at a fixed temperature it is possible to approximate the increase in modulus that occurs due to VACNT reinforcement of the matrix in the transverse direction. Average increases in Storage Modulus were calculated for all three samples and an average improvement of $21 \pm 1.0\%$ was observed at a temperature of 25°C.

4.3.3 Micro Tensile Testing: Experimental Techniques

To further confirm results obtained using DMTA a series of micro tensile tests were conducted on test coupons produced using the methods described previously. The micro tensile test rig used was manufactured by Deben and installed with an accurate 20 N load cell. An image of the tensile rig is shown in **Figure 4.13**. When conducting tensile testing the test coupons were carefully clamped in the rig using a consistent 10 mm gauge length for all samples. The rig is located under an optical microscope which is used to aid accurate sample mounting as it is vital that test coupons are mounted square to the rig to ensure that precise mechanical properties are recorded. Tensile tests

were performed using a constant extension speed of 0.1 mm/min and the tensile load (F) and sample extension (e) were recorded with a sample time of 500 ms until the test coupons failed.

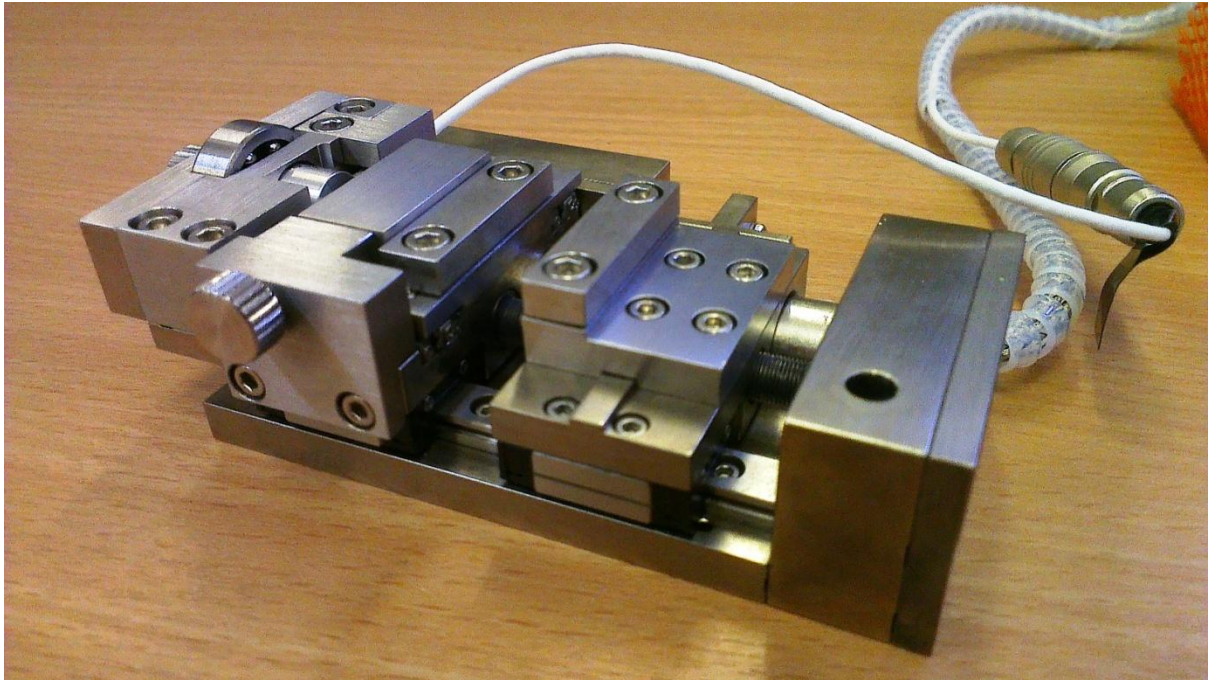


Figure 4.13: The Deben micro tensile test stage used in micro tensile testing experiments, for clarity it has been removed from the microscope assembly.

In total three samples were tested for both neat resin and VACNT composite materials using identical test parameters each time. The data recorded in each test was used to calculate the stress (σ) and strain (ε) values for the samples using the cross sectional area of the sample and gauge length in use. The data can then be plotted as stress-strain curves for each sample allowing calculation of the modulus from the gradient of the curve during the linear region of elastic deformation. Furthermore values for the average tensile strength of the coupons can also be measured although ideally a considerably larger batch of coupons would have been tested in order to increase the reliability of ultimate tensile strength results as these values often vary between samples as a result of minor structural defects.

4.3.4 Micro Tensile Testing: Results

The stress-strain curves obtained for each sample were used to calculate the tensile modulus using the stress strain relationship in **Equation 1**, as follows,

$$E_T = \frac{\sigma}{\varepsilon} = \frac{F/A}{e/l} \quad (1)$$

where E_T is the tensile modulus of the sample, A is the cross sectional area of the sample, l is the gauge length, and all other symbols represent parameters described previously. **Figure 4.14** shows a plot for a single neat resin and VACNT composite sample illustrating how values of elastic modulus were calculated.

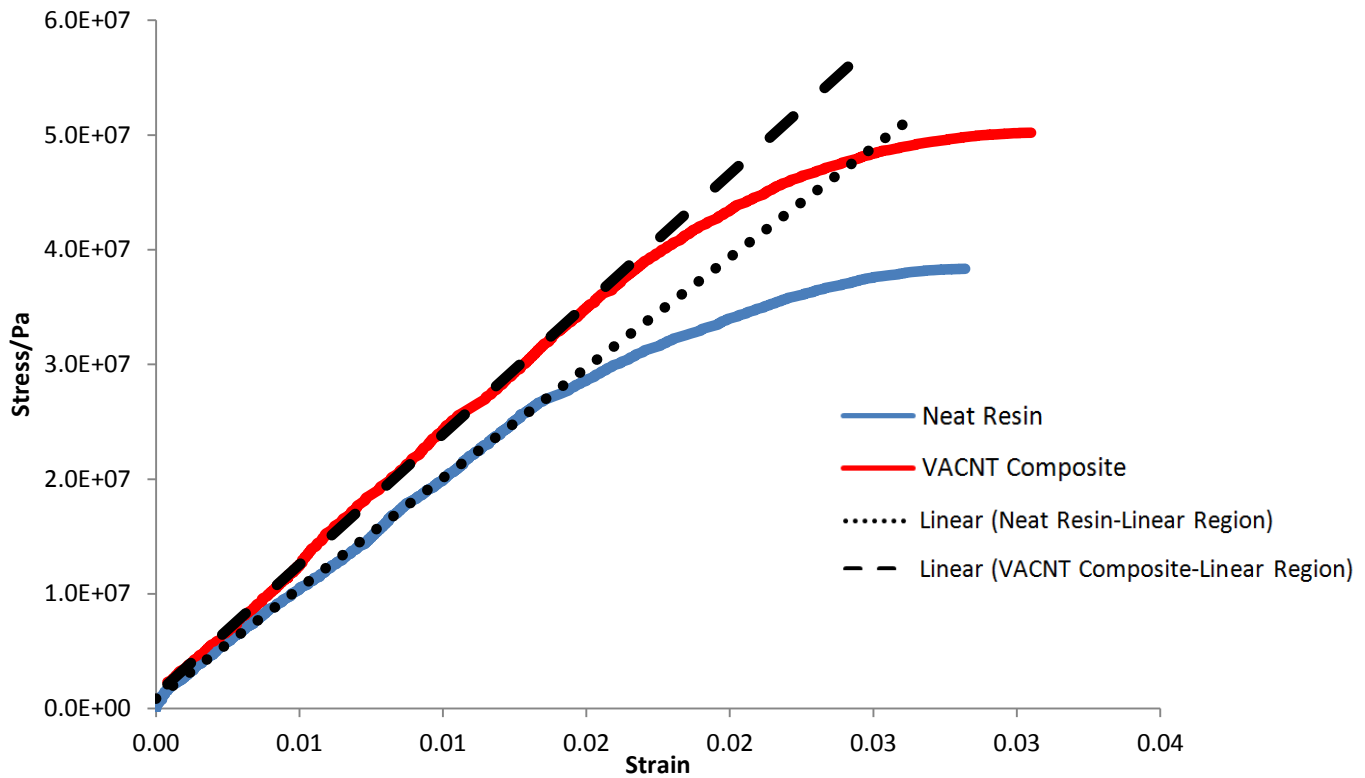


Figure 4.14: An example of stress strain plots for a VACNT composite coupon and a Neat resin coupon. The plots illustrate how tensile modulus and breaking strain were calculated from the data.

The curves clearly illustrate a linear elastic region of deformation before plastically deforming and finally breaking at the ultimate tensile strength. As the samples used in micro tensile testing were considerably thinner than those used in DMTA testing all of the samples were cut from a single VACNT composite sample eliminating any discrepancies that could occur as a result of minor changes in cure profile or mix ratios. By comparing average values of the tensile elastic modulus for neat resin and VACNT samples it was found that an average increase in tensile modulus of $17 \pm 2.6 \%$ was observed. Furthermore an increase of $20 \pm 5.2 \%$ was also observed in tensile strengths of the composite coupons when compared to the neat resin samples

4.3.5 Thermo Gravimetric Analysis: Experimental Techniques

In order to accurately model the VACNT composite structure it is vital to calculate the volume fraction of VACNT reinforcements present in the samples. Although this can be done using several methods, and as a result of the production process should be similar to as grown VACNT forest

structures, around 1-2 vol% [82], the volume fraction was accurately measured using thermo gravimetric analysis (TGA). This method relies on the differences in the thermal stabilities of the resin and the VACNTs and has been used previously in the literature, for example by Bradford et al. [218] TGA experiments were performed on samples of as grown VACNT forest, neat resin, and VACNT composite under a nitrogen flow. Experiments were conducted using a Netzsch TG209 TGA that is pictured in **Figure 4.15**. The samples were ramped to 700 °C at a rate of 10 °C/min whilst the total sample mass was accurately recorded. Both neat resin and VACNT composite samples were again taken from the same batch to remove any discrepancies that could occur during resin mixing and hardening. Experiments were conducted three times for each material and the average mass losses deducted and used to calculate the mass of VACNT present in the composite samples.



Figure 4.15: The Netzsch TGA used to conduct TGA experiments under Nitrogen flow.

4.3.6 Thermo Gravimetric Analysis: Results

As CNTs possess excellent thermal stability up to high temperatures it is expected that they will show no net mass change when heated to 700 °C under a Nitrogen flow, as they will not react with the nitrogen and will not thermally decompose. Conversely thermoset resins are known to degrade into gaseous components at such high temperatures although inevitably some material will remain due to the complex structure of high performance resins. Consequently the percentage mass difference remaining after TGA had been conducted on neat resin and VACNT composite samples reflects the percentage mass of VACNTs present in the composite samples. VACNT volume fractions (f_f) can then be calculated from the data by using the densities of the VACNT composite (ρ_c) and neat resin (ρ_m) samples in the following equation,

$$f_f = 1 - \frac{(1-m_f)\rho_c}{\rho_m} \quad (2)$$

where m_f is the VACNT mass fraction which is calculated to be $\sim 1.7 \pm 0.2$ wt% and all other symbols are defined previously [218]. The densities of the neat resin and composite samples are calculated by accurately measuring and weighing DMTA test samples prior to testing and found to be $\sim 1.3 \text{ gcm}^{-3}$ and $\sim 1.35 \text{ gcm}^{-3}$ respectively. Consequently the approximate volume fraction of VACNTs in the samples was found to be ~ 2 vol% which is typical of as grown VACNT forests. **Figure 4.16** illustrates average plots for percentage mass lost during TGA for all three samples as well as a zoomed in section of the relevant portion of the graph used to calculate the volume fraction of VACNTs. The plot for the as grown VACNT forest indicates no net mass changes over the process and confirms the thermal stability of the VACNTs during TGA testing.

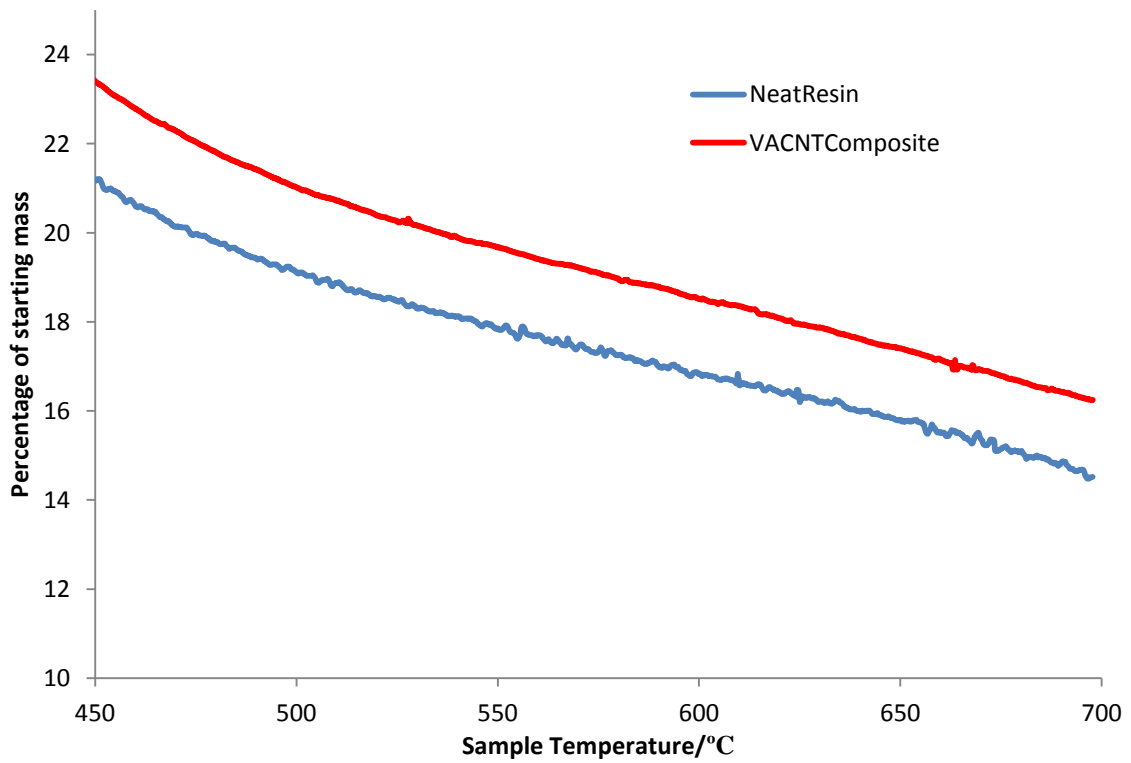
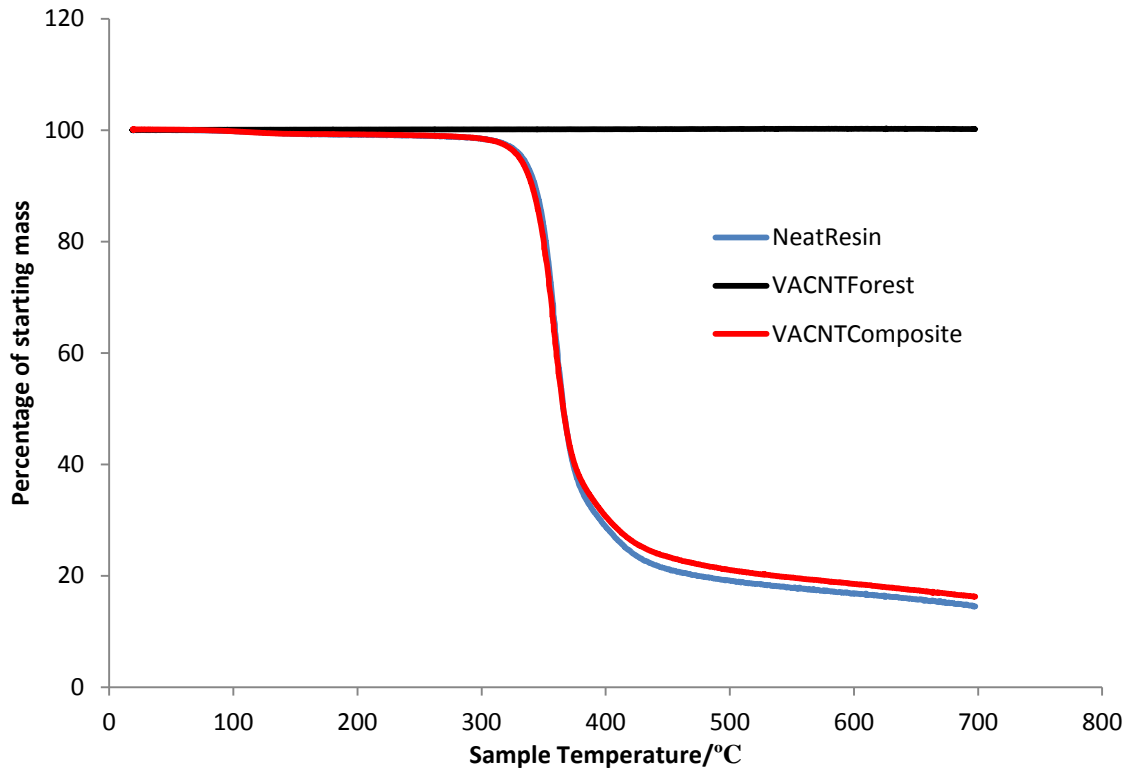


Figure 4.16: Examples of TGA plots that were used in the calculation of VACNT volume fractions in VACNT composite samples. The first graph illustrates that VACNTs are unaffected by the TGA process and the second details the difference between VACNT composite and neat resin samples observed at elevated temperatures.

4.4 Modelling of a VACNT Composite Material

By modelling a composite material using the properties of its components effective predictions of the complete structures properties can be envisaged. In the field of composites materials many models exist that have been shown experimentally to effectively predict the mechanical reinforcement achieved by using various fillers in composite structures. As well as considering the mechanical properties of a composite materials components such models also incorporate the orientation of a composites microstructure. Consequently many models exist for the various fibre and particle reinforced composites that can be produced and have even been used to assist in improving levels of reinforcement that are achieved. In the case of the VACNT composites tested it is often assumed that the VACNTs act as uniaxially aligned fibre reinforcements [160]. However more recently some researchers have begun to consider the wavy structure of VACNTs that can be observed at the nanoscale and the effects of such waviness on the ability of VACNTs to reinforce composite structures [141]. This section will apply such models to the VACNT composites that have been produced and tested previously.

4.4.1 Modelling a VACNT Composite Material using Uniaxially Aligned Fibre Models

Modelling of uniaxially aligned continuous fibre composite materials has traditionally been conducted using two models that predict the so called axial and transverse moduli for a material. These are known as the Voigt and Reuss models respectively [190], [191]. **Figure 4.17** illustrates a simple schematic of a uniaxially aligned composite material and is useful in defining the axial and transverse orientations.

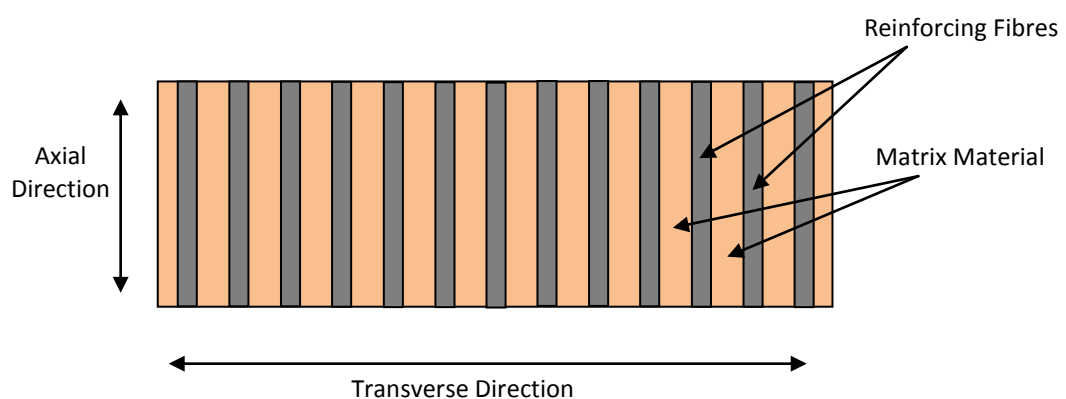


Figure 4.17: Example Schematic of a continuous uniaxially aligned fibre composite material. Although this is a 2D schematic the transverse direction is isotropic throughout the plane and the schematic can be thought of as a cross section of the material

The Voigt model simplistically calculates the predicted maximum axial modulus of a material based on the properties of the matrix and fibres and the volume fractions of each material as follows,

$$E_{Axial} = E_m v_m + E_f v_f \quad (3)$$

where E_m and E_f are the elastic moduli of the matrix and fibre respectively and v_m and v_f are the volume fractions of each. Clearly this model contains some assumptions in order to keep its simplicity and consequently provides a maximum estimate for composite modulus. These assumptions include the uniform distribution of the fibres in the matrix as well as the perfect coupling of matrix and fibre at the interface. Despite such assumptions the model has been shown to give effective predictions with micro scale composites such as GRPs [5]. As Voigt's rule is effective it is reasonable to assume that composites can be improved accordingly by increasing the modulus and volume fraction of fibre reinforcements in a matrix material. As VACNTs have been reported to have a high elastic modulus of up to 1 TPa [7] it is clear that they are ideally suited to reinforcing matrix materials and have the potential to greatly improve the modulus of composite structures. **Table 4.1** details the values used to calculate the predicted axial modulus using the Voigt model for comparison to the experimental results in this work. A value of 200 GPa is used for the CNT modulus as values in the literature vary vastly and this is a sensible mid range approximation for MWCNTs produced using CVD.

| Variable | E_m / GPa | E_f / GPa | v_m | v_f |
|-----------|-----------------|-------------|-----------------|-----------------|
| Value | 3.34 ± 0.03 | 200 | 0.98 ± 0.01 | 0.02 ± 0.01 |
| Reference | DMTA | [7] | TGA | TGA |

Table 4.1: Values of variables used in calculating Reuss and Voigt predicted moduli for a VACNT composite

By inputting the values above to the Voigt model an increase in modulus of approximately ~118 % can be expected in the axial direction for only a 2 vol% VACNT composite thus illustrating a large improvement with only small amounts of VACNTs being added. If the volume fraction of VACNTs was to be increased further then even greater improvements in modulus are to be expected for example if a 50 vol% of VACNTs was used then improvements of up to ~3000 % are theoretically possible. Following from the results obtained using the Voigt model for axial modulus it is also important to understand transverse properties of the composite material which have been tested in this work, particularly when considering building multilayer composite components such as those discussed in **Chapter 2**. The Reuss model predicts the transverse modulus of uniaxially aligned fibre composites as follows,

$$E_{Transverse} = \frac{E_m E_f}{E_m v_f + E_f v_m} \quad (4)$$

where all symbols have identical meaning to those described in the Voigt equation previously. Again using the values indicated in **Table 4.1** it is possible to perform quick calculations of the predicted transverse modulus which for a 2 vol% VACNT content equates to an increase in modulus of just 2 %. This value thus indicates, as expected, that only minimal reinforcement occurs in the transverse orientation despite the high modulus of the VACNT reinforcements and even when volume fraction is increased to 50 vol% modulus increases of only around ~550 % can be expected. Comparing these predictions with the best experimental data in the literature which exist for measurements of the axial modulus of VACNT composite structures still indicates that reinforcement levels are considerably below these values despite impressive improvements in Young Modulus for these materials [141]. Initially various explanations for such discrepancies were offered, such as the modulus of CNTs being considerably lower than values quoted, as well as the presence of voids in composite samples [219]. More recently some researchers realised that these discrepancies may be a result of the microstructure of the as grown VACNTs when used in composite materials. These ideas stem from viewing VACNTs under high magnification SEM where the individual VACNTs appear wavy and disordered compared to the highly ordered aligned structures that are visible at lower magnifications. **Figure 4.18** shows small areas of the same VACNT forest at different magnifications under SEM to clarify the wavy structure of VACNT at this scale. By including this waviness in composite modelling it has been shown that more accurate predictions can be given when comparing models with experimental values for the axial modulus of VACNT composite materials [220].

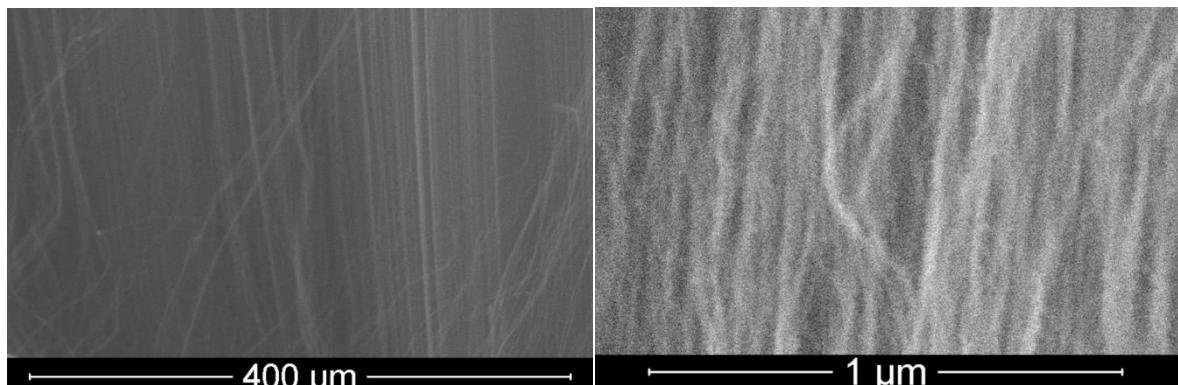


Figure 4.18: SEM images of the same VACNT forest at different magnifications, at low resolution the CNTs appear very straight but at higher magnifications the wavy structure becomes significant.

4.4.2 Modelling a VACNT Composite Material with Wavy Fibre Models

The concept of wavy fibre reinforcements in composite materials has been investigated long before the discovery of CNTs by various researchers [221]. Several models exist and have been tested against experimental data for micro scale composite materials with promising results. More recently Cebeci et al. [141] used an axial Finite Element (FE) model devised by Fisher et al. [214] to investigate how increasing VACNT volume fraction matched with the wavy model through nanoindentation testing of small composite samples in the axial direction. Their results show good agreement with the wavy model for volume fractions of VACNT up to 40 vol% and consequently they believe that VACNT waviness might be the dominating factor in achievable reinforcement in current VACNT reinforced composite materials [141]. In this work, results are compared to a wavy model developed by Chou and Takahashi [221] that is based on traditional rule of mixtures methods and relies on splitting wavy fibres into reinforcing components. This model also contains many assumptions similarly to the Voigt and Reuss models, including again the perfect coupling of fibre and matrix as well as a complete lack of voids in the sample. In the works of Kuo et al. [222] Chou and Takahashi's model is adapted to predict properties for the transverse modulus of a wavy fibre reinforced composite in a similar fashion, and the models are defined as follows. For the axial modulus,

$$E_{axial-wavy} = \frac{(1+c)^{3/2}}{\left(1+\frac{c}{2}\right)S_{11} - \left[1+\frac{3c}{2} - (1+c)^{3/2}\right]S_{22} + \frac{c}{2}(2S_{12}+S_{66})} \quad (5)$$

And for the transverse orientation,

$$E_{transverse-wavy} = \frac{(1+c)^{3/2}}{\left[(1+c)^{3/2} - 1 - \frac{3c}{2}\right]S_{11} + \left(1+\frac{c}{2}\right)S_{22} + \frac{c}{2}(2S_{12}+S_{66})} \quad (6)$$

where,

$$c = \left(\frac{\pi a}{\lambda}\right)^2 \quad (7)$$

and,

$$\left. \begin{aligned} S_{11} &= \frac{1}{E_A}, & S_{22} &= \frac{1}{E_T}, & S_{12} &= -\frac{\nu_{AT}}{E_A}, & S_{66} &= \frac{1}{G_{AT}} \end{aligned} \right\} \quad (8)$$

In the above equations the values of the axial (E_A), and transverse (E_T) moduli are calculated using the Voigt and Reuss equations defined previously and the shear modulus (G_{AT}) and composite Poisson's ration (ν_{AT}) are calculated as follows,

$$\nu_{AT} = \nu_f \nu_f + \nu_m \nu_m, \quad G_{AT} = \nu_f G_f + \nu_m G_m \quad \} \quad (9)$$

where,

$$G_f = \frac{E_f}{2(1+\nu_f)}, \quad G_m = \frac{E_m}{2(1+\nu_m)} \quad (10)$$

where G_f and G_m are the respective shear moduli of the fibre and matrix and ν_f and ν_m are their respective Poisson's ratios. The constant c is used in the formula to define the waviness of the fibre reinforcements in the structure and **Figure 4.19** illustrates how the values of a and λ used in calculating c are related to the fibre geometry. The fibres are treated as uniformly distributed continuous sinusoidal reinforcements in order to simplify calculations.

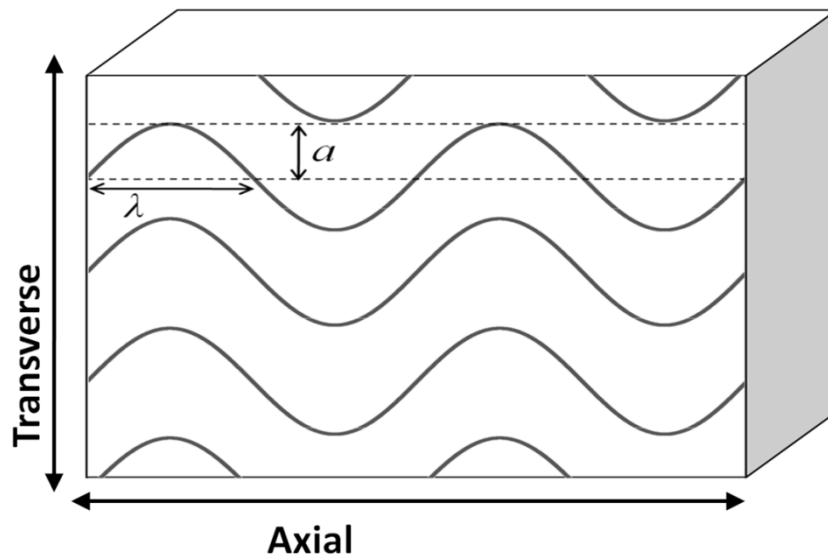


Figure 4.19: Schematic of the wavy composite structure illustrating how waviness is calculated from an assumed sinusoidal form of the CNT reinforcements

Calculation of VACNT waviness, a/λ , in composite structures has been conducted in the literature, for instance by Cebeci et al. [141], by detailed analysis of as grown VACNT forests using high magnification SEM. Their work gives a value of 0.185 ± 0.10 for VACNT waviness for VACNT grown in a similar fashion to those used in this work. For comparison VACNT waviness is calculated in a similar way for 36 VACNTs from several high magnification images and it is found to be 0.20 ± 0.10 in this study which is a comparable value as expected. Calculating waviness in this fashion is far from

perfect as assumptions are made that the VACNT forest's microstructure remains unchanged during resin infiltration, however a fair approximation can be gained and experimental data has previously been shown to be in agreement. Furthermore SEM analysis of composite samples for DMTA testing that were fractured under liquid nitrogen does not clearly reveal the VACNT within the composite sample. Although these images do appear to show alignment within the fracture surface the identification of individual VACNT is challenging and somewhat speculative particularly when using low volume fractions of VACNT as in this case. Wardle et al. [16] have successfully identified VACNT in high volume fraction composite samples but even these images do not accurately reveal the waviness of the as grown VACNTs as is possible with high magnification SEM of as grown structures. **Figure 4.20** illustrates SEM images of fracture surfaces of VACNT samples produced in this work with an indication of the axial direction displayed on the images. These images reflect results observed by other researchers for similar VACNT composite materials and CNT alignment appears visible, although measurement of individual CNT waviness is not viable [16]. Furthermore these images also indicate that little or no voids are present in the samples and that the resin has indeed successfully and fully penetrated into the VACNT forest structure. To further confirm full wetting of samples μ -CT analysis of samples was conducted and no visible micro scale voids were detected. It was hoped that the VACNT might be identifiable when using μ -CT analysis however experiments have shown that VACNT are not detectable, at least at such low volume fractions when using μ -CT analysis and composite samples appear uniform. **Chapter 5** focuses on the results of μ -CT analysis of VACNT-polymer samples and consequently the subject is not discussed further here.

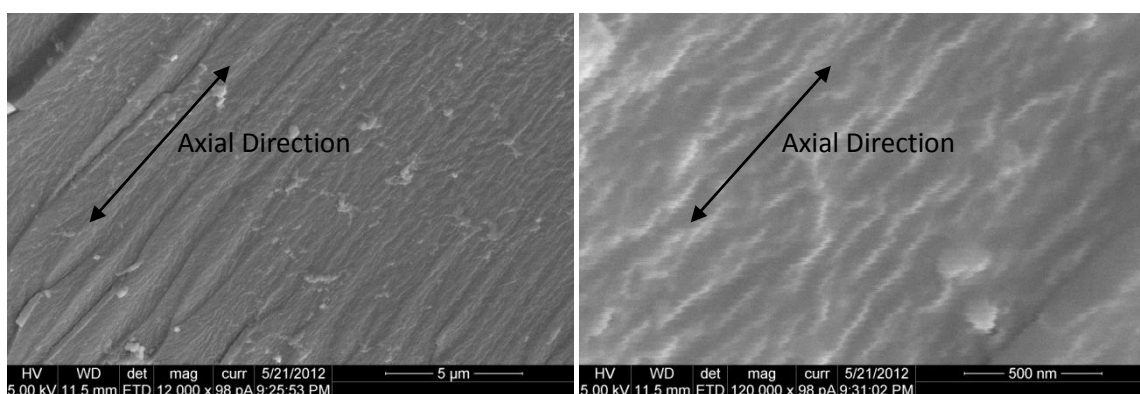


Figure 4.20: SEM images of the VACNT composite sample fracture surfaces at different magnifications. The axial direction is marked and fibre alignment appears visible.

Figure 4.21 details a high magnification SEM image with examples of VACNTs used for the waviness calculation. Individual VACNTs are marked on the image before values of a and λ are measured

digitally and then consequently used to calculate waviness. It is clear that VACNT forests are far from perfect sinusoidal reinforcements but by averaging values over a range of VACNTs a sensible approximation can be drawn.

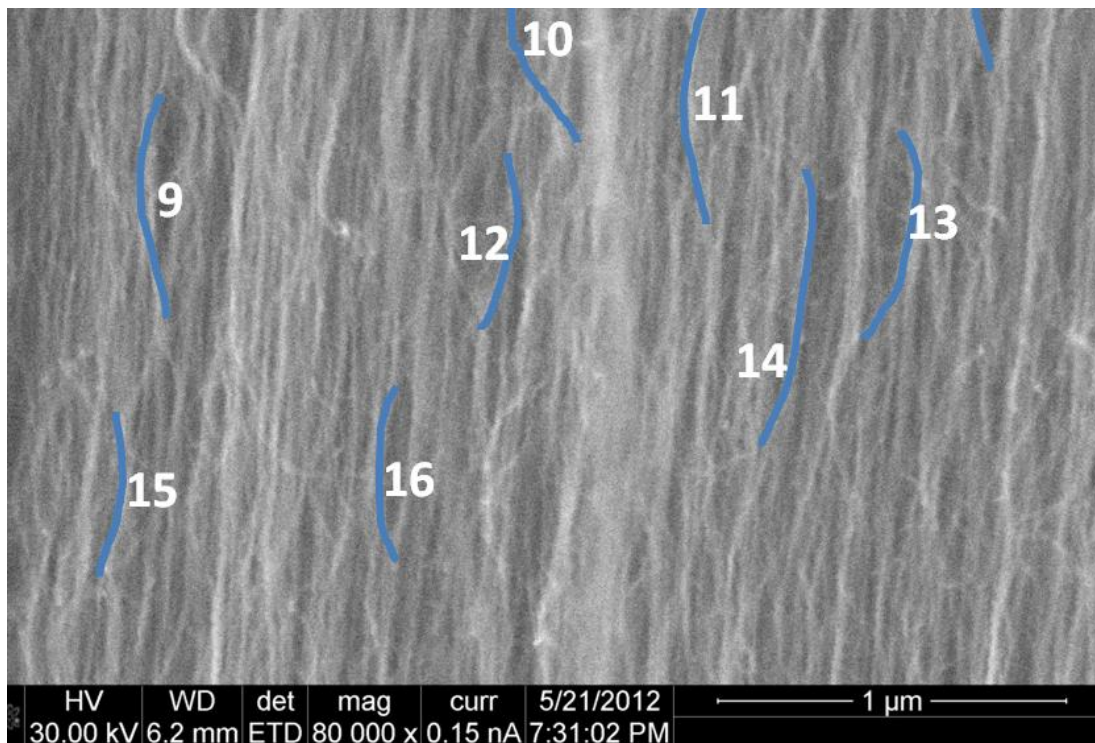


Figure 4.21: High magnification SEM image of an as grown VACNT forest structure indicating how the average VACNT waviness was calculated.

Predicted values of reinforcement for the wavy model can consequently be calculated using the values used previously for the Voigt and Reuss models. When considering Poisson's ratio a value of 0.4 is assumed for both VACNTs and Resin matrix. This is a sensible approximation as it has been shown previously that the Poisson's ratio only influences the results of the predicted elastic moduli in curved fibre rule of mixtures model by approximately $\pm 5\%$ between the values of 0.2 and 0.5 which are sensible limits for the materials in use [220]. By calculating values of predicted reinforcement for axial and transverse moduli compared to Neat resin samples it is possible to plot both moduli as a function of the VACNT waviness for comparison with available experimental data [215] and values calculated for the waviness measured in this work. **Figures 4.22 and 4.23** illustrate plots of this data with **Figure 4.22** illustrating the general trend of reinforcement with waviness over a wide range and **Figure 4.23** details the portion of the curve of interest with various experimental results plotted accordingly.

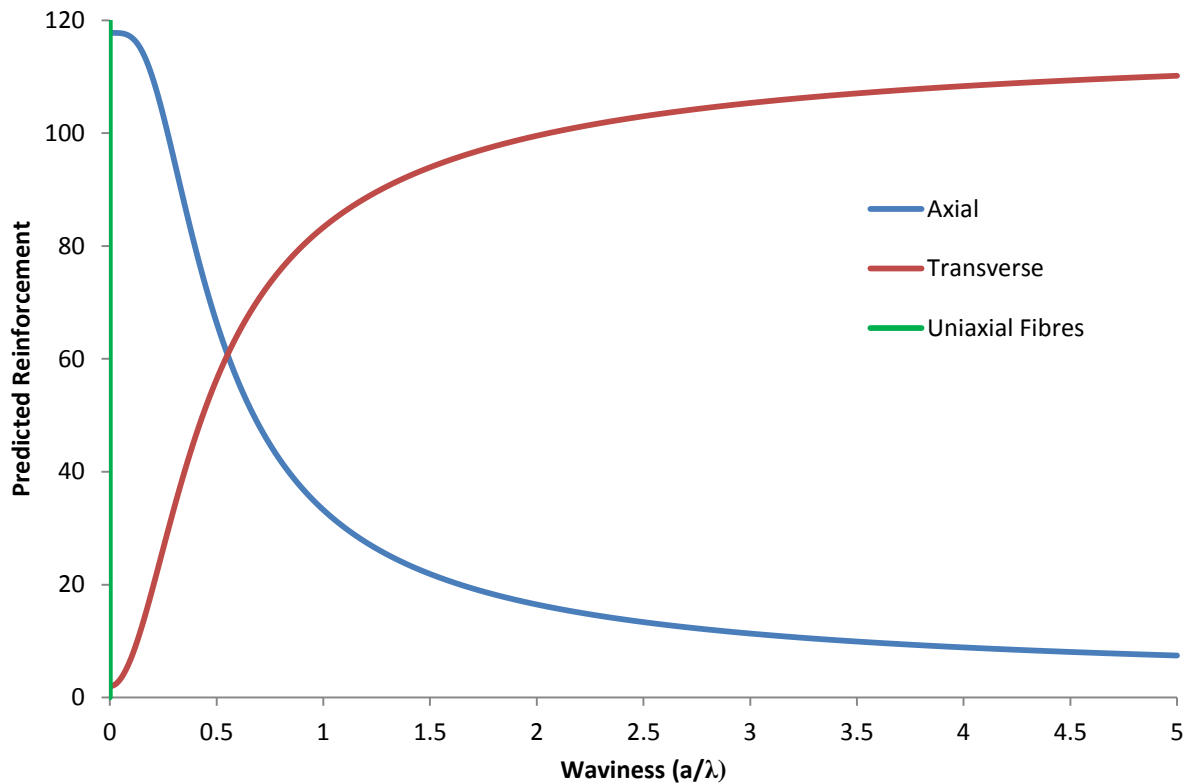


Figure 4.22: Plot of the curved Rule of mixtures model for both Transverse and Axial directions as a function of fibre waviness. The line along the y axis indicates uniaxial straight fibre reinforcement. The plot indicates that extremely wavy fibres will provide greater reinforcement in the Transverse orientation than the axial.

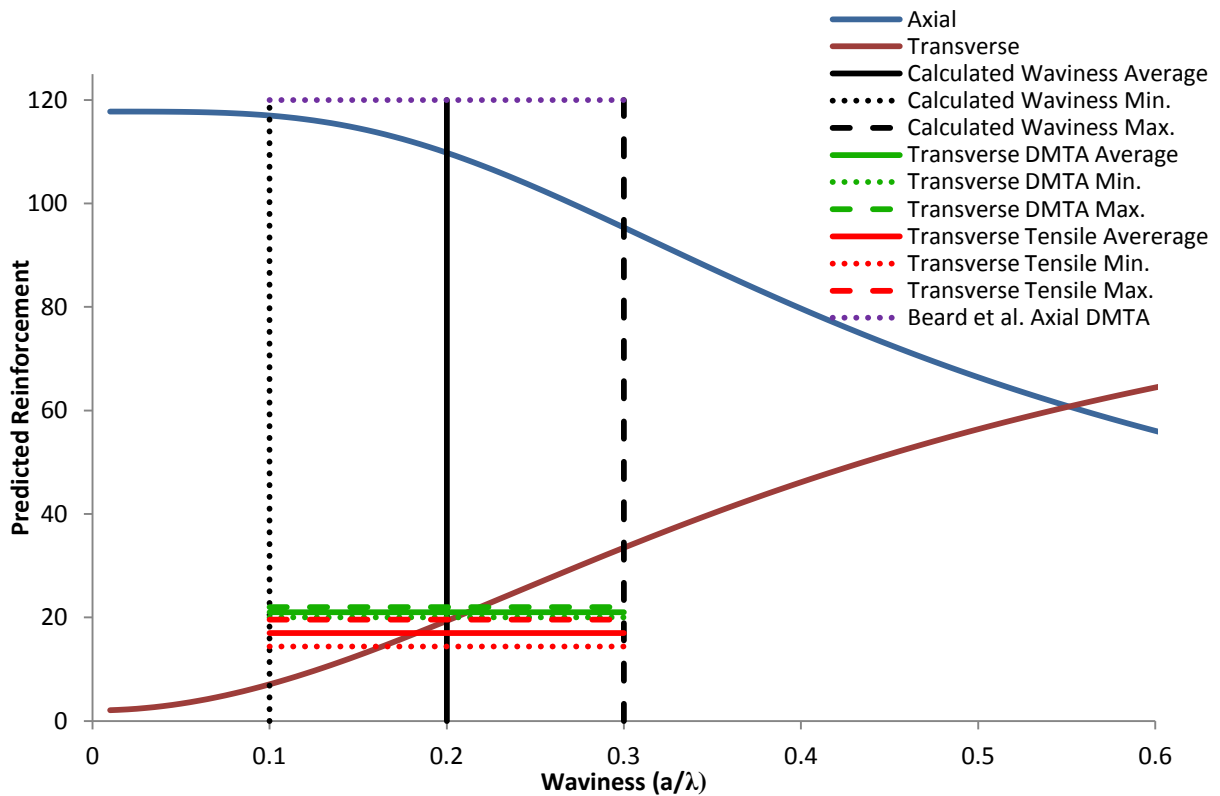


Figure 4.23: Detailed plot of the wavy model with experimental data included from this work for Transverse Modulus and literature values for Axial modulus from Beard et al.'s [215] work

4.5 Discussions and Conclusions

In order to confirm the level of reinforcement in the transverse direction mechanical testing using DMTA and a micro mechanical tensile test rig was conducted in order to measure improvements in the elastic modulus of the composite. The storage modulus of the VACNT composite and neat resin samples as measured using DMTA are plotted in **Figures 4.10-4.12**, previously. The results show that over the temperature sweep a moderate improvement in the storage modulus of the VACNT composite was observed below the glass transition temperature when compared to the neat resin sample. Specifically it is noted that at 25 °C an average improvement in storage modulus of approximately $21 \pm 1.0 \%$ was recorded across the composite samples when compared to the neat resin samples. During the DMTA sweeps the loss modulus was also recorded allowing calculation of the $\tan \delta$ curves for the samples and accurate measurement of the glass transition temperature. The samples show similar glass transition temperatures with differences of less than $\pm 5 \%$ being recorded for both the neat resin and VACNT composite samples in each case. Small deviations observed between VACNT composite and neat resin glass transition temperatures are most likely a result of CNTs slightly affecting the cure mechanism of the resin [223], or experimental errors that may occur due to locating the thermocouple in close proximity to the sample when mounted in the relatively large DMTA steel clamping assembly. As well as DMTA, micro tensile tests were performed in order to confirm the increase observed in flexural storage modulus was also present in reinforced VACNT composite samples under a tensile load. Average values of tensile elastic modulus as well as tensile strength are listed in **Table 4.2**, along with predicted and experimental values obtained in this study and other investigations. An average increase of $17 \pm 2.6 \%$ in tensile modulus and an increase of $20 \pm 5.2 \%$ in tensile strength were observed during micro tensile testing. **Figure 4.24** illustrates a detailed plot of the Transverse model prediction and experimental data from this work with upper and lower bounds based on experimental errors.

| Direction | Traditional Model | Wavy Model | DMTA (Flexural Storage Modulus) (@ 25 °C) | DMTA (Compressive Storage Modulus) (@ 25 °C) | Micro-Tensile (Tensile Modulus) | Tensile Strength |
|------------|-------------------|------------|---|--|---------------------------------|------------------|
| Axial | ~118 % (Voigt) | ~110 % | - | 120 % [215] | - | - |
| Transverse | ~2 % (Reuss) | ~19 % | $21 \pm 1.0 \%$ | - | $17 \pm 2.6 \%$ | $20 \pm 5.2 \%$ |

Table 4.2: A comparison or Rule of Mixtures predictions for straight and curved fibre reinforcement and experimental Data for improvement for Axial and Transverse Moduli. Transverse experimental data has been measured during this work and Axial by Beard et al [215].

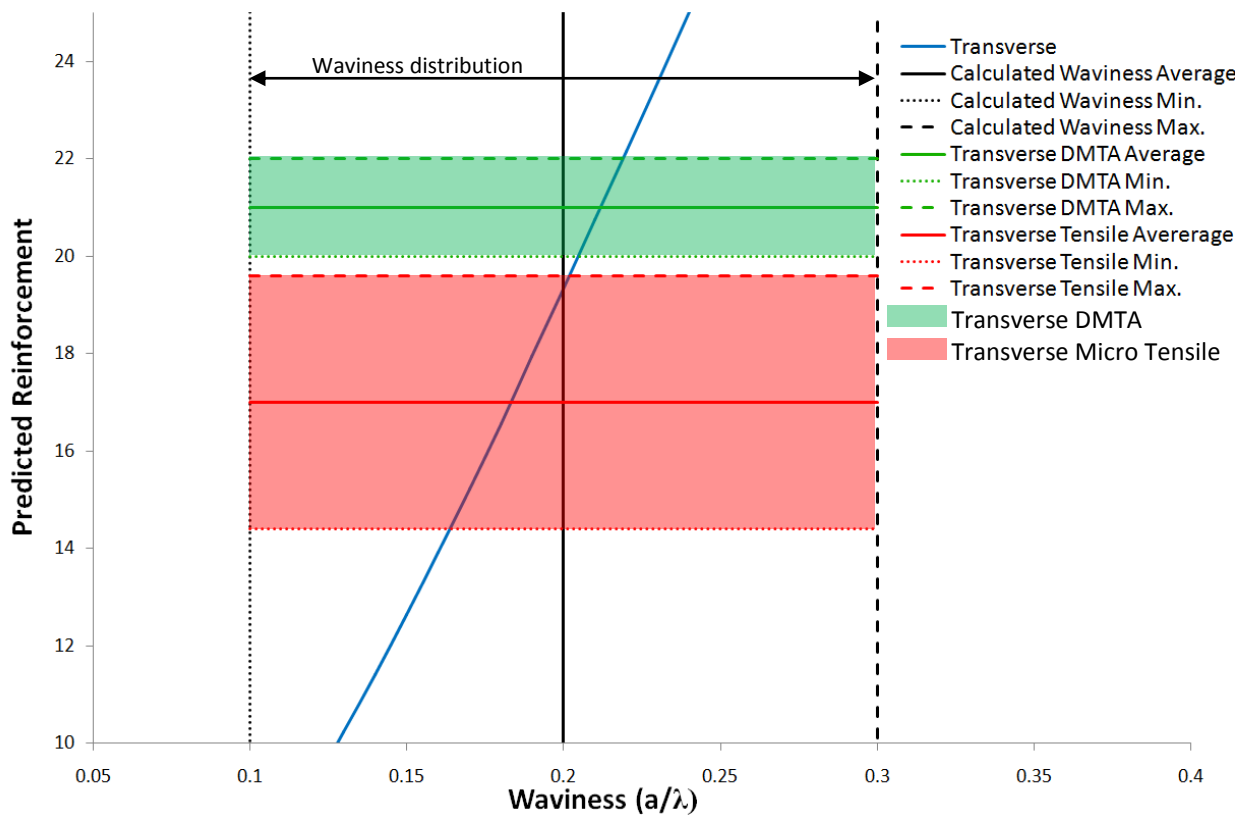


Figure 4.24: A detailed plot of the transverse moduli for VACNT composite samples against VACNT waviness including calculated theoretical values and both experimentally measured values. The measured value of VACNT waviness is also plotted with upper and lower bounds based on the standard deviation of measured VACNTs. This plot is a zoomed region of **Figure 4.23**.

In this work experimental measurement of the improvement in transverse modulus of VACNT composite samples at the millimetre scale has been conducted for the first time. Comparing experimental values with curved fibre reinforcement rule of mixtures modelling indicates good agreement. Transverse reinforcements of up to 20 % have been measured which is an order of magnitude greater than the transverse improvement in modulus expected for a straight aligned VACNT composite sample using the Reuss model. These results indicate that despite VACNT waviness being detrimental to axial modulus as observed in other works, waviness may in fact be beneficial when considering transverse properties of such a material at small volume fractions of VACNTs. These results are of particular significance when considering the feasibility of ideas discussed in the final part of **Chapter 2** as the construction of multi layer composites using AM techniques desires multidirectional reinforcement for many applications. In addition the agreement between experimental data and theoretical modelling indicates that the assumptions used in the model are sensible and that effective coupling of the VACNT reinforcements and epoxy matrix has been achieved. Furthermore it appears no obvious agglomerations are present in the samples when

fractures surfaces were examined using SEM in **Figure 4.20**. Analysis was conducted on several fracture surfaces indicating that the micro structure of the as grown forest has been retained. This is likely as as-grown VACNT structures are known to be extremely stiff and at no point during the production process are the structures exposed to excessive external forces. Consequently further understanding of reinforcing mechanisms exhibited by VACNTs can be drawn and provide a further step towards the production of high performance CNT composite materials that exhibit the levels of reinforcement expected and have potential for use in many applications.

Chapter 5

Investigations into the wetting mechanisms of vertically aligned CNT structures

5.1 Introduction

The recent development of aligned and dispersed CNT polymer composites has begun to practically illustrate the potential of these nanoscale fibres to effectively reinforce polymer matrix materials [224]. To date the most effective reinforcement of polymer matrices has been achieved through the capillary driven wetting of VACNT forests with high performance resins as discussed in depth in **Chapter 4** [141]. Such composite samples are often produced using a single VACNT forests structure which limits the scale of composite components to the millimetre regime. These small samples may have important uses in specific applications such as in the production of Microelectromechanical Systems (MEMS) as suggested by Jiang et al. [225] or in other small scale applications. It has been recognised that to extend beyond these applications and apply aligned and dispersed CNT composites to large scale components and applications it will be necessary to include multiple VACNT forests or structures into a composite material [193]. This realisation occurs from the inherent size limitations in CNT production particularly when considering CVD grown VACNT forests. A number of strategies to build composite structures containing many VACNTs exist including those suggested by Farmer et al. and discussed in depth in **Chapter 2** previously, as well as many other approaches [194]. For example in the literature Bradford et al. [218] produce bucky papers through the mechanical compression of individual VACNT forests and then use several layers of this bucky paper to produce composite test coupons. They show promising results, but even when using several bucky layers still only produce small scale samples that are less than 1 mm in thickness. Windle et al. produce VACNT fibres that are directly spun from a CVD furnace before incorporating these fibres into composite components using traditional composite manufacturing methods and also illustrate effective reinforcement [14]. Another approach has been addressed by Garcia et al, where VACNTs are grown directly onto a woven alumina fibre before resin infiltration and again considerable reinforcement is achieved [147]. Despite such successes little research has investigated the incorporation of multiple as grown VACNT forests into composites. Beard et al. have illustrated effective transfer of stress between two VACNT forests in a composite sample during DMTA compression testing and perhaps provide the closest experimental evidence for effectively

producing multilayer VACNT composites [215]. However in these works it is difficult to conclude whether such effective reinforcement would be achieved under a tensile load as there is no overlapping between the VACNT forest components which is desirable in such structures to avoid matrix rich regions.

As discussed in **Chapter 2** to build composite samples in an AM method the partial wetting of VACNT forests in a controlled fashion will be required. Despite several works illustrating techniques to embed individual VACNT forests into polymer layers [156], [157] the precise mechanism and controlling factors of these processes remains elusive. It is well known that interactions between VACNT forests and liquids is often capillary driven and through the application of traditional capillary theory and comparison with experimental observation further insights into the wetting process may be revealed. In this chapter investigations into the wetting process observed during composite production in **Chapter 4**, and from the literature, are assessed using traditional capillary theory. By understanding the influence of the fluid properties and forest structure on capillary flow further experiments are conducted to achieve partial embedding of VACNT forests within a thermoplastic material. Partially embedded forests are then analysed using micro computed tomography analysis and SEM imaging to assess the flow mechanisms which draw the polymer inside of the forest structure. It is thought that by understanding these capillary driven interactions it could be possible to control the speed and level of penetration of a fluid polymer into a VACNT forest which is of critical importance when building multilayer composite structures. Furthermore it could be possible to effectively predict experimental conditions for partial embedding of VACNT forests into polymeric layers. In doing so it could be possible to carefully select suitable polymer materials for use as a matrix in multilayer VACNT composites by tailoring the fluid properties of such a material. For example in the current advanced composite industry the properties of uncured resin matrices, such as viscosity and cure profile, are often varied to suit highly specific applications and particular production techniques.

5.2 Static Capillary Rise in VACNT forest structures

Capillary effects play a vital role across many scientific fields and consequently have been studied in depth with considerable success. Early studies into capillary effects looked at the simplest case of capillary interactions where a liquid is drawn into a thin capillary tube when inserted into a fluid reservoir. The most common scenario for consideration is that of a glass capillary being inserted into a bath of water, where it is observed that the water will rise to a specific height depending on the diameter of the capillary tube in use. In the equilibrium scenario the force created by surface tension effects occurring at the three phase boundary between the glass capillary, the liquid, and the

surrounding environment, in this case air, is balanced against the weight of the liquid being drawn into the capillary. The capillary force arises as the molecules that are in contact with the glass reach a lower energy state than those in the bulk liquid, and consequently it is energetically favourable for the water molecules to be in contact with the capillary surface and the water is drawn into the tube. It should be noted that it is not always the case that the liquid molecules reach a lower energy state when in contact with a surface and in such a case where the liquid in contact is at a higher energy state the effect is reversed. An example of such a scenario being a mercury bath and a glass capillary tube where a negative capillary rise would be observed owing to the poor interaction between the surfaces. The interaction between a liquid and a surface is often categorised using the contact angle which is calculated from the surface tensions between the fluids and solids involved as shown below in **Figure 5.1**, and is used as a measure of how well the liquid wets the solid surface.

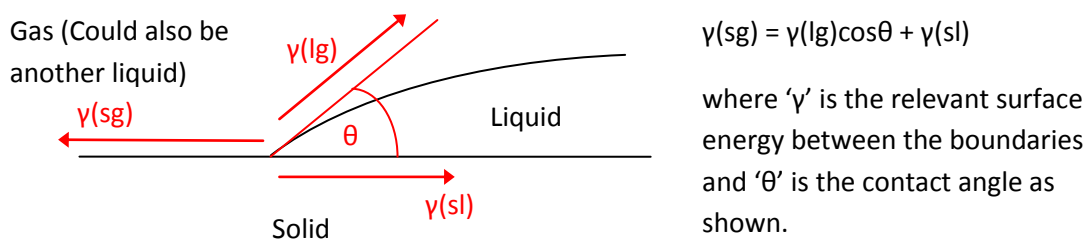


Figure 5.1: A simple schematic detailing the calculation of contact angle at a three phase interface.

Applying this to the case of a capillary follows by considering the interaction between the solid-liquid interface around the inner circumference of the tube. The total upward force resulting from this interaction is the product of the force at a single point and the distance over which it acts, in this case the inner circumference hence, where ' r ' is the inner radius of the capillary. The total force arising from surface interactions (F_{ST}) is,

$$F_{ST} = 2\pi r \gamma_{lg} \cos\theta \quad (1)$$

When capillary action occurs this force is balanced by the weight of the liquid that rises above the level of the bath, this weight is simply the product of the volume of liquid, its density (ρ), and the acceleration due to gravity (g) as follows,

$$W = \pi r^2 h \rho g \quad (2)$$

In an equilibrium case of capillary rise these two forces will be balanced and the liquid will have risen to a stable height (h) above the bath. This means the equation can be simplified to find the height of this rise from the properties of the fluids and capillary in use as follows, **Figure 5.2** shows an example of basic capillary action.

$$\pi r^2 h \rho g = 2\pi r \gamma_{lg} \cos\theta \quad (3)$$

$$r h \rho g = 2\gamma_{lg} \cos\theta \quad (4)$$

$$h = \frac{2\gamma_{lg} \cos\theta}{r \rho g} \quad (5)$$

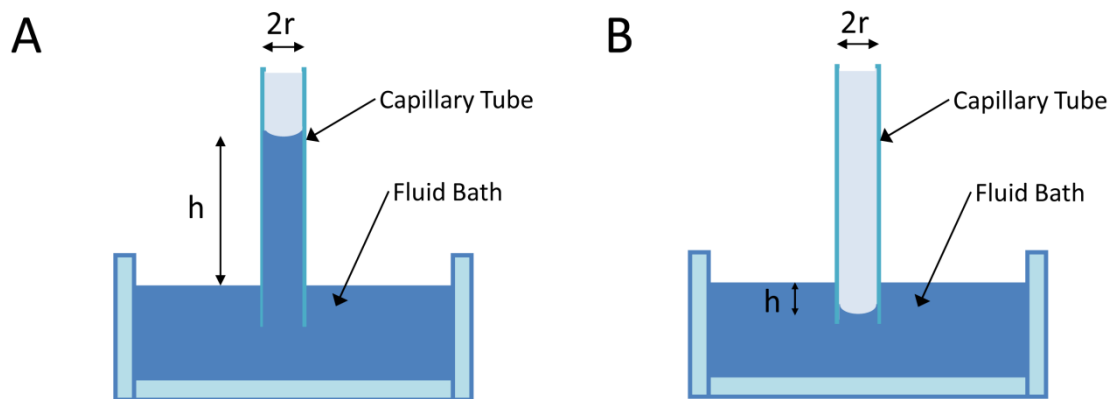


Figure 5.2: Examples of capillary rise, A, where the contact angle is between 0° and 90° , and B, where the value of the contact angle is between 90° and 180° resulting in a negative capillary rise.

Using the above calculations accurate predictions of equilibrium capillary rise have been obtained in many scenarios [226]. Consequently it is of interest to apply such theory to a VACNT forest structure in order to assess the wetting mechanism with an aim of achieving controlled partial wetting of VACNT forests. If these expressions hold true for VACNTs then it may be possible to configure a scenario where VACNT forests will be partially wetted in the equilibrium state, through careful selection of a matrix or precise control of the forest areal density. In order to apply capillary theory to a VACNT forest several assumptions are made in order to simplify the geometry of the forest structure. Subsequently it is logical to model the VACNT forest as a regular array of solid cylinders, where the capillary flow is drawn into the gaps between individual VACNTs rather than into the interior of the VACNTs themselves. This idea was initially addressed by Princen [227] who aimed to quantify the effect of wicking in synthetic textiles by approximating the individual fibres as cylinders

in a regular array. In order to solve this problem capillary theory was initially applied to just two cylinders [228] before progressing to an infinite array of regularly arranged cylinders. Although the expression for small arrays can become complicated due to the interaction between the liquid and the air at the edges of the arrays, these additional terms drop out when considering larger arrays thus simplifying the procedure. To apply the theory to such an array it is necessary to consider a unit cell of the smallest repeatable area, thus the rise in this unit area will be equivalent for as far as the array spans, neglecting any effects occurring at the edges of the array. **Figure 5.3** shows the most suitable unit cell to consider for a rectangular array although the same logic can be applied to other geometric arrays, such as hexagonal arrays.

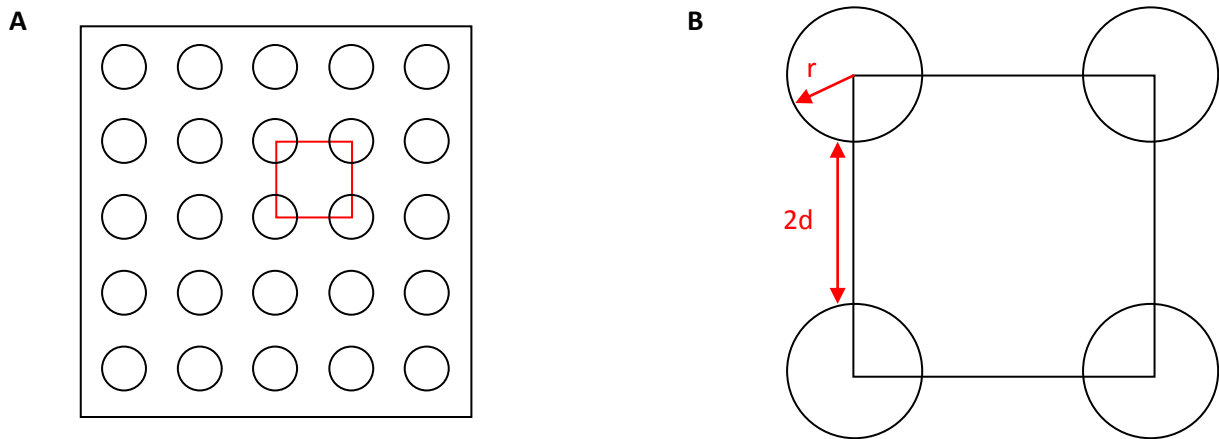


Figure 5.3: A-An example of a rectangular array of solid cylinders in a matrix with unit cell marked in red, and B a unit cell close up with parameters 'r' and 'd' defined.

Considering this unit cell the same theory of surface tension balancing weight is then applied. The surface tension is in fact the same as the case of simple capillary rise as it is once again the product of the perimeter of the solid-liquid interface and the value of the force at a single point. Over the lengths marked 'd', a matrix-matrix boundary occurs and it can be assumed that no net force is acting across the boundary, thus,

$$F_{ST} = 2\pi r \gamma_{lg} \cos\theta \quad (6)$$

where 'r' represents the outer radius of a cylinder in the array and all other symbols have been defined previously. Now considering the weight of the matrix we calculate the area of the square region less the cross sectional area of the cylinders, in the unit cell, multiplied by the density and

acceleration due to gravity as before, this gives the following expression, where 'd' is the distance shown in **Figure 5.3b** above,

$$W = r^2 \left[4 \left(1 + \frac{d}{r} \right)^2 - \pi \right] \rho g h \quad (7)$$

balancing these forces then rearranging for the height of capillary rise and simplifying gives,

$$h = \left(\frac{\gamma_{lg}}{\rho g r} \right) \left[\frac{\pi \cos \theta}{\left[2 \left(1 + \frac{d}{r} \right)^2 - \frac{\pi}{2} \right]} \right] \quad (8)$$

where all symbols have the same meanings as described previously.

Following from this equation some simple predictions about capillary rise in VACNT structures can be drawn by using sensible values, from experiments and literature, for the variables included in Princen's expression [227]. A summary of the variables and their meaning as well as sensible values used in calculations is given in **Table 5.1** below.

| Variable | Value | Description |
|--|--|---|
| The liquid Gas surface tension (γ_{lg}) | 34.1 ± 3.6 mN/m | This value is experimentally measured for mixed LY3505 resin, and is typical of engineering epoxies. Details of experimental measurement are discussed in Chapter 6 . |
| The contact angle (θ) | 30 ° | As it is inherently difficult to measure the contact angle between a fluid and an individual CNT it is necessary to use an approximation instead. Considering that the VACNT structures wet well under capillary effects 30 ° is a sensible approximation and the value of $\cos(\theta)$ only varies from 1.0-0.7 for contact angles between 0 ° and 45 ° its effect on the calculation is minimal if the liquid wets the forest well. |
| The density of the wetting fluid (ρ) | 1300 kg/m ³ | Experimentally measured value of the density of Mixed LY3505 resin from Chapter 4 . |
| The average radius of the CNT (r) | 10 nm | The average radius of VACNT grown using the SabreTube. [16] |
| The average spacing of the CNT (d) | 40 nm | The average spacing of as grown VACNT grown using the SabreTube. [16] |
| The height of the equilibrium capillary rise (h) | Desired value of ~0.1-1.0 mm for partial wetting of as grown VACNT forests | This value represents the equilibrium capillary rise height. In this case it is desirable to achieve partial embedding of a VACNT forest structure for multi layer composite production. Given the maximum height of VACNT forests and the proposed multilayer composite production method a value of approximately half the forest height is chosen. |

Table 5.1: Parameters used in the calculation of equilibrium capillary rise for materials in use in Chapter 4

Initially a quick calculation can indicate a predicted value for equilibrium capillary rise for the materials and parameters in use during **Chapter 4** of this work. This calculation yields a result of approximately ~ 15 m. This value is five orders of magnitudes greater than the largest target value of equilibrium capillary rise to achieve partial wetting in such samples and goes some way towards explaining the strong capillary effects that are observed in the capillary driven wetting of VACNT forest structures. Furthermore by using the above data, plots can be produced to investigate the effect of each variable on the equilibrium capillary rise height prediction, and provide an insight into how changing each parameter affects the process. **Figures 5.4-5.8** illustrate plots displaying how varying each parameter affects the equilibrium capillary rise height while other variables remain constant.

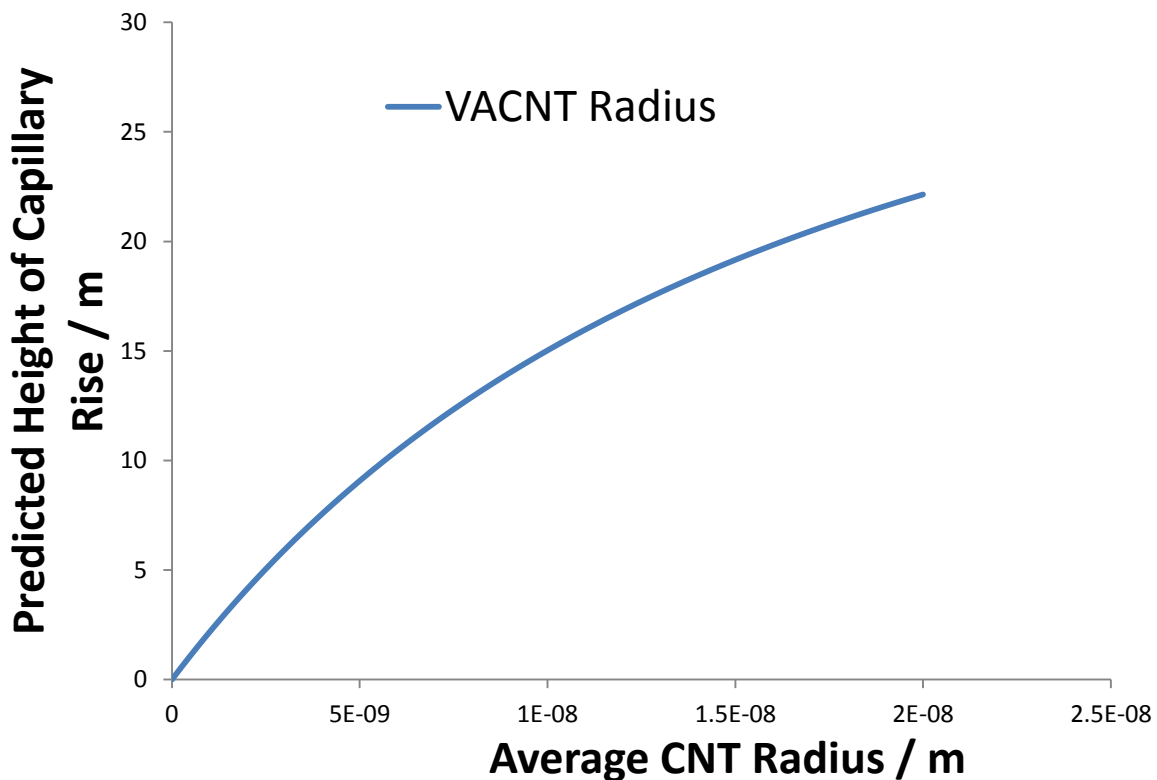


Figure 5.4: Plot detailing how VACNT Radius affects Equilibrium Capillary Rise for parameters from **Table 5.1**

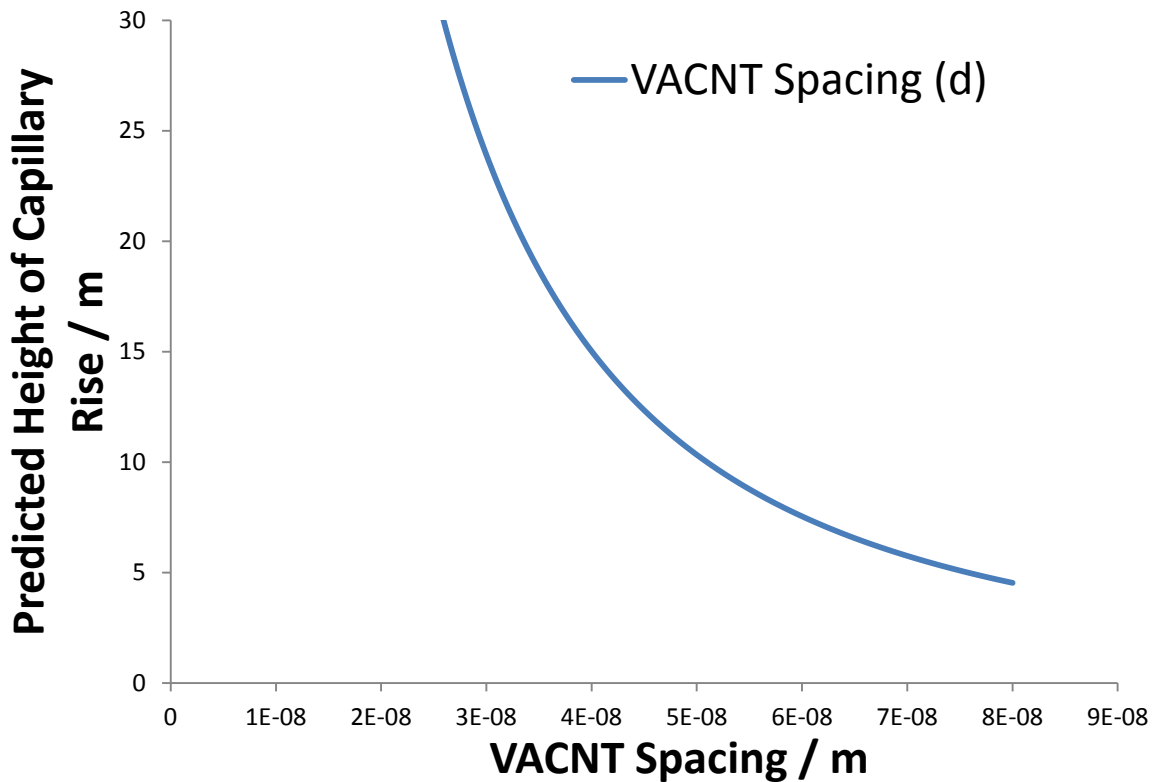


Figure 5.5: Plot detailing how VACNT spacing affects Equilibrium Capillary Rise for parameters from **Table 5.1**

When considering the equilibrium capillary rise scenario in a VACNT structure there are largely two main areas that can be controlled to adjust the height of the equilibrium rise. These are the properties of the VACNT forest and the properties of the wetting liquid. The above plots in **Figures 5.4 and 5.5** illustrate how the properties of the VACNT forest affect the capillary process. As the predicted equilibrium capillary rise height is much greater than the desired value of ~ 0.5 mm the aim of adjusting forest properties is to decrease the value of the equilibrium height. From the plots it is clear that to reduce the capillary height two methods can be used, either decreasing the individual VACNT radii or increasing the VACNT spacing. Although in the literature both of these changes are practically possible but somewhat challenging [16], [229], further problems exist with conducting such adjustments. These are that by shifting either parameter in the desired direction the volume fraction of the VACNT will be reduced. Consequently the level of reinforcement achieved will also decrease which is undesirable for a multilayer VACNT composite as outlined in **Chapter 2**. The next three plots detail the effects of changing the properties of the fluid matrix.

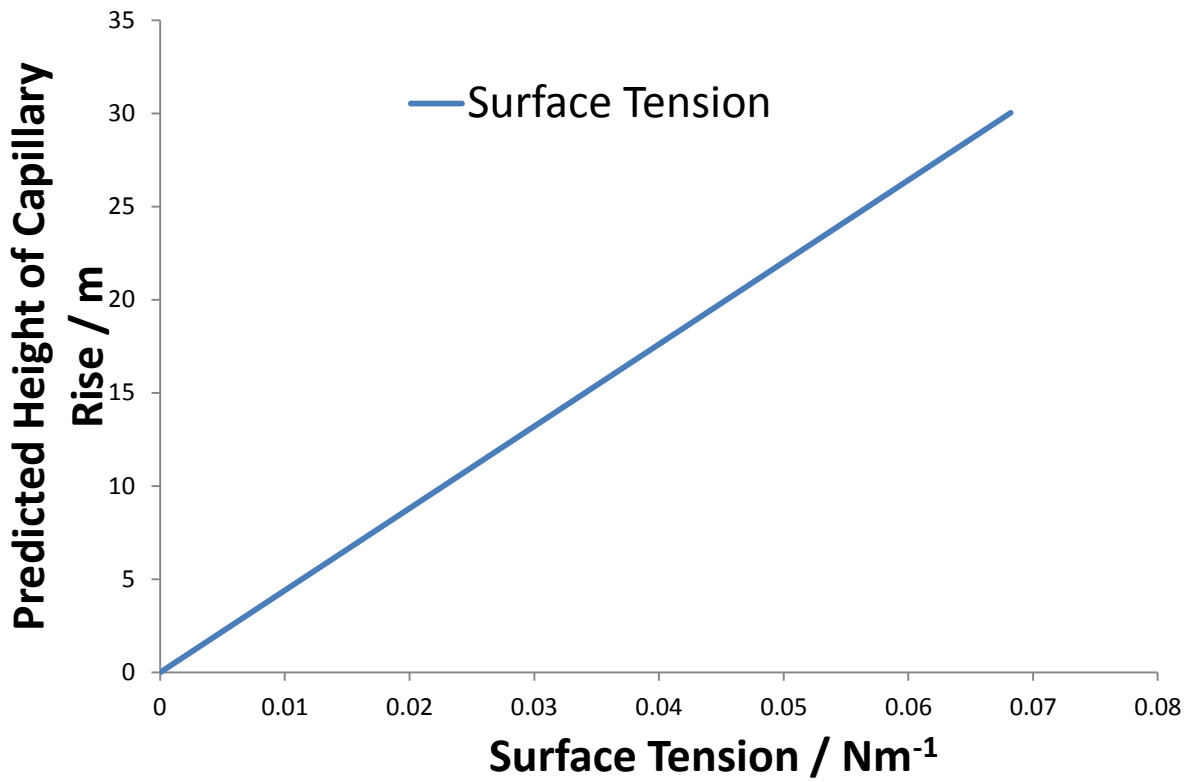


Figure 5.6: Plot detailing how Surface Tension affects Equilibrium Capillary Rise for parameters from **Table 5.1**

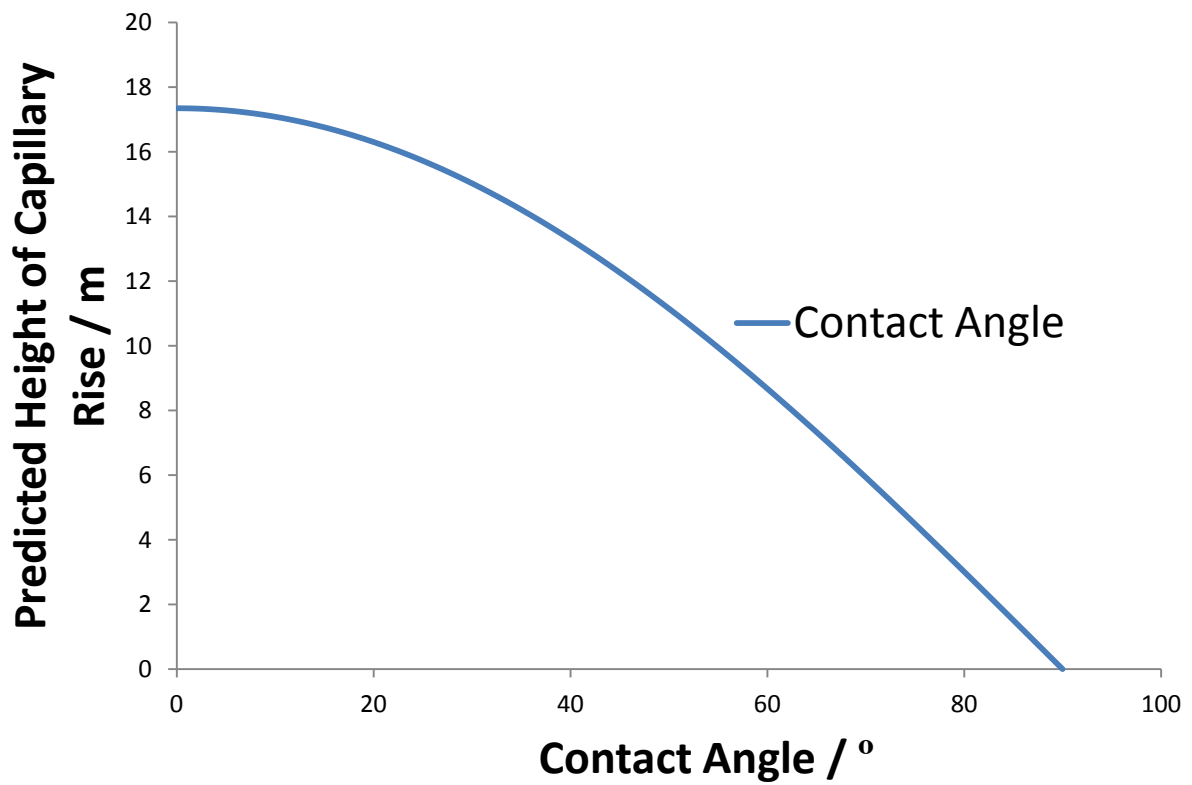


Figure 5.7: Plot detailing how Contact Angle affects Equilibrium Capillary Rise for parameters from **Table 5.1**

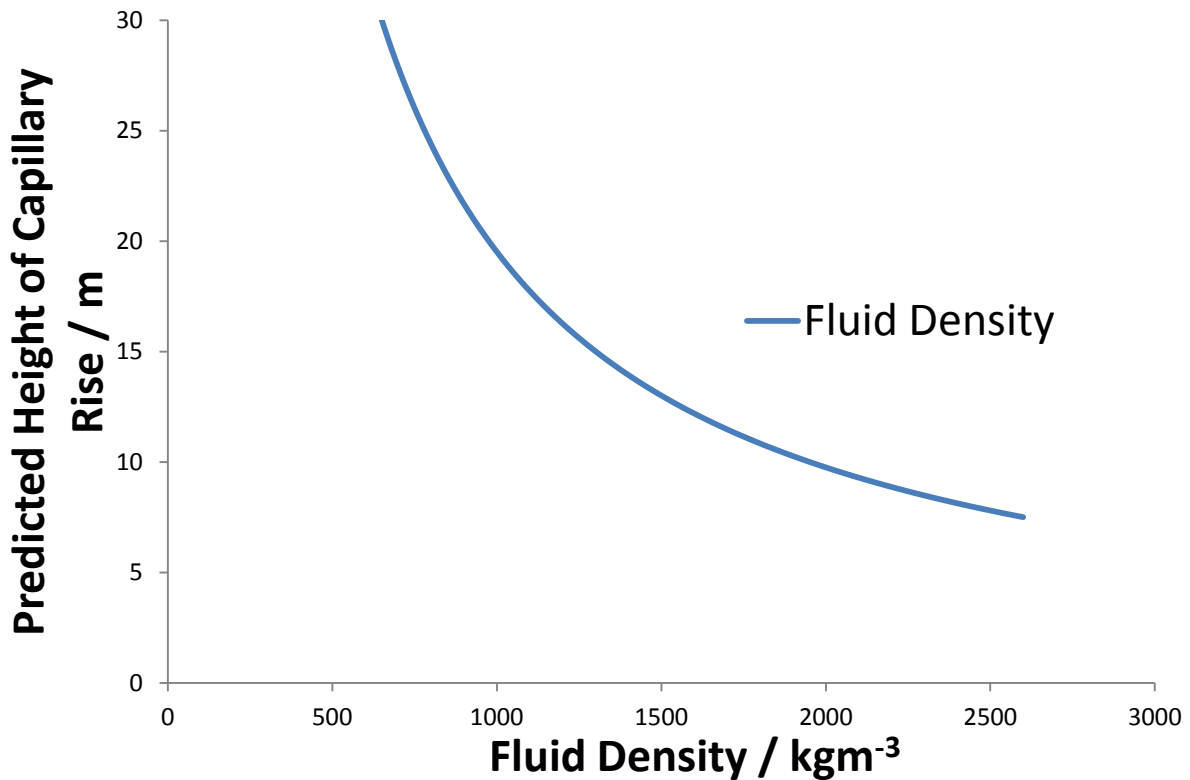


Figure 5.8: Plot detailing how Fluid Density affects Equilibrium Capillary Rise for parameters from **Table 5.1**

Changing the matrix material provides a more interesting solution to the equilibrium capillary rise scenario as shown in **Figures 5.6-5.8**. It is clear that in changing the matrix material that it is likely that all three parameters will also change and in fact contact angle and surface tension are inherently linked as discussed earlier in this chapter. Despite this a brief discussion of each parameters effect follows. Consequently it is perhaps logical to discuss contact angle and surface tension simultaneously as both parameters relate to the ability of the VACNT structure to be wet with a specific fluid. Surface Tension and equilibrium rise height are directly proportional hence reducing the liquid gas surface tension will decrease the rise height. When considering contact angle the most drastic changes in equilibrium capillary rise height are observed and likely explain results in the literature in which VACNT structures have been embedded in polymer layers. For example in the work of Sansom et al. VACNT are successfully embedded in silicone layers and it is well known that silicones do not wet most solid surface particularly well [156]. Consequently if the contact angle approaches 90 ° then little or no capillary driven forces will act and flow of the polymer into the structure will be predominantly driven by gravity or applied external forces, as is likely the case in Sansom’s work. Although these results indicate successful partial embedment, for the production of high performance composites the use of materials such as silicones is undesirable owing to their low modulus values. A more practical solution may exist in the use of thermoplastics as some of the

matrix properties can be controlled thermally, whilst retaining a relatively high modulus once solidified particularly for advanced thermoplastics such as PEEK. The final parameter for consideration is the density of the matrix material. Clearly increasing matrix density will increase the magnitude of the weight term in the balanced equilibrium equation, however practically increasing the density of a polymer matrix to the necessary level, at least ten orders of magnitude, is not viable. To provide an overall understanding of how each parameter affects the process comparatively a plot of **Figures 5.4-5.8** is detailed on the same graph in **Figure 5.9**, the plot illustrates variations from 0-200 % of each parameter from the values listed in **Table 5.1**. Results from static capillary rise modelling of VACNT structures have thus illustrated various possibilities to achieve the partial embedding of VACNT structures but do not provide a clear solution to an effective multilayer manufacture method. However static capillary predictions are only simplistic and the process can be considered as dynamic before the equilibrium scenario is reached. Consequently curing or solidifying of the matrix during the dynamic process may provide further solutions to the problem if the rate of capillary driven wetting can be slowed sufficiently.

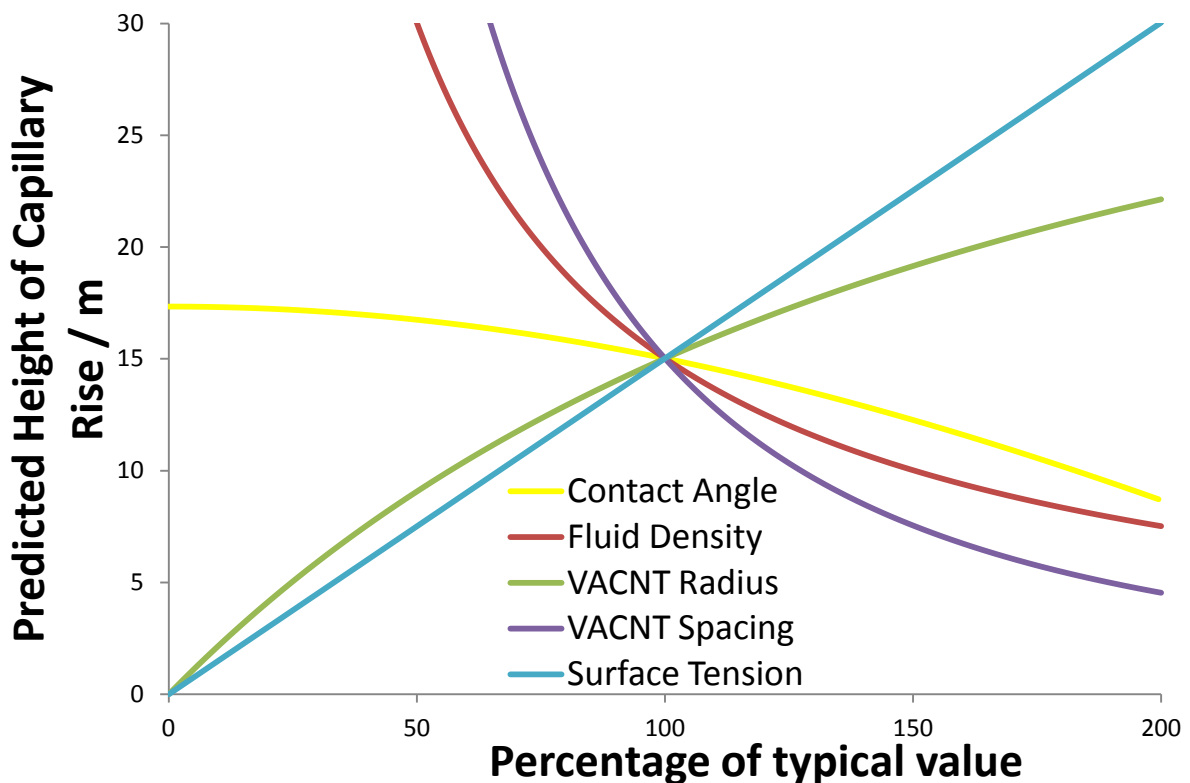


Figure 5.9: A comparison detailing how the various parameters affect equilibrium capillary rise, the point where the lines cross illustrates the value achieved from using the parameters detailed in **Table 5.1**, ~15 m.

5.3 Simple Dynamic Capillary Rise in Capillary Tubes

Dynamic capillary rise is a highly complex phenomenon even for a simple capillary tube and many important factors govern the momentum balance of the fluid including viscous losses, local acceleration of the fluid, entrance effects, the capillary pressure and the hydrostatic pressure. Including all of the prior terms allows calculation of the full linear momentum balance but proves to be complicated and can only be solved numerically [230]. Consequently several terms are often neglected according to the specific situation in order to simplify the equations in an effective and accurate manner. The best example of such simplification and what could be described as the foundation of dynamic capillary rise is the works of Lucas [231] and Washburn [230] in which a relationship where the height of liquid rise in a capillary is found to be proportional to the square root of the time that has passed. Such a result is obtained by simply balancing capillary pressure effects that occur due to the surface interactions between the three phases at the liquid capillary boundary against the viscous pressure loss as the fluid is drawn into the tube as defined by the Hagen-Poiseuille equation. The resulting Lucas-Washburn equation has been used to describe capillary flow dynamically in many situations but is most accurate in the early and intermediate stages of capillary rise as it ignores entrance effects as well as retardation of capillary rise due to gravity and is depicted as follows;

$$h^2 = \frac{\gamma R \cos(\theta)}{2\mu} t \quad (9)$$

where (h) is the height of capillary rise, (γ) is the fluid surface tension, (R) is the inner radius of the capillary, (θ) is the contact angle, (μ) is the fluid viscosity and (t) is the time elapsed since $h=0$. As the equation ignores the influence of gravity it is most appropriate in the early stages of capillary rise and is sometimes called the short term asymptotic solution of the Lucas-Washburn equation.

As well as the traditional Lucas-Washburn equation two further simple analytical models can be used to improve the accuracy of predictions in different time domains. The first is to include the influence of gravity when investigating longer timescales, known as the implicit form of the Washburn equation [230],

$$t(h) = -\frac{8\mu}{\rho g R^2} h - \frac{16\mu\gamma^2 \cos(\theta)}{\rho^2 g^2 R^3} \ln\left(1 - \frac{\rho g R}{2\gamma \cos(\theta)} h\right) \quad (2)$$

where (ρ) is the fluid density and (g) is the acceleration due to gravity. This result was given in Washburn's early work, but is often overshadowed owing to its implicit form and the effectiveness of the short term solution at accurately predicting dynamic capillary rise. Finally Zhmud et al. [232] proposed a long term asymptotic solution (3) to the Washburn momentum balance by considering the turbulent nature of the developed flow of fluid in the capillary.

$$h = \frac{2\gamma \cos(\theta)}{\rho g R} \left[1 - e^{\left(-\frac{\rho^2 g^2 R^3}{16\mu \gamma \cos(\theta)} t \right)} \right] \quad (3)$$

This result provides a long time frame solution that is useful in well developed capillary rise scenarios.

A comparison of these solutions is shown in **Figure 5.10**, where data has been calculated to illustrate the capillary rise of water in a glass capillary of radius of 100 μm . It is suggested that the experimentally observed capillary driven wetting of aligned CNT forests can be fitted to such a model thus allowing a degree of control over the process leading to partial embedment of CNT in a polymer layer. As a rough approximation a CNT forest can be modelled as a bundle of capillary tubes as suggested by Washburn when addressing capillary flows in porous media [230]. More complete models of capillary rise in porous media have also been used by applying Darcy's law [233], and have shown good agreement with experimental data [234]. Considering the complex structure of the as grown VACNT it is likely they will behave more like porous media than bundles of capillaries however both porous and Washburn's models involve the same relationship between height of capillary rise and elapsed time with different constants relating to the properties of the capillary tube or porous structure respectively. Often the use of porous models involves experimental measurement of certain values such as the final capillary rise height, which is not possible for CNT forests and consequently Washburn's simplistic approach will be used as an initial approximation in this case, however a more in depth discussion of porous modelling of VACNT structures is given in **Chapter 6**.

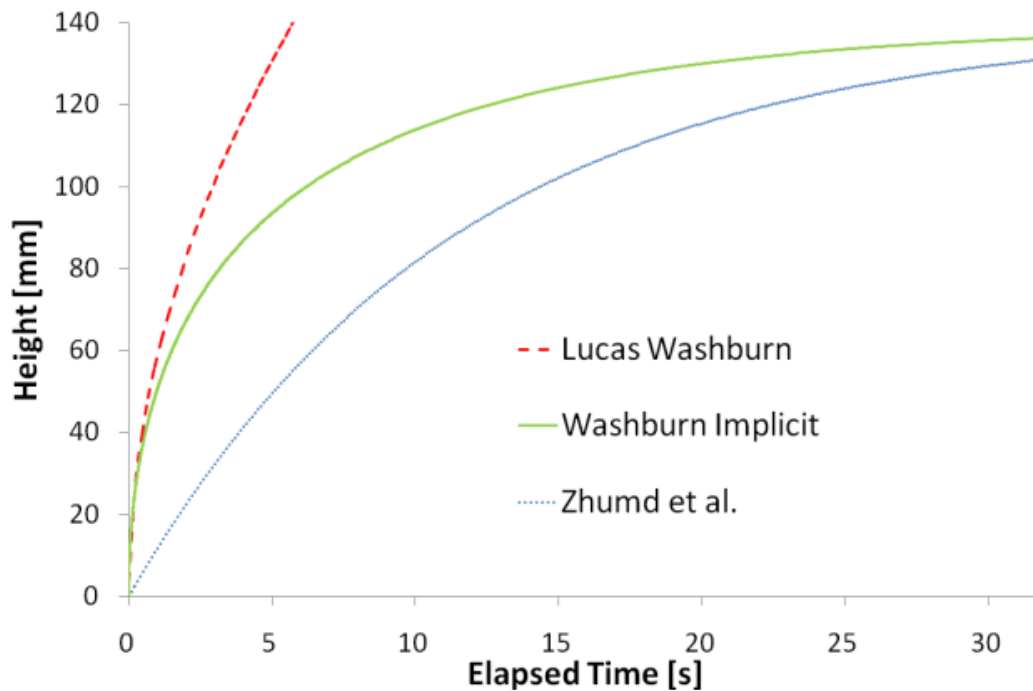


Figure 5.10: A plot of the dynamic capillary rise models for water in a glass capillary of radius $100\mu\text{m}$ illustrating the implicit model as well as the two asymptotic solutions and also illustrating where each approximation is most accurate.

5.4 Application of Simple Dynamic Capillary Rise to VACNT Structures

When considering the penetration of fluids into a VACNT forest a capillary driven process is observed, however the polymer does not penetrate inside of the individual CNT owing to the closed structure of CVD grown CNTs [235], but rather into the voids that exist between the CNT in the overall structure. The as grown CNT forest is characterised as having a certain spatial density, which describes the ratio of the volume of such voids to that of the CNT and can be calculated either through the use of electron microscopy [82], or otherwise [218]. VACNT forests produced using CVD, such as the ones used in this study, have typical densities, or porosities, of $\sim 2\%$ volume fraction as calculated in **Chapter 4** of this work. In the implicit Washburn approximation viscous losses are calculated for laminar flow in a simple pipe, and as a result are not the same as in the unit cell depicted in **Figure 5.3**. Despite this it is possible to calculate an average inter CNT spacing which can be used to calculate an approximate values for an average capillary radius to be used in the dynamic capillary rise models. The values of the average VACNT radius (R) and the spacing between individual CNT (d) are important in different aspects of the momentum balance. The interaction between the CNT and the fluid are the driving force behind the capillary pressure thus using a larger radius than that of the CNT will increase this pressure and also reduce viscous losses calculated at the tube walls. Using the CNT radius will have other implications though and will mean that viscous losses are

increased and gravitational effects are reduced as the volume of liquid being drawn into the structure will be far more than that considered by the model. Considering such details an approximation will be made using a radius of 4 nm and 40 nm to cover the range of scenarios remembering that each term will have a varying effect with development of the capillary flow.

It is possible to estimate expected capillary rise evolution in VACNT forests by inputting data to the models described previously and plotting the expected height against elapsed time. Models were investigated using approximate values for mixed LY3505 resin detailed in **Table 5.1** previously and the data sheet value of ~ 0.35 Pas for the viscosity (μ) of the mixed LY3505 resin.

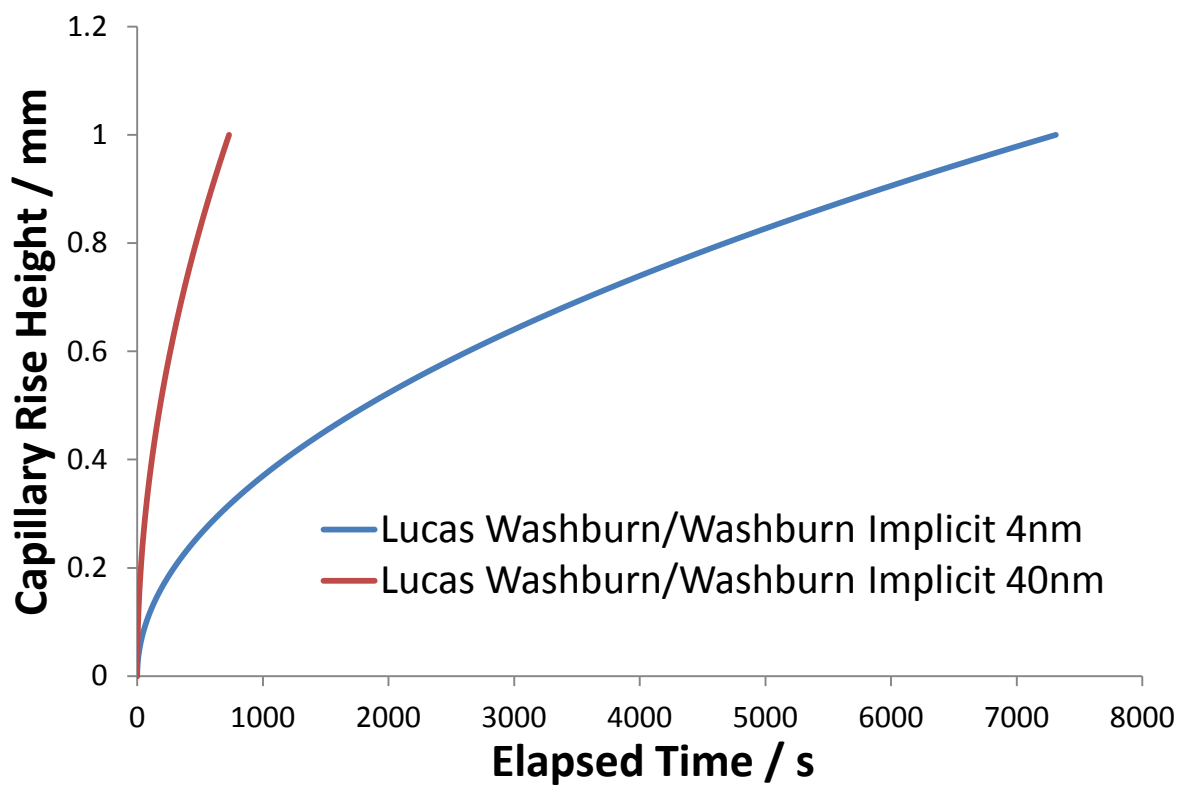


Figure 5.11: Example plots of the Lucas-Washburn/Washburn implicit models using parameters of mixed LY3505 resin and different values of the capillary radius

Figure 5.11 shows the outcome of the short-term and implicit models up to a capillary rise height of ~ 1 mm which is the area of interest when considering the VACNT forests in use. Both short-term and implicit models provide the same result over the area considered which is in the early stages of the capillary rise process and the long time model provides an inaccurate result as expected and hence is not considered further. As the dynamic process is clearly in the early stages of capillary rise, the Lucas-Washburn model will be used to provide an effective prediction of the process as the implicit result tends to this value in this stage of the wetting process. The data for capillary radii of both 4 nm

and 40 nm shows that the expected time for the resin to rise 1 mm inside of the forest is at least several orders of magnitude larger than the experimentally observed result of less than a second [224]. Such a result indicates that the Lucas-Washburn approach to dynamic capillary rise may be inaccurate at nanoscale dimensions, the reasoning for this being that very high viscous losses are expected in such narrow capillaries. These viscous losses then consequently retard the rate of the dynamic capillary rise process thus despite very high equilibrium rise heights being expected the dynamic process should occur at a very slow rate according to these traditional capillary models. Possible explanations for the discrepancies between experimental observations and theoretical predictions include molecular interactions that may occur as the size of the pores in the structure approach that of the molecules in the fluid [82], inaccuracies due to assumptions in the simplistic model or complex wetting mechanisms within the CNT structure perhaps owing to its unpredictable nature at the nanoscale [209]. These results illustrate the need for further investigations into the wetting mechanisms that are occurring inside of these nanoscale structures during capillary driven wetting.

5.5 Experimental investigations into VACNT forest wetting mechanisms

In order to further investigate capillary driven wetting mechanisms in VACNT forests experiments were undertaken to achieve partial capillary driven wetting of VACNT forests using a polymer. The purpose of such experiments is to fix capillary flow in the dynamic regime through solidifying the polymer during the dynamic process thus allowing more detailed analysis of the flow mechanism. The embedding of VACNT structures in polymeric layers is addressed in the literature through various methods. For example Sansom et al. [156] embed VACNTs in silicone layers as discussed previously although this process may not be capillary driven as silicones are known to not wet solid materials well. Furthermore Sansom et al. use 'short' VACNT forests that are less than 100 μm in height, with only approximately 30 μm of the forest interacting with the silicone layer. Other works focus on embedding the tips of VACNT structures into thermoplastic layers but again only a small part of the forest is embedded in the polymer layer [157]. In order to simplify analysis of the wetting mechanism it is desirable to partially wet approximately half of the VACNT structure using a polymer. Consequently it was necessary to identify a suitable polymer material to be used in the wetting process. Using the traditional models discussed earlier predictions of the effect of polymer properties, such as viscosity; on the dynamic wetting process can be made. Initial experiments were conducted using LDPE (Low Density Poly Ethylene) layers as a wetting material. A custom wetting rig was developed in order to provide accurate control over the process as pictured in **Figure 5.12**. By

using this rig accurate temperature control is possible and consequently thin polymer layers can be melted and cooled as required.

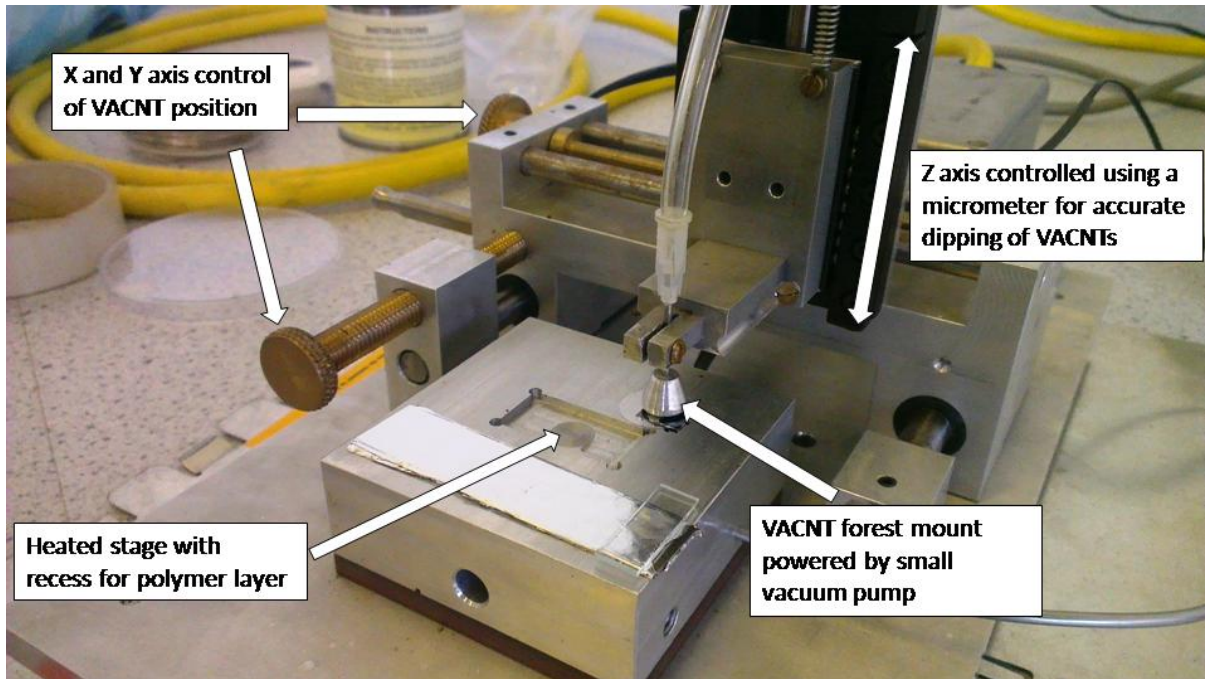


Figure 5.12: Dipping rig for the partial embedment of VACNT forest structures. The heated stage is accurately controlled using an electronic PID controller and is heated using two cartridge heaters embedded in the stage.

Initial experiments conducted using thin LDPE films resulted in successful embedding of VACNT forests at a temperature of 180 °C through the process illustrated in the schematic detailed in **Figure 5.13**. Strong interactions between the LDPE and individual VACNTs were confirmed through the successful mechanical removal of the growth substrate after solidifying the LDPE layer through cooling.

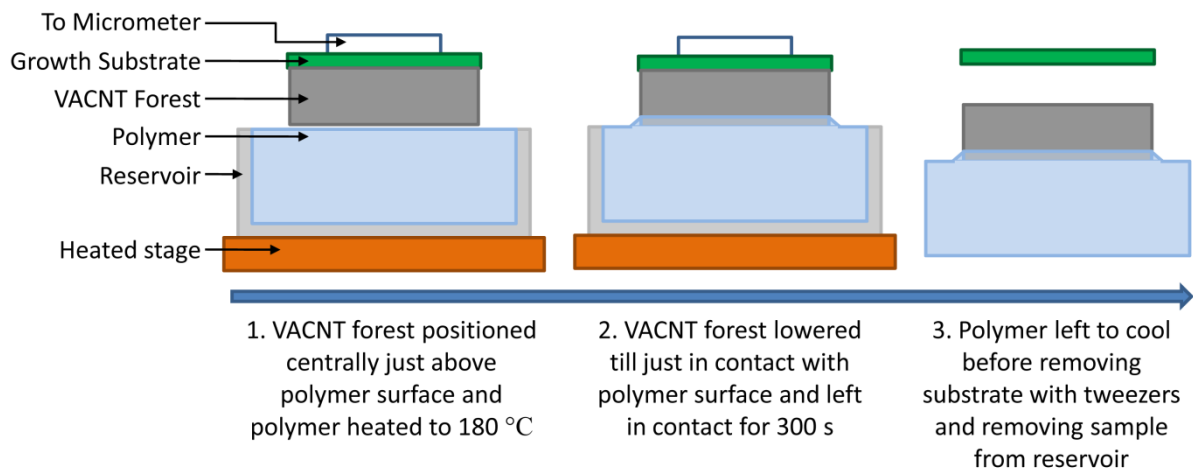


Figure 5.13: Simplified schematic of the partially embedded VACNT production mechanism using the custom rig imaged in **Figure 5.12**.

Although it was apparent that the VACNTs were embedded in the LDPE, confirmed through successful removal of the growth substrate, optical assessment of the degree of wetting achieved remained challenging. However it appeared that only a small fraction of the forests height had been infiltrated by the LDPE when viewed using optical microscopy. To investigate further SEM imaging was conducted on embedded samples which confirmed the interaction between the LDPE and the VACNTs when viewed at high magnification as shown in **Figure 5.14**. Despite confirmation of capillary driven polymer flow using SEM, the topological nature of SEM imaging reveals little detail of polymer flow regimes in the forests interior.

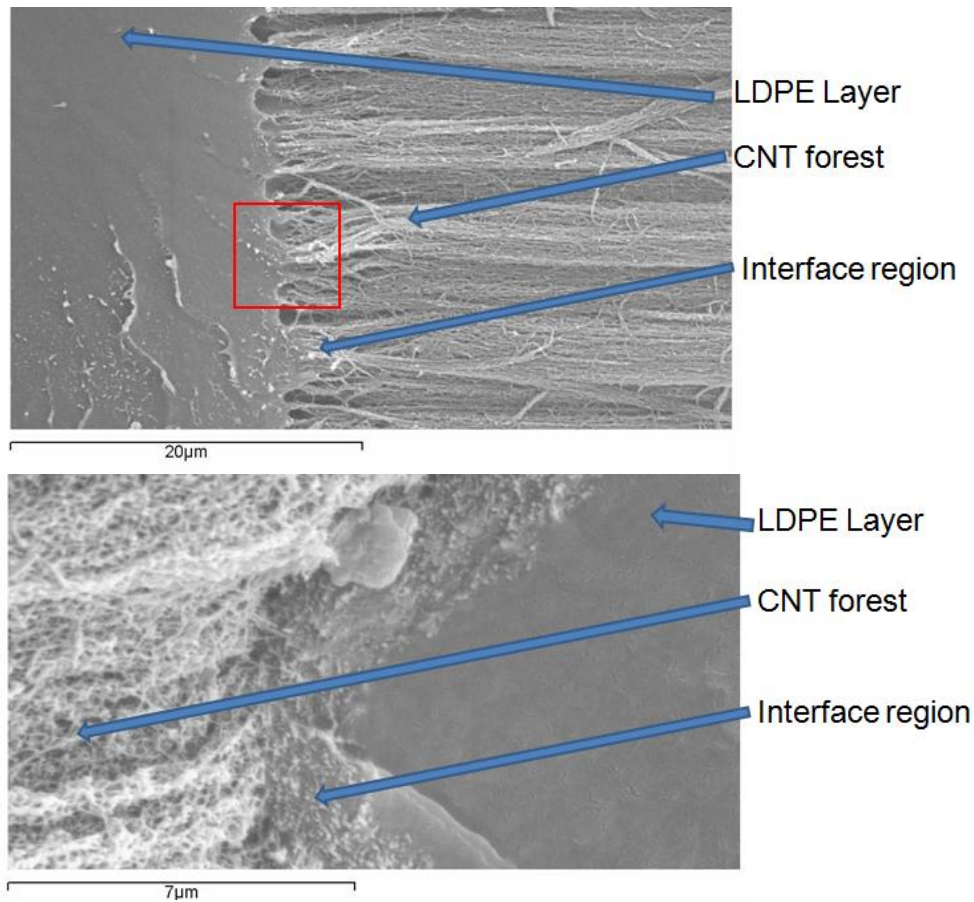


Figure 5.14: SEM images of the interaction between the LDPE and VACNT forest at the interface region.

Considering the difficulties that have been observed experimentally in interpreting the wetting mechanisms occurring in VACNT forests a new approach was devised to investigate the interior of the embedded VACNT forest structure. This approach involved the use of μ -CT analysis to investigate the interior of the embedded samples. In order for successful analysis to be conducted it was advantageous to achieve partial wetting of the forests to a height that was closer to half of the height of the forests in use, owing to the resolution of the CT scanner, and consequently a different thermoplastic was selected for use in a further batch of experiments. Looking at the Lucas-Washburn equation it is clear that lowering the viscosity of the wetting fluid would result in an increase in the speed of the dynamic capillary wetting process. Consequently two samples of the co-polymer EVA (Ethylene-Vinyl Acetate) were sourced as this co-polymer has similar properties to LDPE when molten owing to its ethylene content, but a lower viscosity depending on the volume fraction of vinyl acetate present in the sample. To assess changes in viscosity rotational rheology was conducted on the three polymer samples, LDPE, EVA (12 wt%-Vinyl Acetate), and EVA (40 wt%-Vinyl Acetate), in order to interpret how their viscosities change when molten. In order to select a sensible

range of temperatures to conduct rheology experiments all three polymers were tested using Differential Scanning Calorimetry (DSC) to determine the melt temperature and the onset of significant thermal degradation of the materials, consequently identifying a suitable temperature range to conduct rheology testing. DSC analysis was conducted using a Mettler Toledo DSC823^e between 40 and 250 °C and a plot for each material is given in **Figure 5.15** illustrating the onset of the melt and finally thermal degradation of the material.

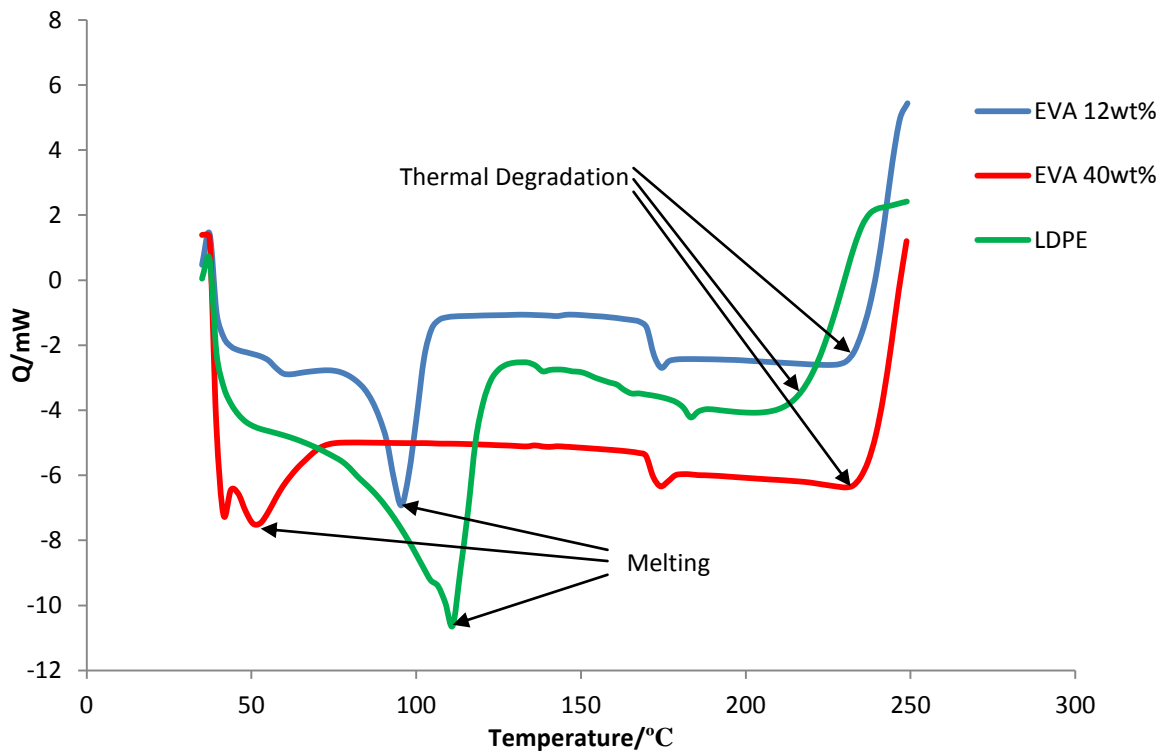


Figure 5.15: DSC traces for the three polymers tested

The DSC plots indicate that a greater content of vinyl acetate in the co-polymer results in an earlier onset of melting, but that the onset of thermal degradation is not significantly affected, and both co-polymers appear to degrade at a slightly higher temperature when compared to the LDPE sample. As a result of DSC analysis suitable temperature ranges were chosen for conducting rotational rheology in order to measure changes in viscosity of each polymer with temperature and plots for each material are given in **Figure 5.16**. Experiments were conducted using a TA Instruments AR2000 rotational rheometer on moulded solid 8mm diameter, 3mm thickness disks of each thermoplastic material at The University of Exeter. An identical sinusoidal rotational motion was applied to the rheometer plates during the experiments, and the complex viscosity of each material measured as it passes through the relevant range of temperatures.

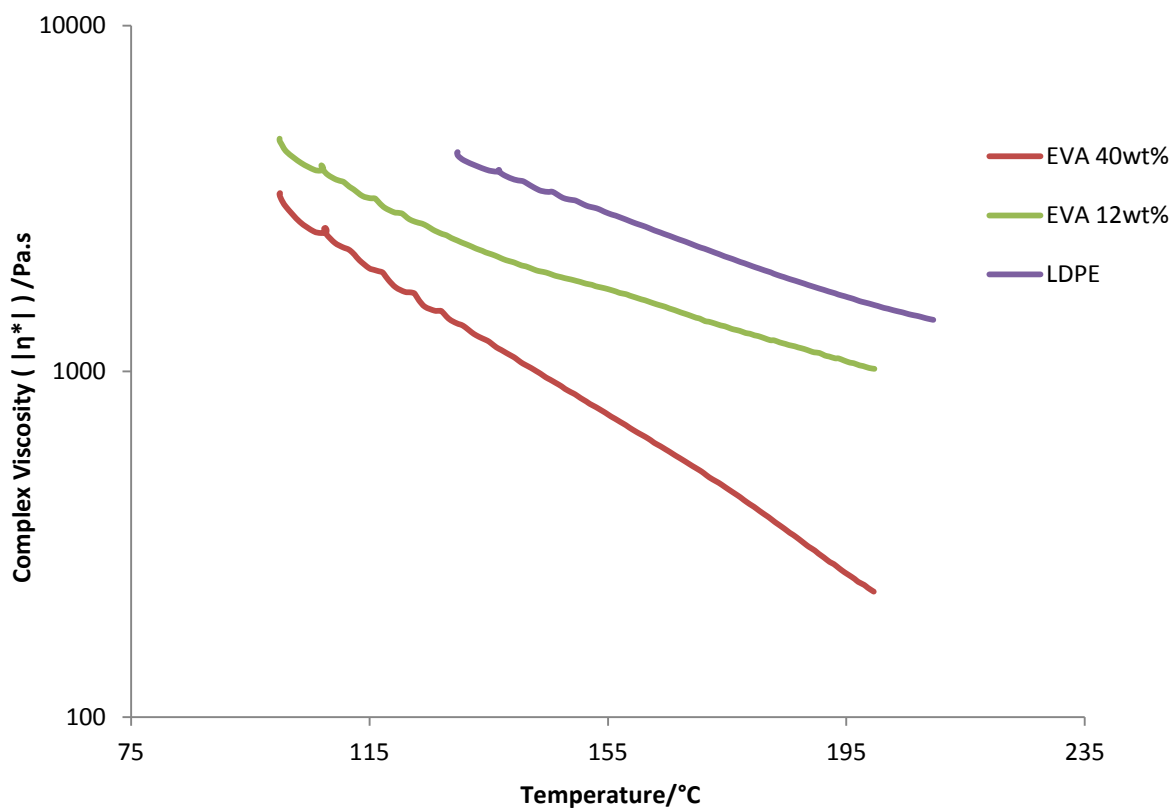


Figure 5.16: Complex viscosity plotted against temperature for the three polymers.

The plots in **Figure 5.16** illustrate a drop of approximately an order of magnitude in the complex viscosity of the EVA 40 wt% when compared to the LDPE used previously at the processing temperature of 180 °C. Consequently further investigations were conducted using the same production method described previously using EVA 40 wt% as the wetting matrix material.

5.6 Experimental investigations into VACNT forest wetting mechanisms with EVA 40wt%

In order to investigate the interactions between VACNT forests and the molten EVA, several forests were embedded into EVA layers using the capillary driven wetting method detailed previously. Detailed analysis was then conducted on these samples using SEM and μ -CT analysis. **Figures 5.17-5.21** illustrate comparisons between SEM images and models constructed using μ -CT analysis of the various samples. The images reveal that the VACNT are not visible in the μ -CT scans indicating that they have a low attenuation coefficient in the x-ray spectrum and consequently it is possible to identify regions of polymer flow in the forests interior [236].

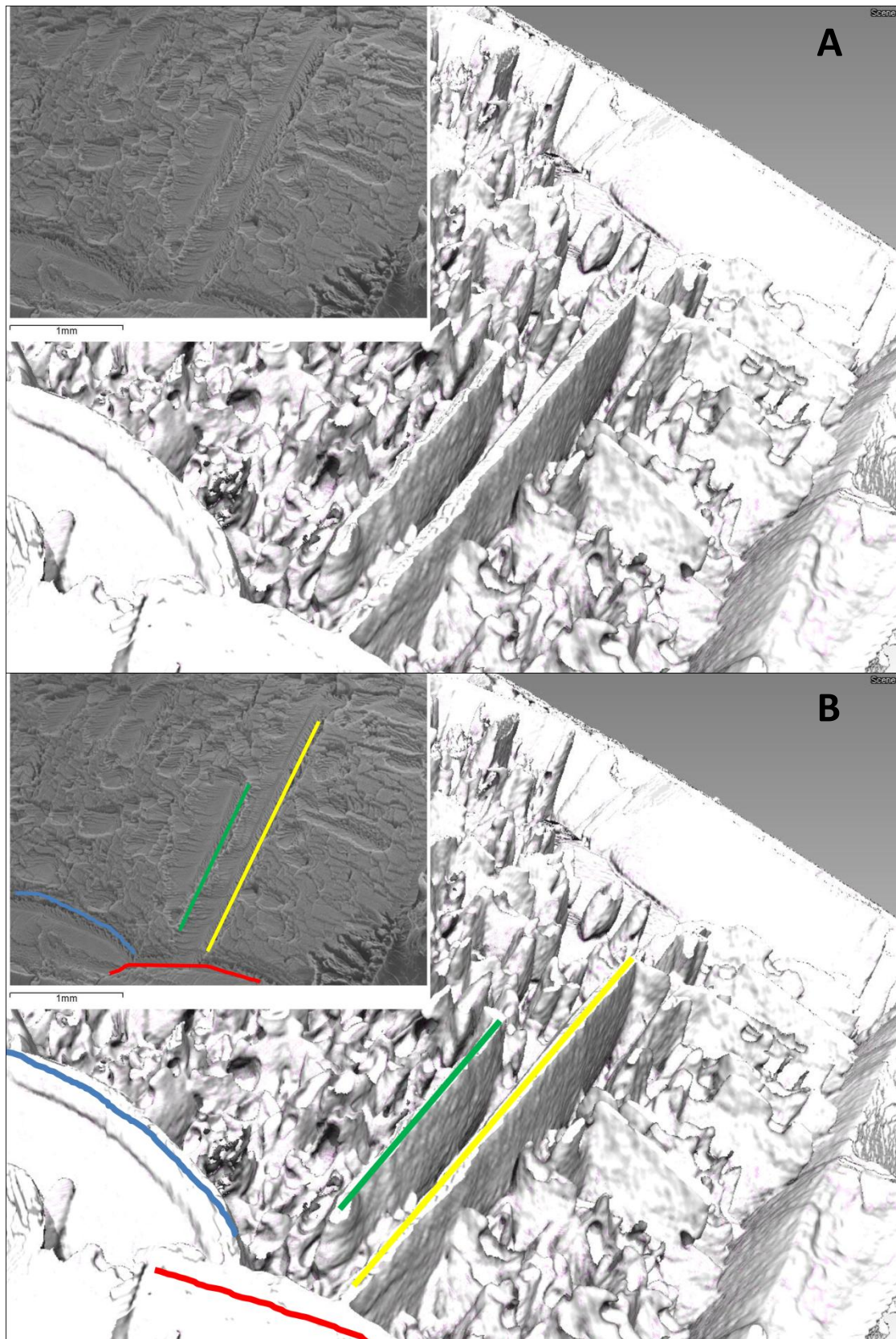


Figure 5.17: A comparison between SEM and μ -CT images for the same area of Sample 1. In B distinguishing features have been marked, the polymer appears to flow in a peaked fashion over the majority of the forest but also appears to fill minor forest defects that likely form during CVD production.

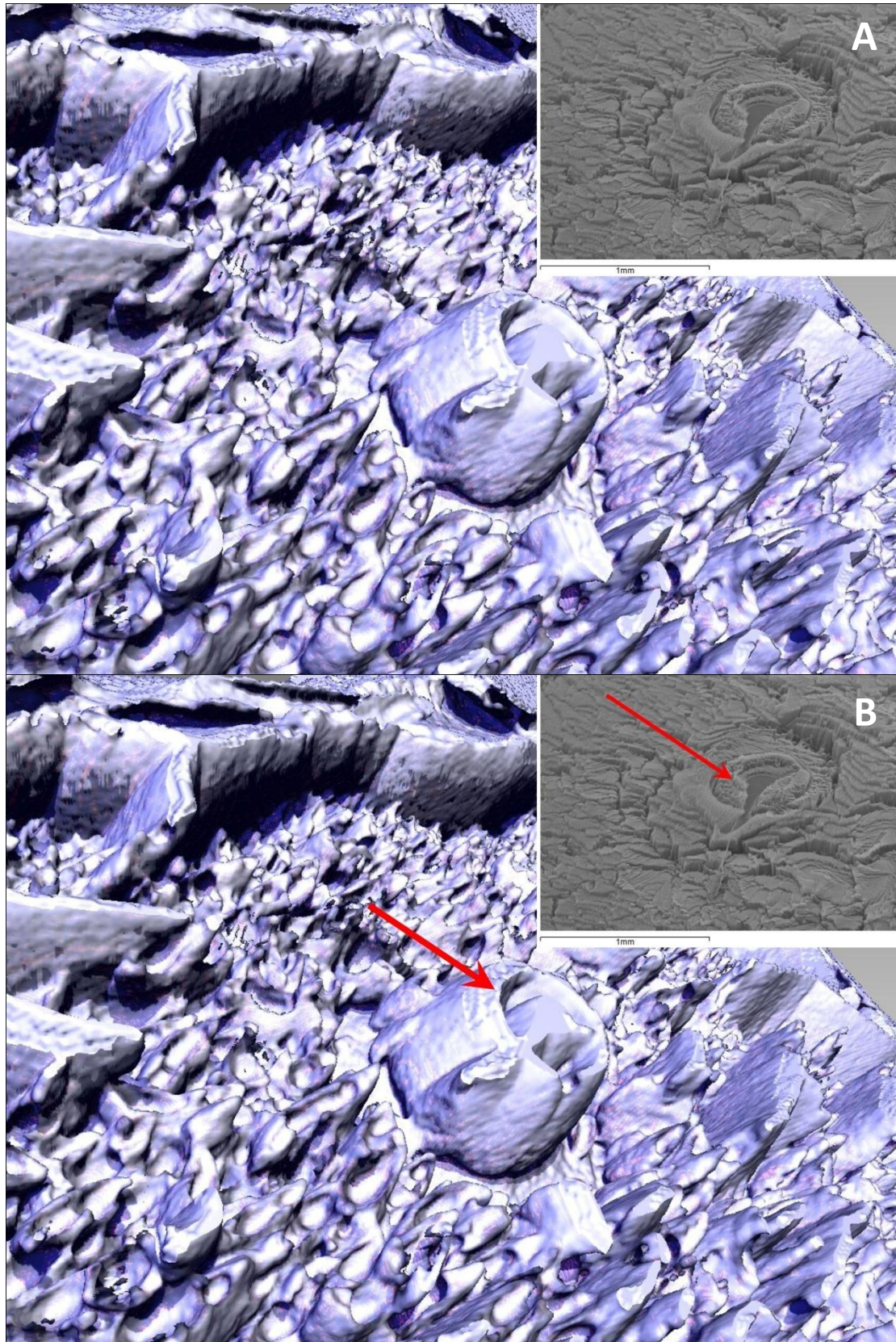


Figure 5.18: A comparison between SEM and μ -CT images for a different area of Sample 1. A large circular defect is present that appears to have channelled polymer flow in the forests interior although this is not clear at the surface of the forest as seen under SEM. Again the majority of the forest appears to channel polymer flow in peaks.

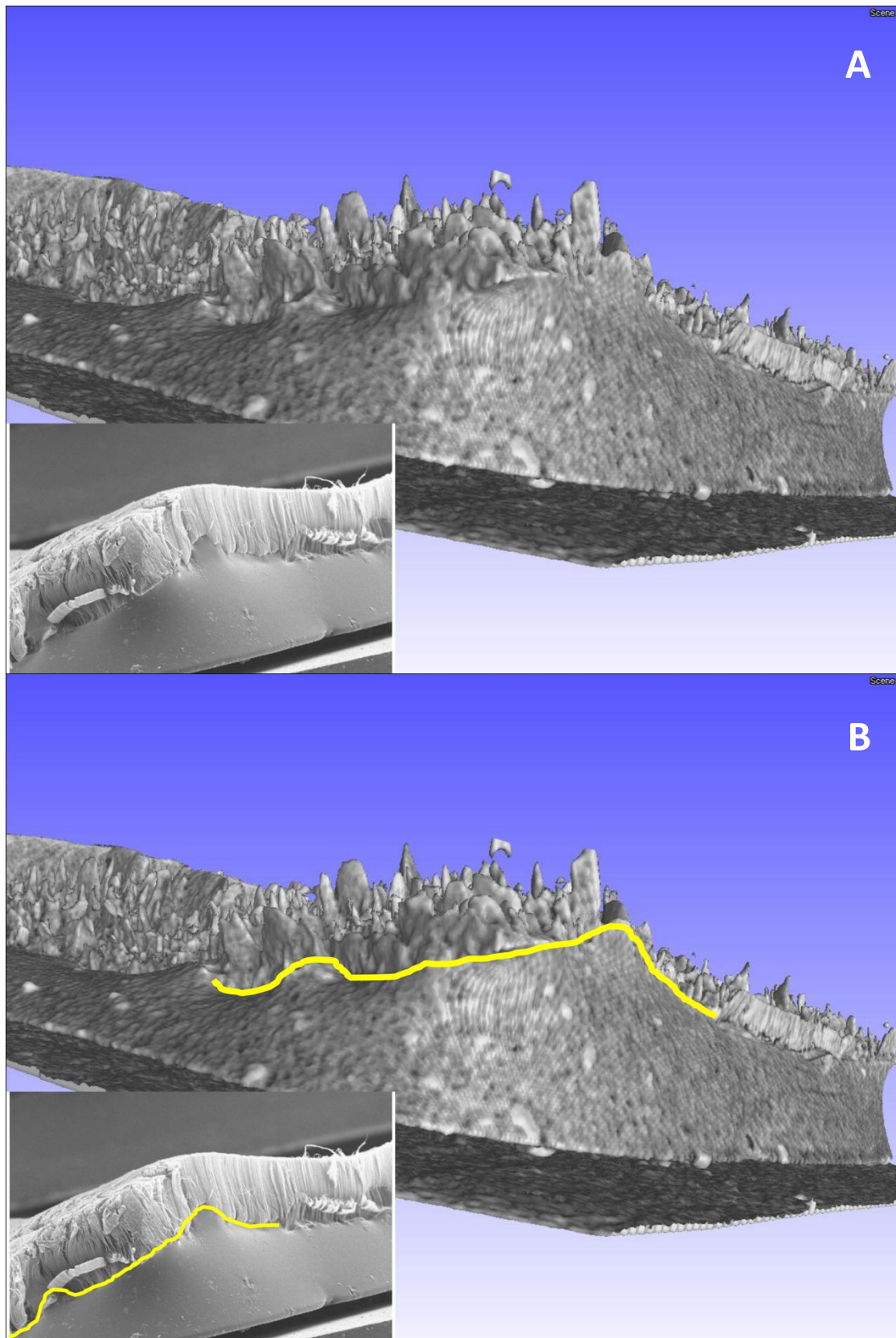


Figure 5.19: A comparison of images from the corner of Sample 2, from this perspective it is observed that as well as flowing inside the interior the polymer also rides up the exterior of the forest slightly.

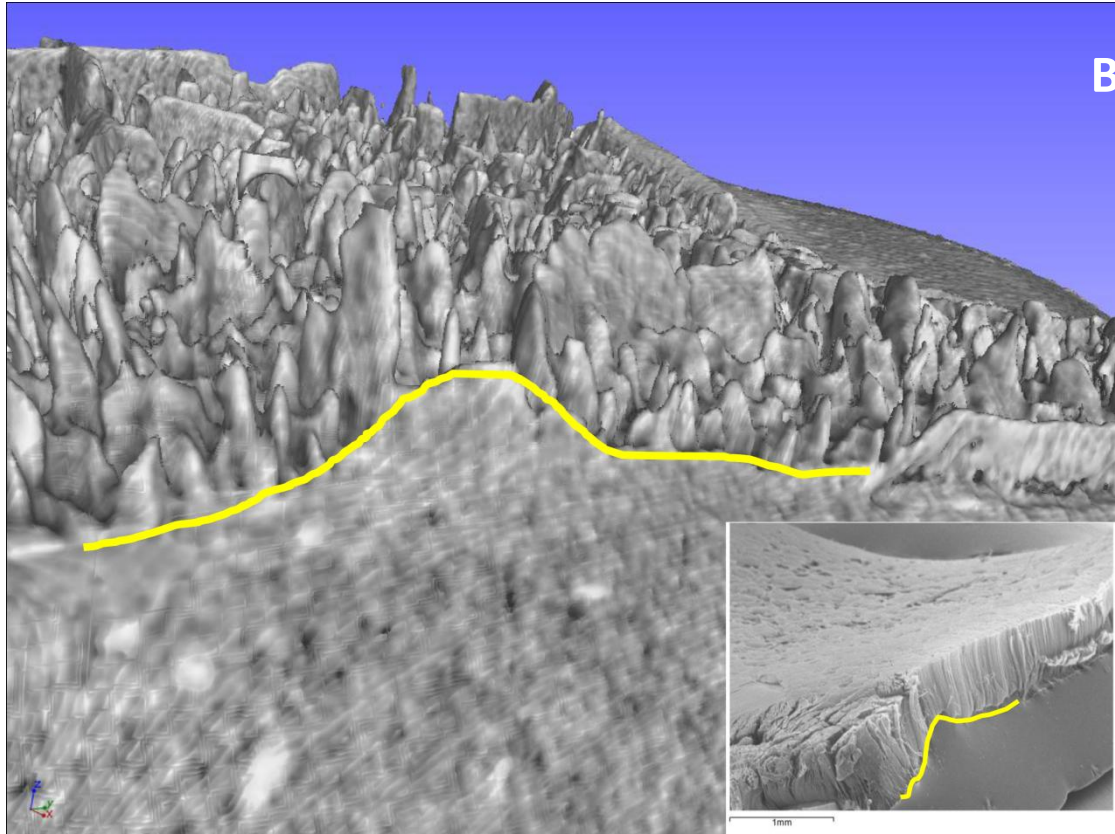
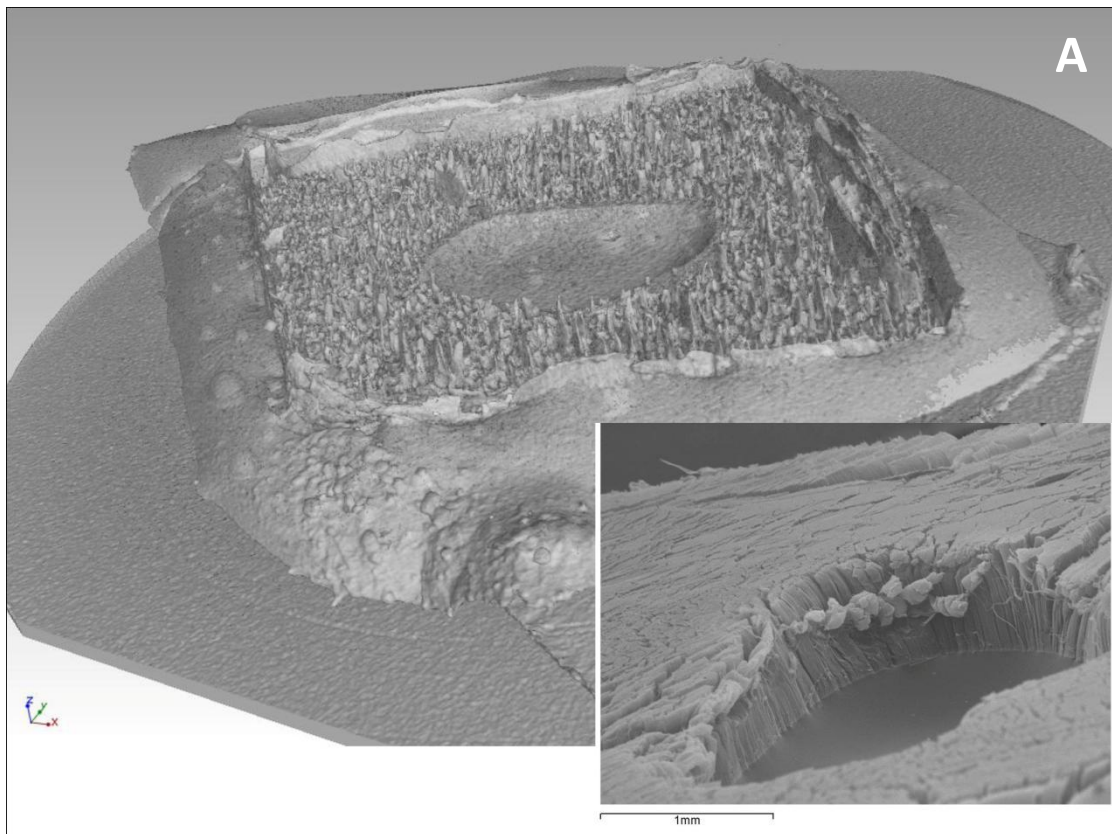
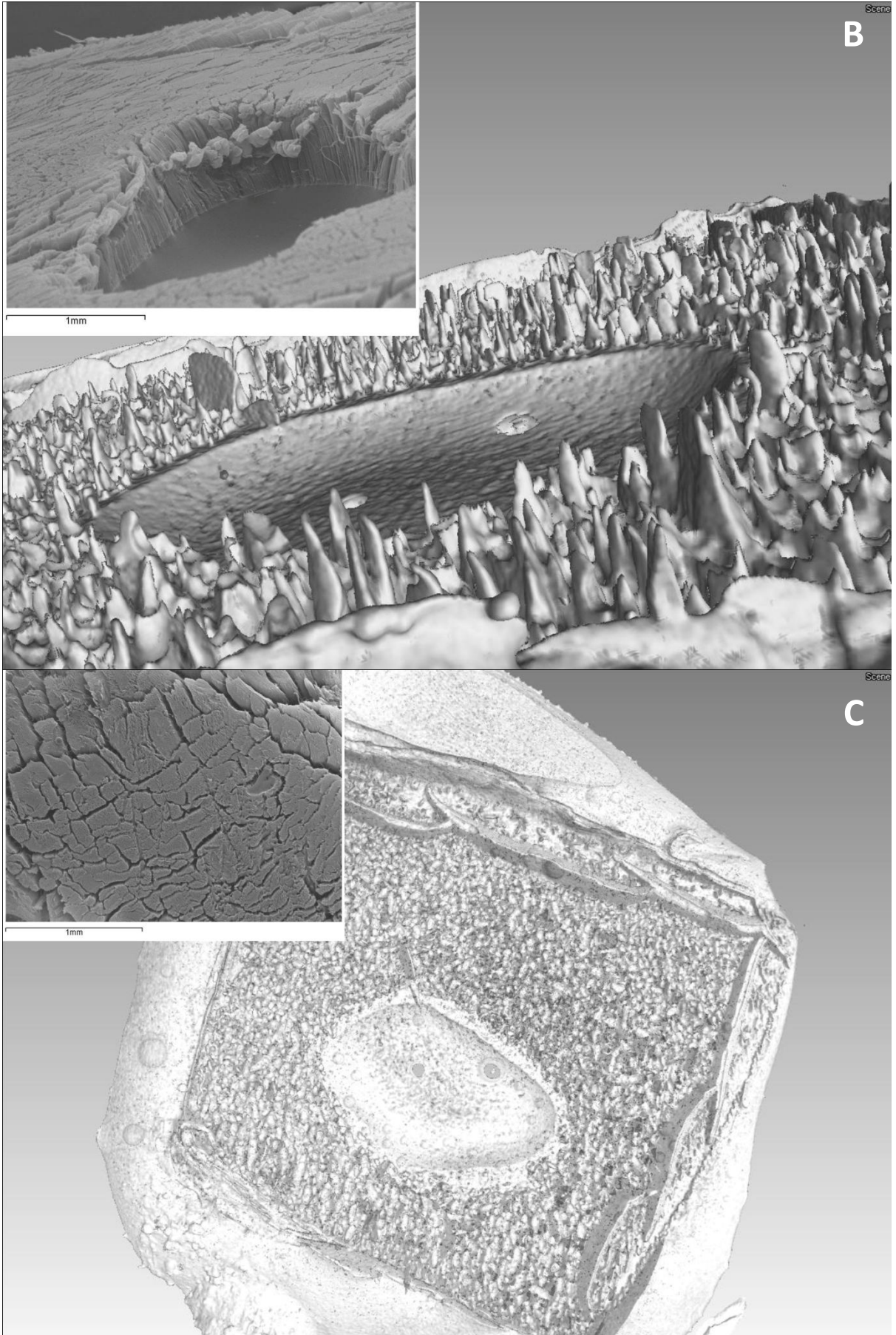


Figure 5.20: A Zoomed image of Sample 2 detailing the peaked structure apparent in the forests interior, the marked yellow line indicates the polymer CNT interface visible under SEM. It appears that the CNT extend to a greater height than the peaks of polymer visible in the CT scan. It is also of interest to note that the surface of the VACNT forest structure remains relatively smooth under SEM imaging.





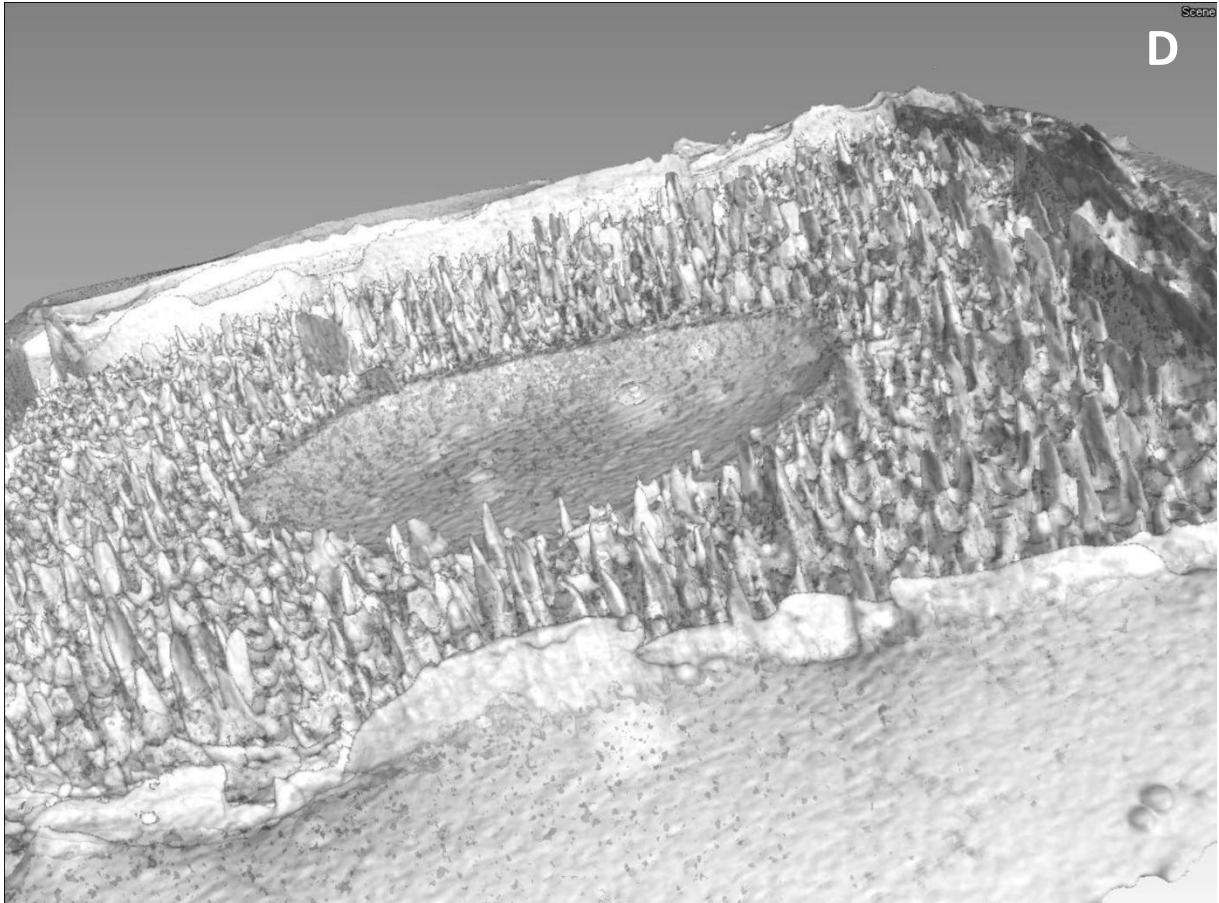


Figure 5.21: A-C, Comparisons of SEM and μ -CT images of sample 3. This sample had a circular portion of the forest missing in the centre owing to the presence of a dust particle during CVD growth of the forest. The presence of which allows an estimation of the height of the rise of the polymer in the forests interior. The final image **D** illustrates that the peaks appear fairly uniform in the uniform defect free regions of the wetted VACNT structure.

The images detailed in the figures above provide evidence of a complicated capillary driven flow of molten polymer occurring within the interior of the VACNT forest structure. Many possible explanations exist for the presence of the observed peaks of polymer flow and include the flow of polymer into voids in the structure created through localised densification of the VACNTs as well as densification of the wetted VACNTs locally via wetting with the polymer matrix. Furthermore the average size of the voids or spaces between the individual VACNTs begins to approach the size of large polymer molecules so molecular interactions may begin to play an important role in the flow of the material, an effect obviously not present in typical traditional capillary theory. Consequently a precise understanding of the wetting mechanism remains elusive. Despite this, it is clear that polymer flow into the forest structure is not simple and these results may begin to explain the discrepancies observed between experimental results and dynamic capillary theory discussed earlier in this chapter. By manipulating the 3D data obtained during μ -CT scanning it is possible to examine slice by slice images of the model and consequently estimate an average diameter of the peaks of

polymer flow observed in the uniform regions of the VACNT forest. These peaks may act to channel flow into the forest thus accounting for a reduction in viscous losses and a considerably faster capillary driven flow than theoretically expected. **Figure 5.22** illustrates the method of measurement of approximate peak diameter using 3D modelling software.

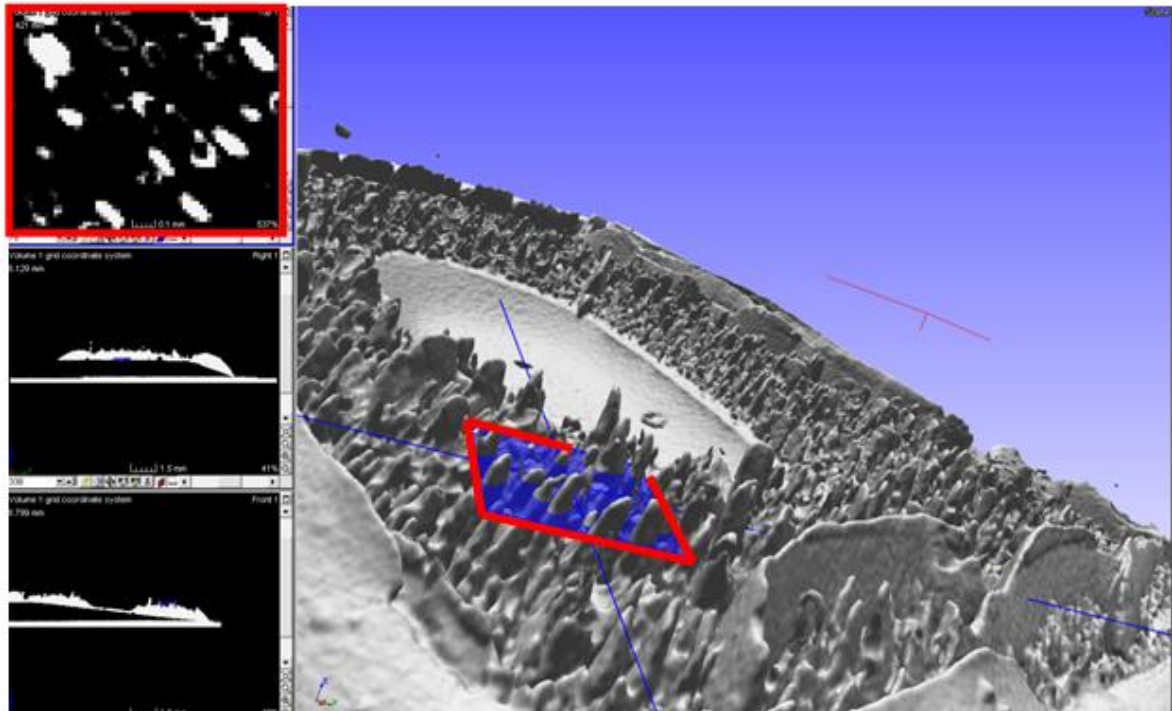


Figure 5.22: Illustration of average peak diameter approximation using the VGstudio software environment the left hand images are indicative of individual x-ray scans used in the construction of the 3D model. Estimations of peak diameter were calculated at approximately half the total height of the peak.

Interestingly the approximate peak diameter yields a value of the order of $120 \pm 60 \mu\text{m}$ which is considerably greater than the diameters used in approximating dynamic capillary driven wetting earlier in this chapter that were based on inter VACNT spacing values. Consequently the Lucas-Washburn Model used previously can be adjusted to account for such effects which may act as a sensible approximation as viscous losses that arise at the boundary between solid and liquid would likely be significantly reduced in the interior of such peaks assuming full wetting has occurred. A simple plot using the identical values used in **Figure 5.11**, but changing the value of capillary radius to $120 \mu\text{m}$ yields the result given in **Figure 5.23** which indicates that the predicted rate of wetting of VACNT forest structures would be considerably faster if these hypotheses are correct.

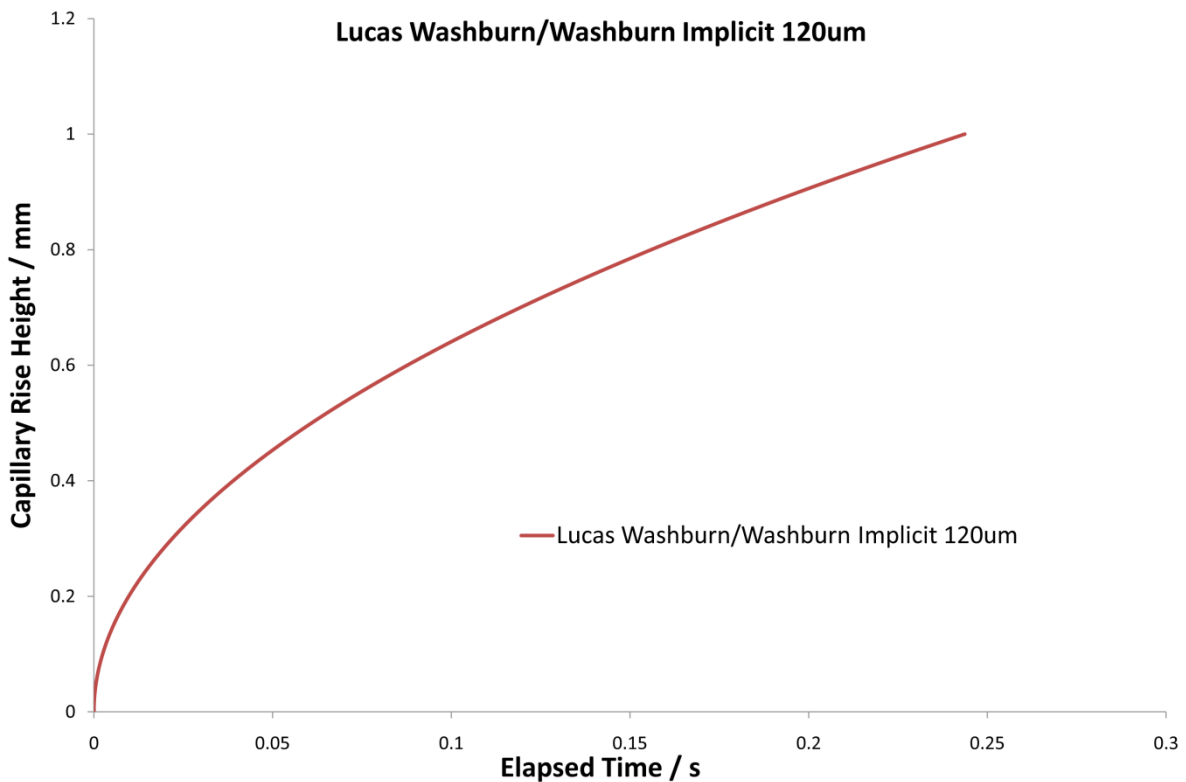


Figure 5.23: Plot of the Lucas Washburn prediction of the evolution of capillary rise in a VACNT structure with an approximate capillary radius of 120 μm , from $\mu\text{-CT}$ measurements, using the same parameters as in **Figure 5.11**.

Despite the numerous assumptions included in the above predictions perhaps the most significant result is that this Lucas Washburn prediction begins to reflect experimental observations observed in this work as well as in the literature for the wetting of VACNT forest with a low viscosity high performance engineering resin [140]. Consequently the feasibility of achieving partial wetting of VACNT structures using a high performance resin matrix may indeed be viable particularly through the fine tuning of the resins cure profile and fluid properties.

5.7 Experimental confirmation of early stage capillary rise in VACNT structures during capillary driven wetting using $\mu\text{-CT}$ analysis

As discussed previously in this work it has been assumed that the capillary driven wetting of VACNTs remains in the early stages throughout at least the first 5 mm of wetting as considered in this work. The most significant point of this assumption is that the capillary process is driven by the balance of viscous losses and capillary interactions with gravitational effects being neglected as their contributions are insignificant in comparison. This assumption has been confirmed experimentally through a simple process in which the method of sample production is modified. **Figure 5.24** details a modified schematic of the sample production method in which the EVA layer is applied to the top

of the forest and consequently gravitational effects occurring from the result of the weight of the polymer layer will aid capillary driven wetting rather than retarding it as in the prior case. As CNTs have been shown to be excellent thermal conductors [41] it can be assumed that the polymer layer will be quickly heated to the temperature of the heated stage when brought into contact with the surface of the VACNT forest. Even so samples produced in this fashion were given an extra 30 s of wetting time in order to ensure similar partial wetting of the VACNT forest structure was achieved.

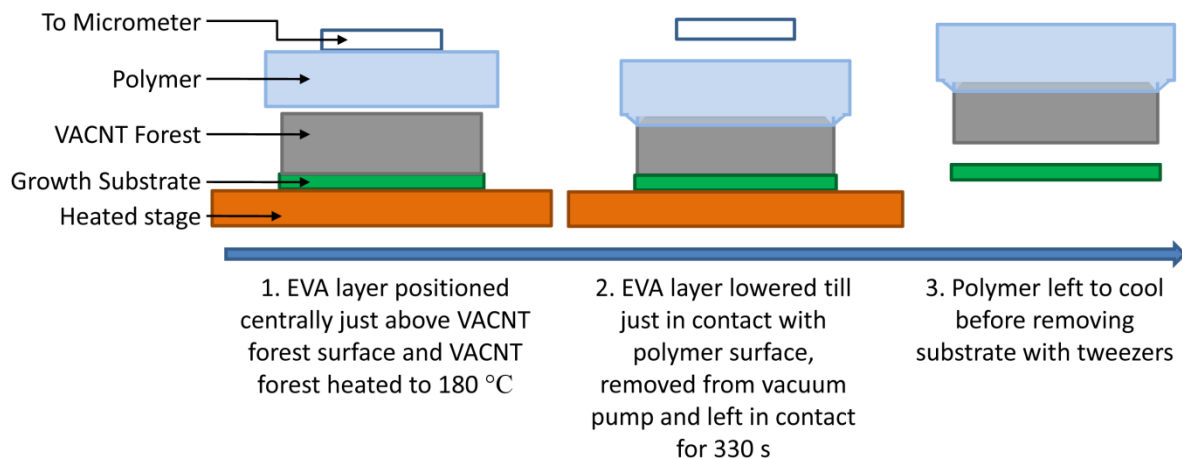


Figure 5.24: Simplified schematic of the modified partially embedded VACNT production mechanism using the custom rig imaged in **Figure 5.12**.

By conducting similar SEM and μ -CT analysis on these samples it was expected that a similar wetting mechanism would be observed thus indicating that the influence of gravitational effects was indeed minor. Wetting of VACNTs in this fashion is slightly more troublesome than in the earlier technique as residual stresses in the polymer layer can cause curling of the material, however successful wetting was achieved and results are imaged in **Figure 5.25**.

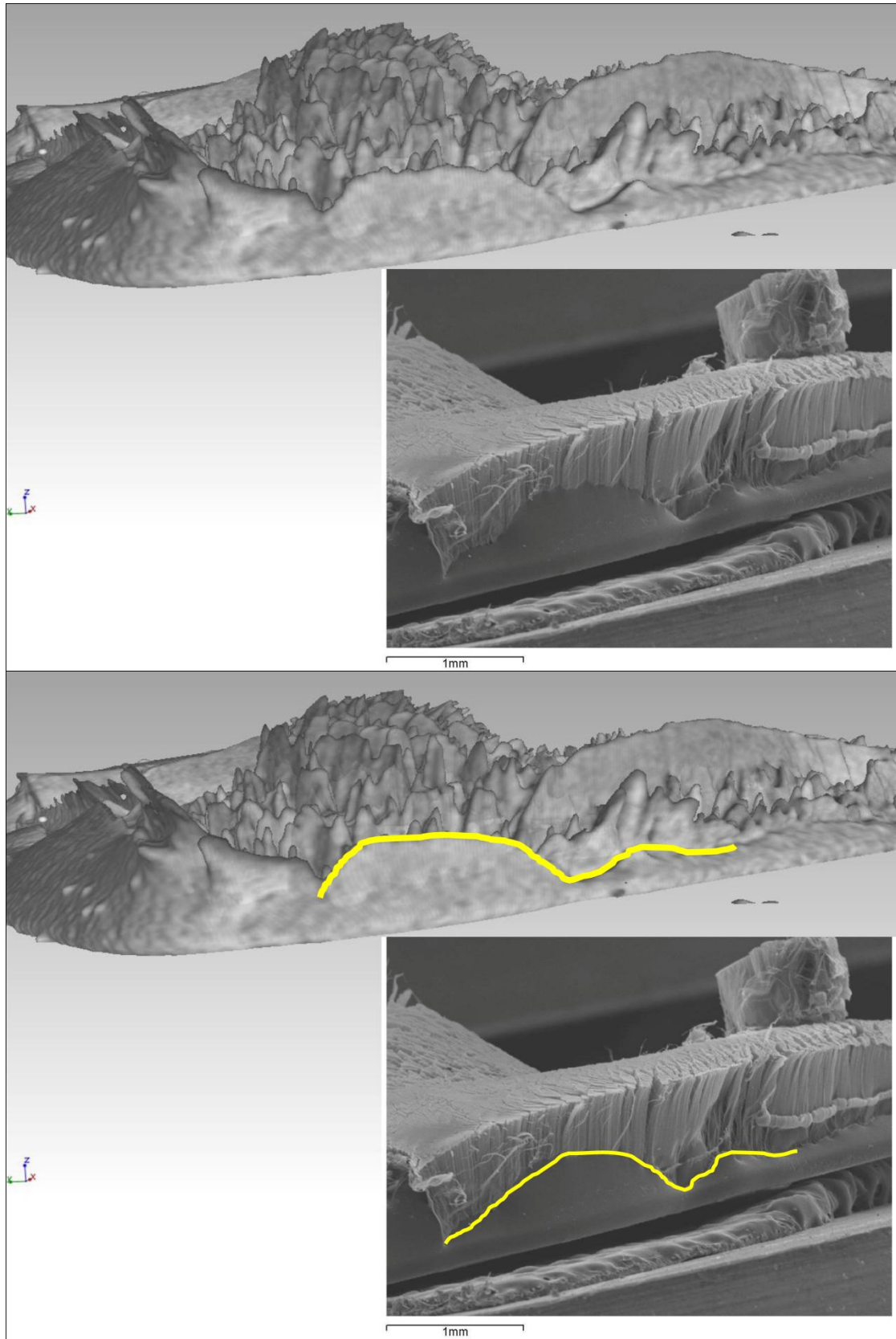


Figure 5.25: SEM and μ -CT analysis results of using the modified sample production technique detailed in **Figure 5.24** to wet VACNT forest structures.

Despite the difficulties in producing samples in this way a similar peaked polymer flow mechanism is still observed in the interior of the VACNT structure when observed using μ -CT analysis and the surface of the VACNT forest remains unchanged when viewed using SEM in a similar fashion to the previously examined samples. These results provide further evidence that indeed the capillary driven flow is largely uninfluenced by gravitational effects at this length scale and consequently confirm that the use of the Lucas Washburn short term asymptotic approximation solution to the implicit model is a sensible one for these structures in this scenario.

5.8 Conclusions

Experiments conducted in this Chapter have confirmed that the capillary driven wetting mechanism of VACNT forest structures with fluid polymers is indeed more complicated than traditional capillary theory predicts. These results are most probably a consequence of the complex architecture that results from the wavy nature of VACNT when viewed at the nanoscale as discussed in depth during **Chapter 4**. However despite such complicated interactions results have confirmed that capillary flow is largely driven by the balance of capillary forces that result at the liquid solid interface and viscous losses that occur as the fluid is drawn into the porous structure. Most interestingly the observation of peaks of polymer material within the structure display a possible mechanism for a reduction of viscous losses in the system during capillary flow and can account for the increased rates of capillary driven wetting observed experimentally when compared to those predicted theoretically. A further point to consider is the implication of the presence of such peaks on a multi layer composite produced using the methods outlined in **Chapter 2**. Despite the presence of these peaks being unexpected, in the case of a multilayer composite they may serve to further interlock the layers of the structure providing that the structure is still fully wetted to the full depth of the troughs that reside between such peaks. Leading from these results it may be possible to use capillary theory to effectively predict the evolution of capillary flow in such structures through fitting experimental observations to traditional models. Similar predictions have been made in other areas of capillary literature that describe capillary flows in other complex porous architectures [237] such as those found in soils or bricks where accurate theoretical prediction of viscous losses is challenging. In such predictions materials are often given effective constants to describe their microstructure which can then be used in consequent capillary calculations regarding the dynamic capillary flow of fluids. Dynamic experimental investigations into capillary flow are conducted in the following Chapter of this work with the aim of confirming these predictions and the end goal of assessing the feasibility of achieving partial wetting for multi-layer composite production.

Chapter 6

Experimental Investigations and Modelling of Dynamic Capillary Driven Wetting in VACNT Forest Structures

6.1 Introduction

In **Chapter 5** of this work initial studies were conducted in order to investigate observed mechanisms of capillary driven wetting in VACNT forest structures [236]. Such experiments not only identified complicated flow regimes within the interior of VACNT forest structures but also illustrated that effective partial embedding of such structures into polymer layers was possible. Considering the highly complex structure of VACNT forests that has been observed at the nanoscale and that accounts for the multidirectional reinforcement provided by such structures and discussed in depth in **Chapter 4**, such complex wetting mechanisms are not overly surprising. The Lucas-Washburn equation has been used to describe the early stages of capillary driven flow in a variety of scenarios [230], [231] and in this Chapter it is utilised in describing the flow of a polymer into a VACNT forest in a dynamic fashion. Despite the highly complex architecture present in the interior of VACNT forests it is shown that approximations can be drawn which allow various effective properties to be assigned to these situations. Using these effective properties predictions about the evolution of dynamic capillary flow in these structures are drawn in a similar fashion to those used to describe fluid flows in other porous media throughout the literature [234]. By using such models it is possible to predict when a VACNT forest will be partially wetted and subsequently terminate further wetting through some means, such as rapid curing or even cooling, thus providing a key step in the route towards a multi-layer VACNT composite [193].

Direct monitoring of wetting in VACNT structures is a challenging process for a number of reasons and consequently it is necessary to overcome several experimental difficulties. These difficulties include the scale of the VACNT forests, as the tallest available forests are only ~ 3 mm tall, the speed of the wetting process, typically less than 1 s for full wetting of a single forest [140], and finally but perhaps most importantly the difficulty in observing the wetting process optically as VACNT forests are almost perfect absorbers of radiation in the visible spectrum [238]. Although such difficulties exist a series of techniques to overcome these problems has been devised and a sequence of experiments conducted in order to investigate if the Lucas Washburn model could be applied to

these nanoscale architectures and whether reliable predictions about capillary flow could be drawn. In order to dynamically measure the speed of wetting a high speed camera was loaned from the ESPRC EIP loan pool that was capable of recording at up to ~100,000 fps [239]. Fitting this camera with a mono-zoom lens solved two of the problems initially encountered when assessing dynamic wetting in VACNT structures as both length and time scales are now easily recordable using such equipment. The final issue of detecting whether a VACNT forest is wetted or not can be solved using a unique method which is made viable through the use of the SabreTube to produce VACNT forests [202]. This technique involves the production of numerous VACNT forests of different heights that remain substrate bound. Consequently when observing the wetting process it is possible to observe when 'full' wetting of the forest has occurred and thus by obtaining numerous results for various forest heights a relationship between VACNT forest height and total wetting time can be found. From such data the presence of a Lucas-Washburn relationship can be confirmed and consequent effective properties for specific systems are also revealed. The experiments undertaken in this chapter have been conducted with the specific purpose of producing multi-layer VACNT composite structures using techniques discussed in **Chapter 3** but it should be noted that there are a vast range of applications and industries that may benefit from the remarkable interactions that occur between fluids and these nanoscale forests of VACNTs.

6.2 Experimental Investigations into Dynamic Capillary flows in VACNT Forest Structures

In order to conduct analysis of dynamic capillary flow in VACNT forests it was necessary to not only use a high magnification, high speed camera but also to accurately measure the surface properties of the resin systems in use that were not detailed on the manufacturer's data sheet. As well as such characterisation a custom rig was also developed which allowed precise control over the capillary driven wetting process. This section provides details of experiments conducted in order to assess the properties of the system and effectively monitor the wetting procedure.

6.2.1 Materials

The VACNT forests used in this study were manufactured in house using the techniques described previously in **Chapter 3** of this work. The resin used is a commercially available high performance, low viscosity two part warm cure resin system consisting of the araldite LY3505 resin and XB3403 hardener manufactured by Huntsman® which has also been used extensively in **Chapter 4** of this work as well as in composite production in the literature. When used as a mixture the resin and hardener were combined by accurate weighing and mechanical mixing in a ratio of 100 parts LY3505

to 35 parts XB3403 by weight as per the manufacturer's recommendations. Weighing and measuring of both components was conducted using syringes and an accurate set of digital scales.

6.2.2 Measurement of the Fluid Surface Tension of the LY3505/XB3403 Resin system

In order to fully analyse the wetting process it is necessary to investigate the fluid-air surface tension (γ) of the neat resin and mixed resin respectively. Although there are various techniques available for accurately measuring the fluid-air surface tension, the pendant drop method was selected in this case as the method could easily be performed using the same equipment available for monitoring the dynamic wetting process [240]. This method was used to provide an approximate value for the surface tension using a syringe and square cut needle to produce the pendant drop. Measurements of the drops were conducted from photographs taken using the same mono zoom lens and camera as used for hi-speed filming of the wetting process, an example image is shown in **Figure 7.1**. The measurements for each sample were accurately recorded using Adobe Photoshop, with drop measurements being scaled to the diameter of the needle, which was measured physically using a digital micrometer.

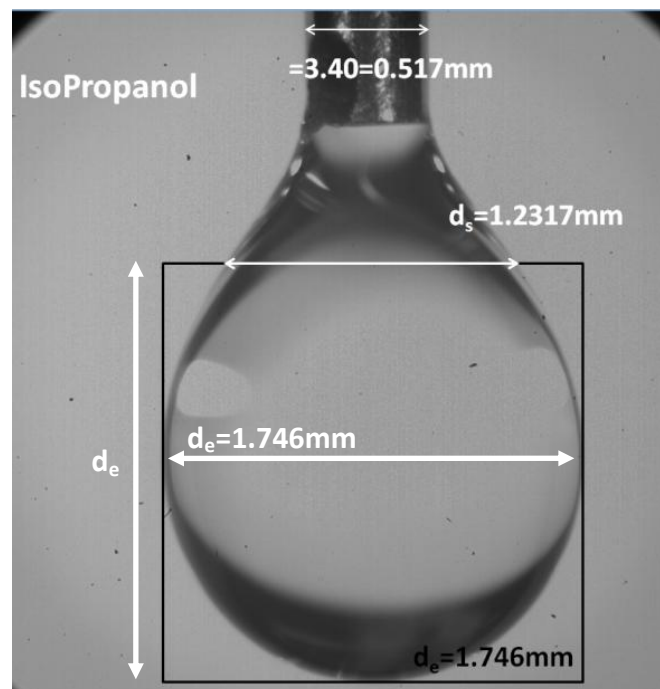


Figure 6.1: Computer analysis of a pendant drop taken from a still from video data collected using the Photron XLR camera for the measurement of fluid surface tension. The measurement of the values of d_e and d_s are shown.

Figure 6.1 also illustrates an example of how values of ' d_s ' and ' d_e ' were measured and consequently used to calculate the shape value ' S ' from the following equation,

$$S = \frac{d_s}{d_e} \quad (1)$$

the value of which is then used to calculate the value of the parameter ' H ' from the H-S function devised by Andreas et al. and described in their work [240]. Values of ' H ' can be drawn from the table pre-calculated in Andreas's paper for the desired shape value ' S ' that have been calculated previously through the use of finite increments. The surface tension, ' γ ', can then be calculated using the following equation, again taken from the work of Andreas et al. [240] and detailed below,

$$\gamma = \frac{(\rho_1 - \rho_2)gd_e^2}{H} \quad (2)$$

where ' ρ_1 ' and ' ρ_2 ' are the respective densities of the fluids present at the interface in this case the wetting fluid being tested and the surrounding air respectively, ' g ' is the acceleration due to gravity, and all other symbols are defined previously.

It should be noted that small errors will likely exist owing to the tendency of the shape of pendant drops to evolve with time, however by maintaining experimental consistency a sufficiently accurate comparison can be obtained. Furthermore as images were recorded using a video camera it was observed that no significant changes in the shape of the drops were apparent during the 10 s of video data that was recorded almost instantaneously after the drops were produced in each case. Measurements were taken from three individual pendant drops for both the neat resin and mixed resin drops and average results for surface tension values are listed in **Table 6.1**. Further experiments were also conducted using isopropanol in an identical fashion in order to assess the accuracy in using this apparatus to measure surface tension. This method is found to be sufficiently accurate through comparison of experimental results for isopropanol with literature values and these values are also detailed in **Table 6.1**. The small discrepancy between literature value and experimental value for isopropanol surface tension can be attributed to the difference in temperature at which each measurement was conducted and is logical considering that various literature documents suggest that surface tensions typically decrease with increasing temperature although clearly such results will depend on the precise chemistry of the specific fluid [241].

| Fluid | Surface Tension @25 °C / mNm ⁻¹ | Literature Value @20 °C / mNm ⁻¹ |
|--------------------------|--|---|
| Neat LY3505 | 44.6±0.6 | -- |
| LY3505/XB3403 Mixture | 34.1±3.6 | - |
| Isopropanol | 18.2±1.8 | 21.7[13] |

Table 6.1: Experimental values of surface tension measured using the pendant drop method

6.2.3 Details of the PHOTRON Fastcam XLR Hi-speed Camera System

The PHOTRON Fastcam XLR system was loaned to the University of Exeter by the ESPRC funded Engineering Instrument Pool (EIP) for duration of three months in order to conduct the experiments detailed in this chapter of this work. This monochromatic camera is capable of recording at rates of up to 100,000 fps which is considerably greater than typical video recording rates that are often well below 50 fps and insufficient to estimate the total wetting time of VACNT forests with fluids as is the purpose of this work. As with the majority of high speed camera systems the limitations of the speed of the device exist due to inherent limitations in the rate at which data can be stored rather than that at which it can be recorded. Consequently when using the camera at its highest frame rates the resolution of recorded video data is reduced to only 128 x 16 pixels per frame. As identifying the point at which a VACNT structure is fully wetted is a challenging process, it is desirable to use a higher resolution when conducting such testing and as a result it is necessary to reduce the frame rate of the camera to allow the capture of a greater number of pixels per frame. In order to increase the image resolution to 1024 x 1024 pixels, sufficient to observe the wetting process in detail, the frame rate must be reduced to around 1000 fps. Although this frame rate is two orders of magnitude lower than the highest performance that the camera is capable of it is still high enough as the timescales that are being considered are of the order of a single second. Using these settings it is possible, owing to the cameras dedicated array of solid state drives (SSDs), to record over 30 minutes of footage in a single shot easily allowing the full wetting procedure to be captured without adversely affecting any experimental procedures. Furthermore the use of the supplied mono-zoom lens allows footage to be recorded at a high enough magnification that the width of the VACNT forest fills the field of view. Video footage can then be exported from the SSDs as a video file or a sequence of individual frames in order to conduct detailed analysis of the procedure, and accurate measurement of the total elapsed time. **Figure 6.2** pictures the PHOTRON Fastcam installed in the

materials testing lab in Exeter, the SSD array is visible in the background of the image and the mono-zoom lens is attached.



Figure 6.2: The PHOTRON Fastcam XLR installed at Exeter.

6.2.4 Monitoring of Dynamic Capillary Rise using the PHOTRON Fastcam XLR Hi-speed Camera System

In order to accurately monitor the dynamic wetting process it was necessary to engineer a unique wetting rig that would allow repeatable and accurate wetting of VACNT forests through capillary effects. Initially a selection of two sets of six individual VACNT forests of various heights between 0.1 and 3.5 mm were produced using the Sabretube system. Forest growth was terminated as best as possible at the desired height by ceasing the flow of ethylene when a suitable growth height was recorded on the laser interferometer as detailed in depth in **Chapter 3**. As previously mentioned despite the Sabretube allowing monitoring and termination of VACNT growth at the user's desired height, the process remains temperamental and consequently is often difficult to predict. As a result a greater focus is placed on using the highest quality forests available as opposed to an even distribution of VACNT forest heights in this work. The PHOTRON Fastcam is controlled using a dedicated computer system with appropriate software installed. This software provides a live feed of the video data allowing accurate focusing and positioning of the camera, which is tripod mounted. The software can be used to initiate and terminate recording when desired and is also used to control the resolution and frame rate of the footage that is being recorded. To conduct accurate wetting of VACNT forests precise control over the vertical displacement of the VACNT forest is required. In order to achieve such precise control a hydraulic piston system is used which allows accurate control over the z-axis position of the forest. The system is constructed from two water

filled syringes that are joined using a polymer tube; one syringe is of considerably smaller volume than the other and consequently can be used to move the larger syringe over small displacements at very low speeds. The VACNT forests are mounted to the larger syringe through the use of a magnet, where the magnet is attached to the end of the syringes plunger using cyanoacrylate. The individual VACNT forests are then attached to a small steel plate again using cyanoacrylate to bond the growth substrate and steel plate thus allowing the VACNT forest to be inverted and mounted to the magnet on the end of the plunger using precision tweezers. **Figure 6.3** illustrates a simplified schematic of the hydraulic syringe system in use.

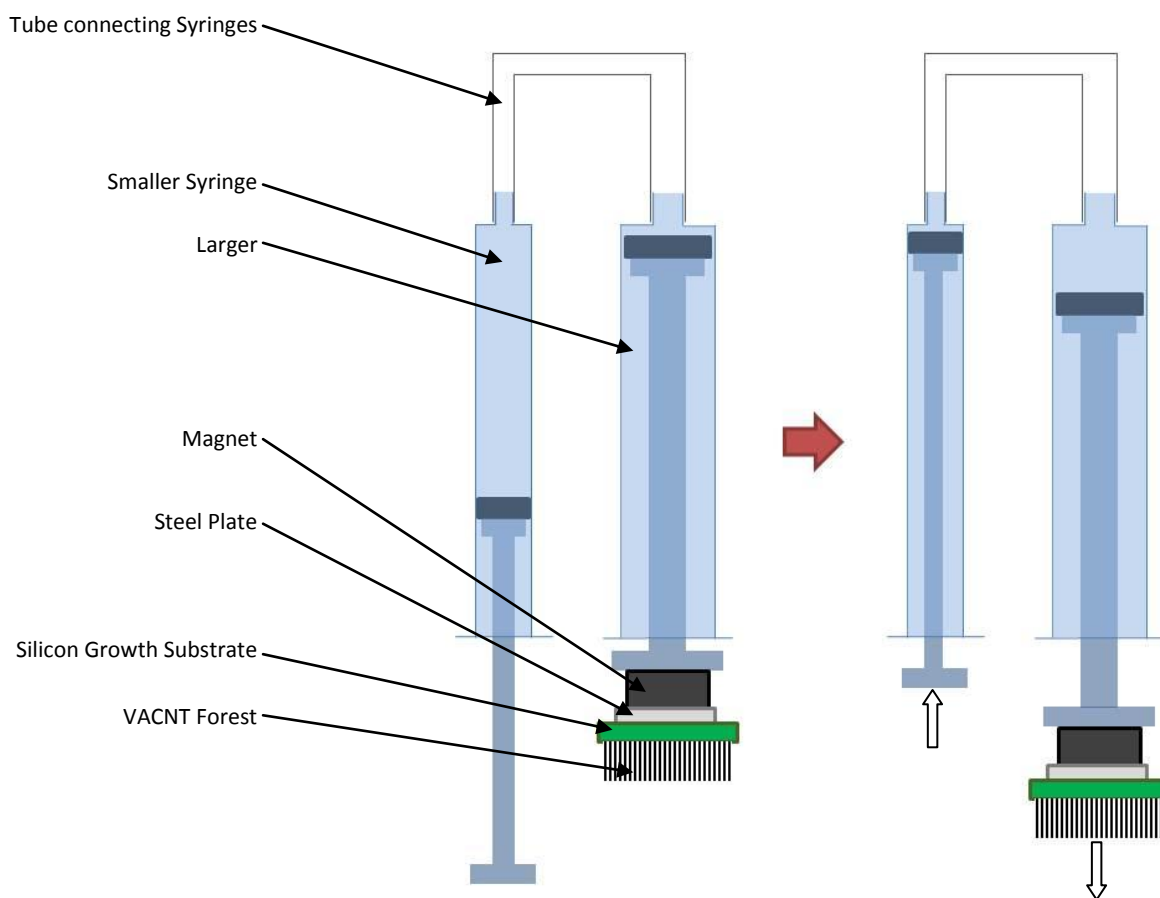


Figure 6.3: A simplified schematic of the hydraulic syringe system used to control z-axis displacement of the VACNT forest (not to scale), note how large displacements on the smaller volume syringe correspond to much smaller displacements of the larger volume syringe.

Using this hydraulic mounting system the larger syringe is then placed into a clamp that is carefully levelled to ensure that when a VACNT forest is attached to the magnet the forest remains perfectly perpendicular to the z-axis. The tube connecting the two syringes is significantly longer than that which is illustrated in **Figure 6.3** and consequently allows control of the z-axis position of the VACNT forest whilst monitoring the live video feed that is visible on the monitor of the cameras control

system. As the larger syringe remains fixed during the experimental procedure VACNT forests can simply be replaced by removing them whilst attached to the steel plate from the magnet via the careful use of a pair of tweezers. The wetting fluid, in this case either neat or mixed LY3505 resin, is carefully placed into an optically clear bath that holds many times the volume of fluid required to fully wet the VACNT forest. When filling the resin bath it is important to ensure that no bubbles are present, this is avoided by deaerating the resin or mixed resin respectively via vacuum treatment in an identical fashion to the method described in **Chapter 4** [224]. The fluid is then carefully transferred to the bath after deaeration using a syringe, and the bath is filled till the meniscus of the fluid rises above the edges of the bath but does not overflow as it is held under its own surface tension. The resin bath is then placed on a stand which has an adjustable height and the bath is positioned centrally below the inverted VACNT forest. The stand is then adjusted till the surface of the resin bath is sufficiently close to that of the VACNT structure that both are clearly visible within the PHOTRON camera's field of view. It should be noted that two powerful spotlights are required to provide enough light for the PHOTRON camera, and that these lights are switched on for the shortest amount of time required and kept as far from the sample as possible in order to minimise thermal effects that might occur as a result of the heat radiating from the spotlights. **Figure 6.4** illustrates an example frame from the PHOTRON camera, where both VACNT forest and resin bath have been accurately positioned ready to initiate capillary driven wetting of the structure.

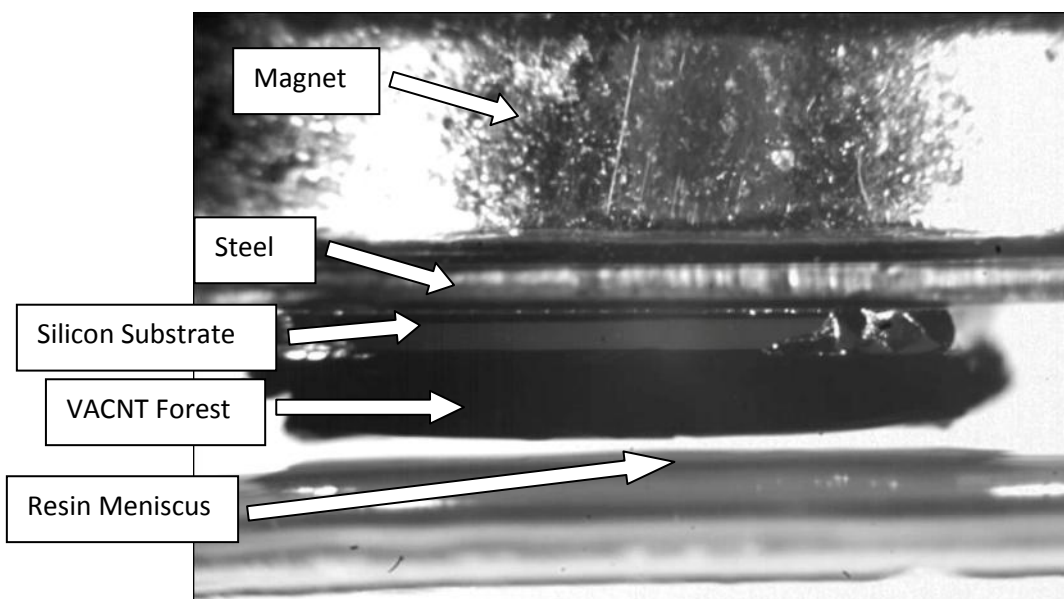


Figure 6.4: Example of a VACNT forest mounted and ready to be *dipped* into the resin bath, the camera has been focused onto the silicon growth substrate.

Once the VACNT forest and resin bath have been carefully positioned the camera recording process can begin and the dynamic wetting process can be initiated. In order to begin wetting the smaller syringe is carefully compressed until the VACNT forest surface just touches the resin bath meniscus as seen on the live feed of the video. As the wetting process is very fast, by moving the VACNT forest into contact as slowly as possible it can be assumed that the VACNT forest is effectively stationary when it contacts the liquid, and the velocity of the forest is consequently neglected from further calculations. This assumption is confirmed as the VACNT forest appears stationary throughout the relevant portion of the video footage when analysed in detail later. Once full capillary driven wetting has occurred the video recording can be terminated and the VACNT forest withdrawn from the resin bath. The video footage is then cropped to only include the relevant section of data before being exported as a video file, as well as a frame by frame high resolution image sequence for further detailed analysis. The process is then repeated for each forest height in order to provide a series of experimental data for comparison with dynamic capillary modelling theory. **Figure 6.5** illustrates a model of the overall unique experimental setup that was used to carry out dynamic monitoring of the capillary driven wetting of VACNT forests in this work.

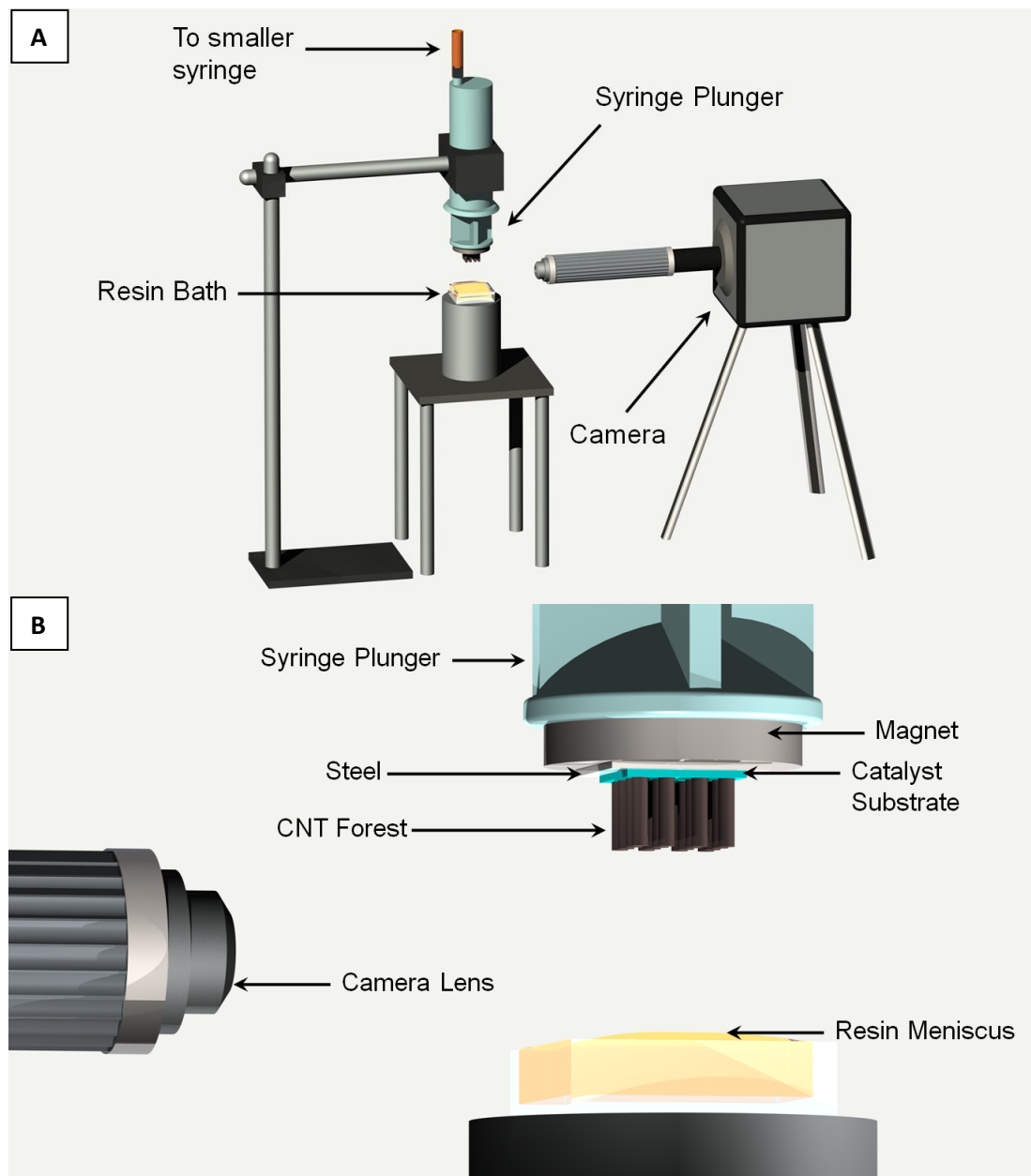


Figure 6.5: **A-** Overall schematic of the Camera and VACNT *dipping* experimental arrangement, **B-** Zoomed detail of the resin bath and VACNT forest mounting arrangement, Note that neither schematic is to scale.

6.3 Modelling of Dynamic Capillary Rise in VACNT Forest Structures

In **Chapter 5** discussions about capillary effects that result from the three phase surface interactions that occur at solid-fluid interfaces were introduced in depth. These effects have been observed to be particularly predominant in VACNT forest structures owing to the nanoscale of the pores that exist between individual CNTs within such structures. Indeed it is as a direct result of both previous theoretical investigations [236] and experimental observations [224] into capillary effects in VACNT forests that the work in this chapter has been conducted.

6.3.1 Simple Capillary Rise Phenomenon in VACNT Forest Structures

As stated an in depth introduction to capillary effects has been discussed in the previous chapter of this work and consequently will not be discussed here. Instead this chapter focuses on using a modified Lucas-Washburn model that has been used effectively throughout the literature to model dynamic capillary driven wetting in complex porous architectures [234]. As flow regimes in intricate networks of pores, such as those found inside bricks, soils, or even columns of beads, can become very complex it is often found that effectively predicting the evolution of capillary rise is challenging. Consequently experiments are often conducted and then matched to theoretical models which subsequently assign effective properties to the specific system being examined. These porous modifications to the Lucas-Washburn model are discussed in the following section; however it is important to remember that many of the assumptions made during the previous chapter still apply in this scenario.

6.3.2 Modelling of Dynamic Capillary Rise in Porous Media and Structures

Most fluid flows are considered in pipes or channels for both simplicity and efficiency. However, as mentioned previously, it remains of interest to understand fluid flows in more complex structures for many applications. In the case of complicated porous structures such as foams, powder columns, or as in this case VACNT forests, the path of the fluid flow through the structure is likely complex and multidirectional thus precise calculation of the viscous drag would be highly complex. Darcy [233] initially addressed this subject and realised that it would be beneficial to consider flow in a single direction at one time and thus considered an average direction of flow. This simplistic approach allowed calculation of a relationship between steady mean velocity and the rate of pressure drop in the direction of the velocity through a constant. This constant is given for a particular temperature, for a particular fluid, and a particular porous structure and is usually determined experimentally as it is difficult to predict in most cases. Kozeny [243] expanded on Darcy's Law by estimating porous structures as bundles of capillaries, an idea originally suggested by Washburn [230], and devised a method for calculating an effective capillary radius based on the associated capillary driven flow. Given the case of a VACNT forest wetting through capillary effects the idea of modelling the structure as an array of vertically aligned cylinders may appear logical but high magnification SEM imaging has revealed that VACNTs are in fact wavy and moderately entangled when viewed individually [141] as discussed in depth earlier in this work. As a result VACNT forests will be modelled as a bulk porous structure where the steady mean velocity is considered in the vertical direction as observed to an extent experimentally. The model used is an adaption of the Lucas-Washburn equation where the momentum balance is changed to calculate the viscous losses and

hydrostatic pressure in terms of the effective pore parameters. These pore parameters are defined as the static radius (R_s), used to calculate hydrostatic pressure, the porosity (φ), the ratio of the volume of voids over the volume of the structure, and the permeability (K), a measure of the resistance to flow caused by the structure, and have been used by others previously. Replacing these terms in the momentum balance discussed in **Chapter 5** previously results in,

$$-\rho \frac{d(h\dot{h})}{dt} = -\frac{2\gamma\cos(\theta)}{R_s} + \frac{\varphi}{K}\mu h \frac{dh}{dt} + \rho gh \quad (3)$$

rearranging and solving, whilst ignoring gravitational effects, as the dynamic capillary rise process is still assumed to be in the early stages where gravitational effects are minimal [234], gives,

$$h^2 = \frac{4\gamma\cos(\theta)}{\varphi\mu} \frac{K}{R_s} t, \quad (4)$$

where all parameters have been defined in **Chapter 5** previously or earlier in this section. This equation is a simple modification of the Lucas-Washburn equation and has been shown experimentally to provide effective prediction of capillary flow in porous structures when matched to experimental data, for instance by Fries et al. [234]. The values of the effective constants cannot be trivially derived as they are highly specific to individual scenarios; however it is possible to draw on results discussed previously in this work in order to estimate suitable predictions for the porosity of a VACNT forest. During **Chapter 4** a value for the porosity of a typical CVD grown VACNT forest such as those used in this work was measured using Thermo Gravimetric Analysis (TGA) and found to be approximately $\sim 98\%$ or 0.98 [224]. The usefulness of this value is however somewhat reduced as changing the density of as grown CVD VACNT forests is non-trivial thus using porosity to control the dynamic wetting process is challenging [208]. Consequently the Lucas-Washburn expression for the VACNT structure and specific wetting fluid, in this case the LY3505 resin, is dependent on the combined effective parameters, $(K/\varphi.R_s)$. If the Lucas-Washburn equation for porous media can be effectively applied to VACNT forests undergoing capillary driven wetting then the combined value of these effective parameters should remain constant throughout the early stages of capillary rise that

are currently under investigation. To assess the validity of this model for VACNT forests undergoing capillary driven wetting with the LY3505 resin experimental data will be plotted and fitted to this modified Lucas-Washburn equation.

6.4 Analysis of Experimental Video Data

Various investigations have been previously conducted into the use of VACNT forests as a black body material, where the radiation absorbance approaches 1.0. Results thus far have shown that VACNT forest structures exhibit an absorbance of greater than 0.98 throughout the visible spectrum [212], [238]. Consequently it is difficult to observe dynamic wetting effects in VACNT forests in detail in similar methods used by others for the characterisation of wetting effects in other materials such as fabrics [234]. In order to understand the wetting process dynamically this work relies on the monitoring of the reflection of the light from the surface of the resin as it is drawn into the VACNT structure under capillary driven flow. Even when using high luminosity spot lights during filming, dynamic monitoring of the wetting front throughout the process remains challenging, as the reflection from the resin surface is inconsistent. These inconsistencies arise due to the variations in the fluids surface geometry as it flows into the porous structure, thus as a result different intensities of light are reflected to the cameras detector as the incident angle of the light changes. Consequently it is necessary to use a different technique in order to measure wetting velocities in VACNT forests and this is achieved by measuring the total wetting time for a given VACNT forest. This total wetting time is calculated by analysing each individual frame using a simple automated procedure in Adobe Photoshop to zoom into a specific section of the VACNT forest and crop each image. It is then possible to identify the exact frame when the forest touches the fluid surface, and also to approximate the specific frame when the fluid reaches the catalyst substrate allowing calculation of the total wetting time. By monitoring the total wetting time it is possible to obtain dynamic wetting data by varying the VACNT forest height from less than 1 mm to greater than 3 mm by terminating the CVD growth of the structures at the desired height as opposed to monitoring the progress of the wetting front dynamically in a single experiment. Experimental data is obtained for a range of six forest heights using both the LY3505/XB3403 mixture and neat LY3505 as wetting fluids and detailed in **Table 6.2**. For each experiment three repeats were recorded by looking at different sections of the VACNT forest which was made possible by the large area of the forests when compared to the forest height. Image batches were cropped and enlarged in order to allow accurate identification of the wetting as well as to compare results for different sections of each forest which was possible through minor adjustments to the automated image sequence editing process. **Figure**

6.6 illustrates an example of how the video data was cropped to allow three measurements of total wetting time from each individual set of video data.

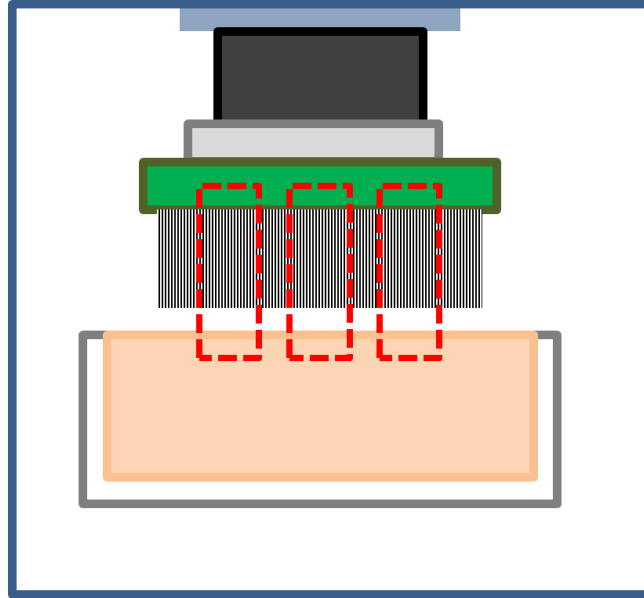


Figure 6.6: A Simple schematic of a typical camera still frame, the dashed red boxes indicate cropped sections of the images that were zoomed and used for repeat readings of the total wetting time for each sample.

In each case the time was measured using frame by frame analysis to assess the degree of wetting and the time for complete wetting calculated from the frame numbers as it is known that each frame corresponds to approximately $\sim 9.9 \times 10^{-4}$ s. An example of a VACNT forest before, during, and after full wetting is shown in **Figure 6.7**. The height of individual forests was also measured using the video data as this provides a more accurate value than using the laser interferometer to monitor VACNT height during growth as discussed in the experimental section included in **Chapter 3** of this work.

| Neat LY3505 | | LY3505/XB3403 mixture | |
|-------------------|-----------------------------------|-----------------------|-----------------------------------|
| Viscosity / mPa.s | 6500-8000 | Viscosity / mPa.s | 300-400 |
| Height / mm | Average Time for full wetting / s | Height / mm | Average Time for full wetting / s |
| 0.655 | 0.685±0.14 | 0.6422 | 0.490±0.04 |
| 0.771 | 0.957±0.08 | 0.6824 | 0.569±0.05 |
| 0.875 | 1.190±0.11 | 1.272 | 2.078±0.24 |
| 0.963 | 1.452±0.02 | 1.875 | 3.070±0.23 |
| 1.870 | 6.860±0.17 | 2.659 | 5.794±0.14 |
| 2.704 | 9.973±0.52 | 3.211 | 9.725±0.14 |

Table 6.2: Experimental values for total wetting time and VACNT forest height for both Neat LY3505 and LY3505/XB3403 mixture experiments, Viscosity values from the manufacturer’s datasheet are also included.

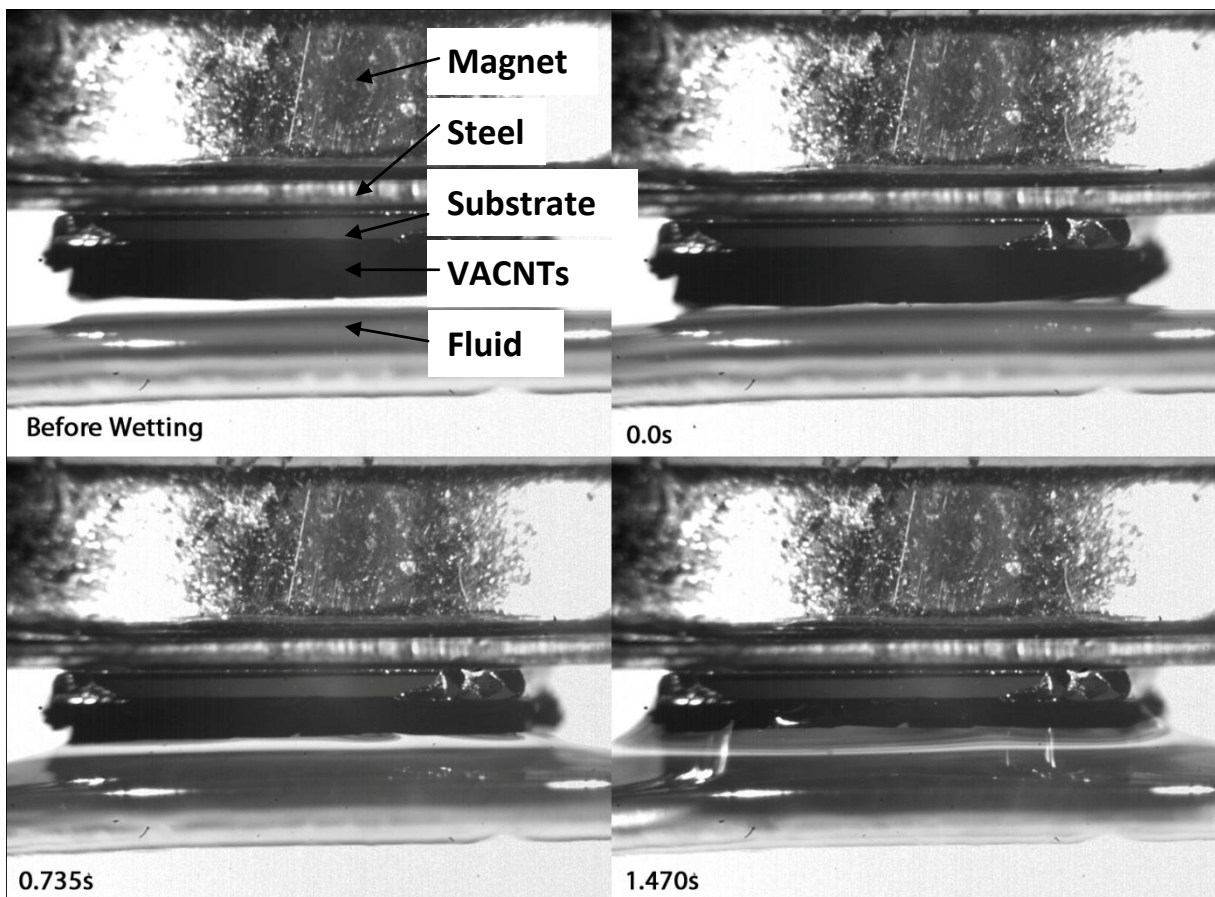


Figure 6.7: Example frame images detailing the various stages of dynamic capillary rise for a single VACNT forest sample undergoing the dipping procedure. Example time scales are provided below each individual frame to provide an indication of the length of the process.

6.5 Fitting Experimental Data to the Porous Lucas-Washburn Model

In order to effectively fit the data acquired to the dynamic porous model a simplistic method was employed which involved calculation of the value of the effective constants discussed previously for each set of experimental data. These combined effective values are simply calculated by rearranging the expression given previously as follows in order to calculate the effective constants from the heights and times that are measured from the video data and listed in **Table 6.2** above,

$$\frac{\varphi R_S}{K} = \frac{4\gamma \cos(\theta)}{\mu} \frac{t}{h^2} \quad (5)$$

In order to calculate these effective values an assumed value of the contact angle (θ) is used and this is chosen to be 30 °. This value is a sensible approximation when considering capillary theory of fluids that wet solids well and has been discussed in depth during **Chapter 5**. Furthermore the value of 30 ° has been used throughout this thesis to approximate the contact angle between individual VACNTs and polymers that readily wet the overall forest structure, as precise measurement of such a value is difficult. The assumption of a value of 30 ° can be further reinforced when considering the modified Lucas-Washburn model only considers the cosine of this angle which will only vary between ~1.0 and ~0.7 for contact angles between 0 and 45 ° in which the value will always fall if the liquid wets the solid surface well in the given environment. Thus as it has been experimentally observed that the resin wets the VACNT forest well [224], 30 ° seems a sensible assumption. Furthermore even if this value is not precise any discrepancies will be included in the calculated values for the effective constants and will not affect the general trends observed in the model. The values of surface tension, (γ), used in these calculations are those measured earlier and detailed in **Table 6.1** previously. Finally the viscosity (μ) values for both mixed resin and neat LY3505 used are those listed on the Material Safety Data Sheet (MSDS) that is supplied by Huntsman. Using the data listed above a value of the combined effective constants is calculated for each VACNT forest height and average total wetting time for both fluids. Consequently a total of six values of the combined effective constants for each scenario can be obtained and then the mean average of the data taken to estimate whether the model provides an effective fit to the data and if the porous model holds in this scenario.

Figures 6.8 and 6.9 plot the data for both the mixed resin and the neat resin experiments respectively, as well as plotting the fitted models that are created from the average values of the

combined constants that have been calculated. Upper and Lower boundaries for the fitted models are also included that indicate the Standard Deviation measured in the values of the combined effective constants for each experiment.

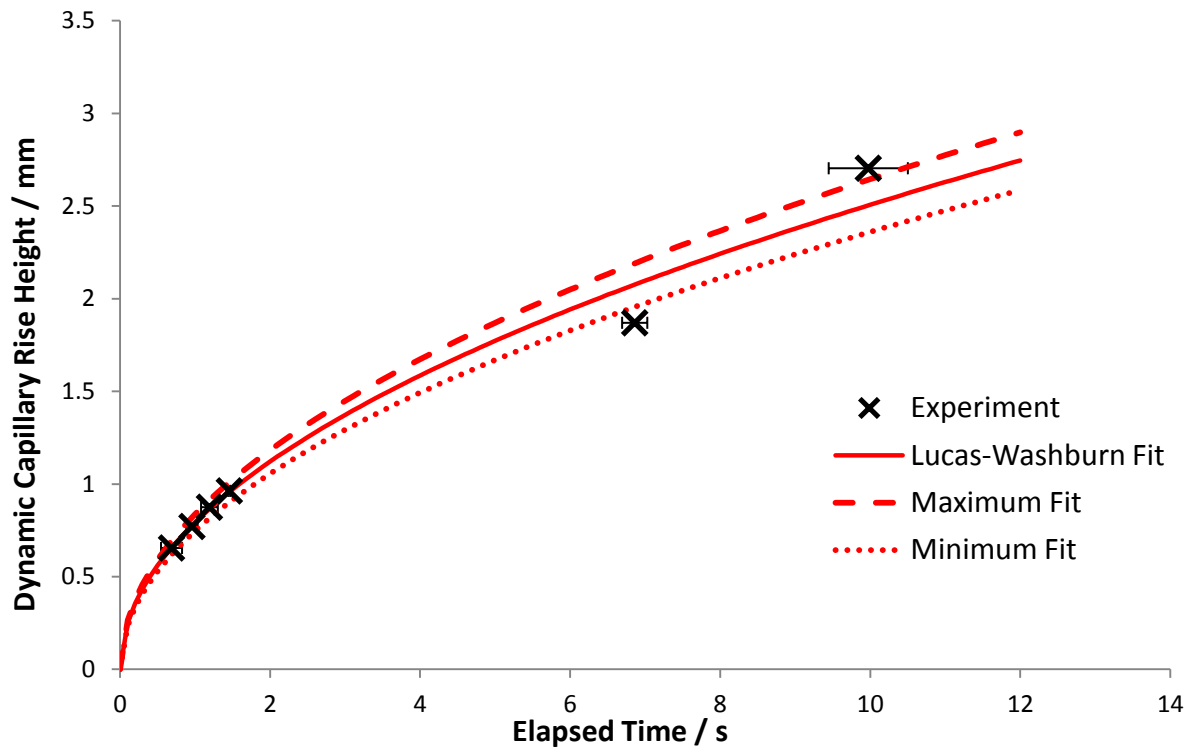


Figure 6.8: Plot of experimental data for total wetting times fitted to a porous model for dynamic capillary rise of neat LY3505 resin in a VACNT forest structure.

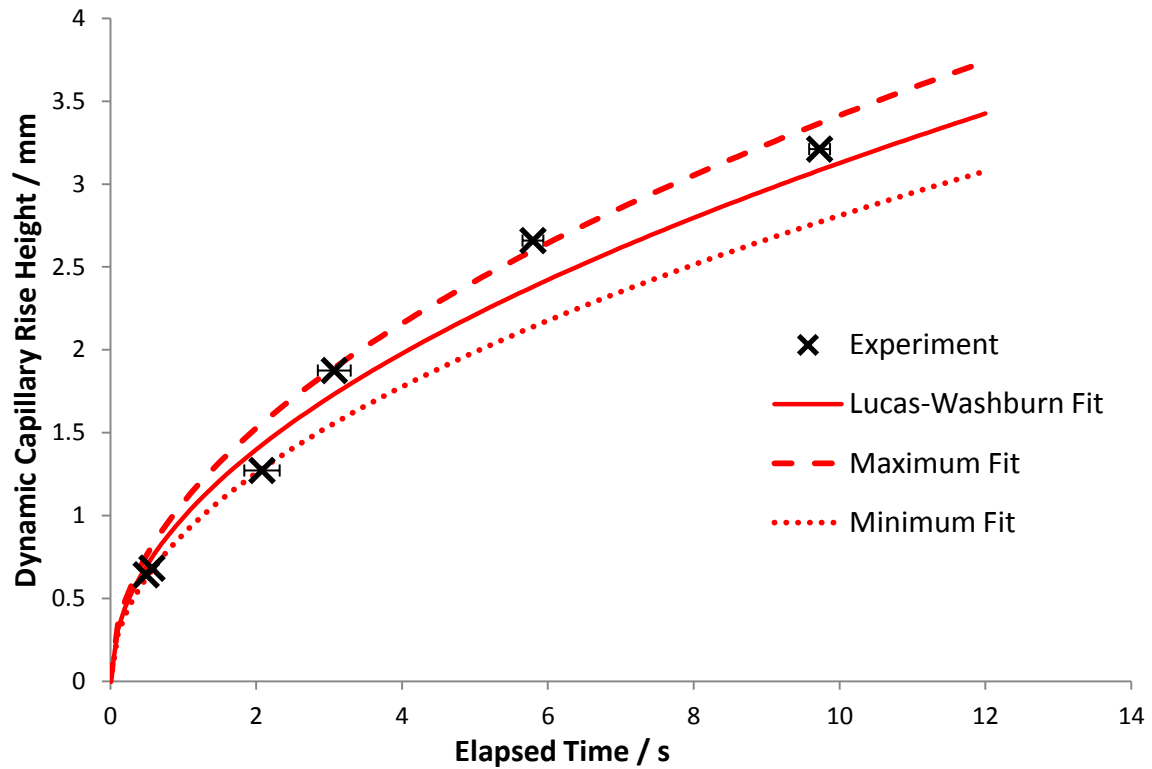


Figure 6.9: Plot of experimental data for total wetting times fitted to a porous model for dynamic capillary rise of mixed LY3505 resin in a VACNT forest structure.

Finally **Figure 6.10** illustrates a plot of all the data and the two matched models on the same graph, indicating how the dynamic process changes for the neat resin and mixed resin, as a result of changes in the surface tension and viscosity of the fluids respectively. The results indicate that reducing the viscosity of the fluid through the addition of the hardener that is of a lower viscosity speeds up the wetting process. Despite this result, accurate interpretation of the effect of viscosity on the wetting process cannot be drawn as the addition of the hardener to the mixture will likely also change other parameters involved in the calculation such as the permeability of the forest. Even so a speculative result can be drawn where it is known that the increasing the viscosity is inversely proportional to the total wetting time as detailed in **Equation 5**.

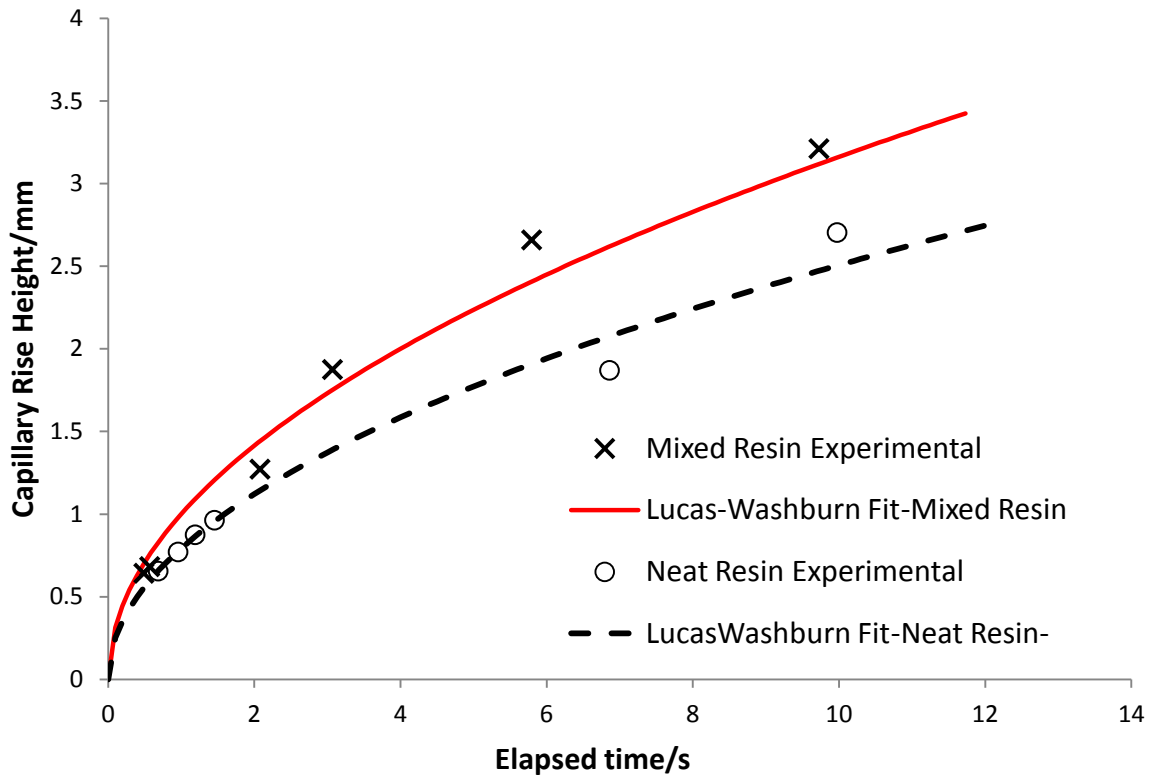


Figure 6.10: Plot of experimental data for total wetting times fitted to a porous model for dynamic capillary rise of both neat LY3505 and mixed LY3505 resin in a VACNT forest structure.

6.6 Conclusions

The results plotted and fitted to the porous Lucas-Washburn model above appear to show that the experimental data obtained in this Chapter follows the matched model well. Such a result is perhaps not altogether surprising when considering if indeed gravitational resistance to flow can be ignored due to the dynamic process being in the early stages then the rate of capillary flow will be governed by viscous losses [244]. Consequently it follows logically that the rate of capillary rise will decrease as the resistance to flow resulting from viscous losses increases as the capillary flow evolves, as observed in the experimental data. Despite the results from this work indicating that the porous Lucas-Washburn model fits with the dynamic wetting of VACNT forest structures there are some key points that must be considered. These include some important assumptions that have not previously been specifically mentioned. Firstly the model assumes that the VACNT forest structure is uniform throughout which is possibly not the case, as it is known that CVD forests often display crust regions in the upper layer [209]. However such regions will be present in all VACNT forests produced using this technique so the model may still provide reasonable predictions but the flow regime may change between different areas of forest structure. Furthermore the interior of VACNT forests at the nanoscale is known to consist of a complex network of wavy entangled individual CNTs.

Consequently, as discussed earlier, the flow profile maybe complex and the capillary rise is unlikely to be uniform as observed previously in **Chapter 5** using μ -CT analysis [236]. This means that although the total wetting time was predicted as being the time when fluid was first observed at the growth substrate this could be a result of fluid rising in peaks or columns up the edge of the forest rather than wetting the full thickness of the structure. Considering these numerous assumptions it is unlikely that accurate predictions about the dynamic wetting process for specific fluids can be drawn without first conducting further experimental analysis of the process. Even so these results provide some useful evidence about the wetting mechanisms occurring in these structures. They illustrate that indeed VACNT forests inhibit the flow of fluids considerably less than expected from traditional models considering they are effectively foam like structures containing nanoscale pores. Such a structure should restrict fluid flow almost completely however only a moderate retardation of flow rate has been observed. This result has important implications across a wide range of carbon nanotube composite research areas and is particularly relevant to efforts involving the incorporation of VACNT forests into composite structures.

Furthermore these results also provide an effective method of predicting capillary flow in highly specific scenarios involving VACNT forests which could prove critical in the achievement of a multilayer composite [194]. As outlined in **Chapter 2** of this work the incorporation of VACNTs into an additive layer manufacture (ALM) method is highly desirable. Indeed by achieving such a composite the potential exists to overcome some of the major problems that exist in both composite ALM techniques as well as inherent problems that exist when incorporating any form of CNTs into a composite structure. The major step in achieving a multilayer structure and extending results beyond the impressive results observed for single layer VACNT composites [16] as discussed previously in **Chapter 4** is achieving partial wetting through the thickness of a single VACNT forest without damaging its mechanical reinforcement capabilities. As these results have identified that the dynamic process follows the Lucas-Washburn relationship to some extent and that the height of the capillary rise is proportional to the square root of the elapsed time this goal becomes a realistic possibility. Unfortunately achieving such a goal using the LY3505 resin is unachievable as this resin is a slow curing material, with curing times that far exceed the time required to fully wet a VACNT forest under capillary driven flow. However in the field of composite materials an ever increasing range of high performance resins exists and cure times of less than a single second are becoming more common. For example the use of resins in SLA based ALM technology is often speed limited owing to the time required for the resin to cure selectively when exposed to a specific wavelength of radiation [245]. Technologies such as the SLA process are driving the cure times of advanced resins down and it is possible that a resin may already exist in the commercial environment that can

precisely partially wet a VACNT structure through a capillary driven process and also be successfully cured before full wetting is achieved. Furthermore as the dynamic process was monitored with both neat and mixed resin samples it is also apparent that both surface tension and fluid viscosity maybe utilised in controlling the dynamic wetting process although it is clear that further investigations will be required to fully understand the effects of these parameters. Assuming that such a resin can be identified that possesses comparable viscous and surface tension properties to the LY3505 resin, then partial wetting in a controlled fashion should be achievable. Following from these results further experiments can be undertaken in a bid to achieve, initially effective partial wetting, and finally a multi-layer composite component with the potential to illustrate the remarkable nanoscale properties of CNT at a macroscale that is only limited by the number of layers that one chooses to employ.

Chapter 7

Conclusions

7.1 Conclusions

The outcomes of the studies contained within this thesis have revealed some important results relating to the incorporation of VACNT forests into composite materials and the interactions that occur between fluid polymers and these nanoscale architectures. Although such results provide useful insight for many applications as discussed in the individual chapters themselves, this section aims to illustrate the implications of such results in the concept of a VACNT reinforced AM process. In **Chapter 3** the feasibility of using a CVD based system to produce large scale VACNT forests for inclusion in a stereo lithography (SLA) based process was assessed. The results indicate that the production of VACNTs in such a manner was indeed a viable strategy and is rapidly becoming the choice method of CNT synthesis owing to high quality of CNTs produced at a low cost. VACNT forests were grown to heights that exceeded 3 mm using the Sabretube desktop CVD system which is much taller than that required for interlayer reinforcement, as the ideal height of a VACNT forest for such a process is of the order of a single layer thickness, typically between 50 and 300 μm . These VACNTs have been imaged through the use of SEM analysis and results have shown that the CNTs are in general well aligned and uniform in the overall microstructure, although as discussed CNTs can often be entangled and wavy when viewed individually in the forest. Furthermore the growth of VACNTs onto silicon substrates provides an effective medium for transporting the VACNT to a polymeric layer as the bonding between the VACNTs and the growth substrate is weak, facilitating the removal of the substrate after the anchoring of the VACNTs into a polymeric layer. Although the area of these forests is limited as a result of the restricted volume of the Sabretube CVD system the achievement of uniform forests of the required heights is sufficient to demonstrate the concepts required for this study, and recent articles have demonstrated the growth of VACNT forests with areas that far exceed the typical layer area of most AM machines [201]. These results are also beginning to bring production costs of CNTs down to the order of \$100/kg for as grown products, another key factor in the implementation of CNT based technology.

After the successful production of sufficiently large VACNT forests it was of interest to ascertain the degree of reinforcement that these structures could offer to a thermosetting resin matrix material. In the literature results have identified that the reinforcement of materials using aligned CNTs is

superior to other methods of incorporating as produced CNTs into a composite material. In this work large scale forests were fully wetted with a high performance thermoset in order to replicate a single reinforced layer from the proposed manufacture process. Unlike other experiments in the literature the scale of these samples allowed transverse mechanical analysis of the samples using dynamic mechanical thermal analysis and micro tensile testing. Results from these tests indicated an interesting effect resulting from the wavy nature of VACNT that is apparent when CNTs are viewed individually in the forest. The influence of the wavy nano structure of VACNTs has previously been investigated with detrimental effects noted in the measured reinforcement achieved in the axial direction when compared to the expected result for equivalent straight fibre reinforcements. Conversely the results from this work illustrate that an increased level of transverse reinforcement is achieved when reinforcing thermosets using aligned CNTs. This occurs due to the wavy VACNTs providing multi directional reinforcement, as a component of each CNT can be considered as falling into the transverse orientation that would not be the case with perfectly straight VACNTs. The implications of these findings when considering an AM process which incorporates VACNTs using the process discussed can provide specific benefits to components manufactured in such a fashion. Initially it was thought that the microstructure of the composite would be critical in providing interlayer reinforcement that would in effect stitch the layers together however a further benefit is now apparent in that significant multi-directional reinforcement is achieved providing reinforcement with in an individual layer simultaneously. Although it is clear that the axial reinforcement will be significantly reduced as a result, considering that the purpose of these investigations is to improve current polymer composite AM materials, significant increases will still be observed when compared to the best currently available composite feed stocks. **Figure 7.1** details a simplified schematic of the expected reinforcement of a multilayer composite sample produced from multiple individual VACNT forests and several thermoset resin layers, calculations are estimated from the mechanical properties of the materials detailed in **Chapter 4**. The schematic illustrates the effects of the individual wavy CNT structure on the measured reinforcement from individual [224] and bi-layer [215] samples and also indicates how the forests may stitch the resin layers together through partial embedding.

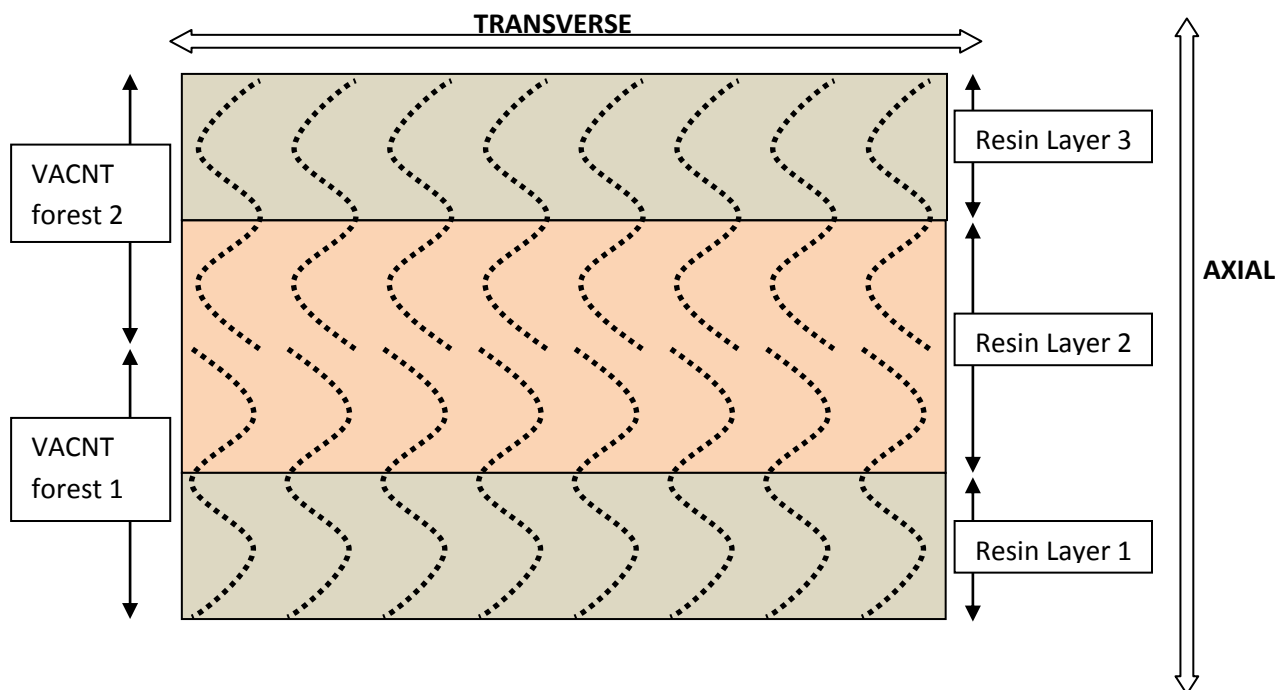


Figure 7.1: Simplified schematic of the current theoretical reinforcing mechanism in a multilayer composite an increase in modulus of approximately 20 % in the transverse orientation and 120 % in the axial direction can be expected with only a 2 vol% loading of VACNTs, not to scale.

The effective reinforcement of a single layer of resin using VACNTs provides a significant step towards the additive manufacture process. However to extend to an effective multi-layer sample the realisation of the partial wetting of VACNT forests with a suitable matrix is critical. In a bid to achieve partial wetting of VACNTs investigations were conducted into the interactions between as-grown VACNT forests and various polymers. It is known that VACNT forests act like porous media that readily wet with fluids under capillary driven effects, which are particularly strong due to the extremely large surface areas that exist as a result of the nanometre scale diameters of the individual CNTs. Consequently low viscosity fluids have been observed to be drawn into VACNT forests under such effects at very high speeds as observed during **Chapters 4 and 6** with a two part resin system. From capillary theory it is known that several methods for slowing capillary flow exist and the most feasible of these in this scenario is the modification of the fluid properties of the matrix. By increasing the viscosity of the matrix the viscous resistance to fluid flow is increased, and partial embedding becomes feasible which has been demonstrated through the use of a molten thermoplastic material in **Chapter 5**. By achieving partial embedding with a thermoplastic characterisation of the flow regime in a VACNT forests interior has been conducted for the first time using micro computed tomography. Scans revealed an interesting result which illustrates the polymer flowing into the forest interior in a series of relatively uniform peaks within the forest. This complicated flow pattern could be caused as a result of a number of different possibilities such as

the partial collapse of the VACNT forest locally where the polymer is trapped in self assembled bundles of VACNTs that may have formed through localised forest collapse as a result of capillary attraction or pushed into voids between such bundles as channels are created for fluid flow. Unfortunately further characterisation is hindered as CNTs cannot be detected using micro CT, and the interior of the forest is not visible through the use of optical or electron microscopy for reasons discussed previously. Consequently the identification of the specific location of the individual CNTs with respect to the polymer peaks is particularly challenging. Even so the formation of these peaks of polymer in the forests interior may prove to assist the production of a multilayer composite. The fixing of these peaks in the structure through curing of the matrix could provide significantly improved interlayer adhesion and help to deter delamination of the structure. **Figure 7.2** details a modified version of the schematic detailed in Figure 8.1 which illustrates the implication of the capillary driven wetting front that has been experimentally observed in VACNT forests using micro CT during **Chapter 5**.

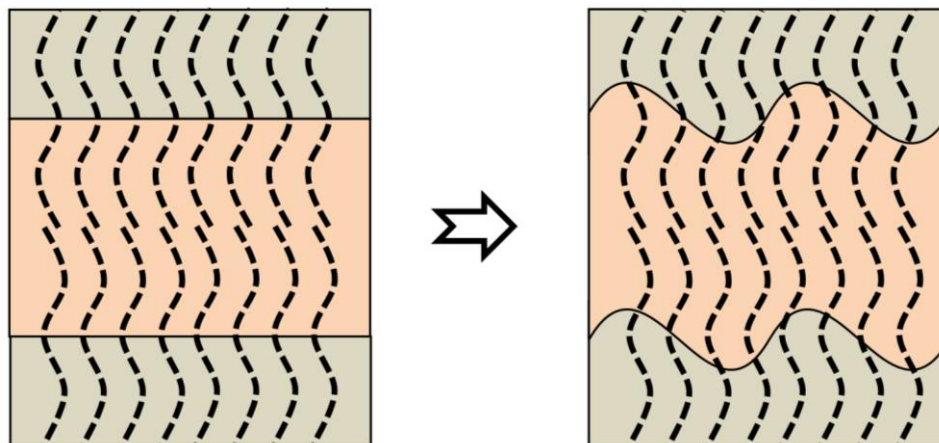


Figure 7.2: Implications of the peaked flow regime on a multilayer composite constructed through the capillary driven wetting of multiple VACNT forests. It is likely that such peaks will improve interlayer bonding through the increased contact area between layers.

The final stages of this thesis focus on further understanding the wetting mechanisms of VACNT forests through experimental monitoring of the dynamic wetting process. By conducting dynamic analysis of the wetting of VACNT forests through the use of a high speed camera, capable of monitoring up to 100,000 fps, an expression to predict the evolution of capillary flow in these nanoscale forests has been found. Although the experiments were conducted using a low viscosity two part resin that was unsuitable for achieving partial wetting of VACNT forests the results

illustrate an experimental method of predicting potential windows for achieving partial wetting of VACNT forests. The model, which is based on a modified Lucas-Washburn equation, illustrates that flow in VACNT forests is in the early stages of the capillary rise process that is driven by the balance of surface tension interactions between the CNTs and the fluid, and the retardation of the flow that results from viscous losses rather than gravitational effects. Consequently the ingress of the fluid into the forest can be characterised as the dynamic height of capillary rise being proportional to the square root of the elapsed time. Although this result is perhaps altogether not unsurprising, as many early stage capillary driven fluid flows fit similar models, it does provide a means to identify the necessary cure times to achieve partial wetting of a VACNT forest using similar materials. Furthermore as experiments were conducted with both the mixed and the neat resin fluids evidence of the influence of fluid viscosity on the wetting process is also observed, and the expected result that lower viscosity fluids wet faster recorded.

These results provide significant steps towards the realisation of a multi-layer CNT composite using an additive layer process; however it is clear that significant further work will be required to achieve a fully effective multilayer composite material in net shape.

7.2 Key Questions and Further work

In order to progress towards multi-layer VACNT composite structures clear pathways have begun to open as a result of the developments contained in this thesis however there are several key issues that require attention as follows:

- Detailed investigation into the structure of resin impregnated VACNT forests remains of interest and further work can be conducted to investigate the effect of wetting on the wavy structure. Samples could for instance be cut with a microtome and analysed using TEM.
- More detail analysis of partially wetted VACNT forests can be conducted. It may be useful to take advantage of modern μ -CT methods that allow nanoscale resolution of 3D data. Using these techniques might reveal further details of polymer flow mechanics in the interior of VACNT forests.
- Further considerations are also required relating to any molecular interaction that could occur at the nanoscale. It is possible that the presence of the VACNT may affect the formation of the crystalline microstructure of a curing or solidifying polymer.

- A material needs to be identified that offers a time-temperature dependent process window to balance the partial wetting required against the dynamic reduction of viscosity that occurs during thermal curing of the matrix material.
- Alternatively, dynamics of partial wetting may be further simplified by utilising a material that can be cured through a non-thermal means, for instance through the use of UV radiation in a similar time frame. Resins that gel in times of a less than a single second are already widely used in SLA processes. [246]
- With the achievement of partially wetted VACNT forests the production of multi-layer macro scale test coupons will be feasible. Initial tests can be conducted on single forest samples that have been wetted in two distinct stages and compared to samples wetted in a single stage.
- The final step in realising an effective multi-layer VACNT composite is to produce a coupon with sufficient layers to allow reliable mechanical testing of the interlayer reinforcement achieved by having aligned and dispersed CNT reinforcements penetrating between layers. The achievement of such a sample will provide conclusive evidence of the feasibility of the process.

7.3 Feasibility of an industrial approach to multi layer VACNT composites through ALM

A final point in concluding this work is to consider the implications of the results reported within on the viability of a realistic manufacturing process. It is clear that significant challenges remain in the path towards this goal; however some promising outcomes have been noted. Firstly the achievement of effective reinforcement of a resin through the use of VACNT forests has illustrated that there is merit in pursuing such a technique. The next consideration is the possibility of achieving partially wetted VACNT forest structures in a controlled fashion. Considering that a typical ALM layer is of the order of 100 μm in thickness an industrial process would rely on the use of VACNT forests of the same height, unlike the tall forests used in this work in order to overcome experimental challenges. Short forests such as these can be produced more reliably and with greater uniformity lending them to the process. Furthermore the production of shorter VACNT structures can be achieved through using catalysts that are deposited through an Ink Jet Print head (IJP). Using an IJP removes the need for expensive and time consuming e-beam evaporation process and allows the rapid construction of net-shape VACNT forests. Furthermore typical SLA machines produce parts at a

rate of around a single 100 μm layer every 15s. Clearly the introduction of VACNT reinforcement will significantly increase this time, however the possibility exists to produce VACNT reinforcements for the next layer as the previous layer is being cured. Consequently the increase in a single layer time is simply the time required to deposit catalyst material, produce short a VACNT forest, and transfer the structure to the layer. The limiting factor in this scenario is likely the CVD growth period which in the lab takes around 5 minutes to grow a 100 μm forest. This time is less than stated in **Chapter 3** as certain steps relating to user safety will not be required in an automated process. In reality it is likely that this process can be further optimised by using flash heating and precision gas delivery methods for accurate repeatable CVD processing rather than an adjustable lab based system. Even so, assuming a 5 minute layer time a typical 2 hour build will be increased to around 40 hours. This is indeed a significant increase however as discussed room for optimisation does exist. Finally it is important to consider that all ALM methods are focused on High Value Manufacturing and it is likely that if success is achieved in such a process it will be restricted to very specific bespoke applications such as the manufacture of precise components for satellites and spacecraft. Despite this it is unlikely that the incorporation of VACNT will add any particularly significant cost to the ALM process as the raw materials used in the production of CVD grown VACNT is fairly low-cost.

This research has provided significant evidence for the feasibility of the process of reinforcing materials through accurate control of the material microstructure through the use of a bottom up approach. The potential applications for such light weight, high strength materials are clearly vast, even without the incorporation of net shape design through additive manufacture. Even so, the potential for such materials to be built in net shape should not be overlooked particularly when considering the high cost of manufacturing materials in this fashion. The potential of producing 2D patterned catalysts for VACNT growth and selectively curing a resin matrix can increase the efficiency of the process by reducing waste materials. Furthermore the net shape production of components can allow significant optimisation of part design, further reducing the volume of material required to produce parts and consequent production speed. To create a viable manufacturing process using such techniques will still require significant optimisation and automation using state of the art additive manufacture software and hardware in a bid to incorporate layered VACNT composite manufacture into a reliable technology. By utilising an autonomous process the currently detached growth of the VACNT forests and production of composites samples can be removed and the use of machines can allow considerably greater levels of precision in the locating of VACNT forests with in the matrix. Using such automation will also allow the use of considerably shorter VACNT forests that approach typical AM z-axis resolutions which are typically of the order of 100 μm . By reducing the height of the VACNT forests in such a

manner superior uniformity of VACNT forest growth can be achieved and highly detailed net shape structure production will be viable. The potential of this technology to enhance additive manufacture processes is an exciting possibility, and will perhaps begin to demonstrate that manufacturing materials in an additive fashion holds significant promise for realising superior composite properties. Following from the results contained in this thesis a further funded research project is being undertaken at the University that will extend this work to investigate patterned interlocking samples that contain multiple VACNT forests on the route towards additive manufacture of large scale VACNT composite components.

References:

- [1] G. N. Levy, R. Schindel, and J. P. Kruth, 'Rapid Manufacturing and Rapid Tooling with Layer Manufacturing (Lm) Technologies, State of the Art and Future Perspectives', *Cirp Ann. - Manuf. Technol.*, vol. 52, no. 2, pp. 589–609, 2003.
- [2] S. Crump, 'The fused deposition modelling (FDM)', *Us Pat.*, no. 5.121, p. 329, 1988.
- [3] O. L. A. Harrysson, O. Cansizoglu, D. J. Marcellin-Little, D. R. Cormier, and H. A. West II, 'Direct metal fabrication of titanium implants with tailored materials and mechanical properties using electron beam melting technology', *Mater. Sci. Eng. C*, vol. 28, no. 3, pp. 366–373, Apr. 2008.
- [4] S. Kumar and J.-P. Kruth, 'Composites by rapid prototyping technology', *Mater. Des.*, vol. 31, no. 2, pp. 850–856, Feb. 2010.
- [5] T.-W. Chou, *Microstructural Design of Fiber Composites*. Cambridge University Press, 1992.
- [6] S. J. Leigh, R. J. Bradley, C. P. Purssell, D. R. Billson, and D. A. Hutchins, 'A Simple, Low-Cost Conductive Composite Material for 3D Printing of Electronic Sensors', *Plos One*, vol. 7, no. 11, p. e49365, Nov. 2012.
- [7] M.-F. Yu, O. Lourie, M. J. Dyer, K. Moloni, T. F. Kelly, and R. S. Ruoff, 'Strength and Breaking Mechanism of Multiwalled Carbon Nanotubes Under Tensile Load', *Science*, vol. 287, no. 5453, pp. 637–640, Jan. 2000.
- [8] O. Breuer and U. Sundararaj, 'Big returns from small fibers: A review of polymer/carbon nanotube composites', *Polym. Compos.*, vol. 25, no. 6, pp. 630–645, 2004.
- [9] W. R. Davis, R. J. Slawson, and G. R. Rigby, 'An Unusual Form of Carbon', *Nature*, vol. 171, no. 4356, p. 756, Apr. 1953.
- [10] H. W. Kroto, J. R. Heath, S. C. O'Brien, R. F. Curl, and R. E. Smalley, 'C60: Buckminsterfullerene', *Nature*, vol. 318, no. 6042, pp. 162–163, Nov. 1985.
- [11] C. W. Hull, 'Apparatus for production of three-dimensional objects by stereolithography', 457533011-Mar-1986.
- [12] S. Iijima, 'Helical microtubules of graphitic carbon', *Nature*, vol. 354, pp. 56–58, Nov. 1991.
- [13] F. Cevolini, 'Rapid Manufacturing with carbon reinforced plastics: applications for motor sport, aerospace and automotive small lot production'. The Fundacio Eduard Soler.
- [14] Y. L. Li, I. A. Kinloch, and A. H. Windle, 'Direct spinning of carbon nanotube fibers from chemical vapor deposition synthesis', *Science*, vol. 304, no. 5668, pp. 276–278, Apr. 2004.
- [15] E. Sells, Z. Smith, S. Bailard, A. Bowyer, and V. Olliver, 'RepRap: The Replicating Rapid Prototyper: Maximizing Customizability by Breeding the Means of Production', Social Science Research Network, Rochester, NY, SSRN Scholarly Paper ID 1594475, May 2010.
- [16] B. L. Wardle, D. S. Saito, E. J. García, A. J. Hart, R. G. de Villoria, and E. A. Verploegen, 'Fabrication and Characterization of Ultrahigh-Volume- Fraction Aligned Carbon Nanotube-Polymer Composites', *Adv. Mater.*, vol. 20, no. 14, pp. 2707–2714, Jul. 2008.
- [17] M. F. L. D. Volder, S. H. Tawfick, R. H. Baughman, and A. J. Hart, 'Carbon Nanotubes: Present and Future Commercial Applications', *Science*, vol. 339, no. 6119, pp. 535–539, Jan. 2013.
- [18] J. A. E. Gibson, 'Early nanotubes?', *Nature*, vol. 359, p. 369, Oct. 1992.
- [19] A. Oberlin, M. Endo, and T. Koyama, 'Filamentous growth of carbon through benzene decomposition', *J. Cryst. Growth*, vol. 32, no. 3, pp. 335–349, Mar. 1976.
- [20] P. W. Fowler, 'Carbon cylinders: a class of closed-shell clusters', *J. Chem. Soc. Faraday Trans.*, vol. 86, no. 12, pp. 2073–2077, 1990.
- [21] S. Iijima, 'Direct observation of the tetrahedral bonding in graphitized carbon black by high resolution electron microscopy', *J. Cryst. Growth*, vol. 50, no. 3, pp. 675–683, Nov. 1980.
- [22] E. Flahaut, R. Bacsa, A. Peigney, and C. Laurent, 'Gram-scale CCVD synthesis of double-walled carbon nanotubes', *Chem. Commun. Camb. Engl.*, no. 12, pp. 1442–1443, Jun. 2003.
- [23] S. Iijima and T. Ichihashi, 'Single-shell carbon nanotubes of 1-nm diameter', *Nature*, vol. 363, no. 6430, pp. 603–605, Jun. 1993.

- [24] D. S. Bethune, C. H. Klang, M. S. de Vries, G. Gorman, R. Savoy, J. Vazquez, and R. Beyers, 'Cobalt-catalysed growth of carbon nanotubes with single-atomic-layer walls', *Nature*, vol. 363, no. 6430, pp. 605–607, Jun. 1993.
- [25] S. J. Tans, M. H. Devoret, H. Dai, A. Thess, R. E. Smalley, L. J. Geerligs, and C. Dekker, 'Individual single-wall carbon nanotubes as quantum wires', *Publ. Online 03 April 1997* vol. 386, no. 6624, pp. 474–477, Apr. 1997.
- [26] E. R. Meshot and A. J. Hart, 'Abrupt self-termination of vertically aligned carbon nanotube growth', *Appl. Phys. Lett.*, vol. 92, no. 11, pp. 113107–3, Mar. 2008.
- [27] M. Jung, K. Yong Eun, J.-K. Lee, Y.-J. Baik, K.-R. Lee, and J. Wan Park, 'Growth of carbon nanotubes by chemical vapor deposition', *Diam. Relat. Mater.*, vol. 10, no. 3–7, pp. 1235–1240, March.
- [28] M. Ge and K. Sattler, 'Vapor-Condensation Generation and STM Analysis of Fullerene Tubes', *Science*, vol. 260, no. 5107, pp. 515–518, Apr. 1993.
- [29] N. Hamada, S. Sawada, and A. Oshiyama, 'New one-dimensional conductors: Graphitic microtubules', *Phys. Rev. Lett.*, vol. 68, no. 10, p. 1579, Mar. 1992.
- [30] R. Saito, G. Dresselhaus, and M. S. Dresselhaus, *Physical Properties of Carbon Nanotubes*, 1st ed. World Scientific Publishing Company, 1998.
- [31] C. J. Lee, J. H. Park, and J. Park, 'Synthesis of bamboo-shaped multiwalled carbon nanotubes using thermal chemical vapor deposition', *Chem. Phys. Lett.*, vol. 323, no. 5–6, pp. 560–565, Jun. 2000.
- [32] S. Amelinckx, X. B. Zhang, D. Bernaerts, X. F. Zhang, V. Ivanov, and J. B. Nagy, 'A Formation Mechanism for Catalytically Grown Helix-Shaped Graphite Nanotubes', *Science*, vol. 265, no. 5172, pp. 635–639, Jul. 1994.
- [33] R. Gao, Z. L. Wang, and S. Fan, 'Kinetically Controlled Growth of Helical and Zigzag Shapes of Carbon Nanotubes', *J. Phys. Chem. B*, vol. 104, no. 6, pp. 1227–1234, Feb. 2000.
- [34] B. W. Smith, M. Monthieux, and D. E. Luzzi, 'Encapsulated C₆₀ in carbon nanotubes', *Nature*, vol. 396, no. 6709, pp. 323–324, Nov. 1998.
- [35] L. X. Zheng, M. J. O'Connell, S. K. Doorn, X. Z. Liao, Y. H. Zhao, E. A. Akhadov, M. A. Hoffbauer, B. J. Roop, Q. X. Jia, R. C. Dye, D. E. Peterson, S. M. Huang, J. Liu, and Y. T. Zhu, 'Ultralong single-wall carbon nanotubes', *Nat Mater*, vol. 3, no. 10, pp. 673–676, Oct. 2004.
- [36] X. Wang, Q. Li, J. Xie, Z. Jin, J. Wang, Y. Li, K. Jiang, and S. Fan, 'Fabrication of Ultralong and Electrically Uniform Single-Walled Carbon Nanotubes on Clean Substrates', *Nano Lett.*, vol. 9, no. 9, pp. 3137–3141, 2009.
- [37] M. Reibold, P. Paufler, A. A. Levin, W. Kochmann, N. Patzke, and D. C. Meyer, 'Materials: Carbon nanotubes in an ancient Damascus sabre', *Nature*, vol. 444, no. 7117, p. 286, Nov. 2006.
- [38] P. M. Ajayan, 'Nanotubes from Carbon', *Chem. Rev.*, vol. 99, no. 7, pp. 1787–1800, Jul. 1999.
- [39] H. Nishijima, S. Kamo, S. Akita, Y. Nakayama, K. I. Hohmura, S. H. Yoshimura, and K. Takeyasu, 'Carbon-nanotube tips for scanning probe microscopy: Preparation by a controlled process and observation of deoxyribonucleic acid', *Appl. Phys. Lett.*, vol. 74, no. 26, pp. 4061–4063, Jun. 1999.
- [40] E. T. Thostenson, Z. Ren, and T.-W. Chou, 'Advances in the science and technology of carbon nanotubes and their composites: a review', *Compos. Sci. Technol.*, vol. 61, no. 13, pp. 1899–1912, Oct. 2001.
- [41] P. Kim, L. Shi, A. Majumdar, and P. L. McEuen, 'Thermal Transport Measurements of Individual Multiwalled Nanotubes', *Phys. Rev. Lett.*, vol. 87, no. 21, p. 215502, Oct. 2001.
- [42] S. Berber, Y.-K. Kwon, and D. Tomnek, 'Unusually High Thermal Conductivity of Carbon Nanotubes', *Phys. Rev. Lett.*, vol. 84, no. 20, p. 4613, May 2000.
- [43] R. H. Baughman, A. A. Zakhidov, and W. A. de Heer, 'Carbon Nanotubes--the Route Toward Applications', *Science*, vol. 297, no. 5582, pp. 787–792, Aug. 2002.

- [44] Y. Mamunya, A. Boudenne, N. Lebovka, L. Ibos, Y. Candau, and M. Lisunova, 'Electrical and thermophysical behaviour of PVC-MWCNT nanocomposites', *Compos. Sci. Technol.*, vol. 68, no. 9, pp. 1981–1988, Jul. 2008.
- [45] T. J. Imholt, C. A. Dyke, B. Hasslacher, J. M. Perez, D. W. Price, J. A. Roberts, J. B. Scott, A. Wadhawan, Z. Ye, and J. M. Tour, 'Nanotubes in Microwave Fields: Light Emission, Intense Heat, Outgassing, and Reconstruction', *Chem. Mater.*, vol. 15, no. 21, pp. 3969–3970, Oct. 2003.
- [46] A. L. Higginbotham, P. G. Moloney, M. C. Waid, J. G. Duque, C. Kittrell, H. K. Schmidt, J. J. Stephenson, S. Arepalli, L. L. Yowell, and J. M. Tour, 'Carbon nanotube composite curing through absorption of microwave radiation', *Compos. Sci. Technol.*, vol. 68, no. 15–16, pp. 3087–3092, Dec. 2008.
- [47] E. Sunden, J. K. Moon, C. P. Wong, W. P. King, and S. Graham, 'Microwave assisted patterning of vertically aligned carbon nanotubes onto polymer substrates', *J. Vac. Sci. Technol. B Microelectron. Nanometer Struct.*, vol. 24, no. 4, pp. 1947–1950, Jul. 2006.
- [48] A. Moiala, Q. Li, I. A. Kinloch, and A. H. Windle, 'Thermal and electrical conductivity of single- and multi-walled carbon nanotube-epoxy composites', *Compos. Sci. Technol.*, vol. 66, no. 10, pp. 1285–1288, Aug. 2006.
- [49] M. J. Biercuk, M. C. Llaguno, M. Radosavljevic, J. K. Hyun, A. T. Johnson, and J. E. Fischer, 'Carbon nanotube composites for thermal management', *Appl. Phys. Lett.*, vol. 80, no. 15, pp. 2767–2769, Apr. 2002.
- [50] T. W. Ebbesen, H. J. Lezec, H. Hiura, J. W. Bennett, H. F. Ghaemi, and T. Thio, 'Electrical conductivity of individual carbon nanotubes', *Nature*, vol. 382, no. 6586, pp. 54–56, Jul. 1996.
- [51] R. Saito, M. Fujita, G. Dresselhaus, and M. S. Dresselhaus, 'Electronic structure of chiral graphene tubules', *Appl. Phys. Lett.*, vol. 60, pp. 2204–2206, May 1992.
- [52] J. Heremans, C. H. Olk, and D. T. Morelli, 'Magnetic susceptibility of carbon structures', *Phys. Rev. B*, vol. 49, no. 21, p. 15122, Jun. 1994.
- [53] A. G. Rinzler, J. H. Hafner, P. Nikolaev, P. Nordlander, D. T. Colbert, R. E. Smalley, L. Lou, S. G. Kim, and D. Tomaneck, 'Unraveling Nanotubes: Field Emission from an Atomic Wire', *Science*, vol. 269, no. 5230, pp. 1550–1553, Sep. 1995.
- [54] W. A. de Heer, A. Chetelain, and D. Ugarte, 'A Carbon Nanotube Field-Emission Electron Source', *Science*, vol. 270, no. 5239, pp. 1179–1180, Nov. 1995.
- [55] Q. H. Wang, A. A. Setlur, J. M. Lauerhaas, J. Y. Dai, E. W. Seelig, and R. P. H. Chang, 'A nanotube-based field-emission flat panel display', *Appl. Phys. Lett.*, vol. 72, no. 22, pp. 2912–2913, Jun. 1998.
- [56] K. H. An, W. S. Kim, Y. S. Park, J.-M. Moon, D. J. Bae, S. C. Lim, Y. S. Lee, and Y. H. Lee, 'Electrochemical Properties of High-Power Supercapacitors Using Single-Walled Carbon Nanotube Electrodes', *Adv. Funct. Mater.*, vol. 11, no. 5, pp. 387–392, 2001.
- [57] L. Hu, J. W. Choi, Y. Yang, S. Jeong, F. La Mantia, L.-F. Cui, and Y. Cui, 'Highly conductive paper for energy-storage devices', *Proc. Natl. Acad. Sci.*, Dec. 2009.
- [58] S. J. Tans, A. R. M. Verschueren, and C. Dekker, 'Room-temperature transistor based on a single carbon nanotube', *Nature*, vol. 393, no. 6680, pp. 49–52, May 1998.
- [59] J. W. G. Wilder, L. C. Venema, A. G. Rinzler, R. E. Smalley, and C. Dekker, 'Electronic structure of atomically resolved carbon nanotubes', *Nature*, vol. 391, no. 6662, pp. 59–62, Jan. 1998.
- [60] M. R. Falvo, R. M. Taylor II, A. Helser, V. Chi, F. P. Brooks Jr, S. Washburn, and R. Superfine, 'Nanometre-scale rolling and sliding of carbon nanotubes', *Nature*, vol. 397, no. 6716, pp. 236–238, Jan. 1999.
- [61] M. S. Dresselhaus, G. Dresselhaus, R. Saito, and A. Jorio, 'Raman spectroscopy of carbon nanotubes', *Phys. Reports*, vol. 409, no. 2, pp. 47–99, Mar. 2005.
- [62] A. M. Rao, E. Richter, S. Bandow, B. Chase, P. C. Eklund, K. A. Williams, S. Fang, K. R. Subbaswamy, M. Menon, A. Thess, R. E. Smalley, G. Dresselhaus, and M. S. Dresselhaus, 'Diameter-Selective Raman Scattering from Vibrational Modes in Carbon Nanotubes', *Science*, vol. 275, no. 5297, pp. 187–191, Jan. 1997.

- [63] A. Jorio, R. Saito, J. H. Hafner, C. M. Lieber, M. Hunter, T. McClure, G. Dresselhaus, and M. S. Dresselhaus, 'Structural (n, m) Determination of Isolated Single-Wall Carbon Nanotubes by Resonant Raman Scattering', *Phys. Rev. Lett.*, vol. 86, no. 6, p. 1118, Feb. 2001.
- [64] H. Kwon, M. Estili, K. Takagi, T. Miyazaki, and A. Kawasaki, 'Combination of hot extrusion and spark plasma sintering for producing carbon nanotube reinforced aluminum matrix composites', *Carbon*, vol. 47, no. 3, pp. 570–577, Mar. 2009.
- [65] X.-L. Xie, Y.-W. Mai, and X.-P. Zhou, 'Dispersion and alignment of carbon nanotubes in polymer matrix: A review', *Mater. Sci. Eng. R Reports*, vol. 49, no. 4, pp. 89–112, May 2005.
- [66] J. L. Bahr and J. M. Tour, 'Covalent chemistry of single-wall carbon nanotubes', *J. Mater. Chem.*, vol. 12, no. 7, pp. 1952–1958, Jun. 2002.
- [67] T. W. Ebbesen, P. M. Ajayan, H. Hiura, and K. Tanigaki, 'Purification of nanotubes', *Nature*, vol. 367, no. 6463, p. 519, Feb. 1994.
- [68] J. Liu, A. G. Rinzler, H. Dai, J. H. Hafner, R. K. Bradley, P. J. Boul, A. Lu, T. Iverson, K. Shelimov, C. B. Huffman, F. Rodriguez-Macias, Y.-S. Shon, T. R. Lee, D. T. Colbert, and R. E. Smalley, 'Fullerene Pipes', *Science*, vol. 280, no. 5367, pp. 1253–1256, May 1998.
- [69] M. S. P. Shaffer, X. Fan, and A. H. Windle, 'Dispersion and packing of carbon nanotubes', *Carbon*, vol. 36, no. 11, pp. 1603–1612, Nov. 1998.
- [70] M. S. P. Shaffer and A. H. Windle, 'Fabrication and Characterization of Carbon Nanotube/Poly(vinyl alcohol) Composites', *Adv. Mater.*, vol. 11, no. 11, pp. 937–941, 1999.
- [71] F. H. Gojny, J. Nastalczyk, Z. Roslaniec, and K. Schulte, 'Surface modified multi-walled carbon nanotubes in CNT/epoxy-composites', *Chem. Phys. Lett.*, vol. 370, no. 5–6, pp. 820–824, Mar. 2003.
- [72] J. E. Riggs, Z. Guo, D. L. Carroll, and Y.-P. Sun, 'Strong Luminescence of Solubilized Carbon Nanotubes', *J. Am. Chem. Soc.*, vol. 122, no. 24, pp. 5879–5880, Jun. 2000.
- [73] L. Cao, H. Chen, M. Wang, J. Sun, X. Zhang, and F. Kong, 'Photoconductivity Study of Modified Carbon Nanotube/Oxotitanium Phthalocyanine Composites', *J. Phys. Chem. B*, vol. 106, no. 35, pp. 8971–8975, 2002.
- [74] D. E. Hill, Y. Lin, A. M. Rao, L. F. Allard, and Y.-P. Sun, 'Functionalization of Carbon Nanotubes with Polystyrene', *Macromolecules*, vol. 35, no. 25, pp. 9466–9471, Dec. 2002.
- [75] E. T. Mickelson, C. B. Huffman, A. G. Rinzler, R. E. Smalley, R. H. Hauge, and J. L. Margrave, 'Fluorination of single-wall carbon nanotubes', *Chem. Phys. Lett.*, vol. 296, no. 1–2, pp. 188–194, Oct. 1998.
- [76] A. G. Nasibulin, P. V. Pikhitsa, H. Jiang, D. P. Brown, A. V. Krasheninnikov, A. S. Anisimov, P. Queipo, A. Moisala, D. Gonzalez, G. Lientschnig, A. Hassanien, S. D. Shandakov, G. Lolli, D. E. Resasco, M. Choi, D. Tomanek, and E. I. Kauppinen, 'A novel hybrid carbon material', *Nat Nano*, vol. 2, no. 3, pp. 156–161, Mar. 2007.
- [77] C. Journet and P. Bernier, 'Production of carbon nanotubes', *Appl. Phys. Mater. Sci. Process.*, vol. 67, no. 1, pp. 1–9, Jul. 1998.
- [78] T. W. Ebbesen and P. M. Ajayan, 'Large-scale synthesis of carbon nanotubes', *Nature*, vol. 358, no. 6383, pp. 220–222, Jul. 1992.
- [79] T. W. Ebbesen, 'Carbon Nanotubes', *Annu. Rev. Mater. Sci.*, vol. 24, no. 1, pp. 235–264, Aug. 1994.
- [80] S.-H. Jung, M.-R. Kim, S.-H. Jeong, S.-U. Kim, O.-J. Lee, K.-H. Lee, J.-H. Suh, and C.-K. Park, 'High-yield synthesis of multi-walled carbon nanotubes by arc discharge in liquid nitrogen', *Appl. Phys. Mater. Sci. Process.*, vol. 76, no. 2, pp. 285–286, Feb. 2003.
- [81] C. Journet, W. K. Maser, P. Bernier, A. Loiseau, M. L. de la Chapelle, S. Lefrant, P. Deniard, R. Lee, and J. E. Fischer, 'Large-scale production of single-walled carbon nanotubes by the electric-arc technique', *Nature*, vol. 388, no. 6644, pp. 756–758, 1997.
- [82] A. J. Hart and A. H. Slocum, 'Rapid Growth and Flow-Mediated Nucleation of Millimeter-Scale Aligned Carbon Nanotube Structures from a Thin-Film Catalyst', *J. Phys. Chem. B*, vol. 110, no. 16, pp. 8250–8257, Apr. 2006.

- [83] H. Zhang, K. Chen, Y. He, Y. Zhu, Y. Chen, C. Wu, J. Wang, J. H. Liao, and S. H. Liu, 'Formation and Raman spectroscopy of single wall carbon nanotubes synthesized by CO₂ continuous laser vaporization', *J. Phys. Chem. Solids*, vol. 62, no. 11, pp. 2007–2010, Nov. 2001.
- [84] T. Guo, P. Nikolaev, A. G. Rinzler, D. Tomanek, D. T. Colbert, and R. E. Smalley, 'Self-Assembly of Tubular Fullerenes', *J. Phys. Chem.*, vol. 99, no. 27, pp. 10694–10697, Jul. 1995.
- [85] T. Guo, P. Nikolaev, A. Thess, D. T. Colbert, and R. E. Smalley, 'Catalytic growth of single-walled nanotubes by laser vaporization', *Chem. Phys. Lett.*, vol. 243, no. 1–2, pp. 49–54, Sep. 1995.
- [86] L. Devetta, P. Canu, A. Bertuccio, K. Steiner, L.-C. Qin, and S. Iijima, 'Structure and formation of raft-like bundles of single-walled helical carbon nanotubes produced by laser evaporation', *Chem. Phys. Lett.*, vol. 269, pp. 65–71, Apr. 1997.
- [87] M. Yudasaka, T. Komatsu, T. Ichihashi, and S. Iijima, 'Single-wall carbon nanotube formation by laser ablation using double-targets of carbon and metal', *Chem. Phys. Lett.*, vol. 278, no. 1–3, pp. 102–106, Oct. 1997.
- [88] A. Thess, R. Lee, P. Nikolaev, H. Dai, P. Petit, J. Robert, C. Xu, Y. H. Lee, S. G. Kim, A. G. Rinzler, D. T. Colbert, G. E. Scuseria, D. Tomanek, J. E. Fischer, and R. E. Smalley, 'Crystalline Ropes of Metallic Carbon Nanotubes', *Science*, vol. 273, no. 5274, pp. 483–487, Jul. 1996.
- [89] E. Muñoz, W. K. Maser, A. M. Benito, M. T. Martínez, G. F. de la Fuente, Y. Maniette, A. Righi, E. Anglaret, and J. L. Sauvajol, 'Gas and pressure effects on the production of single-walled carbon nanotubes by laser ablation', *Carbon*, vol. 38, no. 10, pp. 1445–1451, 2000.
- [90] W. R. Ruston, M. Warzee, J. Hennaut, and J. Waty, 'The solid reaction products of the catalytic decomposition of carbon monoxide on iron at 550°C', *Carbon*, vol. 7, no. 1, pp. 47–50, Feb. 1969.
- [91] M. Jose-Yacamán, M. Miki-Yoshida, L. Rendon, and J. G. Santiesteban, 'Catalytic growth of carbon microtubules with fullerene structure', *Appl. Phys. Lett.*, vol. 62, no. 6, pp. 657–659, Feb. 1993.
- [92] Z. F. Ren, Z. P. Huang, J. W. Xu, J. H. Wang, P. Bush, M. P. Siegal, and P. N. Provencio, 'Synthesis of Large Arrays of Well-Aligned Carbon Nanotubes on Glass', *Science*, vol. 282, no. 5391, pp. 1105–1107, Nov. 1998.
- [93] W. Z. Li, S. S. Xie, L. X. Qian, B. H. Chang, B. S. Zou, W. Y. Zhou, R. A. Zhao, and G. Wang, 'Large-Scale Synthesis of Aligned Carbon Nanotubes', *Science*, vol. 274, no. 5293, pp. 1701–1703, Dec. 1996.
- [94] V. Ivanov, J. B. Nagy, P. Lambin, A. Lucas, X. B. Zhang, X. F. Zhang, D. Bernaerts, G. Van Tendeloo, S. Amelinckx, and J. Van Landuyt, 'The study of carbon nanotubules produced by catalytic method', *Chem. Phys. Lett.*, vol. 223, no. 4, pp. 329–335, Jun. 1994.
- [95] J. Kong, H. T. Soh, A. M. Cassell, C. F. Quate, and H. Dai, 'Synthesis of individual single-walled carbon nanotubes on patterned silicon wafers', *Nature*, vol. 395, no. 6705, pp. 878–881, Oct. 1998.
- [96] S. Huang, X. Cai, and J. Liu, 'Growth of Millimeter-Long and Horizontally Aligned Single-Walled Carbon Nanotubes on Flat Substrates', *J. Am. Chem. Soc.*, vol. 125, no. 19, pp. 5636–5637, May 2003.
- [97] S. B. Sinnott, R. Andrews, D. Qian, A. M. Rao, Z. Mao, E. C. Dickey, and F. Derbyshire, 'Model of carbon nanotube growth through chemical vapor deposition', *Chem. Phys. Lett.*, vol. 315, no. 1–2, pp. 25–30, Dec. 1999.
- [98] A. J. Hart, 'Chemical, mechanical, and thermal control of substrate-bound carbon nanotube growth', 18-Feb-2010. [Online]. Available: <http://dspace.mit.edu/handle/1721.1/38257?show=full>.
- [99] C. J. Lee, D. W. Kim, T. J. Lee, Y. C. Choi, Y. S. Park, W. S. Kim, Y. H. Lee, W. B. Choi, N. S. Lee, J. M. Kim, Y. G. Choi, and S. C. Yu, 'Synthesis of uniformly distributed carbon nanotubes on a large area of Si substrates by thermal chemical vapor deposition', *Appl. Phys. Lett.*, vol. 75, no. 12, pp. 1721–1723, 1999.

- [100] X. H. Chen, S. Q. Feng, Y. Ding, J. C. Peng, and Z. Z. Chen, 'The formation conditions of carbon nanotubes array based on FeNi alloy island films', *Thin Solid Films*, vol. 339, no. 1–2, pp. 6–9, Feb. 1999.
- [101] T. de los Arcos, M. Gunnar Garnier, P. Oelhafen, D. Mathys, J. Won Seo, C. Domingo, J. Vicente García-Ramos, and S. Sánchez-Cortés, 'Strong influence of buffer layer type on carbon nanotube characteristics', *Carbon*, vol. 42, no. 1, pp. 187–190, 2004.
- [102] M. J. Bronikowski, 'CVD growth of carbon nanotube bundle arrays', *Carbon*, vol. 44, no. 13, pp. 2822–2832, Nov. 2006.
- [103] A.-C. Dupuis, 'The catalyst in the CCVD of carbon nanotubes--a review', *Prog. Mater. Sci.*, vol. 50, no. 8, pp. 929–961, Nov. 2005.
- [104] K. B. K. Teo, M. Chhowalla, G. A. J. Amaratunga, W. I. Milne, D. G. Hasko, G. Pirio, P. Legagneux, F. Wyczisk, and D. Pribat, 'Uniform patterned growth of carbon nanotubes without surface carbon', *Appl. Phys. Lett.*, vol. 79, no. 10, pp. 1534–1536, 2001.
- [105] Talapatra S., Kar S., Pal S. K., Vajtai R., Ci L., Victor P., Shaijumon M. M., Kaur S., Nalamasu O., and Ajayan P. M., 'Direct growth of aligned carbon nanotubes on bulk metals:', *Nat Nano*, vol. 1, no. 2, pp. 112–116, Nov. 2006.
- [106] C. Bower, W. Zhu, S. Jin, and O. Zhou, 'Plasma-induced alignment of carbon nanotubes', *Appl. Phys. Lett.*, vol. 77, no. 6, pp. 830–832, Aug. 2000.
- [107] M. Meyyappan, L. Delzeit, A. Cassell, and D. Hash, 'Carbon nanotube growth by PECVD: a review', *Plasma Sources Sci. Technol.*, vol. 12, no. 2, pp. 205–216, May 2003.
- [108] K. Hata, D. N. Futaba, K. Mizuno, T. Namai, M. Yumura, and S. Iijima, 'Water-Assisted Highly Efficient Synthesis of Impurity-Free Single-Walled Carbon Nanotubes', *Science*, vol. 306, no. 5700, pp. 1362–1364, Nov. 2004.
- [109] R. de Villoria, S. Figueredo, A. Hart, S. Steiner, A. Slocum, and B. Wardle, 'High-yield growth of vertically aligned carbon nanotubes on a continuously moving substrate', *Nanotechnology*, vol. 20, no. 40, Oct. 2009.
- [110] E. J. Garcia, B. L. Wardle, and A. John Hart, 'Joining prepreg composite interfaces with aligned carbon nanotubes', *Compos. Part Appl. Sci. Manuf.*, vol. 39, no. 6, pp. 1065–1070, Jun. 2008.
- [111] L. P. F. Chibante, A. Thess, J. M. Alford, M. D. Diener, and R. E. Smalley, 'Solar generation of the fullerenes', *J. Phys. Chem.*, vol. 97, no. 34, pp. 8696–8700, 1993.
- [112] D. Laplaze, P. Bernier, W. K. Maser, G. Flamant, T. Guillard, and A. Loiseau, 'Carbon nanotubes: The solar approach', *Carbon*, vol. 36, no. 5–6, pp. 685–688, 1998.
- [113] W. K. Hsu, J. P. Hare, M. Terrones, H. W. Kroto, D. R. M. Walton, and P. J. F. Harris, 'Condensed-phase nanotubes', *Nature*, vol. 377, no. 6551, p. 687, Oct. 1995.
- [114] W. K. Hsu, M. Terrones, J. P. Hare, H. Terrones, H. W. Kroto, and D. R. M. Walton, 'Electrolytic formation of carbon nanostructures', *Chem. Phys. Lett.*, Jan. 2010.
- [115] J. B. Howard, J. T. McKinnon, Y. Makarovsky, A. L. Lafleur, and M. E. Johnson, 'Fullerenes C60 and C70 in flames', *Nature*, vol. 352, no. 6331, pp. 139–141, Jul. 1991.
- [116] R. all L. V, er Wal, T. M. Ticich, and V. E. Curtis, 'Diffusion flame synthesis of single-walled carbon nanotubes', *Chem. Phys. Lett.*, Jan. 2010.
- [117] L. Yuan, K. Saito, C. Pan, F. A. Williams, and A. S. Gordon, 'Nanotubes from methane flames', *Chem. Phys. Lett.*, vol. 340, no. 3–4, pp. 237–241, Jun. 2001.
- [118] W.-S. Cho, E. Hamada, Y. Kondo, and K. Takayanagi, 'Synthesis of carbon nanotubes from bulk polymer', *Appl. Phys. Lett.*, vol. 69, no. 2, pp. 278–279, Jul. 1996.
- [119] Z. Jiang, R. Song, W. Bi, J. Lu, and T. Tang, 'Polypropylene as a carbon source for the synthesis of multi-walled carbon nanotubes via catalytic combustion', *Carbon*, Jan. 2010.
- [120] P. M. Ajayan, L. S. Schadler, C. Giannaris, and A. Rubio, 'Single-Walled Carbon Nanotube-Polymer Composites: Strength and Weakness', *Adv. Mater.*, vol. 12, no. 10, pp. 750–753, 2000.
- [121] Z. Xia, L. Riester, W. A. Curtin, H. Li, B. W. Sheldon, J. Liang, B. Chang, and J. M. Xu, 'Direct observation of toughening mechanisms in carbon nanotube ceramic matrix composites', *Acta Mater.*, vol. 52, no. 4, pp. 931–944, Feb. 2004.

- [122] K. Ahmad, W. Pan, and S.-L. Shi, 'Electrical conductivity and dielectric properties of multiwalled carbon nanotube and alumina composites', *Appl. Phys. Lett.*, vol. 89, no. 13, pp. 133122–3, 2006.
- [123] C. L. Xu, B. Q. Wei, R. Z. Ma, J. Liang, X. K. Ma, and D. H. Wu, 'Fabrication of aluminum-carbon nanotube composites and their electrical properties', *Carbon*, vol. 37, no. 5, pp. 855–858, Apr. 1999.
- [124] J.-P. Salvetat, G. Briggs, J.-M. Bonard, R. Bacsá, A. Kulik, T. Stöckli, N. Burnham, and L. Forró, 'Elastic and Shear Moduli of Single-Walled Carbon Nanotube Ropes', *Phys. Rev. Lett.*, vol. 82, no. 5, pp. 944–947, Feb. 1999.
- [125] B. Safadi, R. Andrews, and E. A. Grulke, 'Multiwalled carbon nanotube polymer composites: Synthesis and characterization of thin films', *J. Appl. Polym. Sci.*, vol. 84, no. 14, pp. 2660–2669, 2002.
- [126] D. Qian, E. C. Dickey, R. Andrews, and T. Rantell, 'Load transfer and deformation mechanisms in carbon nanotube-polystyrene composites', *Appl. Phys. Lett.*, vol. 76, no. 20, pp. 2868–2870, May 2000.
- [127] K. Mukhopadhyay, C. D. Dwivedi, and G. N. Mathur, 'Conversion of carbon nanotubes to carbon nanofibers by sonication', *Carbon*, vol. 40, no. 8, pp. 1373–1376, Jul. 2002.
- [128] M. Zhang, M. Yudasaka, A. Koshio, and S. Iijima, 'Effect of polymer and solvent on purification and cutting of single-wall carbon nanotubes', *Chem. Phys. Lett.*, vol. 349, no. 1–2, pp. 25–30, Nov. 2001.
- [129] K. L. Lu, R. M. Lago, Y. K. Chen, M. L. H. Green, P. J. F. Harris, and S. C. Tsang, 'Mechanical damage of carbon nanotubes by ultrasound', *Carbon*, vol. 34, no. 6, pp. 814–816, 1996.
- [130] X. Gong, J. Liu, S. Baskaran, R. D. Voise, and J. S. Young, 'Surfactant-Assisted Processing of Carbon Nanotube/Polymer Composites', *Chem. Mater.*, vol. 12, no. 4, pp. 1049–1052, Apr. 2000.
- [131] K. D. Ausman, R. Piner, O. Lourie, R. S. Ruoff, and M. Korobov, 'Organic Solvent Dispersions of Single-Walled Carbon Nanotubes: Toward Solutions of Pristine Nanotubes', *J. Phys. Chem. B*, vol. 104, no. 38, pp. 8911–8915, 2000.
- [132] A. Allaoui, S. Bai, H. . Cheng, and J. . Bai, 'Mechanical and electrical properties of a MWNT/epoxy composite', *Compos. Sci. Technol.*, vol. 62, no. 15, pp. 1993–1998, Nov. 2002.
- [133] M. Kim, Y.-B. Park, O. I. Okoli, and C. Zhang, 'Processing, characterization, and modeling of carbon nanotube-reinforced multiscale composites', *Compos. Sci. Technol.*, vol. 69, no. 3–4, pp. 335–342, Mar. 2009.
- [134] J. K. W. Sandler, J. E. Kirk, I. A. Kinloch, M. S. P. Shaffer, and A. H. Windle, 'Ultra-low electrical percolation threshold in carbon-nanotube-epoxy composites', *Polymer*, vol. 44, no. 19, pp. 5893–5899, Sep. 2003.
- [135] J. Sandler, M. S. P. Shaffer, T. Prasse, W. Bauhofer, K. Schulte, and A. H. Windle, 'Development of a dispersion process for carbon nanotubes in an epoxy matrix and the resulting electrical properties', *Polymer*, vol. 40, no. 21, pp. 5967–5971, Oct. 1999.
- [136] P. M. Ajayan, O. Stephan, C. Colliex, and D. Trauth, 'Aligned Carbon Nanotube Arrays Formed by Cutting a Polymer Resin--Nanotube Composite', *Science*, vol. 265, no. 5176, pp. 1212–1214, Aug. 1994.
- [137] L. Jin, C. Bower, and O. Zhou, 'Alignment of carbon nanotubes in a polymer matrix by mechanical stretching', *Appl. Phys. Lett.*, vol. 73, no. 9, pp. 1197–1199, 1998.
- [138] E. T. Mickelson, I. W. Chiang, J. L. Zimmerman, P. J. Boul, J. Lozano, J. Liu, R. E. Smalley, R. H. Hauge, and J. L. Margrave, 'Solvation of Fluorinated Single-Wall Carbon Nanotubes in Alcohol Solvents', *J. Phys. Chem. B*, vol. 103, no. 21, pp. 4318–4322, May 1999.
- [139] H. Z. Geng, R. Rosen, B. Zheng, H. Shimoda, L. Fleming, J. Liu, and O. Zhou, 'Fabrication and properties of composites of poly(ethylene oxide) and functionalized carbon nanotubes', *Adv. Mater.*, vol. 14, no. 19, pp. 1387–1390, Oct. 2002.

- [140] E. J. Garcia, A. J. Hart, B. L. Wardle, and A. H. Slocum, 'Fabrication of composite microstructures by capillarity-driven wetting of aligned carbon nanotubes with polymers', *Nanotechnology*, vol. 18, no. 16, p. 165602, 2007.
- [141] H. Cebeci, R. G. de Villoria, A. J. Hart, and B. L. Wardle, 'Multifunctional properties of high volume fraction aligned carbon nanotube polymer composites with controlled morphology', *Compos. Sci. Technol.*, vol. 69, no. 15–16, pp. 2649–2656, Dec. 2009.
- [142] F. H. Gojny, M. H. G. Wichmann, U. Köpke, B. Fiedler, and K. Schulte, 'Carbon nanotube-reinforced epoxy-composites: enhanced stiffness and fracture toughness at low nanotube content', *Compos. Sci. Technol.*, vol. 64, no. 15, pp. 2363–2371, Nov. 2004.
- [143] F. H. Gojny, M. H. G. Wichmann, B. Fiedler, I. A. Kinloch, W. Bauhofer, A. H. Windle, and K. Schulte, 'Evaluation and identification of electrical and thermal conduction mechanisms in carbon nanotube/epoxy composites', *Polymer*, vol. 47, no. 6, pp. 2036–2045, Mar. 2006.
- [144] X.-F. Li, K.-T. Lau, and Y.-S. Yin, 'Mechanical properties of epoxy-based composites using coiled carbon nanotubes', *Compos. Sci. Technol.*, vol. 68, no. 14, pp. 2876–2881, Nov. 2008.
- [145] R. J. Mora, J. J. Vilatela, and A. H. Windle, 'Properties of composites of carbon nanotube fibres', *Compos. Sci. Technol.*, vol. 69, no. 10, pp. 1558–1563, Aug. 2009.
- [146] N. A. Siddiqui, M.-L. Sham, B. Z. Tang, A. Munir, and J.-K. Kim, 'Tensile strength of glass fibres with carbon nanotube-epoxy nanocomposite coating', *Compos. Part Appl. Sci. Manuf.*, vol. 40, no. 10, pp. 1606–1614, Oct. 2009.
- [147] E. J. Garcia, B. L. Wardle, A. John Hart, and N. Yamamoto, 'Fabrication and multifunctional properties of a hybrid laminate with aligned carbon nanotubes grown In Situ', *Compos. Sci. Technol.*, vol. 68, no. 9, pp. 2034–2041, Jul. 2008.
- [148] N. Yamamoto, A. Johnhart, E. Garcia, S. Wicks, H. Duong, A. Slocum, and B. Wardle, 'High-yield growth and morphology control of aligned carbon nanotubes on ceramic fibers for multifunctional enhancement of structural composites', *Carbon*, vol. 47, no. 3, pp. 551–560, Mar. 2009.
- [149] A. Godara, L. Mezzo, F. Luizi, A. Warriar, S. V. Lomov, A. W. van Vuure, L. Gorbatikh, P. Moldenaers, and I. Verpoest, 'Influence of carbon nanotube reinforcement on the processing and the mechanical behaviour of carbon fiber/epoxy composites', *Carbon*, vol. 47, no. 12, pp. 2914–2923, Oct. 2009.
- [150] L. L. Lebel, B. Aissa, M. A. E. Khakani, and D. Therriault, 'Ultraviolet-Assisted Direct-Write Fabrication of Carbon Nanotube/Polymer Nanocomposite Microcoils', *Adv. Mater.*, vol. 9999, no. 9999, p. NA, 2009.
- [151] G. H. Kim, J. S. Lee, C. M. Koo, and S. M. Hong, 'Preparation and Characterization of Thermoplastic Composite Based on Poly(vinylidene fluoride) and Multiwalled Carbon Nanotube', *Compos. Interfaces*, vol. 16, pp. 507–518, Jul. 2009.
- [152] J. Gao, M. E. Itkis, A. Yu, E. Bekyarova, B. Zhao, and R. C. Haddon, 'Continuous spinning of a single-walled carbon nanotube-nylon composite fiber', *J. Am. Chem. Soc.*, vol. 127, no. 11, pp. 3847–3854, Mar. 2005.
- [153] Z. Jia, Z. Wang, C. Xu, J. Liang, B. Wei, D. Wu, and S. Zhu, 'Study on poly(methyl methacrylate)/carbon nanotube composites', *Mater. Sci. Eng.*, vol. 271, no. 1–2, pp. 395–400, Nov. 1999.
- [154] A. M. Díez-Pascual, M. Naffakh, M. A. Gómez, C. Marco, G. Ellis, M. T. Martínez, A. Ansón, J. M. González-Domínguez, Y. Martínez-Rubi, and B. Simard, 'Development and characterization of PEEK/carbon nanotube composites', *Carbon*, vol. 47, no. 13, pp. 3079–3090, Nov. 2009.
- [155] D. Zhao, S. Wang, J. Wu, X. Bai, and Q. Lei, 'The mechanical and impact properties of MWNTs/LDPE nanocomposites', *Pigment Resin Technol.*, vol. 38, no. 5, pp. 305–309, 2009.
- [156] E. B. Sansom, D. Rinderknecht, and M. Gharib, 'Controlled partial embedding of carbon nanotubes within flexible transparent layers', *Nanotechnology*, vol. 19, no. 3, p. 035302, 2008.
- [157] A. H. Barber, S. R. Cohen, and H. D. Wagner, 'Measurement of carbon nanotube--polymer interfacial strength', *Appl. Phys. Lett.*, vol. 82, no. 23, pp. 4140–4142, Jun. 2003.

- [158] C. A. Dyke and J. M. Tour, 'Covalent Functionalization of Single-Walled Carbon Nanotubes for Materials Applications', *J. Phys. Chem. A*, vol. 108, no. 51, pp. 11151–11159, Dec. 2004.
- [159] Z. Wang, Z. Liang, B. Wang, C. Zhang, and L. Kramer, 'Processing and property investigation of single-walled carbon nanotube (SWNT) buckypaper/epoxy resin matrix nanocomposites', *Compos. Part Appl. Sci. Manuf.*, vol. 35, no. 10, pp. 1225–1232, Oct. 2004.
- [160] E. J. García, A. J. Hart, B. L. Wardle, and A. H. Slocum, 'Fabrication and Nanocompression Testing of Aligned Carbon-Nanotube–Polymer Nanocomposites', *Adv. Mater.*, vol. 19, no. 16, pp. 2151–2156, 2007.
- [161] J. N. Coleman, U. Khan, W. J. Blau, and Y. K. Gun'ko, 'Small but strong: A review of the mechanical properties of carbon nanotube-polymer composites', *Carbon*, vol. 44, no. 9, pp. 1624–1652, Aug. 2006.
- [162] A. A. Mamedov, N. A. Kotov, M. Prato, D. M. Guldi, J. P. Wicksted, and A. Hirsch, 'Molecular design of strong single-wall carbon nanotube/polyelectrolyte multilayer composites', *Nat Mater*, vol. 1, no. 3, pp. 190–194, Nov. 2002.
- [163] C. K. Chua, K. F. Leong, and C. S. Lim, *Rapid Prototyping: Principles and Applications*. World Scientific, 2010.
- [164] J.-P. Kruth, M. C. Leu, and T. Nakagawa, 'Progress in Additive Manufacturing and Rapid Prototyping', *Cirp Ann. - Manuf. Technol.*, vol. 47, no. 2, pp. 525–540, 1998.
- [165] E. Sachs, E. Wylonis, S. Allen, M. Cima, and H. Guo, 'Production of injection molding tooling with conformal cooling channels using the three dimensional printing process', *Polym. Eng. Sci.*, vol. 40, no. 5, pp. 1232–1247, May 2000.
- [166] M. Schmidt, D. Pohle, and T. Rechtenwald, 'Selective Laser Sintering of PEEK', *Cirp Ann. - Manuf. Technol.*, vol. 56, no. 1, pp. 205–208, 2007.
- [167] E. Sachs, M. Cima, and J. Cornie, 'Three-Dimensional Printing: Rapid Tooling and Prototypes Directly from a CAD Model', *Cirp Ann. - Manuf. Technol.*, vol. 39, no. 1, pp. 201–204, 1990.
- [168] B. Caulfield, P. E. McHugh, and S. Lohfeld, 'Dependence of mechanical properties of polyamide components on build parameters in the SLS process', *J. Mater. Process. Technol.*, vol. 182, no. 1–3, pp. 477–488, Feb. 2007.
- [169] H. Chung and S. Das, 'Functionally graded Nylon-11/silica nanocomposites produced by selective laser sintering', *Mater. Sci. Eng.*, vol. 487, no. 1–2, pp. 251–257, Jul. 2008.
- [170] F. E. Wiria, K. F. Leong, C. K. Chua, and Y. Liu, 'Poly- ϵ -caprolactone/hydroxyapatite for tissue engineering scaffold fabrication via selective laser sintering', *Acta Biomater.*, vol. 3, no. 1, pp. 1–12, Jan. 2007.
- [171] H. Zheng, J. Zhang, S. Lu, G. Wang, and Z. Xu, 'Effect of core–shell composite particles on the sintering behavior and properties of nano-Al₂O₃/polystyrene composite prepared by SLS', *Mater. Lett.*, vol. 60, no. 9–10, pp. 1219–1223, May 2006.
- [172] M. Griffith, D. Keicher, C. Atwood, J. Romero, J. Smugeresky, L. Harwell, and D. Greene, 'Free form fabrication of metallic components using Laser Engineered Net Shaping (LENS(TM))', in *Solid Freeform Fabrication Proceedings, September 1996*, D. Bourell, J. Beaman, H. Marcus, R. Crawford, and J. Barlow, Eds. Austin: Univ Texas Austin, 1996, pp. 125–131.
- [173] W. Liu and J. N. DuPont, 'Fabrication of functionally graded TiC/Ti composites by Laser Engineered Net Shaping', *Scr. Mater.*, vol. 48, no. 9, pp. 1337–1342, May 2003.
- [174] T. R. Jackson, H. Liu, N. M. Patrikakis, E. M. Sachs, and M. J. Cima, 'Modeling and designing functionally graded material components for fabrication with local composition control', *Mater. Des.*, vol. 20, no. 2–3, pp. 63–75, Jun. 1999.
- [175] D. G. Yu, L. Zhu, C. J. Branford-White, and X. L. Yang, 'Three-dimensional printing in pharmaceuticals: Promises and problems', *J. Pharm. Sci.*, vol. 97, no. 9, pp. 3666–3690, Sep. 2008.
- [176] J. H. Sandoval and R. B. Wicker, 'Functionalizing stereolithography resins: effects of dispersed multi-walled carbon nanotubes on physical properties', *Rapid Prototyp. J.*, vol. 12, pp. 292–303, 2006.

- [177] C. M. Cheah, J. Y. H. Fuh, A. Y. C. Nee, and L. Lu, 'Mechanical characteristics of fiber-filled photo-polymer used in stereolithography', *Rapid Prototyp. J.*, vol. 5, pp. 112–119, 1999.
- [178] G. Vaneetveld, A.-M. Clarinval, T. Dormal, J.-C. Noben, and J. Lecomte-Beckers, 'Optimization of the formulation and post-treatment of stainless steel for rapid manufacturing', *J. Mater. Process. Technol.*, vol. 196, no. 1–3, pp. 160–164, Jan. 2008.
- [179] I. Gibson, M. M. Savalani, A. Tarik, and Y. Liu, *The use of multiple materials in Rapid Prototyping*. London: Taylor & Francis Ltd, 2008.
- [180] Y. Zhang, J. Han, X. Zhang, X. He, Z. Li, and S. Du, 'Rapid prototyping and combustion synthesis of TiC/Ni functionally gradient materials', *Mater. Sci. Eng. -Struct. Mater. Prop. Microstruct. Process.*, vol. 299, no. 1–2, pp. 218–224, Feb. 2001.
- [181] L. Weisensel, N. Travitzky, H. Sieber, and P. Greil, 'Laminated object manufacturing (LOM) of SiSiC composites', *Adv. Eng. Mater.*, vol. 6, no. 11, pp. 899–903, Nov. 2004.
- [182] S. Masood and W. Song, 'Development of new metal/polymer materials for rapid tooling using Fused deposition modelling', *Mater. Des.*, vol. 25, no. 7, pp. 587–594, Oct. 2004.
- [183] S. Onagoruwa, S. Bose, and A. Bandyopadhyay, 'Fused Deposition of Ceramics (FDC) and Composites', *Sff 2001*, vol. Texas: 224–31.
- [184] W. Zhong, F. Li, Z. Zhang, L. Song, and Z. Li, 'Short fiber reinforced composites for fused deposition modeling RID C-3025-2011', *Mater. Sci. Eng. -Struct. Mater. Prop. Microstruct. Process.*, vol. 301, no. 2, pp. 125–130, Mar. 2001.
- [185] J. Kim and T. S. Creasy, 'Selective laser sintering characteristics of nylon 6/clay-reinforced nanocomposite', *Polym. Test.*, vol. 23, no. 6, pp. 629–636, Sep. 2004.
- [186] R. Chartoff, B. McMorrow, and P. Lucas, 'Functionally graded polymer matrix nano-composites by solid freeform fabrication: a preliminary report', *Sff 2003*, vol. Texas: 385–91.
- [187] M. Wozniak, T. Graule, Y. de Hazan, D. Kata, and J. Lis, 'Highly loaded UV curable nanosilica dispersions for rapid prototyping applications', *J. Eur. Ceram. Soc.*, vol. 29, no. 11, pp. 2259–2265, Aug. 2009.
- [188] W.-S. Chu, S.-G. Kim, W.-K. Jung, H.-J. Kim, and S.-H. Ahn, 'Fabrication of micro parts using nano composite deposition system', *Rapid Prototyp. J.*, vol. 13, pp. 276–283, 2007.
- [189] J. Czyżewski, P. Burzyński, K. Gawęł, and J. Meisner, 'Rapid prototyping of electrically conductive components using 3D printing technology', *J. Mater. Process. Technol.*, vol. 209, no. 12–13, pp. 5281–5285, Jul. 2009.
- [190] W. Voigt, *Theoretische studien über die elasticitätsverhältnisse der krystalle*. Göttingen: Dieterichsche Verlags-buchhandlung, 1887.
- [191] A. Reuss, 'Berechnung der Fließgrenze von Mischkristallen auf Grund der Plastizitätsbedingung für Einkristalle.', *Zamm - J. Appl. Math. Mech. Z. Für Angew. Math. Mech.*, vol. 9, no. 1, pp. 49–58, 1929.
- [192] A. H. Windle, 'Two defining moments: A personal view by Prof. Alan H. Windle', *Compos. Sci. Technol.*, vol. 67, no. 5, pp. 929–930, 2007.
- [193] B. L. Farmer, M. A. Beard, O. Ghita, R. Allen, and K. E. Evans, 'Assembly Strategies for Fully Aligned and Dispersed Morphology Controlled Carbon Nanotube Reinforced Composites Grown in Net-Shape', *Mrs Online Proc. Libr.*, vol. 1304, 2011.
- [194] B. L. Farmer, R. J. Allen, O. R. Ghita, M. A. Beard, and K. E. Evans, 'Strategies to combine nanocomposite and additive layer manufacturing techniques to build materials and structures simultaneously', *ECCM15 Venice*, vol. 2012, Jun. 2012.
- [195] B. Farmer and D. Johns, 'Method and Apparatus for Manufacturing a Component from a Composite Material', WO/2009/02216720-Feb-2009.
- [196] F. Ko, Y. Gogotsi, A. Ali, N. Naguib, H. Ye, G. I. Yang, C. Li, and P. Willis, 'Electrospinning of Continuous Carbon Nanotube-Filled Nanofiber Yarns', *Adv. Mater.*, vol. 15, no. 14, pp. 1161–1165, 2003.

- [197] C. Park, J. Wilkinson, S. Banda, Z. Ounaies, K. E. Wise, G. Sauti, P. T. Lillehei, and J. S. Harrison, 'Aligned single-wall carbon nanotube polymer composites using an electric field', *J. Polym. Sci. Part B Polym. Phys.*, vol. 44, no. 12, pp. 1751–1762, 2006.
- [198] H. Ago, K. Murata, M. Yumura, J. Yotani, and S. Uemura, 'Ink-jet printing of nanoparticle catalyst for site-selective carbon nanotube growth', *Appl. Phys. Lett.*, vol. 82, no. 5, p. 811, 2003.
- [199] B. Farmer and D. Johns, 'Method of Manufacturing Composite Material by Growing of a Layer of Reinforcement and Related Apparatus', WO/2008/02917914-Mar-2008.
- [200] B. Farmer and D. Johns, 'Method and Apparatus for Manufacturing a Composite Material', WO/2009/01951013-Feb-2009.
- [201] M. Kumar and Y. Ando, 'Chemical Vapor Deposition of Carbon Nanotubes: A Review on Growth Mechanism and Mass Production', *J. Nanosci. Nanotechnol.*, vol. 10, no. 6, pp. 3739–3758, 2010.
- [202] A. J. Hart, L. van Laake, and A. H. Slocum, 'Desktop Growth of Carbon-Nanotube Monoliths with In Situ Optical Imaging', *Small*, vol. 3, no. 5, pp. 772–777, May 2007.
- [203] T. Yamada, T. Namai, K. Hata, D. N. Futaba, K. Mizuno, J. Fan, M. Yudasaka, M. Yumura, and S. Iijima, 'Size-selective growth of double-walled carbon nanotube forests from engineered iron catalysts', *Nat. Nanotechnol.*, vol. 1, no. 2, pp. 131–136, 2006.
- [204] P. Tomaszewski, *Jan Czochralski i jego metoda*, *Jan Czochralski and his method*. Wrocław: Instytut Niskich Temperatur i Badan Strukturalnych PAN : Oficyna Wydawnicza ATUT, Wrocławskie Wydawn. O'swiatowe, 2003.
- [205] '<http://www.idbtechnologies.co.uk/>'.
- [206] S. Noda, K. Hasegawa, H. Sugime, K. Takehi, Z. Zhang, S. Maruyama, and Y. Yamaguchi, 'Millimeter-Thick Single-Walled Carbon Nanotube Forests: Hidden Role of Catalyst Support', *Jpn. J. Appl. Phys.*, vol. 46, pp. L399–L401, May 2007.
- [207] C. P. Deck and K. Vecchio, 'Growth mechanism of vapor phase CVD-grown multi-walled carbon nanotubes', *Carbon*, vol. 43, no. 12, pp. 2608–2617, Oct. 2005.
- [208] E. R. Meshot, D. L. Plata, S. Tawfick, Y. Zhang, E. A. Verploegen, and A. J. Hart, 'Engineering Vertically Aligned Carbon Nanotube Growth by Decoupled Thermal Treatment of Precursor and Catalyst', *Acs Nano*, vol. 3, no. 9, pp. 2477–2486, 2009.
- [209] M. Bedewy, E. R. Meshot, H. Guo, E. A. Verploegen, W. Lu, and A. J. Hart, 'Collective Mechanism for the Evolution and Self-Termination of Vertically Aligned Carbon Nanotube Growth', *J Phys Chem C*, vol. 113, no. 48, pp. 20576–20582, 2009.
- [210] A. J. Hart and A. H. Slocum, 'Force output, control of film structure, and microscale shape transfer by carbon nanotube growth under mechanical pressure', *Nano Lett.*, vol. 6, no. 6, pp. 1254–1260, Jun. 2006.
- [211] D. L. Plata, A. J. Hart, C. M. Reddy, and P. M. Gschwend, 'Early Evaluation of Potential Environmental Impacts of Carbon Nanotube Synthesis by Chemical Vapor Deposition', *Environ. Sci. Technol.*, vol. 43, no. 21, pp. 8367–8373, Nov. 2009.
- [212] K. Mizuno, J. Ishii, H. Kishida, Y. Hayamizu, S. Yasuda, D. N. Futaba, M. Yumura, and K. Hata, 'A black body absorber from vertically aligned single-walled carbon nanotubes', *Proc. Natl. Acad. Sci.*, vol. 106, no. 15, pp. 6044–6047, Apr. 2009.
- [213] G. G. Silva, M.-T. F. Rodrigues, C. Fantini, R. S. Borges, M. A. Pimenta, B. J. Carey, L. Ci, and P. M. Ajayan, 'Thermoplastic Polyurethane Nanocomposites Produced via Impregnation of Long Carbon Nanotube Forests', *Macromol. Mater. Eng.*, vol. 296, no. 1, pp. 53–58, 2011.
- [214] F. T. Fisher, R. D. Bradshaw, and L. C. Brinson, 'Effects of nanotube waviness on the modulus of nanotube-reinforced polymers', *Appl. Phys. Lett.*, vol. 80, no. 24, pp. 4647–4649, Jun. 2002.
- [215] M. A. Beard, O. R. Ghita, B. Farmer, D. Johns, and K. E. Evans, 'Aligned and Dispersed Carbon Nanotube (CNT) Composites: Manufacturing and Characterisation', *14th Eur. Conf. Compos. Mater. ECCM14*, vol. 2010.
- [216] http://www.huntsman.com/advanced_materials/a/Home/Adhesives, .
- [217] S. Tawfick, M. De Volder, and A. J. Hart, 'Structurally Programmed Capillary Folding of Carbon Nanotube Assemblies', *Langmuir*, vol. 27, no. 10, pp. 6389–6394, 2011.

- [218] P. D. Bradford, X. Wang, H. Zhao, J.-P. Maria, Q. Jia, and Y. T. Zhu, 'A novel approach to fabricate high volume fraction nanocomposites with long aligned carbon nanotubes', *Compos. Sci. Technol.*, vol. 70, no. 13, pp. 1980–1985, Nov. 2010.
- [219] R. Andrews and M. C. Weisenberger, 'Carbon nanotube polymer composites', *Curr. Opin. Solid State Mater. Sci.*, vol. 8, no. 1, pp. 31–37, Jan. 2004.
- [220] F. Fisher, 'Fiber waviness in nanotube-reinforced polymer composites—I: Modulus predictions using effective nanotube properties', *Compos. Sci. Technol.*, vol. 63, no. 11, pp. 1689–1703, Aug. 2003.
- [221] T.-W. Chou and K. Takahashi, 'Non-linear elastic behaviour of flexible fibre composites', *Composites*, vol. 18, no. 1, pp. 25–34, Jan. 1987.
- [222] C.-M. Kuo, K. Takahashi, and T.-W. Chou, 'Effect of Fiber Waviness on the Nonlinear Elastic Behavior of Flexible Composites', *J. Compos. Mater.*, vol. 22, no. 11, pp. 1004–1025, Jan. 1988.
- [223] M. Abdalla, D. Dean, P. Robinson, and E. Nyairo, 'Cure behavior of epoxy/MWCNT nanocomposites: The effect of nanotube surface modification', *Polymer*, vol. 49, no. 15, pp. 3310–3317, Jul. 2008.
- [224] R. J. Allen, O. Ghita, B. Farmer, M. Beard, and K. E. Evans, 'Mechanical testing and modelling of a vertically aligned carbon nanotube composite structure', *Compos. Sci. Technol.*, vol. 77, pp. 1–7, Mar. 2013.
- [225] L. Jiang, S. M. Spearing, M. A. Monclus, and N. M. Jennett, 'Formation and mechanical characterisation of SU8 composite films reinforced with horizontally aligned and high volume fraction CNTs', *Compos. Sci. Technol.*, vol. 71, no. 10, pp. 1301–1308, Jul. 2011.
- [226] B. S. Massey and J. W. Smith, *Mechanics of Fluids*, 4th ed. pp24: Taylor & Francis, 1998.
- [227] H. M. Princen, 'Capillary phenomena in assemblies of parallel cylinders : II. Capillary rise in systems with more than two cylinders', *J. Colloid Interface Sci.*, vol. 30, no. 3, pp. 359–371, Jul. 1969.
- [228] H. M. Princen, 'Capillary phenomena in assemblies of parallel cylinders : I. Capillary rise between two cylinders', *J. Colloid Interface Sci.*, vol. 30, no. 1, pp. 69–75, May 1969.
- [229] D. H. Lee, W. J. Lee, and S. O. Kim, 'Highly Efficient Vertical Growth of Wall-Number-Selected, N-Doped Carbon Nanotube Arrays', *Nano Lett.*, vol. 9, no. 4, pp. 1427–1432, Apr. 2009.
- [230] E. W. Washburn, 'The Dynamics of Capillary Flow', *Phys. Rev.*, vol. 17, no. 3, p. 273, Mar. 1921.
- [231] R. Lucas, 'Ueber das Zeitgesetz des kapillaren Aufstiegs von Flüssigkeiten', *Colloid Polym. Sci.*, vol. 23, no. 1, pp. 15–22, 1918.
- [232] B. V. Zhmud, F. Tiberg, and K. Hallstensson, 'Dynamics of Capillary Rise', *J. Colloid Interface Sci.*, vol. 228, no. 2, pp. 263–269, Aug. 2000.
- [233] H. Darcy, *Les fontaines publiques de la ville de Dijon*. Paris: Dalmont, 1856.
- [234] N. Fries, K. Odic, M. Conrath, and M. Dreyer, 'The effect of evaporation on the wicking of liquids into a metallic weave', *J. Colloid Interface Sci.*, vol. 321, no. 1, pp. 118–129, May 2008.
- [235] L. Zhu, Y. Sun, D. W. Hess, and C.-P. Wong, 'Well-Aligned Open-Ended Carbon Nanotube Architectures: An Approach for Device Assembly', *Nano Lett.*, vol. 6, no. 2, pp. 243–247, Feb. 2006.
- [236] R. J. Allen, O. R. Ghita, B. L. Farmer, M. A. Beard, and K. E. Evans, 'Wetting Mechanisms of Vertically Aligned Carbon Nanotube (VACNT) Composite Structures in readiness for Additive Layer Manufacture', *15th Eur. Conf. Compos. Mater. ECCM15*, vol. 2012.
- [237] W. Heber Green and G. A. Ampt, 'Studies on Soil Phycs.', *J. Agric. Sci.*, vol. 4, no. 01, pp. 1–24, 1911.
- [238] Z.-P. Yang, L. Ci, J. A. Bur, S.-Y. Lin, and P. M. Ajayan, 'Experimental observation of an extremely dark material made by a low-density nanotube array', *Nano Lett.*, vol. 8, no. 2, pp. 446–451, Feb. 2008.
- [239] 'http://www.eip.rl.ac.uk/sectc.htm#THE_PHOTRON_Fastcam_XLR'. .
- [240] J. M. Andreas, E. A. Hauser, and W. B. Tucker, 'Boundary Tension by Pendant Drops', *J Phys Chem*, vol. 42, no. 8, pp. 1001–1019, 1937.

- [241] S. Sugden, 'VI.—The variation of surface tension with temperature and some related functions', *J. Chem. Soc. Trans.*, vol. 125, no. 0, pp. 32–41, Jan. 1924.
- [242] N. A. Lange, *Lange's Handbook of Chemistry*. McGraw-Hill, 1967.
- [243] J. Kozeny, *Über kapillare Leitung des Wassers im Boden: (Aufstieg, Versickerung u. Anwendung auf die Bewässerung); Gedr. Mit Unterstützung aus d. Jerome u. Margaret Stonborsugh-Fonds.* Hölder-Pichler-Tempsky, A.-G. Akad. d. Wiss., 1927.
- [244] N. Fries and M. Dreyer, 'The transition from inertial to viscous flow in capillary rise', *J. Colloid Interface Sci.*, vol. 327, no. 1, pp. 125–128, Nov. 2008.
- [245] X. Yan and P. Gu, 'A review of rapid prototyping technologies and systems', *Comput.-Aided Des.*, vol. 28, no. 4, pp. 307–318, Apr. 1996.
- [246] '<http://production3dprinters.com/support/sla-material-safety-datasheets-msds>'.